

Temiz Kum Zeminlerin Kayma Dayanımının Deneysel Olarak Belirlenmesi ve
Karşılaştırmalı Analizi

Türker Güler

DOKTORA TEZİ

İnşaat Mühendisliği Anabilim Dalı

Ocak 2022

Experimental Determination of Shear Strength of Clean Sand Soils and Its Comparative
Analysis

Türker Güler

DOCTORAL DISSERTATION

Department of Civil Engineering

January 2022

Experimental Determination of Shear Strength of Clean Sand Soils and Its Comparative
Analysis

A Thesis Submitted to the Eskişehir Osmangazi University

Graduate School of Natural and Applied Sciences in

Partial Fulfillment of the Requirements for the

Degree of Doctor of Philosophy in Discipline of

Geotechnics of the Department of the

Civil Engineering

by

Türker Güler

Supervisor: Assoc. Prof. Dr. Hasan Savaş

Co-Supervisor: Assoc. Prof. Dr. Kâmil Bekir Afacan

January 2022

ETHICAL STATEMENT

I hereby declare that this thesis titled “**Experimental Determination of Shear Strength of Clean Sand Soils and Its Comparative Analysis**” has been prepared in accordance with the thesis writing rules of Eskişehir Osmangazi University Graduate School of Natural and Applied Sciences under academic consultancy of my supervisor Assoc. Prof. Dr. Hasan Savaş and my co-supervisor Assoc. Prof. Dr. Kâmil Bekir Afacan. I hereby declare that the work presented in this thesis is original. I also declare that, I have respected scientific ethical principle and rules in all stages of my thesis study, all information and data presented in this thesis have been obtained within the scope of scientific and academic ethical principle and rules, all materials used in this thesis which are not original to this thesis have been fully cited and referenced, and all knowledge documents and results have been presented in accordance with scientific ethical principle and rules. 21.01.2022

Türker Güler

SUMMARY

A soil mass must provide stability and deformation conditions under the influence of the loads to which it is exposed. The stability condition deals with the preservation of the stability of the soil against failure as a result of loading, and the deformation condition deals with condition before failure related to the fact that the deformations caused by the loading effect do not exceed certain limits. In the case of both conditions, it is necessary to know the shear strength parameters of the soil. The fact that all structures are founded to the soils makes the shear strength, which is the vital engineering property of geotechnical science, the most important subject of all civil engineering applications. The shear strength, which is defined as the maximum mobilized shear stress formed in the potential plane of failure, is known as the most complex engineering property of soils. This characteristic is quite important, as it directly affects the design parameters of all types of engineering structures. Shear strength parameters of soils are measured by various test methods in field and in laboratories. Although these methods have advantages over each other for different deformation conditions, choosing the appropriate test method according to the current soil conditions is the most important part of the subject. In the first part of the study, the shear strength properties of sand soils were measured by direct shear, triaxial shear and ring shear experimental methods and their comparative analysis was carried out. The results of the analysis were associated with the plane strain method, which more reliably models the field stress conditions in many important geotechnical applications and various relationships were found between them. In the second part of the study, the effect of volumetric strain properties, which are the main determinants of shear strength, on the test methods were examined and comparative analysis were carried out and various relations were obtained for each test method on the basis of the flow rule. Another important subject investigated in the study was the investigation of the effects of geosynthetic reinforcements on the stress-strain and stress-dilatation properties of the soil for each test method and examining the results of the comparative analysis. In the study, effective consolidation stress and relative density intervals which are the most common in geotechnical applications were taken into account, the samples were tested in constant strain rate at a single volumetric reinforcement concentration in drained conditions. As a result of this comprehensive study, in which 1203 experiments were carried out, it was seen that the boundary conditions belonging to the experimental methods affect the shear strength properties of sand soils depending on the geometrical interference capacity, and the presence of fiber makes this effect more specific in different concepts.

Keywords: Direct Shear Test, Triaxial Test, Ring Shear Test, Plane Strain Test, Shear Strength Parameters, Volumetric Strain Parameters, Sand, Reinforcement

ÖZET

Bir zemin kütlesi maruz kaldığı yükler etkisinde stabilite ve deformasyon koşullarını sağlamak zorundadır. Stabilite koşulu yükleme sonucunda zeminin yenilmeden duraylılığını korumasıyla, deformasyon koşulu ise yükleme etkisinde oluşan deformasyonların belli sınırları aşmaması ile ilgili yenilme öncesi durumla ilgilenir. Her iki koşulun incelenmesinde de zeminin kayma dayanımı parametrelerinin bilinmesi gerekir. Tüm yapıların zeminle ilişkili olması geoteknik biliminin en önemli mühendislik özelliği olan kayma dayanımını tüm inşaat mühendisliği uygulamalarının en önemli konusu haline getirmektedir. Potansiyel kırılma düzleminde oluşan mobilize en büyük kesme gerilmesi olarak tanımlanan kayma dayanımı zeminlerin en karmaşık mühendislik özelliği olarak bilinir. Bu özellik her tür mühendislik yapısının tasarım parametrelerini doğrudan etkilediğinden oldukça önemlidir. Zeminlerin kayma dayanımı parametreleri arazi ve laboratuvarlarda çeşitli deney yöntemleriyle ölçülür. Bu yöntemlerin farklı deformasyon koşulları için birbirlerine üstünlükleri bulunsa da mevcut zemin koşullarına göre uygun deney yönteminin seçilmesi konunun en önemli kısmını oluşturmaktadır. Çalışmanın ilk bölümünde kum zeminlerin kayma dayanımı özellikleri direkt kesme, üç eksenli basınç ve halka kesme deney yöntemleriyle ölçülerek karşılaştırmalı analizleri yapılmıştır. Analiz sonuçları birçok önemli geoteknik uygulamada arazi gerilme koşullarını daha güvenilir bir şekilde modelleyen düzlem deformasyon yöntemi ile ilişkilendirilerek aralarında çeşitli ilişkiler türetilmiştir. Çalışmanın ikinci bölümünde kayma dayanımının asıl belirleyicisi olan hacimsel deformasyon özelliklerinin deney yöntemlerine etkisi incelenerek karşılaştırmalı analizleri yapılmış akış kuralı esasında her bir deney yöntemi için çeşitli ilişkiler elde edilmiştir. Çalışmada araştırılan bir diğer önemli konu ise geosentetik donatıların zeminin gerilme-deformasyon ve gerilme-dilatasyon özelliklerine olan etkisinin her bir deney yöntemi için araştırılarak karşılaştırmalı analiz sonuçlarının incelenmesi olmuştur. Çalışmada geoteknik uygulamalarda en çok karşılaşılan efektif konsolidasyon gerilmesi ve sıklık aralıkları dikkate alınmış, numuneler sabit deformasyon hızında ve tek bir hacimsel donatı konsantrasyonunda drenajlı olarak test edilmiştir. Toplam 1203 adet deneyin gerçekleştirildiği bu kapsamlı çalışma sonucunda deney yöntemlerine ait sınır koşulların geometrik interferans kapasitesine bağlı olarak kum zeminlerin kayma dayanımı ve deformasyon özelliklerini etkilediği, fiber varlığının ise bu etkiyi farklı kavramlarda daha özel bir hale getirdiği görülmüştür.

Anahtar kelimeler: Direkt Kesme Deneyi, Üç Eksenli Deney, Halka Kesme Deneyi, Düzlem Deformasyon Deneyi, Kayma Dayanımı Parametreleri, Hacimsel Deformasyon Parametreleri, Kum, Donatı

TABLE OF CONTENTS

	<u>Page</u>
SUMMARY	vi
ÖZET	vii
ACKNOWLEDGMENTS	viii
TABLE OF CONTENTS	ix
LIST OF FIGURES	xi
LIST OF TABLES	xxiv
LIST OF SYMBOLS AND ABBREVIATIONS	xxvi
1. INTRODUCTION AND PURPOSE	1
2. LITERATURE REVIEW	3
3. SHEAR STRENGTH AND FAILURE CRITERIA OF SOILS	70
3.1. Introduction	70
3.2. Stress State at a Point in Soil Mass	70
3.3. Mohr-Coulomb Failure Criterion	76
3.4. Stress-Strain Behavior of Sands	80
3.5. Factors Acting on the Shear Strength of Sands	93
4. MATERIALS AND METHODS	97
4.1. Introduction	97
4.2. Material Specifications	97
4.2.1. CEN Standard Sand	97
4.1.2. Fiber reinforcement	106
4.3. Test Procedure and Study Program	108
4.3.1. Sample preparation method and application principles	108
4.3.2. Selection of test parameters and study program	111

TABLE OF CONTENTS (Continued)

	<u>Page</u>
4.4. Test Systems and Application Details	118
4.4.1. Direct shear test	119
4.4.2. Triaxial shear test	126
4.4.3. Ring shear test	136
5. RESULTS AND DISCUSSION	143
5.1. Introduction	143
5.2. Direct Shear Test Results	145
5.2.1. Stress-strain relationship	146
5.2.2. Shear strength parameters	162
5.2.3. Volumetric strains	169
5.3. Triaxial Test Results	170
5.3.1. Stress-strain relationship	170
5.3.2. Shear strength parameters	184
5.3.3. Volumetric strains	190
5.4. Ring Shear Test Results	191
5.4.1. Stress-strain relationship	193
5.4.2. Shear strength parameters	204
5.4.3. Volumetric strains	210
5.5. Comparative Analysis of Direct Shear, Triaxial and Ring Shear Test Methods...211	
5.5.1. Shear Strength Parameters	211
5.5.2. Volumetric strain parameters	241
6. CONCLUSIONS AND RECOMMENDATIONS	254
LIST OF REFERENCES	258

LIST OF FIGURES

<u>Figure</u>	<u>Page</u>
2.1. Variation of shear strength angle as a function of porosity by different test methods (Nash, 1953)	6
2.2. Comparison of the failure characteristics as a function of porosity (pre-test) for different test methods: (a) Angle of shearing resistance, (b) Volumetric deformation, and (c) Axial deformation (Cornforth, 1964)	8
2.3. Illustration of strength parameters from different methods in Mohr circle with Davis hypothesis (Davis, 1968).....	9
2.4. Representation of stress and strain increments in the Mohr circle (Rowe, 1969).....	12
2.5. The relationship between the peak strengths measured in the direct shear, plane strain, and triaxial compression tests (quartz mineral sand from Mersey River) (Rowe, 1969)	14
2.6. Variation of the material constants as a function of the effective ambient pressure by different test methods: (a) Initial tangent module, (b) Poisson ratio (Lee, 1970) ..	15
2.7. Mohr failure envelopes (Cape coast sand), (Pells et al., 1973)	16
2.8. Effect of the moderate principal stress on the effective friction angle of sands (Ladd et al. 1977)	19
2.9. Effect of the angle δ on principal stress ratio: (a) Plane strain, (b) Triaxial (Oda et al., 1978)	21
2.10. Evaluation of the Mohr failure envelopes for certain angles δ (Oda et al., 1978)	21
2.11. Relationship between ambient pressure and internal friction angle (Marachi et al., 1981)	25
2.12. Comparison of axial strains at failure obtained by different test methods (Marachi et al., 1981)	25

LIST OF FIGURES (Continued)

<u>Figure</u>	<u>Page</u>
2.13. Comparison of the plane strain strengths observed with those estimated (Ramamurthy & Tokhi, 1981)	28
2.14. Failure surface sections in principal stress space (Wroth, 1984)	29
2.15. Relationship of shear strength angle obtained from the Matsuoka failure criterion for different test conditions (Wroth, 1984)	31
2.16. Theoretical relationship of shear friction angles tested and calculated (Jewell & Wroth, 1987)	33
2.17. Relationship between the tangent ratio of peak shear friction angles and the critical-state friction angle (Jewell & Wroth, 1987)	33
2.18. Comparison of the maximum strengths for different strain conditions (Schanz and Vermeer, 1996)	36
2.19. Triaxial dilation deviation from the biaxial state (Schanz and Vermeer, 1996).....	37
2.20. Investigation of the variation of shear strength angle by the void ratio with different test methods (Okada et al., 1998)	39
2.21. Comparison of the plane strain test results and the triaxial test results: (a) Low density - high ambient pressure, (b) High density - low ambient pressure (Alshibli et al., 2003)	41
2.22. On deviatoric plane (Georgiadis et al., 2004)	42
2.23. On $(J - p')$ plane (Georgiadis et al., 2004)	42
2.24. According to the Matsuoka-Nakai failure criterion (Georgiadis et al., 2004)	43
2.25. According to the Lade-Duncan failure criterion (Georgiadis et al., 2004)	43
2.26. Comparison of the peak direct shear and plane strain data: (a) Using the combination of different parameters, (b) Evaluating the winged direct shear and Stroud (1971) with the flow rules ($\phi'_{cv} = 35^\circ$), (Lings & Dietz, 2004)	45

LIST OF FIGURES (Continued)

<u>Figure</u>	<u>Page</u>
2.27. Variation of the peak shear strength measured by the drained triaxial tests and by other shear tests (Mirata & Erzin, 2007)	47
2.28. Variation of the δ angle and the peak shear strength angle measured by different tests (Mirata & Erzin, 2007)	47
2.29. Failure states obtained from different strain conditions (Wanatowski & Chu, 2007)....	48
2.30. Stress-dilation relationships of different sands (Wanatowski & Chu, 2007)	50
2.31. Failure envelopes of different scale and methods (Specimen <i>D</i>) (Bareither et al., 2008)	52
2.32. Geometric description of shear plane direction and large principal stress direction relative to bedding plane (Guo, 2008)	53
2.33. Effect of angle δ on anisotropic strength properties of sands (Guo, 2008)	55
2.34. Relationships $\phi' - I_D$ for shear tests (Park et al., 2008)	56
2.35. Specimens before and after ring shear test (from the shear band) (Sadrekarimi & Olson, 2010)	58
2.36. CSL and RSL lines of different sands: (a) Ottawa (20/40), (b) Illinois river sand, (c) Mississippi river sand (Sadrekarimi & Olson, 2014)	59
2.37. Initial shear modules for different stress paths ($\gamma_s = 0.05\%$, $p_{ref} = 101.3 \text{ kPa}$), (Strahler et al., 2016b)	61
2.38. Comparison of effective friction and dilation angle (Strahler et al., 2016)	62
2.39. Comparison of the test results as a function of mean effective ambient pressure with Bolton's (1986, 1987) approaches (Strahler et al., 2016)	62
2.40. Failure envelopes of sands containing reinforcement from different methods (Dev et al., 2016)	63

LIST OF FIGURES (Continued)

<u>Figure</u>	<u>Page</u>
2.41. Mobilized shear strength distribution (kPa) in shearing plane and in ($A - A$) cross section (Medzvieckas et al., 2017)	65
2.42. Displacement distribution $u_x(10^{-3}m)$ in shearing plane and in ($A - A$) cross section (Medzvieckas et al., 2017)	65
2.43. Distribution of vertical stresses $\sigma_y(kPa)$ after an initial compression phase in shearing plane and in cross section ($A - A$) (Medzvieckas et al., 2017)	65
2.44. Distribution of vertical stresses $\sigma_y(kPa)$ at failure in shearing plane and in cross section ($A-A$) (Medzvieckas et al., 2017)	65
2.45. Distribution of horizontal stresses $\sigma_x(kPa)$ at ambient pressure and failure phase (Medzvieckas et al., 2017)	66
2.46. Distribution of horizontal stresses $\sigma_y(kPa)$ in the whole specimen and in cross section ($A-A$) at failure (Medzvieckas et al., 2017)	66
2.47. Distribution of shear stress $\tau_{xy}(kPa)$ under the cap at failure (Medzvieckas et al., 2017)	66
2.48. Peak shear strength angles from different methods, as a function of porosity (Hanna & Ayadat, 2019)	67
2.49. Effect of porosity on volumetric strains from different methods (Hanna & Ayadat, 2019)	68
3.1. Stress definition of an infinitesimal soil that is exposed to external loads, around a point on any separated plane	71
3.2. (a) Stress components of infinitesimal soil element, (b) Representative stress state reduced to two dimensions	72
3.3. (a) Stresses acting on the triangle element, (b) Positive sign directions, (c) Separation of principal stresses in XZ plane into components	73

LIST OF FIGURES (Continued)

<u>Figure</u>	<u>Page</u>
3.4. Mohr stress circle for plane stress condition	75
3.5. Mohr diagram and failure envelopes	77
3.6. Failure state according to Mohr-Coulomb criterion	78
3.7. Shear strength components of sand (based on porosity) (Rowe, 1962; Lee & Seed, 1967)	81
3.8. Mohr failure envelope components of sand at high ambient pressures (Lee & Seed, 1967)	82
3.9. Effect of shearing force on the volume of soils (Casagrande, 1936)	83
3.10. Contribution of dilation to internal friction (Bolton, 2018)	86
3.11. Illustration of dilatation behavior with saw tooth model (Bolton, 1979, 1986)	87
3.12. Critical state lines at q', p', v space (Schofield & Wroth, 1968; Bolton, 1979; Wood, 1990; Jefferies & Been, 2016)	88
3.13. Variation of dilation and critical state line at $p' - e$ space (Bolton, 2018)	89
3.14. Non-linear strength envelope of sand soil (Bolton, 2018).....	92
3.15. Friction angle envelope of quartz sands as a function of grain size (Rowe, 1962)...	95
3.16. Relationship between effective friction angle, dry density, and soil classification (Holtz et al., 2011).....	96
4.1. CEN standard sand produced in accordance with TS EN 196-1	99
4.2. The particle size distribution (granulometry) curve of the CEN standard sand	100
4.3. Particle size distribution range of CEN standard sand (USCS)	100
4.4. Relationship between density index and void ratio (Venkatramaiah, 2018)	101
4.5. Compaction curves of CEN standard sand	105
4.6. SEM outputs of CEN standard sand: (a) 50X, (b) 2500X	105

LIST OF FIGURES (Continued)

<u>Figure</u>	<u>Page</u>
4.7. Standard STRUX® 90/40 synthetic macro fiber	106
4.8. Dimensions of standard STRUX® 90/40 fiber	106
4.9. Historical development process of polyolefin (Sauter et al., 2017)	107
4.10. Phase diagram for fiber reinforced samples	112
4.11. Schematic section diagram of the direct shear test tool (Wood, 2009)	119
4.12. Representation of stress states on the shear plane with Mohr circle (Taylor, 1948)	120
4.13. Dynamic shear area diagram of circular shear box	121
4.14. Direct shear apparatus manufactured by ELE International (26-2114/01)	122
4.15. Auxiliary equipment of the circular shear box: (a) Shear box, (b) Loading head, (c) Porous stones, (d) Sample shearer, (e) Sample extractor (26-2213)	123
4.16. System tools used in the study: (a) LVDT, (b) Load cell, (c) Data acquisition unit	123
4.17. General view of the direct shear apparatus from the top profile: (a) Loading shaft, (b) Train of components, (c) Vertical displacement transducer, (d) Load pin, (e) Loading yoke, (f) Shear box, (g) Drain plug, (h) Swan neck, (i) Locking screw, (j) Swan neck guide shaft arm, (k) Split bracket, (l) Horizontal displacement transducer, (m) Load cell, (n) Load cell adjustment lever	125
4.18. Pre-test procedure: (a) Sample preparation, (b) Consolidation stage	125
4.19. Post-test procedure: Shear completion and disassembly of the shear box	125
4.20. Schematic diagram of consolidated drained triaxial apparatus (ASTM, 2020)	126
4.21. Triaxial shear panel manufactured by ELE International (25-3516/01)	130
4.22. Auxiliary equipment of the triaxial shear test: (a) Two-part vacuum split mold, (b) Filter Disc, (c) Porous plate, (d) O-ring, (e) Membrane, (f) Membrane placing tool, (g) Base adapter, (h) Porous top cap	131

LIST OF FIGURES (Continued)

<u>Figure</u>	<u>Page</u>
4.23. System tools used in the study: (a) Pressure transducer, (b) Clamped boss load ring, (c) LVDT, (d) Volume change unit	131
4.24. Other details of the sample setup and system valves for the triaxial test: (a) Drain/pressure valve, (b) De-airing Block, (c) Pressure transducer, (d) Cell water supply valve, (e) Cell base, (f) Suction pressure application valve, (g) Membrane vacuum line, (h) Base adapter, (i) O-ring, (j) Two-part vacuum split mold, (k) Membrane, (l) Porous plate	133
4.25. Stages of the triaxial shear test: (a) Preparing the sample, (b) Removing the mold, (c) Filling the cell with water, (d) Saturating the sample, (e) Consolidation stage, (f) Shear stage	134
4.26. General view of ring shear test apparatus (Type B) (BS, 1990; ISO, 2018)	135
4.27. Plan view of bottom platen, center pin and torque arms of ring shear test apparatus (Type B)	137
4.28. Stress state of the shear band in the ring shear test: a) Resultant of forces, b) Unbalanced forces (Detailed explanations of notation representation can be found in Sadrekarimi's study (2009).)	137
4.29. Ring shear test system (VJT5600A/01) manufactured by VJ Tech Limited.....	139
4.30. Auxiliary equipment of ring shear box: (a) Specimen container and lifting handle (bottom part), (b) Bronze porous torsion beam (top cap, modified type), (c) Clamping screws, (d) Circular tamping tool	140
4.31. System tools used in the study: (a) LSCT, (b) Load cell, (c) Converter interface ...	140
4.32. Details of ring shear box: (a) Load ring arm, (b) Water chamber, (c) Lifting handle, (d) Specimen container, (e) Angular indicator, (f) Clamping screw, (g) Graduated scale, (h) Torsion beam (top cap)	141
4.33. Pre-shear procedure: (a) Sample preparation, (b) Consolidation stage	142

LIST OF FIGURES (Continued)

<u>Figure</u>	<u>Page</u>
4.34. Post-shear procedure: (a) Material extrusion ($\delta_r > 1 m$), (b) Disassembly of the ring shear box	142
5.1. Specimen stress, deformation and boundary conditions for the test methods used in the study (NA: Not Applicable) (O’Kelly, 2015)	143
5.2. Scaled test specimens for the direct shear, triaxial and ring shear apparatus	144
5.3. The stress ratio - Relative lateral displacement relationship for direct shear ($e_0 = 0.50$): (a) 50 kPa, (b) 100 kPa, (c) 200 kPa	149
5.4. The stress ratio - Relative lateral displacement relationship for direct shear ($e_0 = 0.55$): (a) 50 kPa, (b) 100 kPa, (c) 200 kPa	152
5.5. The stress ratio - Relative lateral displacement relationship for direct shear ($e_0 = 0.60$): (a) 50 kPa, (b) 100 kPa, (c) 200 kPa	154
5.6. The stress ratio - Relative lateral displacement relationship for direct shear ($e_0 = 0.65$): (a) 50 kPa, (b) 100 kPa, (c) 200 kPa	155
5.7. Effect of effective normal stress (σ'_n), initial void ratio (e_0) and volumetric reinforcement concentration (v_f) on the peak effective stress ratio for the direct shear tests (τ_p/σ'_n): (a) $\sigma'_n = 50 kPa, v_f-e_0$, (b) $\sigma'_n = 100 kPa, v_f-e_0$, (c) $\sigma'_n = 200 kPa, v_f-e_0$, (d) $v_f = 0.0\%, \sigma'_n-e_0$, (e) $v_f = 0.3\%, \sigma'_n-e_0$, (f) v_{fr}, σ'_n-e_0	159
5.8. Effect of effective normal stress (σ'_n), initial void ratio (e_0) and volumetric reinforcement concentration (v_f) on the critical state stress ratio for the direct shear tests (τ_{cs}/σ'_n): (a) $\sigma'_n = 50 kPa, v_f-e_0$, (b) $\sigma'_n = 100 kPa, v_f-e_0$, (c) $\sigma'_n = 200 kPa, v_f-e_0$, (d) $v_f = 0.0\%, \sigma'_n-e_0$, (e) $v_f = 0.3\%, \sigma'_n-e_0$, (f) v_{fr}, σ'_n-e_0	161
5.9. Effect of effective normal stress (σ'_n), initial void ratio (e_0) and volumetric reinforcement concentration (v_f) on the peak effective friction angle (ϕ'_p) in direct shear tests: (a) $\sigma'_n = 50 kPa, v_f-e_0$, (b) $\sigma'_n = 100 kPa, v_f-e_0$, (c) $\sigma'_n = 200 kPa, v_f-e_0$, (d) $v_f = 0.0\%, \sigma'_n-e_0$, (e) $v_f = 0.3\%, \sigma'_n-e_0$, (f) v_{fr}, σ'_n-e_0	165

LIST OF FIGURES (Continued)

<u>Figure</u>	<u>Page</u>
5.10. Effect of effective normal stress (σ'_n), initial void ratio (e_0) and volumetric reinforcement concentration (v_f) on the critical state friction angle (ϕ'_{cs}) in direct shear tests: (a) $\sigma'_n = 50 \text{ kPa}$, v_f - e_0 , (b) $\sigma'_n = 100 \text{ kPa}$, v_f - e_0 , (c) $\sigma'_n = 200 \text{ kPa}$, v_f - e_0 , (d) $v_f = 0.0\%$, σ'_n - e_0 , (e) $v_f = 0.3\%$, σ'_n - e_0 , (f) v_{fr} , σ'_n - e_0	167
5.11. Effect of initial void ratio (e_0) and volumetric reinforcement concentration (v_f), on cohesion parameter (c') in direct shear tests: (a) v_f - e_0 , (b) v_{fr}	168
5.12. Volumetric strain curves obtained from direct shear tests	169
5.13. Principal stress ratio - Axial strain relationship for triaxial ($e_0 = 0.50$): (a) 50 kPa , (b) 100 kPa , (c) 200 kPa	173
5.14. Principal stress ratio - Axial strain relationship for triaxial ($e_0 = 0.55$): (a) 50 kPa , (b) 100 kPa , (c) 200 kPa	174
5.15. Principal stress ratio - Axial strain relationship for triaxial ($e_0 = 0.60$): (a) 50 kPa , (b) 100 kPa , (c) 200 kPa	176
5.16. Principal stress ratio - Axial strain relationship for triaxial ($e_0 = 0.60$): (a) 50 kPa , (b) 100 kPa , (c) 200 kPa	177
5.17. Effect of effective cell pressure (σ'_c), initial void ratio (e_0) and volumetric reinforcement concentration (v_f) on the peak effective stress ratio for the triaxial tests (τ_p/σ'_c): (a) $\sigma'_c = 50 \text{ kPa}$, v_f - e_0 , (b) $\sigma'_c = 100 \text{ kPa}$, v_f - e_0 , (c) $\sigma'_c = 200 \text{ kPa}$, v_f - e_0 , (d) $v_f = 0.0\%$, σ'_c - e_0 , (e) $v_f = 0.3\%$, σ'_c - e_0 , (f) v_{fr} , σ'_c - e_0	181
5.18. Effect of effective cell pressure (σ'_c), initial void ratio (e_0) and volumetric reinforcement concentration (v_f) on the critical state stress ratio for the triaxial tests (τ_{cs}/σ'_c): (a) $\sigma'_c = 50 \text{ kPa}$, v_f - e_0 , (b) $\sigma'_c = 100 \text{ kPa}$, v_f - e_0 , (c) $\sigma'_c = 200 \text{ kPa}$, v_f - e_0 , (d) $v_f = 0.0\%$, σ'_c - e_0 , (e) $v_f = 0.3\%$, σ'_c - e_0 , (f) v_{fr} , σ'_c - e_0	183

LIST OF FIGURES (Continued)

<u>Figure</u>	<u>Page</u>
5.19. The effect of effective all around pressure (σ'_c), initial void ratio (e_0) and volumetric reinforcement concentration (v_f) on the effective peak friction angle (ϕ'_p) for triaxial tests: (a) $\sigma'_c = 50 \text{ kPa}$, v_f - e_0 , (b) $\sigma'_c = 100 \text{ kPa}$, v_f - e_0 , (c) $\sigma'_c = 200 \text{ kPa}$, v_f - e_0 , (d) $v_f = 0.0\%$, σ'_c - e_0 , (e) $v_f = 0.3\%$, σ'_c - e_0 , (f) v_{fr} , σ'_c - e_0	186
5.20. The effect of effective all around pressure (σ'_c), initial void ratio (e_0) and volumetric reinforcement concentration (v_f) on the critical state friction angle (ϕ'_{cs}) for triaxial tests: (a) $\sigma'_c = 50 \text{ kPa}$, v_f - e_0 , (b) $\sigma'_c = 100 \text{ kPa}$, v_f - e_0 , (c) $\sigma'_c = 200 \text{ kPa}$, v_f - e_0 , (d) $v_f = 0.0\%$, σ'_c - e_0 , (e) $v_f = 0.3\%$, σ'_c - e_0 , (f) v_{fr} , σ'_c - e_0	188
5.21. The effect of initial void ratio (e_0) and volumetric reinforcement concentration (v_f) on cohesion parameter (c') in triaxial tests: (a) v_f - e_0 , (b) v_{fr}	189
5.22. Volumetric strain curves obtained from triaxial tests.....	190
5.23. The stress ratio - Shear displacement relationship for ring shear ($e_0 = 0.50$): (a) 50 kPa , (b) 100 kPa , (c) 200 kPa	194
5.24. The stress ratio - Shear displacement relationship for ring shear ($e_0 = 0.55$): (a) 50 kPa , (b) 100 kPa , (c) 200 kPa	195
5.25. The stress ratio - Shear displacement relationship for ring shear ($e_0 = 0.60$): (a) 50 kPa , (b) 100 kPa , (c) 200 kPa	197
5.26. The stress ratio - Shear displacement relationship for ring shear ($e_0 = 0.65$): (a) 50 kPa , (b) 100 kPa , (c) 200 kPa	198
5.27. Effect of effective normal stress (σ'_n), initial void ratio (e_0) and volumetric reinforcement concentration (v_f) on the peak effective stress ratio for the ring shear tests (τ_p/σ'_n): (a) $\sigma'_n = 50 \text{ kPa}$, v_f - e_0 , (b) $\sigma'_n = 100 \text{ kPa}$, v_f - e_0 , (c) $\sigma'_n = 200 \text{ kPa}$, v_f - e_0 , (d) $v_f = 0.0\%$, σ'_n - e_0 , (e) $v_f = 0.3\%$, σ'_n - e_0 , (f) v_{fr} , σ'_n - e_0	201

LIST OF FIGURES (Continued)

<u>Figure</u>	<u>Page</u>
5.28. Effect of effective normal stress (σ'_n), initial void ratio (e_0) and volumetric reinforcement concentration (v_f) on the critical effective stress ratio for the ring shear tests (τ_{cs}/σ'_n): (a) $\sigma'_n = 50 \text{ kPa}$, v_f - e_0 , (b) $\sigma'_n = 100 \text{ kPa}$, v_f - e_0 , (c) $\sigma'_n = 200 \text{ kPa}$, v_f - e_0 , (d) $v_f = 0.0\%$, σ'_n - e_0 , (e) $v_f = 0.3\%$, σ'_n - e_0 , (f) v_{fr} , σ'_n - e_0	203
5.29. Effect of effective normal stress (σ'_n), initial void ratio (e_0) and volumetric reinforcement concentration (v_f) on the peak effective friction angle (ϕ'_p) for ring shear tests: (a) $\sigma'_n = 50 \text{ kPa}$, v_f - e_0 , (b) $\sigma'_n = 100 \text{ kPa}$, v_f - e_0 , (c) $\sigma'_n = 200 \text{ kPa}$, v_f - e_0 , (d) $v_f = 0.0\%$, σ'_n - e_0 , (e) $v_f = 0.3\%$, σ'_n - e_0 , (f) v_{fr} , σ'_n - e_0	206
5.30. Effect of effective normal stress (σ'_n), initial void ratio (e_0) and volumetric reinforcement concentration (v_f) on the critical effective stress ratio (τ_{cs}/σ'_n) for ring shear tests: (a) $\sigma'_n = 50 \text{ kPa}$, v_f - e_0 , (b) $\sigma'_n = 100 \text{ kPa}$, v_f - e_0 , (c) $\sigma'_n = 200 \text{ kPa}$, v_f - e_0 , (d) $v_f = 0.0\%$, σ'_n - e_0 , (e) $v_f = 0.3\%$, σ'_n - e_0 , (f) v_{fr} , σ'_n - e_0	208
5.31. Effect of initial void ratio (e_0) and volumetric reinforcement concentration (v_f), on cohesion parameter (c') in ring shear tests: (a) v_f - e_0 , (b) v_{fr}	209
5.29. Volumetric strain curves obtained from ring shear tests	210
5.30. Peak shear strength failure envelopes for various initial void ratios: (a) $e_0 = 0.50$, (b) $e_0 = 0.55$, (c) $e_0 = 0.60$, and (d) $e_0 = 0.65$	208
5.31. Critical shear strength failure envelopes for various initial void ratios: (a) $e_0 = 0.50$, (b) $e_0 = 0.55$, (c) $e_0 = 0.60$, and (d) $e_0 = 0.65$	209
5.32. The following are the relationships between effective peak and critical friction angles and tightness: (a) 50 kPa, (b) 100 kPa, and (c) 200 kPa.....	210
5.33. Comparison of effective friction angles with the general diagrams reproduced by triaxial method for typical intervals: (a) Hough (1957), (b) Means and Parcher (1963), (c) Terzaghi and Peck (1967), (d) Schmertmann (1978), (e) NAVFAC (1982), (f) Holtz et al., (2011)	217

LIST OF FIGURES (Continued)

<u>Figure</u>	<u>Page</u>
5.34. Peak shear strength failure envelopes for various initial void ratios: (a) $e_0 = 0.50$, (b) $e_0 = 0.55$, (c) $e_0 = 0.60$, and (d) $e_0 = 0.65$	219
5.35. Critical shear strength failure envelopes for various initial void ratios: (a) $e_0 = 0.50$, (b) $e_0 = 0.55$, (c) $e_0 = 0.60$, and (d) $e_0 = 0.65$	224
5.36. The following are the relationships between effective peak and critical friction angles and density: (a) 50 kPa, (b) 100 kPa, and (c) 200 kPa	227
5.37. Correlation of ϕ'_{cs} with index properties for sands (Knappett and Craig, 2019) ...	229
5.38. Maximum strength under direct shear and triaxial test (ϕ'_{ds} & ϕ'_{tx})	230
5.39. Comparison of the derived equation with the theoretical relations (ϕ'_{ds} & ϕ'_{tx})	232
5.40. Maximum strength under ring shear and triaxial test (ϕ'_{rs} & ϕ'_{tx})	233
5.41. Maximum strength under ring shear and direct shear test (ϕ'_{rs} & ϕ'_{ds})	234
5.42. Maximum strength under plane strain and triaxial test (ϕ'_{ps} & ϕ'_{tx})	235
5.43. Maximum strength under plane strain and triaxial test (ϕ'_{ps} & ϕ'_{tx})	236
5.44. Cohesion strengths of reinforced specimens (ϕ'_{ds} & ϕ'_{tx} & ϕ'_{rs}).....	239
5.45. Volumetric strain at failure in direct shear, triaxial and ring shear tests versus initial void ratio ($v_f = 0.0\%$)	242
5.46. Volumetric strain at failure in direct shear, triaxial and ring shear tests versus initial void ratio ($v_f = 0.3\%$)	243
5.47. Volumetric strain at failure in direct shear, triaxial and ring shear tests versus initial void ratio ($v_f = 0.0\%$)	244
5.48. Volumetric strain at failure in direct shear, triaxial and ring shear tests versus initial void ratio ($v_f = 0.3\%$)	245

LIST OF FIGURES (Continued)

<u>Figure</u>	<u>Page</u>
5.49. Variations of the excess friction angle ($\phi'_p - \phi'_{cs}$) with the angle of dilation (ψ) for unreinforced specimens	248
5.50. Variations of the excess friction angle ($\phi'_p - \phi'_{cs}$) with the angle of dilation (ψ) for reinforced specimens	248
5.51. Influence of initial void ratio on maximum dilation angle for unreinforced specimens	249
5.52. Influence of initial void ratio on maximum dilation angle for reinforced specimens	249
5.53. Relationship between effective peak friction angle and maximum dilation angle for unreinforced specimens	251
5.54. Relationship between effective peak friction angle and maximum dilation angle for reinforced specimens	251
5.55. Relationship between excess friction angle and maximum dilation angle	253

LIST OF TABLES

<u>Table</u>	<u>Page</u>
1.1. Guidelines for selection of laboratory tests (FHWA, 2007).....	2
2.1. Comparison of the peak shear strength angles (Taylor, 1939).....	4
2.2. Comparison of the critical void ratios (Taylor, 1939).....	4
2.3. Comparison of the shear strength parameter by different test methods (Hennes, 1953)	5
2.4. Comparison of the tested and calculated plane strain angles (Lee, 2000).....	17
2.5. Details of the literature resources used (Ladd et al., 1977).....	18
2.6. Physical properties of Toyoura sand (Oda et al., 1978).....	20
2.7. Details of plane strain and triaxial tests (Oda et al., 1978).....	20
2.8. Class and description of the materials by the Unified Soil Classification System (USCS) (Superfesky and Williams, 1978).....	22
2.9. Comparison of the shear strength parameters by different test methods and humidity conditions (Superfesky and Williams, 1978).....	23
2.10. Dimensions of the specimens used in the plane strain test (Marachi et al., 1981)....	24
2.11. Physical properties of Monterey sand (No.20) (Marachi et al., 1981).....	24
2.12. Physical properties of Leighton Buzzard sand (Jewell and Wroth, 1987).....	32
2.13. Physical properties of Hostun sand (Schanz and Vermeer, 1996).....	35
2.14. Physical properties of Ottawa sand (F-75) (Alshibli et al., 2003).....	40
2.15. Material properties of sand specimens (Mirata and Erzin, 2007).....	46
2.16. Physical properties of Changi sand (Wanatowski and Chu, 2007).....	48
2.17. Physical properties of the tested sands (Bareither et al., 2008).....	51
2.18. Peak shear strength angles of different test types (Bareither et al., 2008).....	52
2.19. Physical properties of Ottawa sand (C190) (Guo, 2008).....	53

LIST OF TABLES (Continued)

<u>Table</u>	<u>Page</u>
2.20. Material properties of Jumunjin sand (Park et al., 2008)	56
2.21. Physical properties of the tested sands (Sadrekarimi and Olson, 2014)	57
2.22. Details of the ring shear and triaxial tests (Sadrekarimi and Olson, 2014).....	57
2.23. Material properties of Babolsar coast sand (Noorzad and Zarinkolaei, 2015).....	60
2.24. Material properties of polypropylene fiber (Noorzad and Zarinkolaei, 2015).....	60
2.25. Effective shear strength angles from different methods (Dev et al., 2016).....	63
2.26. Details of direct shear and triaxial tests (Medzvieckas et al., 2017)	64
3.1. Friction angles between mineral surfaces (under saturated conditions) (Procter and Barton, 1974)	94
4.1. Number of tests performed in the study	102
4.2. Maximum and minimum dry density test results of CEN standard sand	102
4.3. Specific gravity test results of CEN standard sand.....	103
4.4. Index properties of CEN standard sand.....	104
4.5. Other properties of CEN standard sand.....	105
4.6. Technical specifications of standard STRUX® 90/40 fiber (GCP, 2020)	107
4.7. Test Program	117
4.8. Specifications of direct shear test device (ELE, 2015, 2019).....	123
4.9. Specifications of triaxial shear test device (ELE, 1993, 2019)	131
4.10. Specifications of the ring shear test tool (VJTech, 2018).....	140
5.1. Internal friction angle relationships for direct shear, triaxial, ring shear, and plane strain experiments	238

LIST OF SYMBOLS AND ABBREVIATIONS

<u>Symbol</u>	<u>Description</u>
A	Cross-sectional area
A_c	Corrected cross-sectional area
A_o	Initial area
a	Current soil state
$\overline{A}_1, \overline{B}_1, \overline{C}_1$	Constants that depend on dilation factor
AR	Aspect ratio
B	Skempton's pore pressure parameter
b	Relative value of effective intermediate principal stress
B_g	Breakage factor
b_ψ	Bolton's dilation coefficient
c'	Effective cohesion
c'_{dsd}	Dry direct shear cohesion
c'_{dsm}	Moist direct shear cohesion
c'_{tcm}	Moist triaxial cohesion
C_u	Coefficient of uniformity
D	Dilation factor
d	Specimen width
$\partial v / \partial \varepsilon_1$	Dilation rate
D_{50}	Mean particle size
D_{tc}	Triaxial grain diameter
D_{ds}	Direct shear grain diameter
$d\varepsilon_1$	Major principal strain increments
$d\varepsilon_3$	Minor principal strain increments
dv	Volumetric strain increment

LIST OF SYMBOLS AND ABBREVIATIONS (Continued)

D_r, R_d	Relative density
e_0	Initial void ratio
e_{cr}	Critical state void ratio
e_{max}	Maximum void ratio
e_{min}	Minimum void ratio
E_{ps}	Plane strain initial tangent modulus
E_{tx}	Triaxial initial tangent modulus
E_{sps}	Plane strain secant modulus
E_{stc}	Triaxial secant modulus
F, F_1, F_2	Yield surface expressions
G_s	Specific gravity
h	Specimen height
I_1, I_2, I_3	Stress invariants
I_{CR}	Relative crushability index
I_d	Density index
I_D	Dilatancy index
I_R	Relative dilatancy index
K	Material parameter
k_c	Anisotropic consolidation ratio between major and minor principal stresses
l	Specimen length
M	η at critical state
M_e	Torque error
M_s	Mass of soil
M_t	Torsion moment

LIST OF SYMBOLS AND ABBREVIATIONS (Continued)

n	Porosity
q	Deviatoric stress
Q	Shear force
q_c	Critical deviatoric stress
P	Normal load
p	Probability value
p'	Mean effective normal stress
p'_c	Critical mean effective normal stress
R	Principal stress ratio
R_c	Relative compaction
r_{in}	Inner radius
r_{out}	Outer radius
u	Pore water pressure
v	Specific volume
V	Volume
v_d	Dense specific volume
v_f	Volumetric reinforcement concentration
v_{fr}	Strength increase rate
v_l	Loose specific volume
v_{ps}	Plane strain Poisson ratio
v_s	Volumetric unit strain
v_{tx}	Triaxial Poisson ratio
v_f	Volumetric reinforcement concentration
W_f	Reinforcement weight

LIST OF SYMBOLS AND ABBREVIATIONS (Continued)

w_{opt}	Optimum water content
W_s	Dry sand weight
α	Geometrical angle, $\sin \alpha = (dv/2 - d\varepsilon_{yy})/(d\gamma/2)$
β	Expansion in yield surface
Γ	Specific volume at a reference stress
γ	Shear strain
γ_d	Dry unit weight
Δ	Angle between principal stress and principal strain increment direction (non-coaxial angle)
ΔA	Field element
Δ_d	Maximum principal stress difference
ΔF	Internal force acting on element
$\Delta\theta$	Deviation between the axes of principal stress and incremental strain
$\Delta\psi$	Deviation in the angle of dilation
δ	Angle of bedding plane normal with major principal stress (σ_1) direction, tilting angle
δ_h	Horizontal displacement
δ_v	Vertical displacement
$\varepsilon_a, \varepsilon_1$	Axial strain
ε_{a_s}	Axial strain due to grain movement
ε_2	Longitudinal strain
ε_3	Radial strain
ε_{ps}	Plane strain axial strain
ε_{tc}	Triaxial axial strain

LIST OF SYMBOLS AND ABBREVIATIONS (Continued)

ε_v	Volumetric strain
η'_{ps}	Plane strain effective stress ratio
η'_{tc}	Triaxial effective stress ratio
θ	Lode's angle
λ	Slope of the CSL on e - $\log p'$ plane
μ	Friction coefficient
ξ	Angle of the same plane with intermediate principal stress (σ_2) direction
ρ_d	Dry density
σ'_1	Major principal effective stress
σ'_1/σ'_3	Maximum principal effective stress ratio
σ_1/σ_3	Maximum principal total stress ratio
σ'_2	Intermediate principal effective stress
σ'_3	Minor principal effective stress, effective confining pressure
σ'_c	Effective isotropic confining pressure
σ'_n	Effective normal stress
σ_v	Vertical normal stress
τ	Shear stress
τ_{ds}	Direct shear test shear stress
τ_{ps}	Plane strain shear stress
τ_{cs}/σ'_n	Critical state effective stress ratio
τ_p/σ'_n	Peak effective stress ratio
ϕ'	Effective friction angle
$\phi'_{cs}, \phi'_{cv}, \phi'_{crit}$	Critical state friction angle
ϕ'_{cw}	Cylindrical wedge effective friction angle

LIST OF SYMBOLS AND ABBREVIATIONS (Continued)

ϕ'_{ds}	Effective direct shear friction angle
ϕ'_{dsd}	Dry direct shear effective friction angle
ϕ'_{dsm}	Moist direct shear effective friction angle
ϕ_f	Friction component of shear strength angle
ϕ'_{ps}	Effective plane strain friction angle
ϕ'_{pw}	Prismatic wedge effective friction angle
ϕ'_{rs}	Effective ring shear friction angle
ϕ'_{tcd}	Dry triaxial effective friction angle
ϕ'_{tcm}	Moist triaxial effective friction angle
ϕ'_{tx}, ϕ'_{tc}	Effective triaxial shear friction angle
ϕ_μ	Kinetic friction, mineral friction
ψ	Dilation angle
ψ_{max}	Maximum dilation angle

Abbreviation

AASHTO

ASTM

BSI

CD

CEN

CSL

CU

DS

FHWA

Description

American Association of State Highway and Transportation Officials

International American Society for Testing and Materials

British Standard Institute

Consolidated drained

Comité Européen de Normalisation

Critical state line

Consolidated undrained

Direct shear test

Federal Highway Administration

LIST OF SYMBOLS AND ABBREVIATIONS (Continued)

GW	Well graded gravel
ISO	International Organization for Standardization
LSCT	Linear strain converter transducers
LSDS	Large-scale direct shear test
LVDT	Linear variable differential transformer
MC	Material class
PS	Plane strain test
PSC	Plane strain condition
R	Reinforced sample
RS	Ring shear test
RSL	Residual state line
SC	Clayey sand
SM	Silty sand
SP	Poorly graded sand
SSDS	Small-scale direct shear test
SW	Well graded sand
TX	Triaxial test
USCS	Unified Soil Classification System
U	Unreinforced sample
UU	Unconsolidated undrained
XRF	X-Ray Fluorescence

1. INTRODUCTION AND PURPOSE

At a point in a soil mass, stress occur due to both the weight of the soil itself and the loads on it. When these stresses reach a limit value, shear deformations occur that will lead to the failure of the soil mass. Therefore, it is a essential to understand the shear strength in order to know the behaviour of a soil mass. Shear strength is defined as the resistance of the soil grains to relative movements of each other under continuous displacements applied to the soil. Expressed as a function of shear stress or the principal stress with respect to the deformation mode, this concept is of critical importance, since it controls the stability and deformation properties that cause the failure of the soil mass.

The development of the engineering properties of soils is a topic that has been honed since ancient times, and its importance has been further realized in the last century. For this purpose, although insufficient soil improvement methods that people with limited opportunities previously experienced through trial and error are used, quite good results can be obtained for most cases with the techniques developed depending on the advancing science and developing technology. Fiber materials, which are one of the methods and have various advantages such as efficiency and economy compared to many other methods, have been one of the most popular applications in recent years.

It is not possible to represent geotechnical applications in different deformation conditions with a single testing method. For this reason, a large number of field and laboratory testing methods have been developed to determine the engineering properties of soils. In tests conducted in a laboratory environment, it is very important to accurately simulate the current field conditions. Therefore, when deciding which experiment will be used to determine the shear stress of soils, the disadvantages and advantages of this experiment should be taken into account for which purpose the experiment will be performed (Table 1.1). In this study, two widely preferred methods; direct shear test and triaxial test methods and a less studied method; ring shear test used for the determination of the shear strength properties of sand and comparative analysis of reinforced and unreinforced cases are included.

Table 1.1. Guidelines for selection of laboratory tests (FHWA, 2007)

Analysis Type	Laboratory tests selection frequency											
	A	B	C	D	E	F	G	H	I	J	K	L
Structural Foundation	F	F	M	F	L	L	L	M	F	M	L	L
Landslides	F-M	F	F	F	L	R	L	R	F-M	F-M	L	F
Retaining Wall	F-M	F	M	F	L	R	L	M	F-M	F-M	L	M-L
Material Source	F	F	F	F	F	F	F	R	R	M-L	R	M
Fill/Cut	F	F	F	F	F	M	F-L	M	M-L	M	F	F-M
Roadway Soil	F	F	F	F	F	F	F	L	L	M	R	M-L
Test description:									Selection legend:			
A	Index properties		G	Compaction					F	Frequent use		
B	Gradation (Classification)		H	Consolidation					M	Moderate use		
C	Fine grain analysis		I	Unconfined compression					L	Limited use		
D	Atterberg limits		J	Direct shear					R	Rarely use		
E	Permeability tests		K	Triaxial								
F	CBR		L	Ring shear								

The aims of the studies carried out within the scope of this thesis can be summarized as follows: The main aim of the study is investigating stress-strain and stress-dilatation behaviors of sands for the most common density and effective consolidation stress ranges in practice via direct shear, triaxial and ring shear test methods and their comparative analysis. In particular, it is aimed to contribute to the literature by investigating the strength-strain properties of ring shear tests of cohesionless soils. By comparing the friction term, which is the main strength parameter of the sands, for each test method and plane strain method that reliably represents the stress condition for many geotechnical applications, it is aimed to derive significant relationships that can be used in practical applications. Another important aim of the study is to investigate the effect of the presence of reinforcement, the use and importance of which is increasing, on the strength and strain characteristics of different test methods.

In order to understand the soil properties, the experiences obtained from past studies are presented in Chapter 2, how we defined stress in geotechnical engineering and failure theories are given in Chapter 3, the experiments that are often used to measure the engineering properties of soils are presented in Chapter 4, evaluation of experimental results and comprehensive comparative analysis results are given in Chapter 5.

2. LITERATURE REVIEW

In this section, the comparative analysis results of direct shear, triaxial shear, and ring shear test methods used in the literature in order to determine the strength characteristics of sands under static loading conditions. For this purpose, **all** publications in the indexes were reviewed and the studies on the subject were summarized. The literature studies on the subject were deemed important and included in the section because, in geotechnical engineering applications, most cases can be represented by the plane strain condition, and due to the difficulties in obtaining devices meeting this condition. The scope of the thesis subject and the evaluation methods showed that it would be better to present the subject as a whole, instead of separate titles. Unless otherwise specified, the "shear strength" parameter was symbolized by (ϕ_{ds}) for direct shear, (ϕ_{tc}) for triaxial compression, (ϕ_{rs}) for ring shear, and (ϕ_{ps}) for plane strain.

The comparison of shear strength parameters of soils with different test methods was first performed by Taylor (1939). The researcher compared the peak shear strength angles of four different sands with low and high density, the shape of the stress-strain curve, and the critical void ratios using the direct shear and triaxial compression tests. In the study, Ottawa standard sand consisting of angular *Sand A* of which 90% is finer than 0.8 mm and 10% is finer than 0.18 mm; angular and colloidal *Sand B* of which 90% is finer than 0.4 mm and 10% is finer than 0.15 mm and *Sand BW* that is the same as *Sand B* but clean was used. All the tests were performed at constant strain rates and the initial void ratio, and the stress values are given in Table 2.1 and Table 2.2. The study concluded that the shear strength angle is affected by void ratio, stress condition, different test methods, and the physical properties of grains and that the most important factor in experimental comparison is the void ratio. When the peak shear strength angles of the two test methods were compared, it was seen that the difference between them was $1^\circ - 2^\circ$ on average, and the results of the triaxial tests had a higher scattering due to their sophisticated structure. The researcher stated that the strains were not in agreement although the curves were significantly similar when the stress-strain relationships were compared. When the peak and ultimate critical state void ratios were compared, it was seen that the results of the direct shear test were higher for both cases.

Finally, the researcher suggested a new critical void ratio concept called as "*equal strength void ratio*" for the purpose of controlling the volume change at failure. Since the value of this concept can be determined with constant volume tests, it cannot be directly obtained by direct shear. On the other hand, the researcher stated that this value is closely associated with the critical void ratio obtained by direct shear method.

Table 2.1. Comparison of the peak shear strength angles (Taylor, 1939)

Soil	Stress, σ_3 (kN/m ²)	Initial void ratio, e_0	Peak shear strength angle (°)		
			direct shear	triaxial	difference
Ottawa sand	20	0.65	28.5	26.7	1.8
		0.55	34.1	30.3	3.8
	60	0.65	27.2	26.4	0.8
		0.55	31.1	30.3	0.8
Sand A	15	0.75	33.9	35.1	-1.2
		0.60	41.7	40.5	1.2
	30	0.75	33.5	33.8	-0.3
		0.60	39.9	39.3	0.6
Sand B	18	0.85	33.8	33.8	0.0
		0.60	42.8	41.9	0.9
	34	0.85	33.2	31.6	1.6
		0.60	42.0	40.7	1.3
Sand BW	30	0.85	33.8	34.0	-0.2
		0.65	44.4	41.8	2.6
	60	0.85	32.7	32.2	0.5
		0.65	42.6	39.6	3.0

Table 2.2. Comparison of the critical void ratios (Taylor, 1939)

Soil	Stress, σ_3 (kN/m ²)	Peak critical void ratio			Ultimate void ratio	Equal strength void ratio
		direct shear	triaxial	difference	direct shear	triaxial
Ottawa sand	20	0.66	0.65	0.01	0.68	...
	40	0.65	0.645	0.005	0.67	...
	60	0.645	0.64	0.005	0.66	...
Sand A	15	0.75	0.68	0.07	0.77	...
	30	0.73	0.64	0.09	0.74	...
Sand B	18	0.85	0.81	0.04	0.86	...
	34	0.81	0.76	0.05	0.82	...
Sand BW	30	0.86	0.815	0.045	0.88	0.85
	60	0.84	0.78	0.06	0.87	...

The relation between the grain shape and size of cohesionless soils and the shear strength was studied by Hennes (1953) using different test methods. In the study, a material with smooth, round-shaped grains that is obtained from the river, and a crushed stone basalt material with rough, angular grains were used. The specific gravities of the materials were 2.62 and 2.66, respectively. The researcher used dry material in all tests and took into account the results of one test for triaxial shear and the mean of a few test results for direct shear, for each grain diameter. The study concluded that the shear strength angle was the common function of void ratio, grain diameter, and grain shape and the results are detailed in Table 2.3. Minor differences were observed between the two tests for loose and medium dense materials; however, it was seen that this difference increased up to $(\phi_{ds} - \phi_{tc}) 5^\circ$ with the increasing grain diameter and the decreasing void ratio. In conclusion, the researcher stated that the shear strength angle was strongly affected by grain diameter up to a certain level (6.35 mm), and that the materials with a grain size of higher than 19 mm gave inconsistent test results.

Table 2.3. Comparison of the shear strength parameter by different test methods (Hennes, 1953)

Grain size(mm)	Round		Angular	
	direct shear ($\tan \phi$)	triaxial ($\tan \phi$)	direct shear ($\tan \phi$)	triaxial ($\tan \phi$)
1.18 – 2.36	0.903	0.91	0.98	1.00
	0.698*	0.63*	0.92*	0.93*
2.36 – 4.75	-	-	1.09	0.99
	-	-	0.90*	0.92*
4.75 – 6.73	1.12	0.93	-	-
	0.622*	0.61*	-	-
12.5 – 19.0	1.17	1.03	-	-
	0.85*	0.58*	-	-

*Initial void ratio

The drained and undrained shear strength characteristics of fine-grained sands were investigated by Nash (1953) using triaxial and direct shear test methods. In the study, natural river sand with rough surface and with main mineral component of quartz was used. The effect of moisture on the specimens was also investigated for a wide porosity range (39 – 46.95%) at effective normal and various confining pressures. The study concluded that moisture had no effect on compressibility of sands and shear strength in the tests performed under the same conditions. Lower shear strength was obtained under undrained conditions and the result data were spread over a wider range of values. Finally, the researcher compared the results of triaxial, and direct shear tests based on porosity and obtained almost equal shear strength angles for medium porosity in both tests, 5% lower shear strength angles for high porosity in direct shear, and 10% higher shear strength angles for low porosity (Figure 2.1).

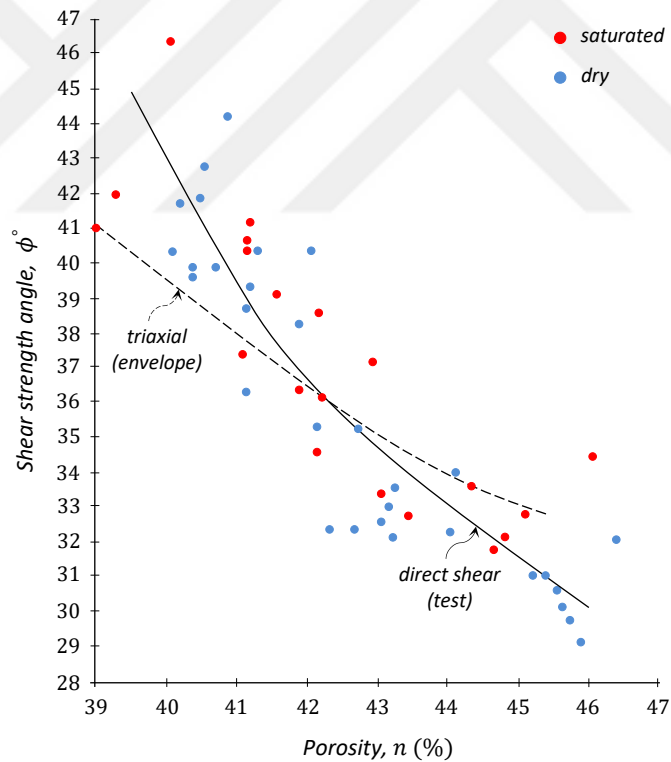
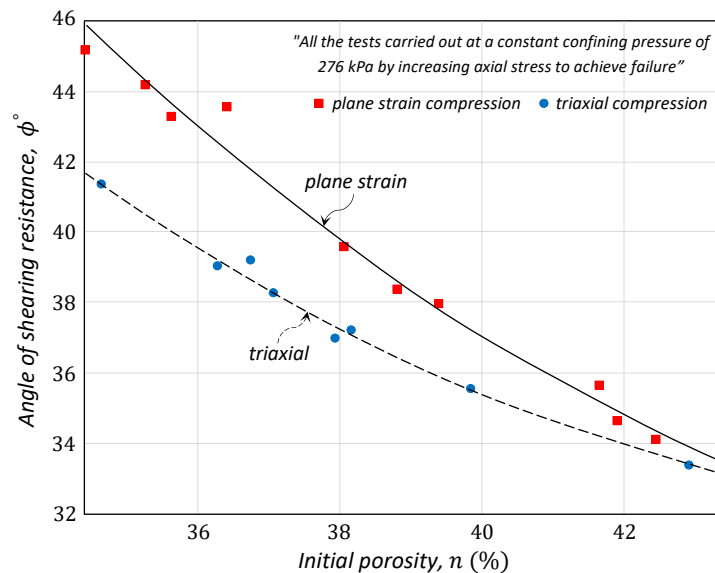
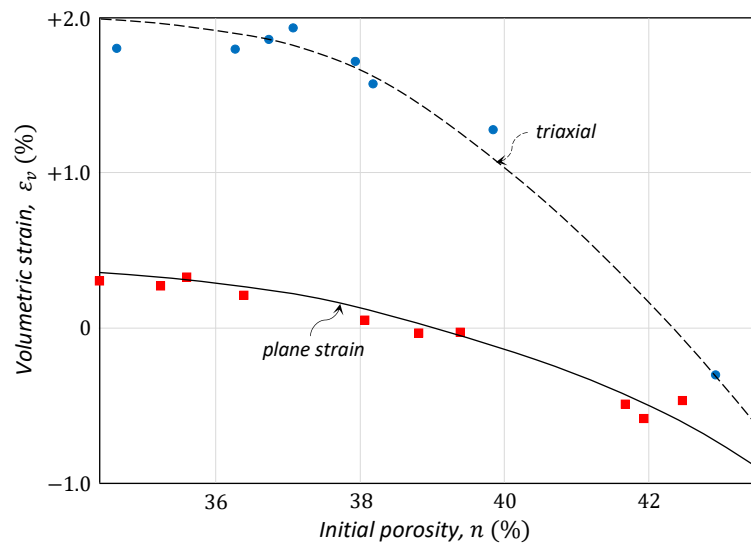


Figure 2.1. Variation of shear strength angle as a function of porosity by different test methods (Nash, 1953)

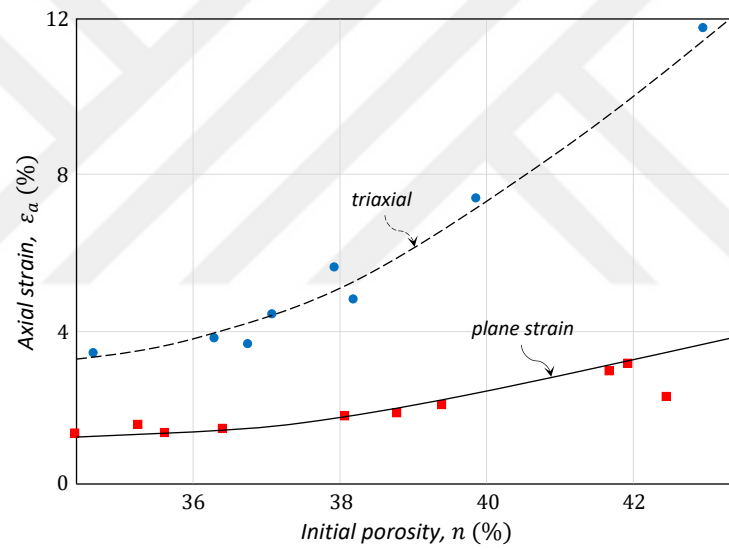
One of the first comprehensive studies conducted to compare the strength properties of sands by different test methods was performed by Cornforth (1964). The researcher performed a range of plane strain and triaxial tests in a wide density range and under constant confining pressure (276 kPa) using uniform Brasted sand ($\leq 2 \text{ mm}$). In the study, 0.03 mm/min and 0.15 mm/min were used for plane strain test and triaxial test, respectively, assuming that constant strain rate has no effect on the strength of sands (Casagrande and Shannon, 1948). As a result of the study, higher shear strength angles were obtained in the plane strain test, and it was seen that the difference between the tests has reduced with the increasing porosity ($0.5^\circ \leq \phi_{ps} - \phi_{tc} \leq 4^\circ$) (Figure 2.2a). When the volumetric strains were compared, a greater volumetric increase was observed in triaxial tests at low porosities and the difference between the two tests reduced with the increasing porosity (Figure 2.2b). When the axial strains at the time of failure were compared, higher values were obtained in triaxial state for the same density values ($\varepsilon_{tc} \cong 3\varepsilon_{ps}$) (Figure 2.2c). This shows a lower module value for triaxial tests. When the ultimate strengths were compared, it was seen that the triaxial test gave 0.7° higher results in average ($33.0 - 32.3^\circ$). The researcher concluded that intermediate principal stress had no significant effect on shear strength.



(a)



(b)



(c)

Figure 2.2. Comparison of the failure characteristics as a function of porosity (pre-test) for different test methods: (a) Angle of shearing resistance, (b) Volumetric deformation, and (c) Axial deformation (Cornforth, 1964)

To explain the behavior of granular soils under plane strain conditions, Mohr-Coulomb yield surface should be defined in terms of plane strain friction angle (ϕ'_{ps}). Davis (1968) theoretically showed that this angle could be obtained from the relation between the friction angle (ϕ'_{ds}) from the direct shear test method and the angle of dilation (ψ) (Figure 2.3). The researcher, in his hypothesis, assumed that shear behavior in the direct shear test method represented the plane strain condition.

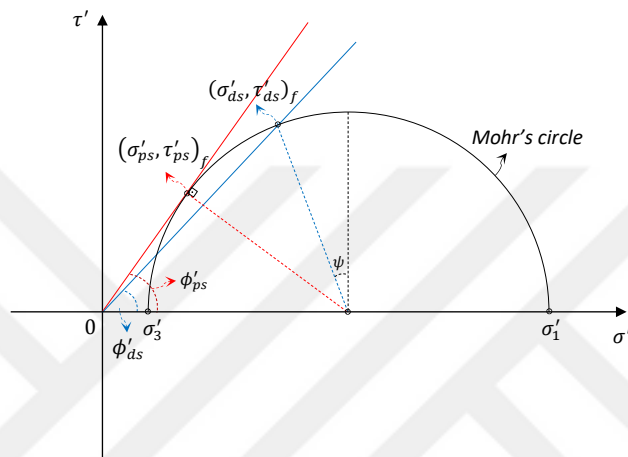


Figure 2.3. Illustration of strength parameters from different methods in Mohr's circle with Davis hypothesis (Davis, 1968)

The researcher assumed that for both test methods, stress and strain increment was coaxial in the principal axis, there was no linear strain increment in the horizontal direction (zero extension), and soil grains were perfect elastic bodies at failure. Equation 2.1 and Equation 2.2 were obtained from Figure 2.3 based on all these assumptions.

$$\phi'_{ps} = \sin^{-1} \left(\frac{\sigma'_1 - \sigma'_3}{\sigma'_1 + \sigma'_3} \right) \quad (2.1)$$

$$\tan \phi'_{ds} = \frac{\cos \psi (\sigma'_1 - \sigma'_3)}{(\sigma'_1 + \sigma'_3) - \sin \psi (\sigma'_1 - \sigma'_3)} \quad (2.2)$$

In the equations, the major and the minor principal stresses were represented by σ'_1 and σ'_3 , respectively, the angle of dilation by $\psi = \tan^{-1}(-\delta_v/\delta_h)$, and the vertical and horizontal displacement by δ_v and δ_h , respectively.

Using Equation 2.1 and Equation 2.2, the friction angle and the critical state angle are written in terms of the parameters of direct shear method, as in Equation 2.3 and Equation 2.4, respectively:

$$\sin \phi'_{ps} = \frac{\tan \phi'_{ds}}{\cos \psi + \tan \phi'_{ds} \sin \psi} \quad (2.3)$$

$$\sin(\phi'_{crit})_{ps} = \tan(\phi'_{crit})_{ds} \quad (2.4)$$

This hypothesis is very helpful for comparing the flow rules that were derived by Taylor (1948) based on direct shear and those that were derived by Rowe (1962) and Bolton (1986) and for using them in a common form.

Note: The relation between the test methods for the most general state with no assumption is as follows:

$$\sin \phi'_{ps} = \frac{\tan \phi'_{ds}}{\cos(\alpha - 2\Delta) + \sin(\alpha - 2\Delta) \tan \phi'_{ds}} \quad (2.5)$$

Where, the deviation of strain increment from the vertical and the angles obtained with the geometrical relations from the Mohr's stress circle for non-coaxial states were symbolized with α and Δ , respectively.

When explaining the stress-strain relation of sands, the leading study by Rowe (1962) that took into account internal work and whose details are given in Section 3.4 is highly important. Rowe has used these fundamental relations to estimate the volumetric strain of slopes and earth pressures (Rowe, 1963; 1964a), and the effect of strain conditions on the strength properties of sands (Rowe, 1964b) and to establish various correlations between the shear strength parameters obtained by different tests by comparing them (Rowe et al., 1964; Rowe, 1969). In this section, the study by Rowe (1969) is discussed.

Rowe (1969) studied the strength parameters of saturated sands obtained by direct shear, plane strain and triaxial test methods under drained conditions and performed a comparative analysis of them. In the study, quartz and feldspar mineral sands, crushed glass and glass ballotini, and previous experimental studies and theoretical relations were used. The researcher aimed to establish a new relationship between the strength properties of sand, which are also defined as peak effective stress ratio and measured by plane strain and direct shear tests and compared the theoretical and empirical results with the strength limits already derived from the triaxial compression method. It was assumed that the principal strain increment and principal stress directions coincided based on the stress-dilation theory of Rowe (1962) (Figure 2.4). As a result of the study, the highest strength values were obtained with the plane strain method in all materials used (with different mineral friction and critical state strength values) and a new relationship was suggested for the solution of practical problems between the peak effective shear strength angles measured by plane strain and direct shear test methods (Figure 2.18). This relationship gave very consistent results in a certain range of values of the mineral friction of cohesionless soils ($\phi_{\mu} = 17^{\circ} - 39^{\circ}$) and a difference of about $4^{\circ} - 5^{\circ}$ was obtained between the peak strength angles ($\phi'_{ps} - \phi'_{ds}$) for quartz sand ($\phi_{\mu} = 26^{\circ}, \phi_{cv} = 32^{\circ}$) (Figure 2.5). The researcher concluded that most earth pressure and stability problems could be evaluated under plane strain conditions, the shear strength angle varied as a function of density by different test methods, and the triaxial method with lower means than the peak plane strain angles and the direct shear method which was more conservative for the loose state should be used for practical purposes.

Rowe (1969) followed the following method when deriving the equation (Equation 2.18).

Rowe (1962) defined the stress-dilation relationship as in Equation 2.6 for triaxial and plane strain loading conditions:

$$R = DK \quad (2.6)$$

Where, the principal stress ratio was symbolized by R , the dilation factor by D , and the material parameter by K :

$$R = \frac{\sigma'_1}{\sigma'_3} ; D = \left(1 - \frac{dv_s}{d\varepsilon_{a_s}} \right) ; K = \tan^2 \left(\frac{\pi}{4} + \frac{\phi_f}{2} \right) \quad (2.7)$$

In Equation 2.7, the major effective principal stress is represented by σ'_1 , the minor effective principal stress by σ'_3 , the volumetric unit strain by v_s , the axial strain due to grain movement by ε_{a_s} , and the friction component of shear strength angle by ϕ_f . Rowe (1969) suggested the D factor as 2 for $\phi_f = \phi_\mu$ in dense state and as 1 for $\phi_f = \phi_{cv}$ in loose state for triaxial and plane strain conditions.

Considering that the principal stress increment directions and the principal strain increment directions coincide in direct shear tests (Figure 2.4), the following relationships between the stress and strain increments are obtained from the Mohr's circle geometry.

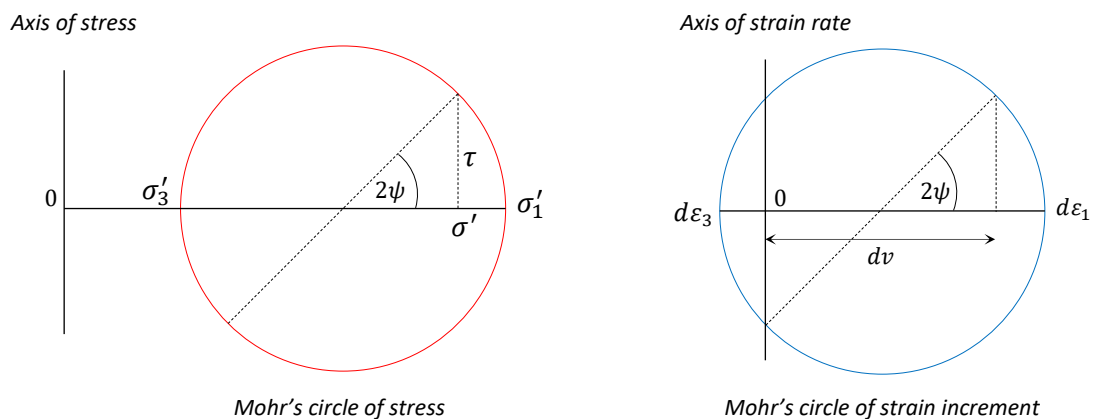


Figure 2.4. Representation of stress and strain increments in the Mohr's circle (Rowe, 1969)

From the two-dimensional strain relationship in Figure 2.4:

$$\frac{dv}{2} = \frac{d\varepsilon_1 - d\varepsilon_3}{2} \cos 2\psi \quad (2.8)$$

$$dv = d\varepsilon_1 + d\varepsilon_3 \quad (2.9)$$

From Equation 2.8 and Equation 2.9

$$\cos 2\psi = \frac{dv}{2d\varepsilon_1 - dv} = \frac{dv/d\varepsilon_1}{2 - dv/d\varepsilon_1} = \frac{1 - D}{1 + D} \quad (2.10)$$

From the two-dimensional stress relationship in Figure 2.4:

$$\frac{\sigma'_1 + \sigma'_3}{2} = \sigma' - \tau \cot 2\psi \quad (2.11)$$

$$\frac{\sigma'_1 - \sigma'_3}{2} = \tau \csc 2\psi \quad (2.12)$$

From Equation 2.11 and Equation 2.12:

$$\frac{\sigma'_1 + \sigma'_3}{\sigma'_1 - \sigma'_3} = \frac{R + 1}{R - 1} = \frac{\sigma'}{\tau} \sin 2\psi - \cos 2\psi \quad (2.13)$$

Using Equation 2.10:

$$\frac{R + 1}{R - 1} = \frac{\sigma'}{\tau} \sqrt{1 - \frac{(1 - D)^2}{(1 + D)^2}} - \frac{(1 - D)}{(1 + D)} = \frac{\sigma'}{\tau} \frac{2\sqrt{D}}{(1 + D)} - \frac{(1 - D)}{(1 + D)} \quad (2.14)$$

Hence,

$$\frac{\tau}{\sigma'} = \sqrt{\frac{1}{D} \frac{(R - 1)}{(R/D + 1)}} \quad (2.15)$$

If we add the flow rule equation (Equation 2.6) to Equation 2.15:

$$\frac{\tau}{\sigma'} = \sqrt{\frac{K(R-1)}{R(K+1)}} \quad (2.16)$$

As mentioned above, since $\phi'_\mu = \phi'_{cv}$, the expression K turns into the following equation. If we substitute the conjugates of R and (τ/σ') in Equation 2.16, we obtain the general expression in Equation 2.18:

$$K = \tan^2\left(\frac{\pi}{4} + \frac{\phi'_{cv}}{2}\right) ; R = \tan^2\left(\frac{\pi}{4} + \frac{\phi'_{ps}}{2}\right) ; \left(\frac{\tau}{\sigma'}\right) = \tan \phi'_{ds} \quad (2.17)$$

$$\tan \phi'_{ds} = \tan \phi'_{ps} \cos \phi'_{cv} \quad (2.18)$$

Where, the effective shear strength angles are represented by ϕ'_{ds} in direct shear, ϕ'_{ps} in plane strain, and ϕ'_{cv} in critical state. In the critical state at which no volume change occurs, $R = K$ and $\phi'_{ps} = \phi'_{cv}$. Thus, Equation 2.18 becomes as follows:

$$\tan \phi'_{ds} = \sin \phi'_{ps} \quad (2.19)$$

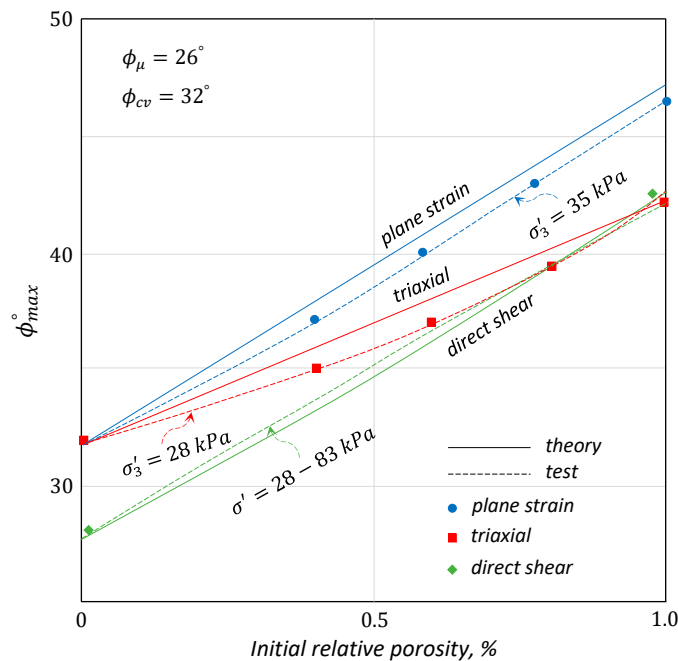


Figure 2.5. The relationship between the peak strengths measured in the direct shear, plane strain, and triaxial compression tests (quartz mineral sand from Mersey River) (Rowe, 1969)

Lee (1970) evaluated and compared the shear strength properties, failure envelopes, and material constants of sands under drained and undrained conditions based on the plane strain and triaxial compression methods. In the study, fine-grained (0.149 – 0.297 mm), clean, uniform Antioch sand composing of subangular and subrounded grains and with the main mineral content of quartz was used. In all the tests, the anisotropic consolidation ratio between major and minor principal stresses was selected as 2 ($k_c = \sigma'_{1c}/\sigma'_{3c}$), the confining pressures as 30, 100, 1000 (kN/m^2), and the relative density as 38% and 78% for loose and medium dense sands, respectively. The researcher also included his previous test data (Lee et al., 1966; Lee and Seed, 1967) in the study. As a result of the study, for the drained state, the greatest difference ($\phi'_{ps} - \phi'_{tc}$) between the peak shear strength angles was obtained in medium dense sands at low confining pressure (8°) and it was seen that this difference was lower in loose sands or in medium dense sands at high confining pressures. For the undrained state, greater strengths were obtained by the triaxial test method at low confining pressures and by the plane strain test method at high confining pressures. On the other hand, it was observed that in both methods, the failure envelopes became straight with the increasing confining pressure and their slopes were the same. The researcher investigated the material constants in the final section and stated that the initial tangent modules were $E_{ps} > E_{tc}$ and increased as exponential function with the increasing confining pressure (Figure 2.6a), while the Poisson ratios were $\nu_{ps} > \nu_{tc}$ and the difference between them decreased with the increasing confining pressure (Figure 2.6b). All these results are important because they indicate the effect of boundary conditions and dilation on the strength and deformation properties of sands.

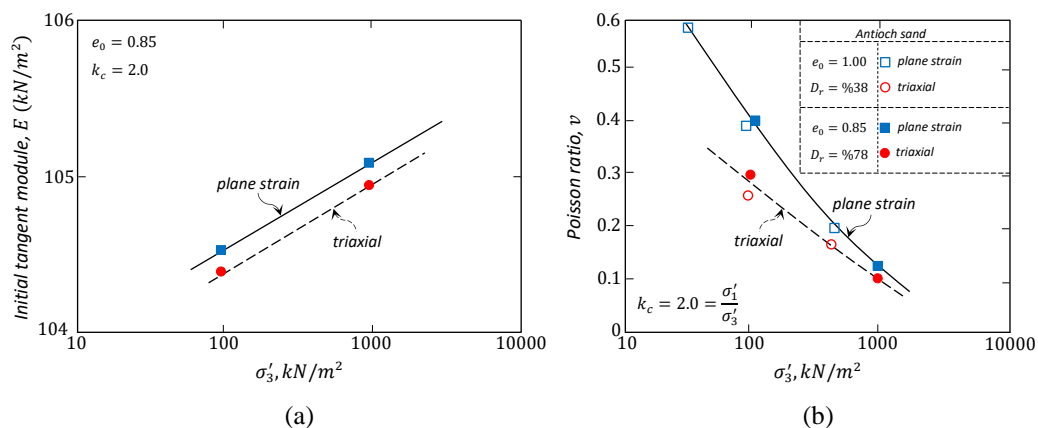


Figure 2.6. Variation of the material constants as a function of the effective confining pressure by different test methods: (a) Initial tangent module, (b) Poisson ratio (Lee, 1970)

In general, direct shear and triaxial test methods are preferred when determining the strength properties of granular soils. Pells et al. (1973) performed a range of tests using these test methods to determine the strength properties of two different sands to be used as filling material (Cape coast-fine, crushed quartzite-coarse). In the study in which all the tests were performed under drained conditions, the specimens ($B > 0.90$) prepared in medium dense form (66 – 71%) and saturated with back pressure ($\leq 850 \text{ kN/m}^2$) were sheared at wide effective normal and confining pressure (70 – 700 kN/m^2) range under strain-controlled conditions. As a result of the study, it was observed that the curvature of the Mohr failure envelope was greater in the direct shear test method and there was a slight difference between the shear strength parameters obtained from both methods for the specified stress range and density form (Figure 2.7). The researchers stated that these results were consistent with the literature data (Taylor, 1939; Nash, 1953; Rowe, 1969) and empirical comparisons are needed to be performed for high relative compaction ($R_c > 100\%$) and high stress conditions ($\sigma' > 700 \text{ kN/m}^2$).

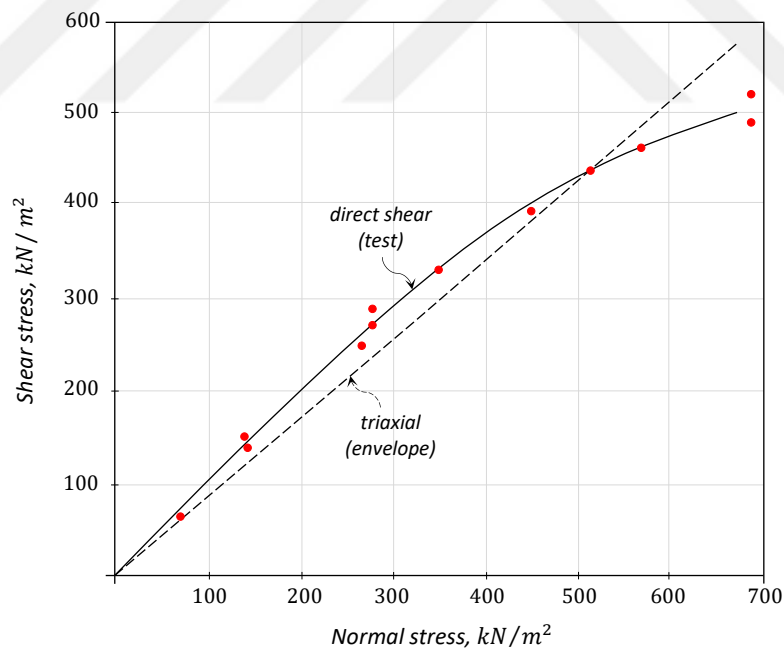


Figure 2.7. Mohr failure envelopes (Cape coast sand), (Pells et al., 1973)

Lade and Lee (1976) aimed to estimate the peak strength parameter of the plane strain method from the triaxial test results by observing the effect of critical state shear strength on test methods. For this purpose, they derived the following equations using lots of data that they previously obtained by the triaxial compression and plane strain test methods with sands that are mainly composed of quartz mineral. These equations are more conservative than most relations proposed in the literature.

$$\phi'_{ps} = 1.5\phi'_{tc} - 17 \quad (\phi'_{tc} > 34^\circ) \quad (2.20)$$

$$\phi'_{ps} = \phi'_{tc} \quad (\phi'_{tc} \leq 34^\circ) \quad (2.21)$$

Lee (2000) studied the effect of grain shape and different confining pressures on the equations above. The researcher evaluated the strength parameters obtained by different test methods using RMC sand with angular and subangular grain shape (Riemer, 1999), round Ottawa sand, and angular Rainier sand (Boyle, 1995) and compared with the equations in question (Table 2.4). As a result of the study, the plane strain angles were found higher in sands with round grain shape and lower in angular sands at low confining pressure and it was seen that the results were consistent with the increasing confining pressure. This result is important because it shows that Equation 2.20 and Equation 2.21 should be used conservatively.

Table 2.4. Comparison of the tested and calculated plane strain angles (Lee, 2000)

Soil	Confining pressure (kPa)	Predicted plane strain soil friction angle ^a (°)	Test results of plane strain soil friction angle (°)
Ottawa sand	25	50.5	47 ^b
	50	46	42 ^b
Rainier sand	25	57	59 ^b
	50	54	56 ^b
	75	54	55 ^b
RMC sand	20/25	39	41 ^c
	50/30	40	42 ^c
	100/80	42	43 ^c

^a(Lade and Lee, 1976), ^b(Boyle, 1995), ^c(Riemer, 1999)

Ladd et al. (1977) investigated the effect of intermediate principal stress (σ_2) on the effective shear strength of sands using five different studies in the literature whose details are given in Table 2.5. The researchers measured the relative value of effective intermediate principal stress (Habib, 1953):

$$b = \frac{(\phi'_2 - \phi'_3)}{(\phi'_1 - \phi'_3)} \quad (2.22)$$

As a function of the friction angle of Mohr-Coulomb failure criterion expressed in terms of effective principal stresses:

$$\phi' = \sin^{-1} \frac{(\phi'_1 - \phi'_3)}{(\phi'_1 + \phi'_3)} \quad (2.23)$$

and obtained the relationships in Figure 2.8. Since the value b continuously changes (0.25 – 0.40) due to σ_2 during the plane strain test, the relationships were drawn according to the value of b at failure ($b = 0$ for triaxial pressure condition).

Table 2.5. Details of the literature resources used (Ladd et al., 1977)

<i>Line</i>	<i>Sand</i>	<i>D_r(%)</i>	<i>Reference</i>
<i>A₁</i>	<i>Ottawa</i>	<i>medium-loose</i>	<i>Ko and Scott (1968)</i>
<i>A₂</i>		<i>medium-dense</i>	
<i>B₁</i>	<i>Med Fine</i>	<i>30</i>	<i>Sutherland and Mesdary (1969)</i>
<i>B₂</i>	<i>Loch Aline</i>	<i>80</i>	
<i>C</i>	<i>River Welland</i>	<i>dense</i>	<i>Proctor and Barden (1969)</i>
<i>D₁</i>	<i>Monterey (No.0)</i>	<i>27</i>	<i>Lade and Duncan (1973)</i>
<i>D₂</i>		<i>98</i>	
<i>E₁</i>	<i>Ham River</i>	<i>loose</i>	<i>Reades and Green (1974)</i>
<i>E₂</i>		<i>dense</i>	

As a result of the study, it was seen that the effective friction angle increased from zero to the value of (0.25 – 0.40), which represents the plane strain condition (*PSC*). This increase ($\phi'_{ps} - \phi'_{tc}$) occurred in the range of 2° – 4° for loose sands and of 4° – 9° for dense sands (Figure 2.8). At higher b values, it was seen that this effect caused an increase

in some sands, while a decrease in other sands. The researchers stated that they have not yet known whether this behavior difference was real difference or a function of variation in the test apparatus. On the other hand, it was seen that the young modulus often significantly increased with the increase in the practical range of (0.25 – 0.40). This result is important to understand the effect of changes in intermediate principal stress on the stress-strain properties of sand soils.

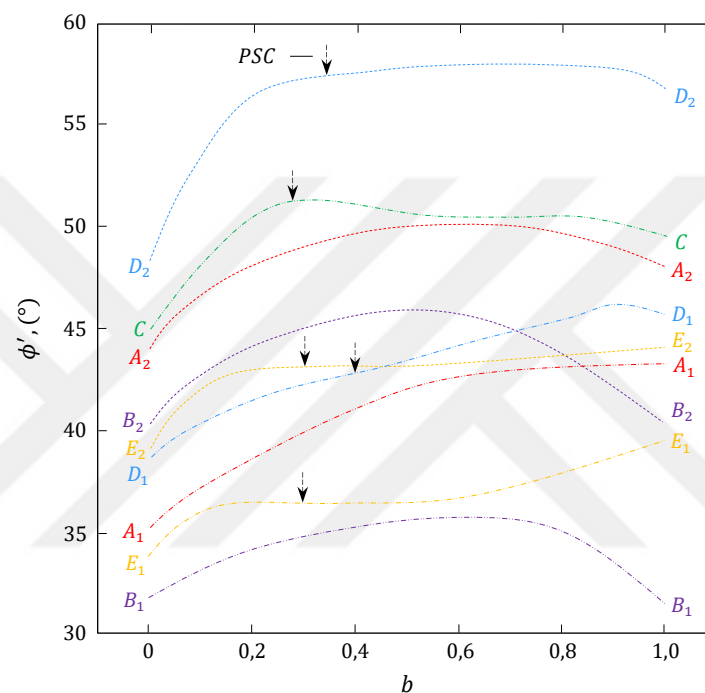


Figure 2.8. Effect of the intermediate principal stress on the effective friction angle of sands (Ladd et al. 1977)

The researchers, in the final part of the study, investigated the relationship of the value b with the failure criteria. Accordingly, it was seen that the effective friction angle (ϕ') was independent of the value b in Mohr-Coulomb criterion and expanded Von Mises (Drucker and Prager, 1952) and expanded Tresca (Drucker, 1953) criteria overestimated ϕ' at higher values of b ($b = 0.5$) (Bishop, 1966). On the other hand, it was reported that the criterion where Lade and Duncan (1975) used the stress invariants (I_1, I_3) was more consistent with the data in Figure 2.8.

Oda et al. (1978) studies and performed comparative analysis on the effect of anisotropic arrangement on the shear plane, stress-strain relationship, and shear strength properties of sands using the plane strain and triaxial test methods. The details of the procedure applied in preparing the specimens in anisotropic arrangement (in the desired tilting angle, δ) were explained by Menzies (1970) and Oda (1971). The details of uniform Toyoura sand used in the study are given in Table 2.6, while the details of the tests performed under drained conditions are given in Table 2.7.

Table 2.6. Physical properties of Toyoura sand (Oda et al., 1978)

Property	$D_{50}(mm)$	C_u	G_s	Void ratio		Particle size	Particle shape	Mineral	USCS
				e_{max}	e_{min}				
Value	0.18	1.5	2.65	0.99	0.63	fine	subangular	quartz (75%) and others	SP

Table 2.7. Details of plane strain and triaxial tests (Oda et al., 1978)

Test type	Dimensions of specimens ^a (cm)			$e_0 (D_r)$	$\sigma_3(kPa)$	δ°
	l	d	h			
Plane strain	8	4.4	6	0.66-0.67 ($\approx 90\%$)	50 - 400	0, 15, 24, 30, 45, 60, 90
Triaxial	7.5 (diameter)		8	0.67-0.68	50 - 200	0, 30, 60, 90

^a(l : Long, d : Wide, h : High)

As a result of the study, it was seen that the friction in end platens was effective in determining the shear planes, especially in triaxial method, and this plane coincided with the layer plane of angle δ at 24° or 30° , in both methods. When the stress-strain relationships were compared, it was seen that the angle δ had an effect in both methods, but this effect was more obvious in the plane strain method ($\varepsilon_2 = 0$). It was seen that as the angle δ increased, the deviator stress at failure ($\sigma_1 - \sigma_3$)_f and the dilation rate ($\partial v / \partial \varepsilon_1$)_f, but the deviator stress remained lower for $\sigma_3 = 200 kPa$ and $24^\circ - 30^\circ$ in the plane strain method. It was observed that the strain ratio at failure slightly increased as the confining pressure increased, regardless of the angle δ (in plane strain test method 2.5 – 5%, in triaxial test method higher than 5%). When the shear strengths were compared, it was seen that the stress ratio (σ_1 / σ_3)_f was mostly higher in the plane strain tests, while it was minimum at $\delta = 24^\circ$ for $\sigma_3 = 200, 400 (kPa)$ (Figure 2.9a). In the triaxial tests, a gradual decrease was observed, instead of an obvious bottom point (Figure 2.9b). The failure envelopes drawn for

certain angles δ based on all these results are given in Figure 2.10. Contrary to common belief, the researchers concluded that the plane strain strengths of sands could not be greater than the triaxial test for all states. This result is important because it shows that the anisotropic effect is too important to ignore in problems that can be represented with plane strain condition such as stability and earth pressure.

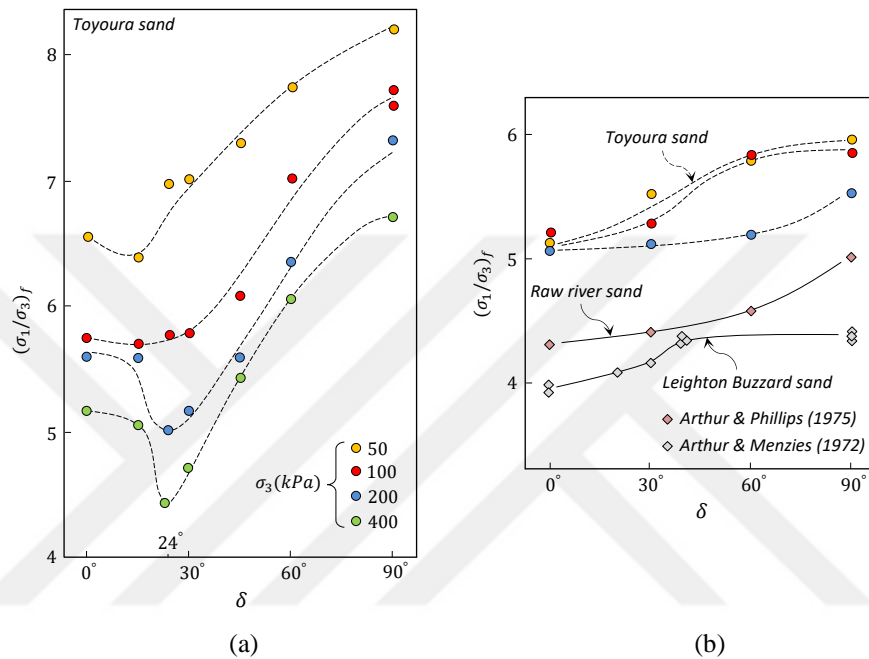


Figure 2.9. Effect of the angle δ on principal stress ratio: (a) Plane strain, (b) Triaxial (Oda et al., 1978)

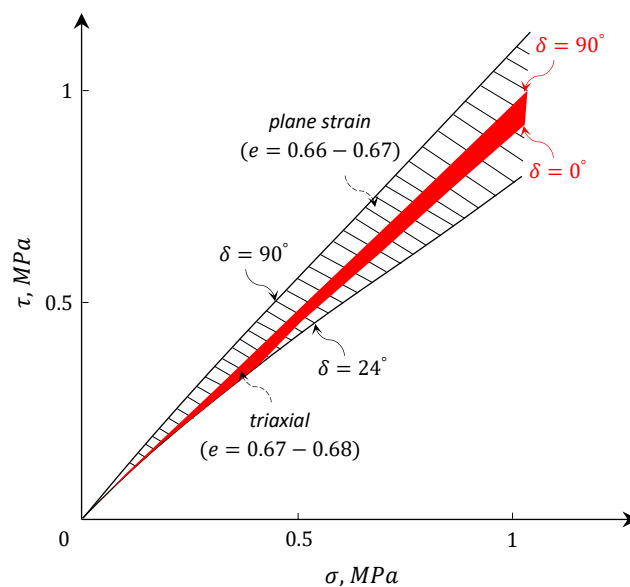


Figure 2.10. Evaluation of the Mohr's failure envelopes for some angles δ (Oda et al., 1978)

The shear strength parameters of seven different granular materials were compared by Superfesky and Williams (1978) using the triaxial and direct shear test methods. These materials as detailed in Table 2.8 were obtained from Kentucky open pit mining site, their main mineral was quartz, and their grain diameters were $D_{tc} < 19.0 \text{ mm}$ and $D_{ds} < 4.75 \text{ mm}$ to prevent possible errors arising from the testing apparatus. The researchers obtained separate material classes (*MC 1*, *MC 2*, *MC 3*) by mixing new (fresh) crushed aggregates obtained by crusher in the range of $19.0 - 4.75 \text{ (mm)}$ in the triaxial test method and of $4.75 - 2.0 \text{ (mm)}$ in the direct shear test method, with the available specimen at certain proportions. Thus, the effect of moisture that is the main subject of the study as well as the effect of newly crushed materials on strength could be measured. The direct shear tests were performed on dry and wetted samples at loose density, at constant vertical normal stress of 46, 100, 167 (*kPa*), at constant shear displacement rate of 1.22 mm/min , while the triaxial tests were performed at constant confining pressure of 103, 207, 414 (*kPa*) under undrained conditions.

Table 2.8. Class and description of the materials by the Unified Soil Classification System (USCS) (Superfesky and Williams, 1978)

<i>Material</i>	<i>Description</i>	<i>Triaxial</i>	<i>Direct shear</i>
<i>G</i>	<i>1/3 sandstone, 1/3 siltstone, 1/3 acid shale</i>	<i>SP-SC*</i>	<i>SP</i>
<i>H</i>	<i>1/3 sandstone, 1/3 siltstone, 1/3 calcareous shale</i>	<i>SW-SM* or SP-SM*</i>	<i>SW</i>
<i>I</i>	<i>1/3 sandstone, 1/3 acid shale, 1/3 calcareous shale</i>	<i>SP-SC*</i>	<i>SP</i>
<i>J</i>	<i>1/3 siltstone, 1/3 acid shale, 1/3 calcareous shale</i>	<i>SP-SC*</i>	<i>SP</i>
<i>MS 1</i>	<i>Similar to J but different batch and gradation</i>	<i>GW*</i>	<i>SW</i>
<i>MS 2</i>	<i>Shale from 10-foot thick stratum</i>	<i>GW</i>	<i>SW</i>
<i>MS 3</i>	<i>Sands and silty shales from several overburden strata; as blended during mining and grading operations</i>	<i>SP</i>	<i>SP</i>

* From composite of constituents

As a result of the study in which the evaluations were made in terms of effective parameters, higher mean shear strength angles were obtained by the direct shear method in dry sand ($\phi'_{dsd} - \phi'_{tcd} = 5.2^\circ$) and by the triaxial method in the presence of moisture ($\phi'_{tcm} - \phi'_{dsm} = 3^\circ$). It was seen that while the presence of moisture significantly reduced

the shear strength angle in the direct shear method ($\phi'_{dsd} - \phi'_{dsm} = 8.2^\circ$), its effect on cohesion term was insignificant ($c'_{dsd} - c'_{dsm} = 1.1 \text{ kPa}$). On the other hand, when the average cohesion strengths of both methods were compared, it was seen that the difference between them was still small ($c'_{tcm} - c'_{dsm} = 2.3 \text{ kPa}$). All these results are importance since they showed that the presence of moisture had a significant effect on the shear strength angle of soils, but its effect on cohesion was limited. In the final section, the researchers compared the mechanical properties of the new material classes by different test methods. It was seen that the new crushed materials had a significant contribution on strength in the triaxial method, while they had no effect in the direct shear test method. The researchers interpreted this as the fact that the new crushed aggregate formed a more compact structure with materials with larger diameters used in the triaxial method. The detailed results of the study are given in Table 2.9.

Table 2.9. Comparison of the shear strength parameters by different test methods and humidity conditions (Superfesky and Williams, 1978)

Material	Triaxial		Direct shear			
			dry		wet	
	$\phi'_{tc}(\circ)$	$c'_{tc}(\text{kPa})$	$\phi'_{ds}(\circ)$	$c'_{ds}(\text{kPa})$	$\phi'_{ds}(\circ)$	$c'_{ds}(\text{kPa})$
<i>G</i>	30.8	19	37.9	11.3	32.2	3
<i>H</i>	31.5	17	37.3	5.3	26.9	9.1
<i>I</i>	31.3	9	38.4	7.5	33.7	3.7
<i>J</i>	28.6	20	39.8	11.2	30.8	1.6
<i>MS 1</i>	33.2	4.9	38.7	14.6	27.4	11.6
<i>MS 2</i>	38.7	0	38.8	3.9	30.1	10.6
<i>MS 3</i>	39.8	0	39.1	0	31.5	6.3
Mean	33.4	10	38.6	7.7	30.4	6.6

Another study in which the strength and strain properties of sands were compared by different test methods was carried out by Marachi et al. (1981). In the study, in addition to the empirical comparison, the effect of specimen shape (Table 2.10) and longitudinal strain on the test results was also investigated. The specimens as detailed in Table 2.11, which were prepared using uniform Monterey sand (No.20) through vibration at different void ratios ($e_0 = 0.55 - 0.75$) were tested at a wide confining pressure range ($\sigma_3 = 70 - 3450 \text{ kPa}$) under drained conditions.

Table 2.10. Dimensions of the specimens used in the plane strain test (Marachi et al., 1981)

Width(cm)	Length(cm)	Height(cm)	Length/Width Ratio
2.5	21.6	10.1	8.5
2.5	14.0	10.1	5.5
4.6	11.4	11.4	2.5
11.4	28.4	28.4	2.5
11.9	11.9	29.2	1.0

Table 2.11. Physical properties of Monterey sand (No.20) (Marachi et al., 1981)

Property	$D_{50}(\text{mm})$	C_u	G_s	Void ratio		Particle size	Particle shape	Mineral	USCS
				e_{max}	e_{min}				
Value	0.55	1.25	2.64	0.83	0.53	fine-medium	rounded subrounded	quartz and others	SP

As a result of the study, greater shear strength angles were obtained by the plane strain method ($\phi'_{ps} > \phi'_{tc}$) and it was seen that the greatest difference occurred in dense sands under low stress conditions ($\sim 7^\circ$) and the difference between them significantly decreased ($\sim 1^\circ$) at high confining pressures (3450 kPa) (Figure 2.11). When the axial strains at failure were compared, greater values were measured in the triaxial method for all cases ($\epsilon'_{1ps} < \epsilon'_{1tc}$) and it was stated that this parameter was a function representing the common effect of density of sands and confining pressure (Figure 2.12). Although the strain levels at failure were close, the secant modulus ratios (E_{Sps}/E_{Stc}) were found greater in dense sands, contrary to the study by Cornforth (1964). Another important conclusion of the study is the fact that the shapes of specimens used in the plane strain test had no significant effect on the test results. In other words, square specimens might be used instead of

rectangular specimens. Finally, it was seen that the ratio of longitudinal strain at failure to axial strain up to a certain value ($\varepsilon_2/\varepsilon_1 < 0.4$) had a very limited effect on the effective shear strength angle ($< 1^\circ$). This result is importance since it shows the theoretical assumption in the plane strain method ($\varepsilon_2 = 0$) can be tolerated for certain strain levels.

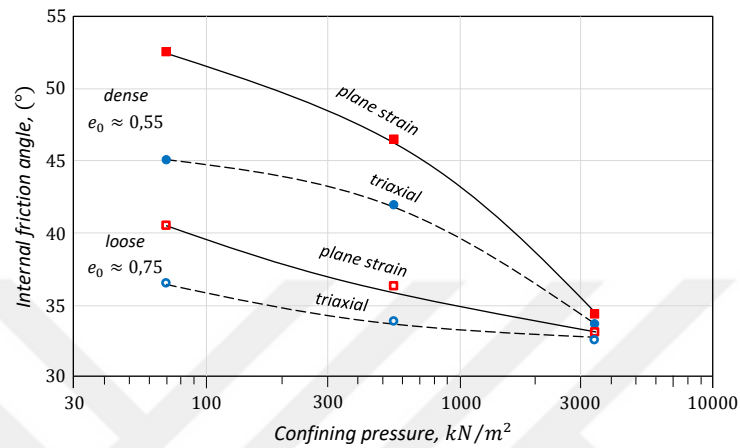


Figure 2.11. Relationship between confining pressure and internal friction angle (Marachi et al., 1981)

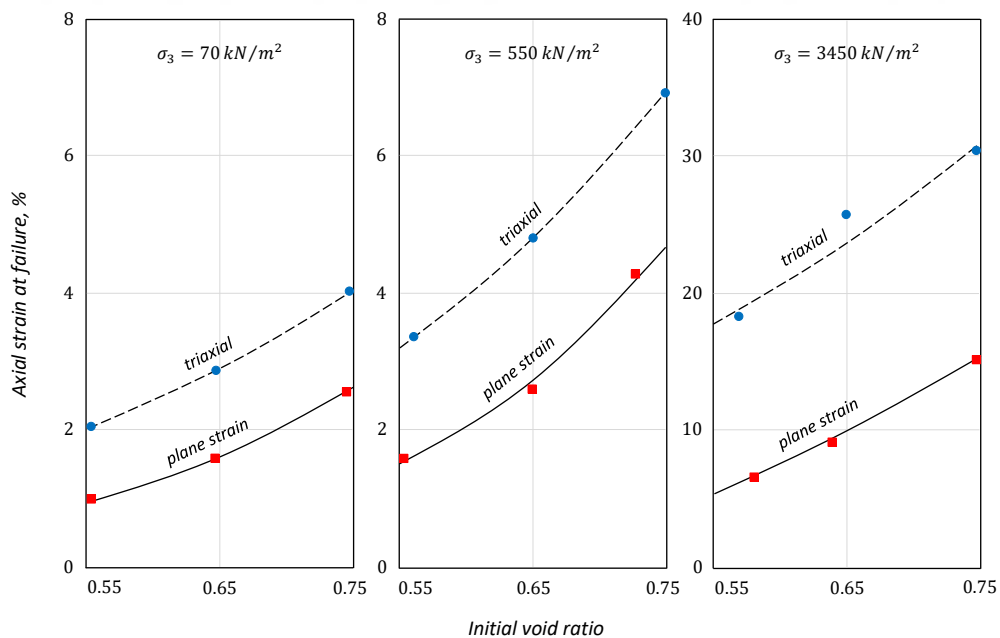


Figure 2.12. Comparison of axial strains at failure obtained by different test methods (Marachi et al., 1981)

Ramamurthy and Tokhi (1981) derived two different theoretical expressions depending on the dilation characteristic to estimate the plane strain strength from the triaxial (compression) test results. Under axisymmetric stress conditions, the intermediate principal stress (σ_2) was equal to the major or minor principal stress, while the inequality $\sigma_1 \neq \sigma_2 \neq \sigma_3$ was taken into account for plane stress conditions, as in the real stress conditions in the field. The researchers used the ratio of mean effective stress (at failure) to deviator stress for the axisymmetric condition:

$$\frac{1}{3} \frac{(\sigma'_1 + \sigma'_2 + \sigma'_3)_{tc}}{(\sigma'_1 - \sigma'_3)_{tc}} = \frac{1}{3} \left[\frac{(\sigma'_1 + \sigma'_3)}{(\sigma'_1 - \sigma'_3)} + \frac{\sigma'_3}{(\sigma'_1 - \sigma'_3)} \right]_{tc} \quad (2.24)$$

When the Mohr-Coulomb failure criteria is expressed in terms of effective principal stresses:

$$\frac{(\sigma'_1 - \sigma'_3)}{(\sigma'_1 + \sigma'_3)} = \sin \phi' \quad (2.25)$$

Rearranging Equation 2.25:

$$\frac{\sigma'_3}{\sigma'_1 + \sigma'_3} = \frac{1}{2} \left(\frac{1}{\sin \phi'_{tc}} - 1 \right) \quad (2.26)$$

If we solve Equation 2.24 and Equation 2.26 together:

$$\frac{1}{3} \frac{(\sigma'_1 + \sigma'_2 + \sigma'_3)_{tc}}{(\sigma'_1 - \sigma'_3)_{tc}} = \frac{1}{3} \left(\frac{3}{2 \sin \phi'_{tc}} - \frac{1}{2} \right) \quad (2.27)$$

If the method is repeated for the plane strain condition:

$$\frac{1}{3} \frac{(\sigma'_1 + \sigma'_2 + \sigma'_3)_{ps}}{(\sigma'_1 - \sigma'_3)_{ps}} = \frac{1}{3} \left[\frac{(\sigma'_1 + \sigma'_3)}{(\sigma'_1 - \sigma'_3)} + \frac{\sigma'_2}{(\sigma'_1 - \sigma'_3)} \right]_{ps} \quad (2.28)$$

Expressing the dilation expression in terms of effective principal stresses:

$$(\sigma'_2)_{ps} = \psi (\sigma'_1 + \sigma'_3)_{ps} \quad (2.29)$$

Substituting Equation 2.29 in Equation 2.28:

$$\frac{1}{3} \frac{(\sigma'_1 + \sigma'_2 + \sigma'_3)_{ps}}{(\sigma'_1 - \sigma'_3)_{ps}} = \frac{1}{3} \frac{1}{\sin \phi'_{ps}} (1 + \psi) \quad (2.30)$$

If Equation 2.30 and 2.27 representing two different conditions are combined and rearranged:

$$\frac{(\sigma'_1 + \sigma'_2 + \sigma'_3)_{tc}}{(\sigma'_1 - \sigma'_3)_{tc}} - \frac{(\sigma'_1 + \sigma'_2 + \sigma'_3)_{ps}}{(\sigma'_1 - \sigma'_3)_{ps}} = \frac{3}{2} \frac{1}{\sin \phi'_{tc}} - \frac{1}{\sin \phi'_{ps}} (1 + \psi) - \frac{1}{2} \quad (2.31)$$

A soil has a unique shear strength and dilation angle for any stress path, stress history, density, and particle structure. Therefore, the difference between the shear strength angles obtained for different methods under the same conditions is constant. The researchers calculated the parameter b representing the intermediate principal stress ratio in terms of the dilation expression, considering the fact that cohesion is zero under drained conditions:

$$\psi = \frac{1}{2} - \sin \phi' \left(\frac{1}{2} - b \right) \quad (2.32)$$

Thus, assuming that the expression $\sigma'_2/(\sigma'_1 + \sigma'_3)$ is constant, they suggested the relationship between the shear strength angles for the plane strain and triaxial condition:

$$\frac{1}{\sin \phi'_{tc}} - \frac{1}{\sin \phi'_{ps}} = \frac{2}{3} b \quad (2.33)$$

Using the expression in Equation 2.34 as suggested by Bishop (1966) for various clays and sands, for Equation 2.33:

$$\left(\frac{\sigma'_2}{\sigma'_1 + \sigma'_3} \right)_{ps} = \frac{1}{2} \cos^2 \phi'_{ps} \quad (2.34)$$

The researchers derived the following relationship for loose sands showing slight compression or dilation:

$$\sin \phi'_{ps} + 3 \left(\frac{1}{\sin \phi'_{tc}} - \frac{1}{\sin \phi'_{ps}} \right) = 1 \quad (2.35)$$

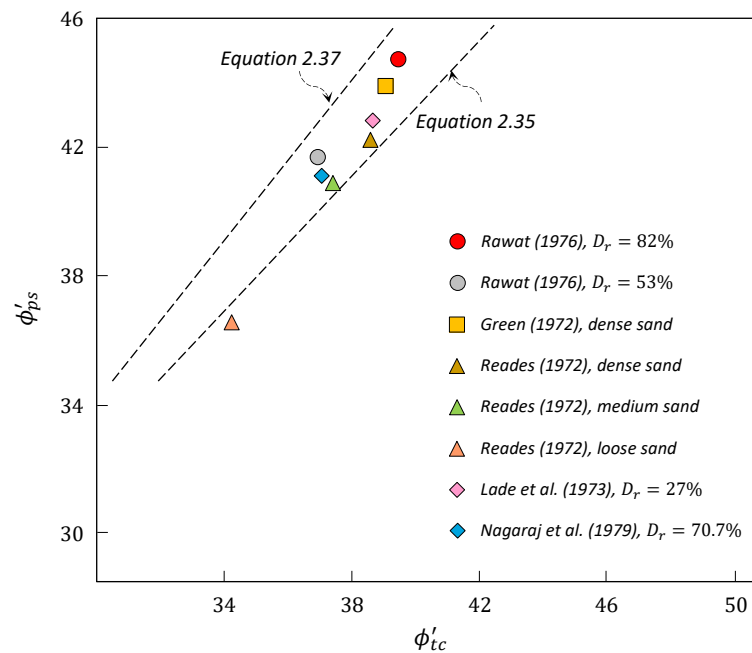
The expression suggested by Green (1972) for dense sands:

$$(\sigma'_2)_{ps} = \sqrt{(\sigma'_1 \sigma'_3)_{ps}} \quad (2.36)$$

is used together with Equation 2.33 and the following expression was obtained for dense sands showing significant dilations (at failure):

$$3 \sin \phi'_{ps} - \sin \phi'_{tc} (\sin \phi'_{ps} + \cos \phi'_{ps}) = 2 \sin \phi'_{tc} \quad (2.37)$$

As a result of the study, an excellent consistency was obtained between the literature data and the theoretical equations derived for drained conditions (especially for dense sands), based on many empirical observations (Figure 2.13). The researchers derived a new valid relationship for all densities, mostly with empirical data, using the coordinate direction-independent stress invariants (Ramamurthy and Tokhi, 1989)



Equation 2.13. Comparison of the plane strain strengths observed with those estimated (Ramamurthy and Tokhi, 1981)

Wroth (1984) investigated the strength properties of soils measured under different strain conditions and suggested a new relationship based on the shear angle of friction. The researcher stated that the intermediate principal stress effect should be taken into account and the strength parameters should be expressed with effective stress in order to make accurate comparisons between different types of tests. For this purpose, he used the generalized Mohr-Coulomb (1900), Lade (1972), Matsuoka (1974) failure criteria expressed in terms of all three effective principal stress (Figure 2.14).

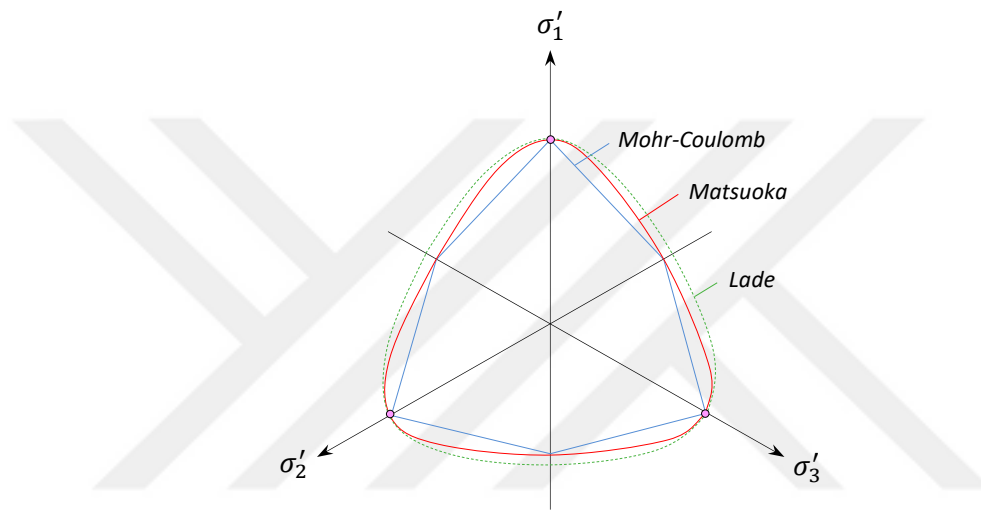


Figure 2.14. Failure surface sections in principal stress space (Wroth, 1984)

The figure above is a section of the principal stress space made by an octahedral plane or π -plane that is perpendicular to the space diagonal. This section represents three possible surfaces of failure from the origin, each in the cone form. The innermost, non-uniform hexagon section belongs to the expanded Mohr-Coulomb failure envelope, while the outermost curve belongs to the failure surface suggested by Lade. The Lade criterion is expressed in the form of stress invariants (Equation 2.38) as follows (Equation 2.39):

$$I_1 = \sigma'_1 + \sigma'_2 + \sigma'_3 \quad ; \quad I_2 = \sigma'_2\sigma'_3 + \sigma'_3\sigma'_1 + \sigma'_1\sigma'_2 \quad ; \quad I_3 = \sigma'_1\sigma'_2\sigma'_3 \quad (2.38)$$

$$\frac{I_1^3}{I_3} = \text{constant} \quad (2.39)$$

Matsuoka suggested an alternative failure criterion, which is represented by the red inner curve in Equation 2.14. In the form of invariant:

$$\frac{I_1 I_2}{I_3} = \text{constant} \quad (2.40)$$

In Figure 2.14, the sections of Lade and Matsuoka failure surfaces were drawn so that they coincided with the Mohr-Coulomb criterion for the triaxial compression tests. It's seen that, contrary to the Lade curve, the Matsuoka and the Mohr-Coulomb curves coincided at all corners and fit each other very well. The researcher used the Matsuoka criterion in his study due to the reasons such as the theoretical representation of mobilized spatial planes where slip in the soil was assumed to have occurred, the consistency with empirical data, and the expression in terms of all three stress invariants.

In the study, the parameter (b) defined by Habib (1953) was used to express the relative value of effective intermediate principal stress:

$$b = \frac{\sigma'_2 - \sigma'_3}{\sigma'_1 - \sigma'_3} \quad (2.41)$$

In the triaxial compression test 0, this parameter, which was taken as 0.5 approximately (at failure) in the plane strain test (Bishop, 1966), was valued in the range of $0 \leq b \leq 1$.

In the triaxial condition, since $\sigma'_2 = \sigma'_3$ (and $b = 0$), the Matsuoka criterion can be expressed as in Equation 2.42:

$$\frac{I_1 I_2}{I_3} = \frac{(\sigma'_1 + 2\sigma'_3)(\sigma_3'^2 + 2\sigma'_1 \sigma'_3)}{\sigma'_1 \sigma_3'^2} = \frac{(\sigma'_1/\sigma'_3 + 2)(1 + 2\sigma'_1/\sigma'_3)}{\sigma'_1/\sigma'_3} \quad (2.42)$$

The expression above can be expressed in terms of shear friction angle ($\sin \phi = (\sigma'_1 - \sigma'_3)/(\sigma'_1 + \sigma'_3)$) as follows for the triaxial compression state:

$$\frac{I_1 I_2}{I_3} = \frac{(3 - \sin \phi_{tc})(3 + \sin \phi_{tc})}{(1 - \sin \phi_{tc})(1 + \sin \phi_{tc})} = 9 + 8 \tan^2 \phi_{tc} \quad (2.43)$$

For the plane strain state, the parameter b can be redefined and its invariants can be arranged and then can be expressed in terms of the shear strength angle as follows:

$$b_{ps} = \frac{\sin \phi_{ps} + \cos \phi_{ps} - 1}{2 \sin \phi_{ps}} \quad (2.44)$$

If the method used in the triaxial compression test is applied for the plane strain state and the results between them are compared, the following relationship is obtained:

$$\sec^2 \phi_{ps} + \sec \phi_{ps} = 2 \sec^2 \phi_{tc} \quad (2.45)$$

As a result of the study, Figure 2.15 was obtained based on Equation 2.45. Thus, the approximate linear relationship between the two test methods, as in Equation 2.46, was derived, which can be used for engineering purposes. This relationship is important as it shows that the triaxial test can be approximately underestimated by 10% than the plane strain test for a soil.

$$8\phi_{ps}^{\circ} \approx 9\phi_{tc}^{\circ} \quad (2.46)$$

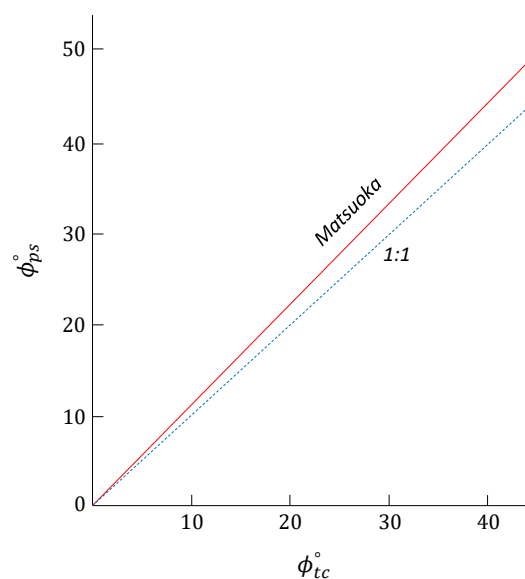


Figure 2.15. Relationship of shear strength angle obtained from the Matsuoka failure criterion for different test conditions (Wroth, 1984)

Jewell and Wroth (1987) investigated the strength properties of sands by the direct shear method and suggested a new equation in which the data obtained were associated with the plane strain parameters in the flow rule formation. In the study, in addition to the empirical comparison, the contribution of polymer material on strength and the effect of shear box scale on boundary conditions were also investigated. A modified shear box with dimensions of $25.4 \times 15.2 \times 15.2$ (cm) (length x width x height) was used in the tests (Jewell, 1980) and uniform Leighton Buzzard sand specimens (BS 14/25), as detailed in Table 2.12, were prepared in dense form ($e_0 = 0.52$) by a pluvial method and sheared under three different constant vertical loads.

Table 2.12. Physical properties of Leighton Buzzard sand (Jewell and Wroth, 1987)

Property	$D_{50}(mm)$	C_u	G_s	Void ratio		Particle size	Particle shape	Mineral	USCS
				e_{max}	e_{min}				
Value	0.90	1.20	2.65	0.78	0.49	medium	rounded	quartz	SP

As a result of the study, the researchers analyzed the direct shear test results by the expression obtained from the dilation ($\tan \psi = \partial y / \partial x = -\partial \varepsilon_{yy} / \partial \varepsilon_{yx}$) and the Mohr's stress circle geometry (based on plane strain) and showed that the results were consistent with the results of the same sand obtained by the simple shear method (Stroud, 1971; Budhu, 1979). When the strength parameters of the plane strain and direct shear ($\tan \phi_{ds} = \tau_{yx} / \sigma_{yy}$) methods were compared with the same procedure, the typical critical friction angle range ($\phi_{cv} = 33 - 37$)° suggested by Bolton (1986) was taken as basis and Equation 2.16 and Equation 2.17 were obtained using Equation 2.3 (Davis, 1968) and Equation 3.27 (Bolton, 1986). Figure 2.16 shows that the difference between strength angles ($\phi_{ps} - \phi_{ds}$) is independent of the dilation angle and the density of sand. In Figure 2.17, it is seen that there is a difference of 20 – 25 (%) between the tangent ratios of friction angle of both methods and the safety factor of 1.2 can be used in designs on a peak or critical state basis.

$$\phi_{ps} = \tan^{-1}(1.2 \tan \phi_{ds}) \quad (2.47)$$

It was also shown that Equation 2.47 had a strong agreement with Equation 2.18 (Rowe, 1969).

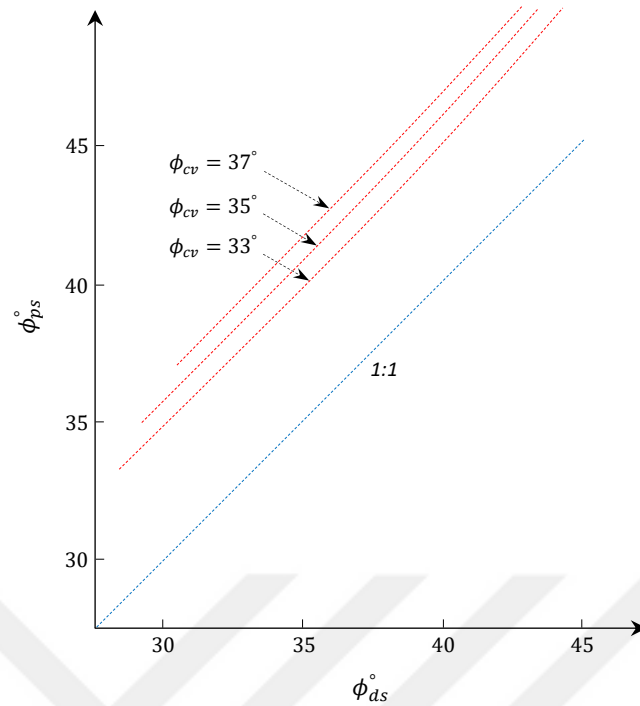


Figure 2.16. Theoretical relationship of shear friction angles tested and calculated (Jewell and Wroth, 1987)

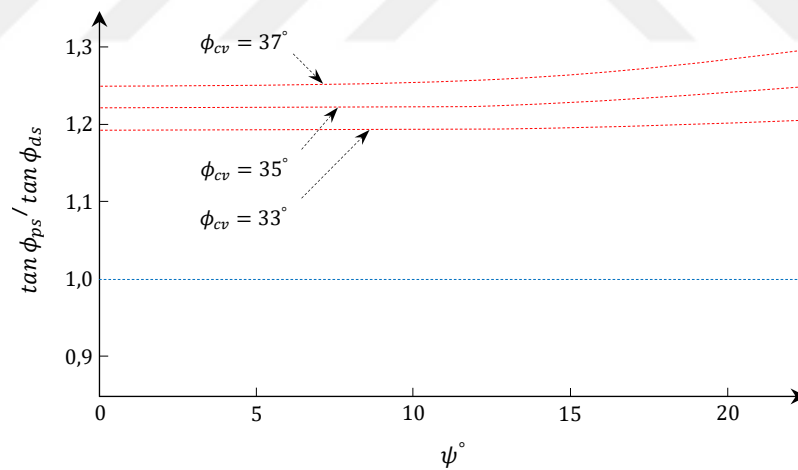


Figure 2.17. Relationship between the tangent ratio of peak shear friction angles and the critical state friction angle (Jewell and Wroth, 1987)

The researchers observed that polymer reinforcement enhanced the strength properties of sand and explained the extent of this effect with a new relationship using the two-dimensional limit equilibrium analysis. On the other hand, they stated that the scale was effective on boundary conditions in the direct shear test and suggested that the ratio of shear box length to the average particle size (D_{50}) should be between 50 – 300.

Jewell (1989), who investigated the effect of boundary conditions on the direct shear test results, compared the strength parameters for different strain conditions, with the rearranged equation and flow rules. In the study, the test results reported by Stroud (1971), Jewell (1980) and Palmeira (1987) under different boundary conditions and the relationships reported by Davis (1968) and Bolton (1986) were used. The evaluated test results were for the high specimen density ($D_r = 90\%$) and low normal stress ($\sigma_v < 60 \text{ kN/m}^2$) conditions at which uniform Leighton Buzzard sand (BS 14/25), as detailed in Table 2.12, was used. As a result of the study, greater shear strength (τ_{yx}/σ_{yy}) and shear displacement values (at failure) were obtained in the conventional (asymmetrical) arrangement in which the top loading platen can freely move, however, it was seen that the volumetric changes ($\partial y/\partial x$) were smaller. It was stated that in symmetrical conditions where the top loading platen is fixed, effects such as stress concentration, rotation, etc., which occur with the free top platen, are eliminated; strains and stress distribution in the center plane are more uniform, and thus the soil behavior can be represented more accurately. On the other hand, the friction angles obtained by different methods were scattered over a wide range in the conventional method, but it was seen that they were closer to each other in the symmetrical arrangement. When the flow rules were evaluated, it was stated that some of them underestimated the plane strain angle, while some of them overestimated the plane strain angle and it was emphasized that the most conservative value should be used. The researcher finally stated that the accuracy of direct shear test results was affected by non-uniform strain (lower dilation angle) (Equation 2.48, Equation 2.49) and non-coaxial principal axes (stress-strain increment) (Equation 2.50) and suggested the following relationships for these factors:

$$\phi_{ps} = \phi_{cv} + 0.8(\psi - \Delta\psi) \quad (2.48)$$

$$\sin \phi_{ps} = \frac{\tan \phi_{ds}}{\cos(\psi - \Delta\psi) + \sin(\psi - \Delta\psi) \tan \phi_{ds}} \quad (2.49)$$

$$\tan \phi_{ds} = \frac{\sin \phi_{ps} \cos(\psi - 2\Delta\theta)}{1 - \sin \phi_{ps} + \sin(\psi - 2\Delta\theta)} \quad (2.50)$$

In the equations, the deviation in dilation angle and between principal axes was represented by $\Delta\psi$ and $\Delta\theta$, respectively ($8^\circ \geq (\Delta\psi, \Delta\theta) \geq 0^\circ$), ($\phi_{cv} = 35^\circ$, $\psi = 0^\circ - 20^\circ$).

Schanz and Vermeer (1996) evaluated the dilation and friction angles of sands under different strain conditions. The researchers associated the general volumetric strain concepts with the studies by Rowe (1962) and Bolton (1986) and aimed to expand the dilation angle defined for the plane strain state to include the triaxial strain state. In the study, Hostun sand as detailed in Table 2.13 was used, and the specimens that were prepared in two different relative density (I_D) (dense (1.15) and loose (0.38)) by the pluvial method were tested at constant cell pressure ($\sigma_3 = 300 \text{ kPa}$) and axial strain (1% per minute) conditions by a range of drained triaxial strain methods. The researchers stated that the critical friction angle was independent of strain conditions and took the unique critical friction angle as a basis.

Table 2.13. Physical properties of Hostun sand (Schanz and Vermeer, 1996)

Property	$D_{50}(\text{mm})$	C_u	G_s	Void ratio		Particle size	Particle shape	Mineral	USCS
				e_{max}	e_{min}				
Value	0.32	1.70	2.65	1.041	0.648	fine-medium	angular	quartz	SP

As a result of the study, the dilation angle was associated with triaxial strain condition using the superposition concepts, thus a new dilation angle definition that is applicable to triaxial and plane strain conditions and the same around the peak for these conditions was obtained (Equation 2.58). Contrary to the dilation angle, the friction angles showed significant differences for both strain states. The researchers associated this with different critical state friction angles in the literature. In other words, they stated that strain conditions might change the critical state friction angle, but this had no scientific precision. The researchers finally matched the equations suggested by Bolton (1986) for different strain condition (Equation 2.62 and Equation 2.63) on relative dilation indexes basis (I_R) and derived a linear relationship between the peak friction and the critical friction terms (Equation 2.64). Figure 2.18 shows that this relationship is in good agreement with the literature. The definitions of the derived dilation and friction angles are detailed in the continuation of the section.

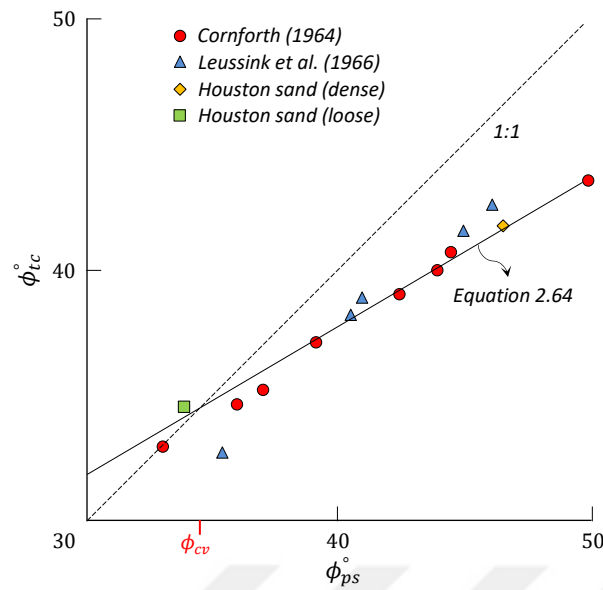


Figure 2.18. Comparison of the maximum strengths for different strain conditions (Schanz and Vermeer, 1996)

The researchers suggested a new method similar to the energy principle of Rowe (1962), using the strain-dilation expressions in Equation 2.6 and Equation 2.7, for the transition from plane strain condition to triaxial strain condition. In this method, the strain ratios $(\sigma_1 - \sigma_2, \sigma_1 - \sigma_3)$ in different planes were represented by two different mechanisms (A and B) (Figure 2.19). Hence:

$$-\left(\frac{\dot{\varepsilon}_2}{\dot{\varepsilon}_1}\right)_A = D_A = \frac{R_A}{K} \quad (2.51)$$

$$-\left(\frac{\dot{\varepsilon}_3}{\dot{\varepsilon}_1}\right)_B = D_B = \frac{R_B}{K} \quad (2.52)$$

Since $R_A = R_B = R$ and $\dot{\varepsilon}_2 = \dot{\varepsilon}_3$ under triaxial testing conditions, the contribution of components in different planes into strain:

$$\dot{\varepsilon}_1 = \dot{\varepsilon}_{1A} + \dot{\varepsilon}_{1B} = -2\dot{\varepsilon}_3 \frac{K}{R} \quad (2.53)$$

Thus, unlike the expression suggested by Rowe (1962), the following expression is obtained:

$$D = -2 \frac{\dot{\epsilon}_3}{\dot{\epsilon}_1} \quad (2.54)$$

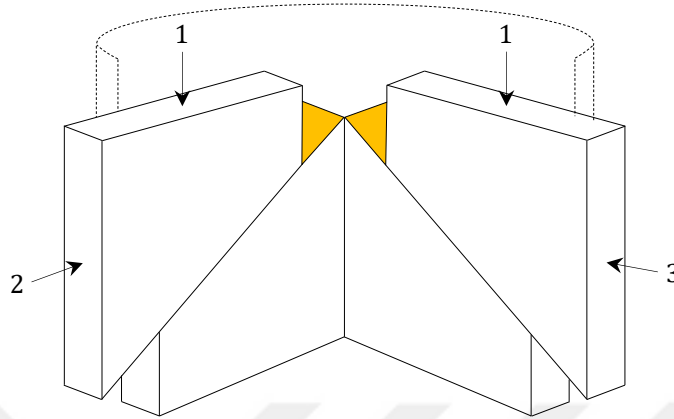


Figure 2.19. Triaxial dilation deviation from the biaxial state (Schanz and Vermeer, 1996)

However, Bolton (1986) defined the following plane strain relationship:

$$\sin \psi_{ps} = -\frac{\dot{\epsilon}_1 + \dot{\epsilon}_3}{\dot{\epsilon}_1 - \dot{\epsilon}_3} \quad (2.55)$$

Considering that the axial strain is the combination of the *A* and *B* mechanisms:

$$\dot{\epsilon}_v = \dot{\epsilon}_{1A} + \dot{\epsilon}_{1B} = \frac{\dot{\epsilon}_2}{D_A} + \frac{\dot{\epsilon}_3}{D_B} \quad (2.56)$$

The expression ψ from Equation 2.55 and Equation 2.56:

$$D_A = D_B = -\frac{1 - \sin \psi}{1 + \sin \psi} \quad (2.57)$$

$$\sin \psi = -\frac{\dot{\epsilon}_v / \dot{\epsilon}_1}{2 - \dot{\epsilon}_v / \dot{\epsilon}_1} \quad (2.58)$$

Thus, a new relationship by which the dilation angle could be measured for both strain conditions was obtained.

Combining the dilation angle expression above with the stress-dilatancy relationships in Equation 2.6 and Equation 2.7, for the plane strain condition:

$$\sin \psi = \frac{\sin \phi_{ps} - \sin \phi_{psf}}{1 - \sin \phi_{ps} \sin \phi_{psf}} \quad (2.59)$$

Similarly, combining the dilation angle expression in Equation 2.58 with the stress-dilatancy relationship in Equation 2.54, for the triaxial strain condition:

$$\sin \psi = \frac{\sin \phi_{tc} - \sin \phi_{tcf}}{1 - \sin \phi_{tc} \sin \phi_{tcf}} \quad (2.60)$$

The expression in Equation 2.54 was combined with the relationship suggested by Bolton (1986) for plane strain and triaxial strain conditions ($-\dot{\epsilon}_v/\dot{\epsilon}_1 = 0.3I_R$) and presented as a general equation as follows:

$$\sin \psi = \frac{0.3I_R}{2 + 0.3I_R} = \frac{I_R}{6.7 + I_R} \quad (2.61)$$

The researchers obtained Equation 2.64 using the relationships suggested by Bolton (1986) for different strain conditions to estimate the friction angles:

For the plane strain state:

$$\phi_{ps_p} - \phi_{ps_{cv}} = 5I_R \quad (2.62)$$

For the triaxial strain state:

$$\phi_{tc_p} - \phi_{tc_{cv}} = 3I_R \quad (2.63)$$

Bolton assumed the critical state friction angles as equal for both strain states:

$$\phi_{tc_p} = \frac{1}{5} (3\phi_{ps_p} + 2\phi_{cv}) \quad (2.64)$$

Okada et al. (1998) investigated the peak and ultimate strengths of sands by ring shear method, triaxial compression method and direct shear method at different arrangements (constant volume, constant stress) and performed comparative analyses of them. In the study, standard Toyoura sand as detailed in Table 2.6 was used and the tests were performed with the void ratio in the range of ($e_o = 0.63 - 0.91$), at constant stress loads ($\sigma = 100, 200 \text{ kPa}$) by taking the shear displacement rate and distance as $0.3 - 3 \text{ mm/s}$; $1 - 10 \text{ m}$ for ring shear test and as $0.05 \text{ mm/s} - 30 \text{ mm}$ for triaxial test under drained conditions. The researchers included the literature data summarized in Figure 2.20 into the study to make the comparisons more meaningfully. As a result of the study, it was seen that the peak shear strength angles from the ring and direct shear methods were close to each other at every void ratio level, that when the results of these tests were compared with the triaxial method, they were similar at high void ratios, and that the difference between them increased distinctively at low void ratios ($0.75 - 0.85$). When the ultimate strengths were evaluated, it was stated that although very high displacement levels (10^4 mm) were reached by the ring shear method and $\tan\phi = 65^\circ$ was obtained, because the triaxial method had a limited axial strain level (15%), the ultimate strength values could not be reached, thus an empirical comparison cannot be performed for this parameter.

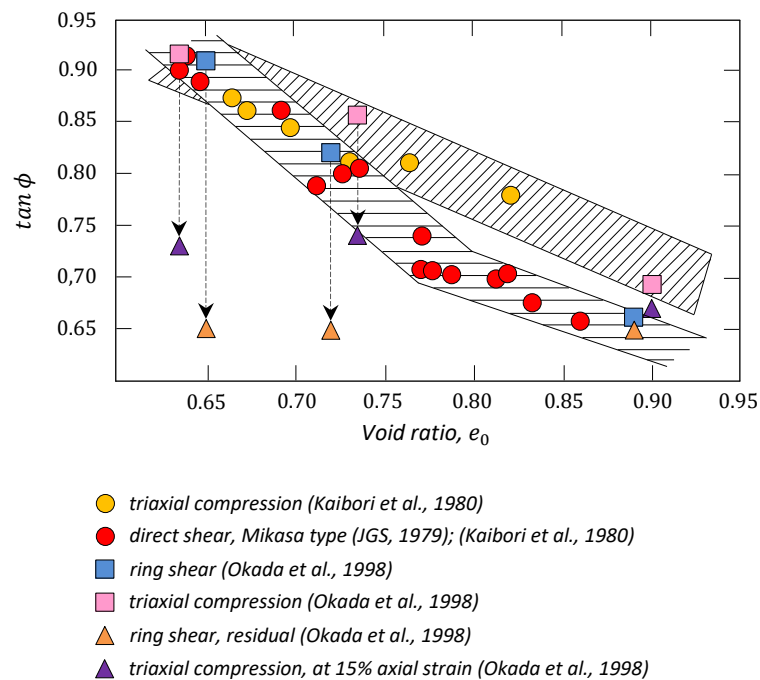


Figure 2.20. Investigation of the variation of shear strength angle by the void ratio with different test methods (Okada et al., 1998)

Alshibli et al. (2003) investigated the effect of density and confining pressure on the peak shear strength properties of sands and performed a comparative analysis of them using different test methods. In the study where uniform Ottawa sand (F-75) as detailed in Table 2.14 was used, the plane strain tests (PS) were performed in the relative density range of 47 – 97(%) and confining pressure of 15, 100 (kPa), while the triaxial tests (TC) were performed in the relative density range of 66.5 – 91.3(%) and confining pressure of 11.5 – 70 (kPa).

Table 2.14. Physical properties of Ottawa sand (F-75) (Alshibli et al., 2003)

Property	$D_{50}(mm)$	C_u	G_s	Porosity		Particle size	Particle shape	Mineral	USCS
				n_{max}	n_{min}				
Value	0.22	1.83	2.65	0.446	0.327	fine	rounded	quartz	SP

As a result of the study, it was seen that the shear strength of loose sands was slightly higher in the plane strain method under low stress conditions, while it was the same in the triaxial method under high stress conditions (Figure 2.21a). For the dense sands, the test method had a more significant effect on strength (Figure 2.21b). When the volumetric strains were compared, greater values were obtained by the triaxial method for all densities tested. The researchers compared the post-peak strain conditions and observed strain hardening in the plane strain tests, and strain softening in the triaxial tests, regardless of the density. The researchers explained this behavior difference with the limiting factors of the test methods.

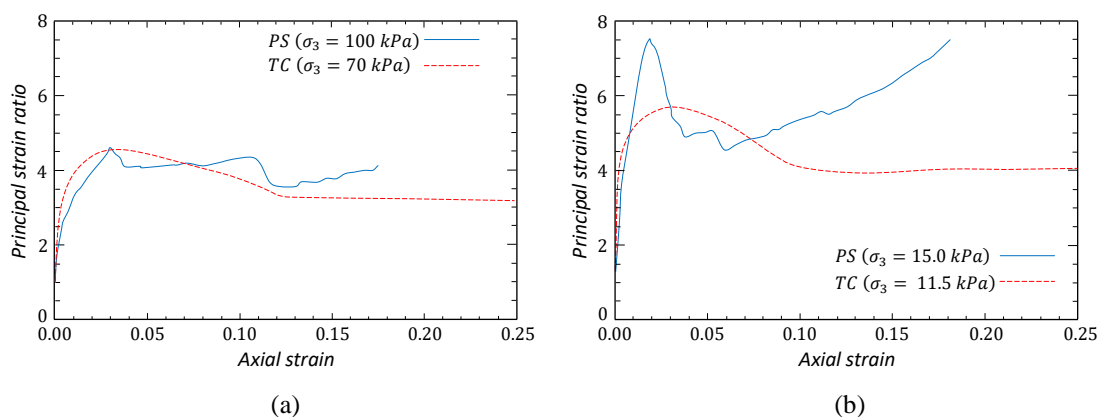


Figure 2.21. Comparison of the plane strain test results and the triaxial test results: (a) Low density - high confining pressure, (b) High density - low confining pressure (Alshibli et al., 2003)

Georgiadis et al. (2004) reevaluated different failure criteria and various empirical data based on plane strain and triaxial test methods and suggested a new yield surface that is applicable to loose and dense soils. The researchers used Mohr-Coulomb (1900), Matsuoka-Nakai (1974), and Lade-Duncan (1975) as failure criteria; and the results of studies by Cornforth (1964), Leussink et al. (1966), Rowe (1969), Green and Reades (1975), Lam & Tatsuoka (1988), and Schanz & Vermeer (1996) as test data. In the study, evaluations were made for failure criteria on plane strain and triaxial test basis and a new yield surface expression was suggested (Equation 2.65) and then this expression was compared with the results of various tests. As a result of the study, an experimental difference ($\phi'_{ps} - \phi'_{tc}$) was observed in the range of 5 – 14(%) in the Matsuoka-Nakai criterion, of 10 – 20(%) in the Lade-Duncan criterion, and the researchers attributed this difference to the dilation capacity and the difference between the criteria to their definitions. It was stated that since $\phi'_{ps} = \phi'_{tc}$ is expected for loose sands and those reached the critical state, the Mohr-Coulomb criterion would be sufficient for the strength modeling of these soils. When the criteria were compared with the test results in the literature, higher ϕ'_{ps} values were obtained for Matsuoka-Nakai and Lade-Duncan at small values of ϕ'_{tc} , however it was seen that Matsuoka-Nakai gave results that were more consistent with ϕ'_{ps} at higher values of ϕ'_{tc} . Thus, the researchers suggested the following new expression based on the Mohr-Coulomb failure criterion for loose soils and the Matsuoka-Nakai failure criterion for dense soils:

$$F = \alpha F_1 + (1 - \alpha) F_2 \quad (2.65)$$

Where, the yield surface is represented by F , F_1 , F_2 for Georgiadis et al., Matsuoka-Nakai, Mohr-Coulomb, respectively and the soil state is represented by α . The expression α may be expressed with Equation 2.66 with the effective friction angle relationship or Equation 2.67 with the dilation angle relationship:

$$\alpha = \beta \frac{\phi'_{tc} - \phi'_{cv}}{\phi'_{cv}} \quad (2.66)$$

$$\psi = \alpha \psi_p \quad (2.67)$$

Where, expansion in yield surface is represented by β , critical friction angle by ϕ'_{cv} , and the peak dilation angle by ψ_p .

The expression α representing the current soil state is equal to zero in loose soils but varies depending on the parameter β in dense soils and takes its maximum value at peak state (by having the peak shear strength angle at all Lode angles (θ) and with the maximum divergence of the failure surface from the Mohr-Coulomb hexagon). Figure 2.22 shows the effect of this expression on the shape and position of yield surface on deviatoric plane and Figure 2.23 shows its effect on deviatoric stress-mean effective stress plane.

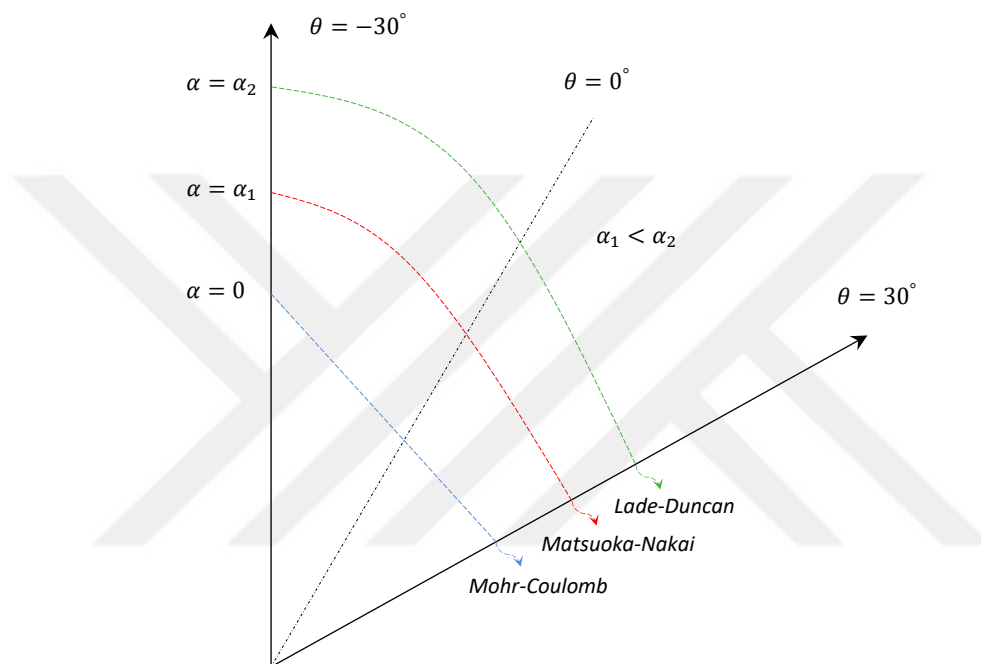


Figure 2.22. On deviatoric plane (Georgiadis et al., 2004)

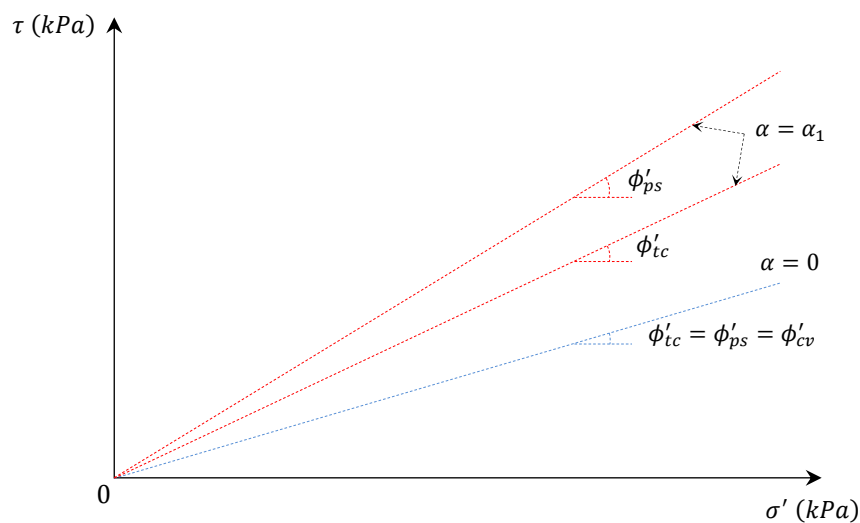


Figure 2.23. On $(J - p')$ plane (Georgiadis et al., 2004)

The researchers compared the expression they suggested (Equation 2.65) with the results of various tests whose details are shown in figures, for the different values of β , using the Matsuoka-Nakai (Figure 2.24) and Lade-Duncan (Figure 2.25) failure criteria. Accordingly, they obtained consistent results at $\beta = 3$ for the Matsuoka-Nakai criterion (for $\alpha = 1$) and at $\beta = 2$ for the Lade-Duncan criterion (the expression gives unrealistic results for $\alpha > 1$).

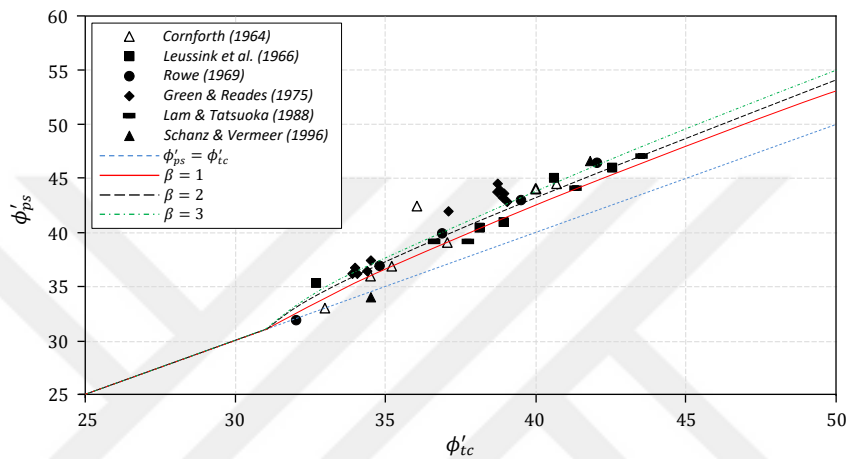


Figure 2.24. According to the Matsuoka-Nakai failure criterion (Georgiadis et al., 2004)

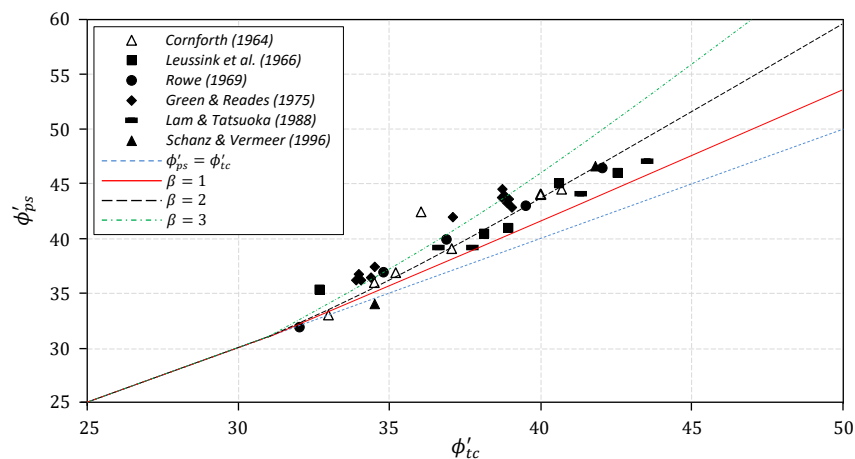


Figure 2.25. According to the Lade-Duncan failure criterion (Georgiadis et al., 2004)

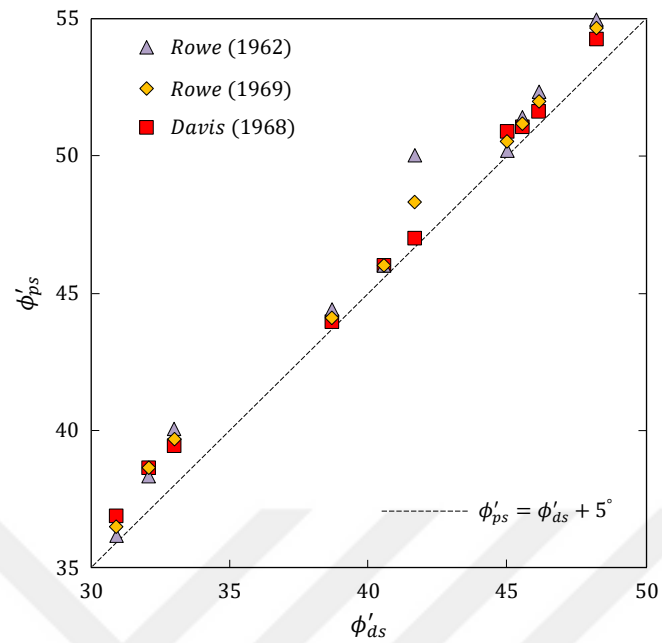
Consequently, it was stated that the new yield surface presented as the combination of the Mohr-Coulomb, Matsuoka-Nakai, and Lade-Duncan expressions represent the post critical state and thus can be used for all soil densities. It was also concluded that using the Matsuoka-Nakai criterion, instead of the Lade-Duncan making fungible predictions would be more meaningful, as compared to the literature results.

Lings and Dietz (2004) developed a new modified direct shear apparatus with new wings that are attached to both sides, based on Jewell's (1989) symmetrical arrangement in order to minimize the faults arising from the conventional direct shear test. The researchers stated that with this apparatus, shear loads could be applied to the specimen center more uniformly as well as the boundary effect on volume changes measured by conventional instruments could be eliminated. In the study, uniform Leighton Buzzard sand (BS 14/25) as detailed in Table 2.12 was used and the specimens prepared in loose, medium dense, and dense sands by pluvial method were sheared at the stress range of 25 – 252 (*kPa*) and the constant shear displacement rate of 1.2 *mm/min*. As a result of the study, greater dilation rates were obtained by the winged direct shear apparatus and contrary to the literature (Jewell, 1980; Jewell and Wroth, 1987), a rotational effect, even slightly, was observed in the symmetrically arranged top platen. It was concluded that the shear strength properties were highly affected by the horizontal distance between platens and the side material and the edge material, but the lever arm effect was negligible. This result is important because it significantly affects the measurements obtained by the direct shear method. The researchers associated the measured parameters with the equations and yield rules in the literature for plane strain condition (Figure 2.26a). When the data derived using these relationships, are examined, it is seen that the most consistent results were obtained by Davis (1968). The researchers attributed the different scatterings of the expressions to the differences in the definitions of critical state angle and suggested the following equation that forms a lower limit for the data in Figure 2.26a:

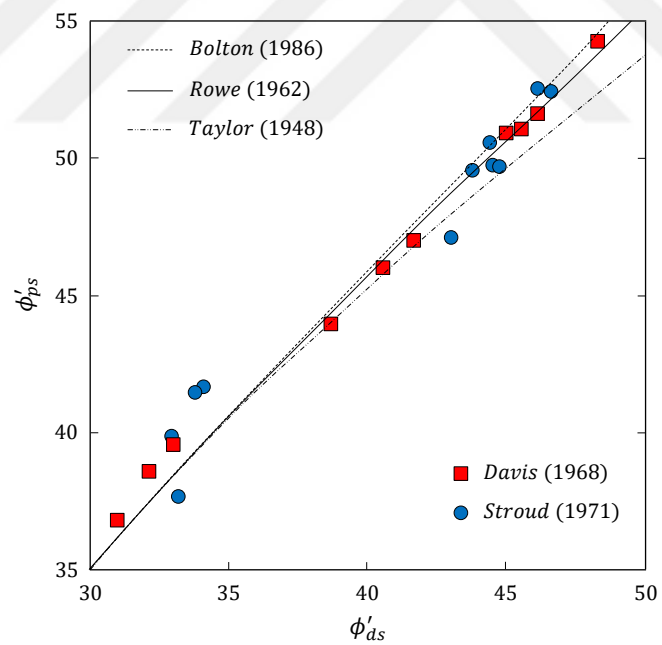
$$\phi'_{ps} = \phi'_{ds} + 5^\circ \quad (2.77)$$

The winged direct shear test data interpreted by Davis (1968) and the simple shear test data reported by Stroud (1971) were also evaluated by adding different flow rules (Figure 2.26b). Thus, it was seen that the flow rule that was the best representative of both data sets that appeared to be in the same trend was Rowe's rule (1962). The researchers finally evaluated the critical shear strength angle using the winged direct shear apparatus and stated that the results were in good agreement with the values measured by Stroud (1971) and suggested the following equation for these large displacement conditions:

$$\tan \phi'_{ds} = \sin \phi'_{cv} \quad (2.78)$$



(a)



(b)

Figure 2.26. Comparison of the peak direct shear and plane strain data: (a) Using the combination of different parameters, (b) Evaluating the winged direct shear and Stroud (1971) with the flow rules ($\phi'_{cv} = 35^\circ$), (Lings and Dietz, 2004)

The peak shear strength angles obtained by cylindrical and prismatic wedge shear, triaxial and direct shear test methods were compared by Mirata and Erzin (2007) on different bases and their comparative analysis was performed. In the study, sand materials ($D < 3.35 \text{ mm}$) which were obtained from different locations of our country and of which details are presented in Table 2.15 were used, the tests were performed at different values (δ) of the angle between the shear plane and the bedding planes for low and high relative density and stress states under drained conditions. The researchers defined the particle crushing that they encountered at all stress levels, with Marsal's (1967) breakage factor (B_g) and neglected the cohesion effect.

Table 2.15. Material properties of sand specimens (Mirata and Erzin, 2007)

Sample	Location of sampling sites	$D_{50}(\text{mm})$	C_u	G_s	Void ratio		$B_g(\%)$	Particle shape	Mineral	USCS
					e_{max}	e_{min}				
A	Kazan	0.94	5.80	2.64	0.66	0.40	3.1	angular	quartz and other	SP
B	Şereflikoçhisar	1.17	2.24	2.62	0.86	0.50	6.6	angular	quartz and other	SP
C	Bafra	0.67	3.48	2.68	0.62	0.41	7.6	angular	quartz and other	SP
D	Sinop	0.41	1.24	2.64	0.80	0.58	13.7	subangular	quartz and other	SP
E	Yumurtalık	0.33	1.76	2.70	0.82	0.56	13.8	subangular	quartz and other	SP
F	Ceyhan	0.40	2.19	2.70	0.81	0.54	10.2	subangular	quartz and other	SP

As a result of the study, the relationship $\phi'_{cw} = 1.075 \phi'_{tc}$ was obtained between the triaxial method ($\delta \approx 65^\circ$) and the cylindrical wedge shear method ($\delta = 60^\circ$) under low stress conditions and it was seen that this relationship was close to the equation ($\phi'_{ps} = 1.125 \phi'_{tc}$) suggested by Wroth (1984) for plane strain condition. When the triaxial method was compared with the prismatic wedge shear method ($\delta = 30^\circ$), the relationships $\phi'_{tc} = 0.982 \phi'_{pw}$ and $\phi'_{tc} = 0.983 \phi'_{pw}$ were obtained for low and high stress conditions, respectively; when it was compared with the direct shear method ($\delta = 0^\circ$), the relationships $\phi'_{tc} = 0.914 \phi'_{ds}$ and $\phi'_{tc} = 0.983 \phi'_{pw}$ were obtained for low and high stress conditions, respectively (Figure 2.27). The researchers attributed the fact that ϕ'_{pw} was lower than ϕ'_{cw} to the low δ angle of ϕ'_{pw} and stated that their strengths could be close for similar angles ($\delta_{pw} \approx \delta_{cw}$). When the angle δ was increased to 60° in the direct shear method, the shear strength angle increased significantly (4.2°). With this increase, close results were obtained

by the cylindrical method ($\phi'_{cw} = 0.972 \phi'_{ds}$) as well as the plane strain method at the same δ angle. On the other hand, it was seen that the results obtained by the triaxial method, and the prismatic method were on the same trend. All these results are important because the angle δ is effective both in the strength properties of sands and in the comparison of experimental methods (Figure 2.28). The researchers stated that the critical state angle (ϕ'_{cv}) that depends on the particle mineral composition is independent of the test type and the angle δ .

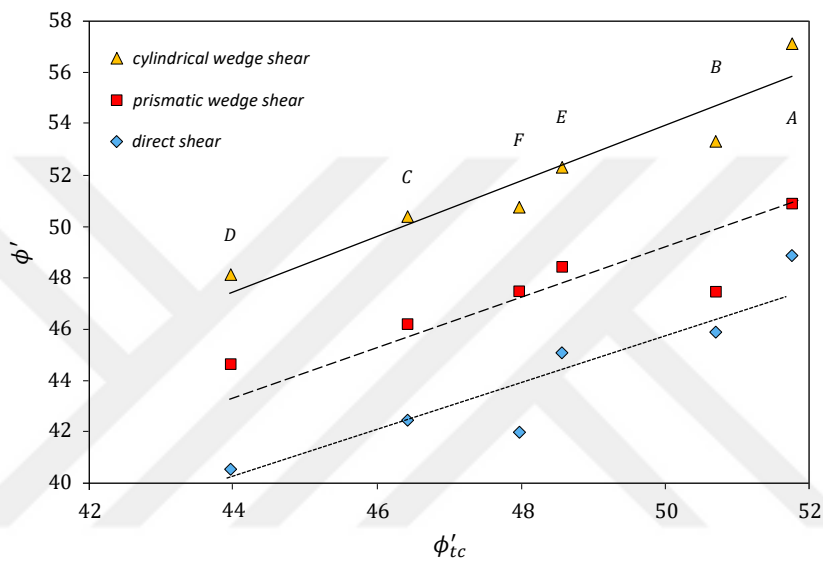


Figure 2.27. Variation of the peak shear strength measured by the drained triaxial tests and by other shear tests (Mirata and Erzin, 2007)

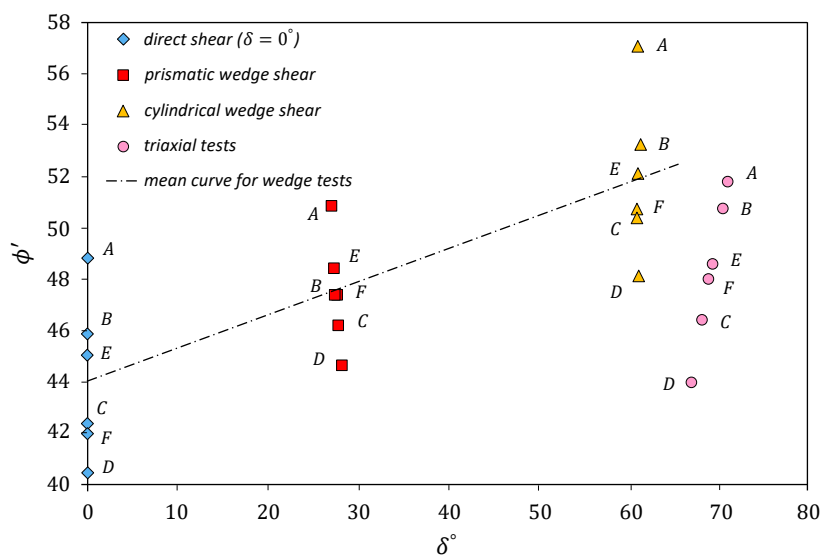


Figure 2.28. Variation of the δ angle and the peak shear strength angle measured by different tests (Mirata and Erzin, 2007)

Wanatowski and Chu (2007a) investigated the strength and dilation characteristics of sands under axisymmetric and plane strain conditions and performed their comparative analysis. For the plane strain tests, test apparatus as described by Wanatowski and Chu (2006), by which the intermediate principal stress (σ_2) can be measured by eliminating the corner effects with four transducers on two rigid vertical platens, was used. In the study where all the tests were performed under drained conditions, the specimens that were prepared in loose ($e_c \approx 0.90$) and medium dense ($e_c \approx 0.66$) form and saturated with back pressure (400 kPa) ($B > 0.96$) were sheared in a wide range of mean effective stress ($p'_c = 35 - 300$ kPa) as strain controlled (0.05% per minute). The properties of Changi sand used in the study are given in Table 2.16.

Table 2.16. Physical properties of Changi sand (Wanatowski and Chu, 2007a)

Property	$D_{50}(mm)$	C_u	G_s	Void ratio		Particle size	Particle shape	Mineral	USCS
				e_{max}	e_{min}				
Value	0.30	2.00	2.60	0.916	0.533	fine-medium	subangular	quartz	SP

As a result of the study, higher shear strength angles were obtained by the plane strain method as compared to the triaxial method ($\phi'_{ps} > \phi'_{tc}$) and it was seen that the difference between them was higher at low void ratios. When the failure lines at $q - p'$ space was compared, higher stress ratios ($\eta'_{tc} > \eta'_{ps}$) were obtained by the triaxial method and it was seen that the difference between them was lower at low void ratios (Figure 2.29).

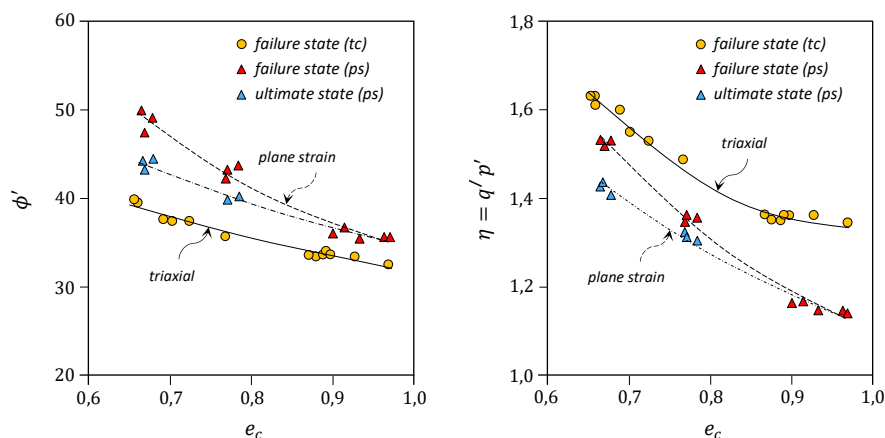


Figure 2.29. Failure states obtained from different strain conditions (Wanatowski and Chu, 2007a)

The researchers stated that this inconsistency from ϕ' and η definitions should not be ignored in geotechnical designs. On the other hand, it was stated that since the critical state lines (CSL) were of different values at $e - p'$ ($\phi'_{pscv} = 36^\circ$; $\phi'_{tc cv} = 33.6^\circ$) and $q - p'$ ($M_{ps} = 1.16$; $M_{tc} = 1.33$) spaces for both methods, the CSL obtained by the triaxial method cannot be applied to other generalized methods. The researchers finally investigated the effect of different materials and test methods on the stress-dilation relationship using the empirical data from the study performed by Cornforth (1961) using Brasted sand. According to the results as detailed in Figure 2.30, different stress-dilation relationships were obtained under plane strain and axisymmetric loading conditions for both Changi sand and Brasted sand. For Changi sand under plane strain and axisymmetric conditions (at failure), respectively:

$$\phi'_{ps} = \phi'_{pscv} + 0.34\psi_{ps} \quad (2.79)$$

$$\phi'_{tc} = \phi'_{tc cv} + 0.18\psi_{tc} \quad (2.80)$$

For Brasted sand under plane strain and axisymmetric conditions (at failure), respectively:

$$\phi'_{ps} = \phi'_{pscv} + 0.30\psi_{ps} \quad (2.81)$$

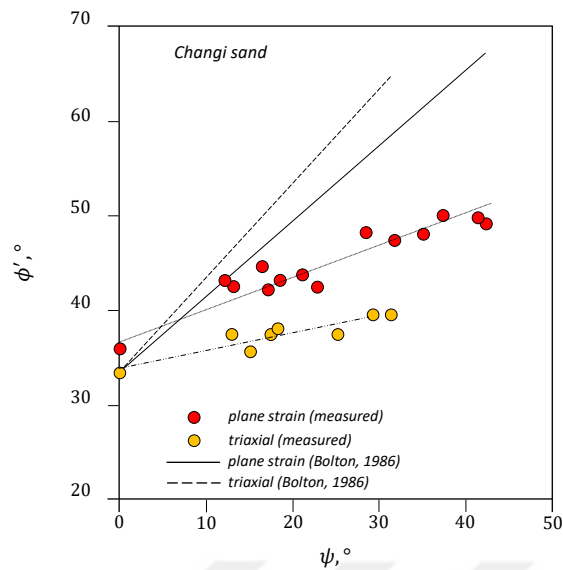
$$\phi'_{tc} = \phi'_{tc cv} + 0.24\psi_{tc} \quad (2.82)$$

Stress-dilation relationship derived by Bolton (1986) for plane strain and axisymmetric conditions (at failure), respectively:

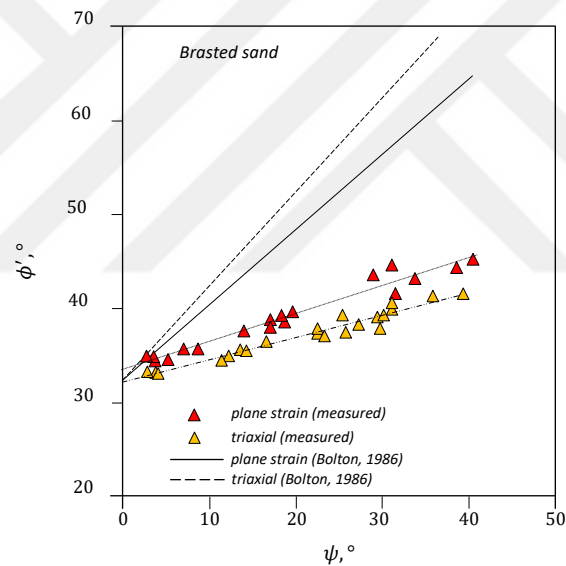
$$\phi'_{ps} = \phi'_{pscv} + 0.80\psi_{ps} \quad (2.83)$$

$$\phi'_{tc} = \phi'_{tc cv} + 1.00\psi_{tc} \quad (2.84)$$

Bolton defined the critical effective friction angle as equal ($\phi'_{pscv} = \phi'_{tc cv}$) for both methods. The schematic representation of the comparison of all these relationships is given below.



(a)



(b)

Figure 2.30. Stress-dilation relationships: (a) Changi sand, (b) Brasted sand (Wanatowski and Chu, 2007a)

Although the Figure 2.30 shows that the presented relationships are on similar trends as a function of dilation, it was observed that both the relationships between different strain methods and the stress-dilation relationships presented by Bolton were not consistent with the results of Changi and Brasted sands. Therefore, the researchers concluded that the stress-dilation relationships derived for any sand and method cannot be applied for other sands and methods.

Bareither et al. (2008) investigated the scale effects on the shear strength in the direct shear tests and compared them with the test results of the triaxial method. For this purpose, the researchers used two different square shear boxes; standard small-scale $64 \times 64 \times 31$ (mm) and large-scale $305 \times 305 \times 152$ (mm). The direct shear tests were performed at a normal stress range of $26 - 184$ (kPa) and the constant shear displacement rate of 0.24 mm/min; up to a maximum horizontal displacement of 7 mm with materials passing the 4.75 mm sieves in the small-scale direct shear test (SSDS) and up to a maximum horizontal displacement of 38 mm with materials passing the 25.4 mm sieves in the large-scale direct shear test (LSDS). The triaxial tests were performed with materials passing the 4.75 mm sieves, the specimen sizes of 74×147 (mm) (diameter, height, respectively), the confining pressure range of $21 - 83$ (kPa), and the axial strain rate of 0.11 mm/min under drained conditions. In the study where the specimens were prepared with a medium relative density of (60 – 75%), four different filling materials as detailed in Table 2.17 were used as well as the contribution of gravel aggregate ($25.4 > D_g > 4.75$ mm) to strength was tested with a large-scale shear box.

Table 2.17. Physical properties of the tested sands (Bareither et al., 2008)

Sample	Gravel (%)	C_u	C_c	G_s	e_{max}	e_{min}	$\gamma_{d_{max}}$ (kN/m ³)	R^*	USCS
A	0.0	1.86	1.12	2.64	0.76	0.48	17.36	0.50	SP
B	1.8	2.35	1.15	2.63	0.69	0.43	17.59	0.62	SP
C	22.1	4.16	0.68	2.67	0.56	0.33	18.11	0.43	SP
D	2.2	3.06	0.85	2.70	0.64	0.39	18.64	0.42	SP

* Roundness

As a result of the study, a strong agreement was obtained between the failure envelopes obtained by different tests for each specimen (this agreement was also shown statistically with the covariance analysis model, $p > 0.05$), (Figure 2.31). The shear strength angles varied up to 3.3 degrees depending on the test method and specimen (Table 2.18) and it was stated that the results were consistent with the literature data of medium dense sands (Taylor, 1939; Nash, 1953; et al.). When the strain characteristics were examined, it was seen that the strains required to reach the peak were greater (0.88%) in the large-scale direct shear method, which was attributed by the researchers to the dimensions of shear box that

caused significant differences in the relative movement of particles. On the other hand, it was stated that the gravel content (up to 30%) had limited effect on the shear strength angles.

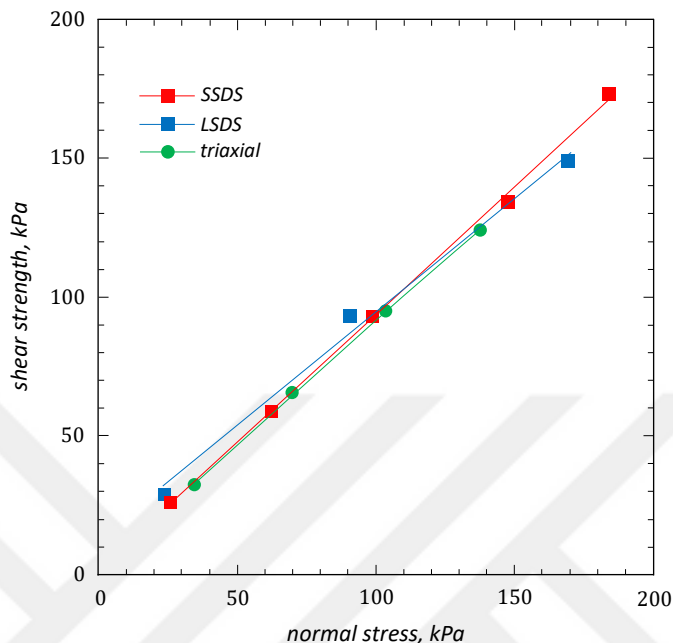


Figure 2.31. Failure envelopes of different scale and methods (Specimen *D*) (Bareither et al., 2008)

Table 2.18. Peak shear strength angles of different test types (Bareither et al., 2008)

Test type	A	B	C	D
Small-scale direct shear	35.8	32.5	38.5	42.6
Large-scale direct shear	38.1	31.8	36.6	40.5
Triaxial	34.8	34.2	39.5	41.3
<i>p</i> * value	0.70	0.07	0.09	0.45

*Probability value

The researchers concluded that material properties may significantly affect the test results of different scales and suggested that the results should be always checked with different tests. This is important since it explains that the scale effect should be considered when making experimental comparisons and that the experimental relationships suggested in the literature should be evaluated and used on the basis of these principles.

Guo (2008) compared the anisotropic strengths of sands obtained using a new modified shear box with the results of the studies by Tatsuoka et al. (1986) and Lam and Tatsuoka (1988) where the anisotropic plane strain strengths of sands were measured and performed their comparative analysis. The modified shear box (60 x 60 x 45 mm) was made of four interlocking sides. When preparing the specimen, the shear box consisting of two orthogonal sides was positioned in the plexiglass mold according to the desired bedding plane inclination angle (θ), the sand material was placed in the reservoir by the pluvial method and then the angular positions of the shear box were changed and the sides No. 3 and 4 were added. After the specimen was saturated, it was frozen and then thawed at room temperature by applying isotropic stress and the void ratios were measured. The tests were performed with dense specimen density ($e_0 = 0.48 - 0.52$), normal stress loads of 50, 100, 200 (kPa) and constant shear displacement rate of 1 mm/min. The properties of standard Ottawa sand (C190) are given in Table 2.19.

Table 2.19. Physical properties of Ottawa sand (C190) (Guo, 2008)

Property	$D_{50}(mm)$	C_u	G_s	Void ratio		Particle size	Particle shape	Mineral	USCS
				e_{max}	e_{min}				
Value	0.72	1.25	2.65	0.67	0.45	medium	rounded	quartz	SP

The angle of bedding plane normal with major principal stress (σ_1) direction was represented by (δ), the angle of the same plane with intermediate principal stress (σ_2) direction by (ξ) (Figure 2.32).

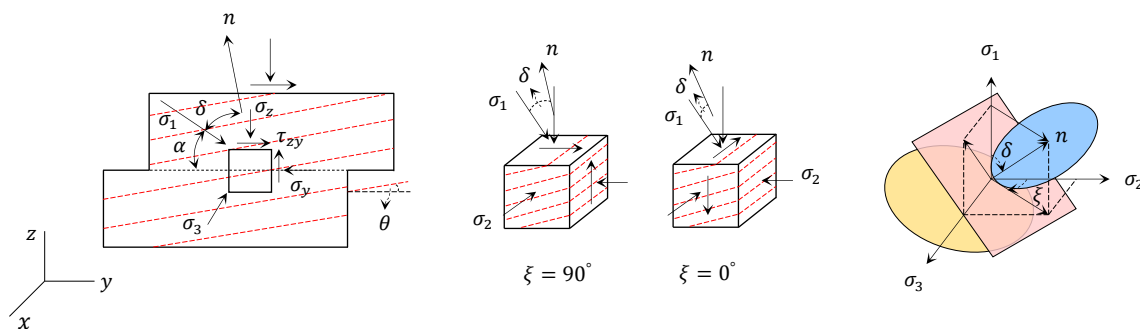


Figure 2.32. Geometric description of shear plane direction and major principal stress direction relative to bedding plane (Guo, 2008)

As a result of the study, it was seen that the shear strengths were affected by the bedding plane direction in the direct shear tests where modified shear box was used. It was seen that at different angles ($\theta = 0^\circ - 90^\circ$) of the shear box being identical to this plane direction, the peak shear strengths ($\tan \phi = \tau/\sigma_n$) got the minimum value at 30° and the maximum value at 90° [$(\phi_{90} - \phi_{30}) > 4^\circ$] and almost equal ($\phi_0 \approx \phi_{60}$) at 0° and 60° .

The researcher investigated the effect of shear stress direction (ξ_0, ξ_{90}) on the shear strengths of sand specimens with the same bedding layer plane inclination, using the angular expression defined by Lam and Tatsuoka (1988) ($0^\circ \leq \xi \leq 90^\circ$; parallel ($\xi = 0^\circ$), perpendicular ($\xi = 90^\circ$)). For this purpose, a series of direct shear tests were performed using the modified shear box under $\theta = 30^\circ$, $e_0 = 0.48 - 0.52$, $\sigma_n = 50, 100$ (kPa) conditions and it was seen that the effect of the angular expression was negligible. This result is important since it shows the strengths obtained from the direct shear tests were a function of angle θ rather than shear stress acting on the shear plane.

The researcher compared the test results obtained by the direct shear and plane strain methods using the expression of Tatsuoka (1985) showing that the anisotropic plane strain strengths of sands could also be expanded for the direct shear method by expressing them in terms of δ . For this purpose, the following expressions derived from Mohr-Coulomb criterion (assuming the angle $(\pi/4 - \phi/2)$ relative to the direction of failure plane σ_1):

$$\xi = 90^\circ;$$

$$\delta = \frac{\pi}{4} + \frac{\phi}{2} - \theta \quad (2.85)$$

$$\xi = 0^\circ;$$

$$\cos \delta = \cos \theta \cos \left(\frac{\pi}{4} + \frac{\phi}{2} \right) \quad (2.86)$$

Within these principles, the results normalized with the shear strength angle ($\phi_{\delta=0^\circ}$) at $\delta = 0^\circ$ were compared in the form of plane strain to bring out the effect on anisotropic strengths (Figure 2.33). The researcher stated that the curves in the figure from different methods were on the same trend and anisotropic strengths could also be obtained by direct shear tests.

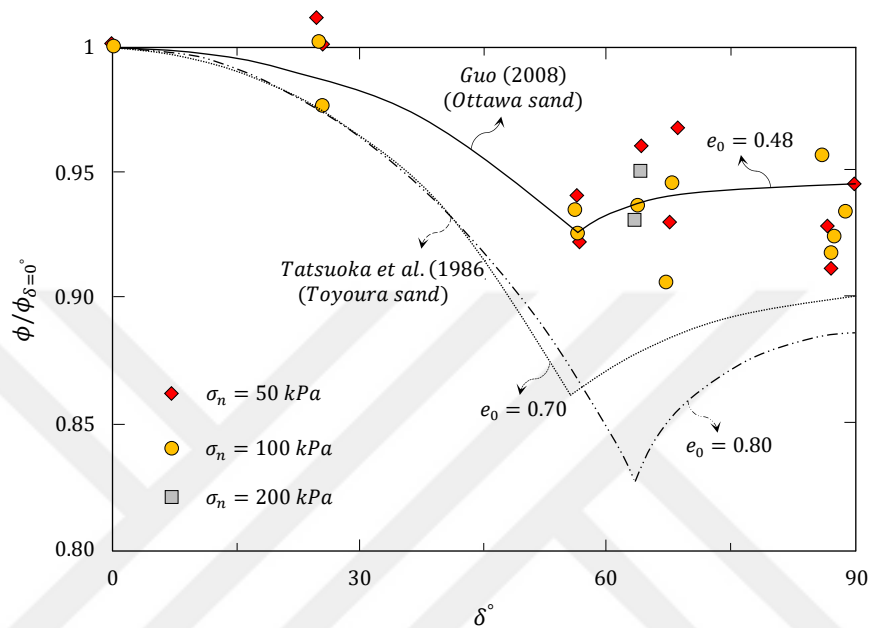


Figure 2.33. Effect of angle δ on anisotropic strength properties of sands (Guo, 2008)

When the results were evaluated in general, it was seen that both angular terms δ and ξ were effective on anisotropic strength in the studies based on plane strain (Tatsuoka et al., 1986; Lam and Tatsuoka, 1988), while the expression ξ was not effective on the basis of direct shear as mentioned before. Furthermore, since the principal stress axes rotate within the shear zone in the direct shear test (during strain), care should be exercised when comparing the results of plane strain test results (particularly when the effect of principal stress directions on sand behavior cannot be neglected).

Park et al. (2008) investigated the effect of relative density on the strength and strain properties of sands by plane strain, direct shear, and triaxial test methods and comparatively analyzed them. In the study where Jumunjin sand as detailed in Table 2.20 was used, all the tests were performed at a constant shear rate, with a relative density of 0 – 100(%) and normal and confining pressure range of 100 – 200 (kPa) under drained conditions.

Table 2.20. Material properties of Jumunjin sand (Park et al., 2008)

Property	$D_{50}(mm)$	C_u	G_s	Void ratio		Particle size	Particle shape	Mineral	USCS
				e_{max}	e_{min}				
Value	0.595	1.402	2.65	0.843	0.617	medium	angular	quartz and others	SP

As a result of the study, strain softening and shear band formation were similar in the plane strain and triaxial methods for low and high densities, while they were not observed in the triaxial method for medium density. When the shear strength angles (ϕ') were compared, the highest values were obtained in the plane strain method for all density (I_D) cases ($\phi'_{ps} - \phi'_{tc} = 4^\circ - 9.5^\circ$; $\phi'_{ps} - \phi'_{ds} = 5^\circ - 10^\circ$), (Figure 2.34). The researchers derived various numerical correlations from the relationships $\phi' - I_D$ of different test methods, which could be used only for prediction purposes (independent of cohesion and disintegration effect).

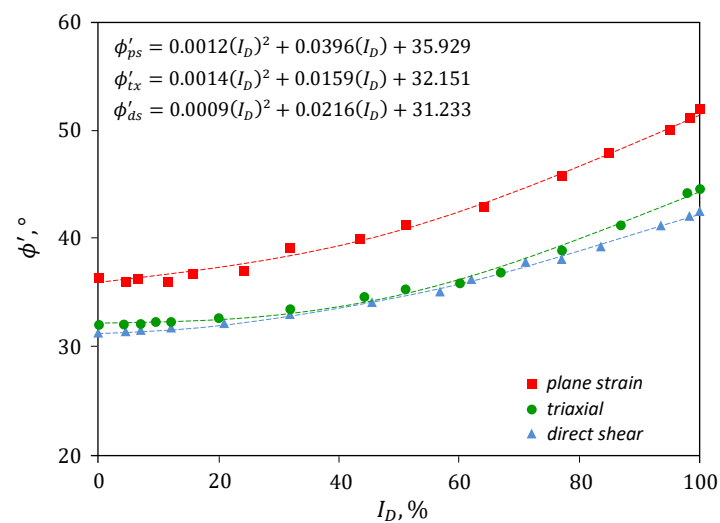


Figure 2.34. Relationships $\phi' - I_D$ for shear tests (Park et al., 2008)

Sadrekarami and Olson (2014) investigated the effect of particle crushing on critical state line (*CSL*) using granular materials as detailed in Table 2.21. In the study, the effects of particle characteristics, different specimen preparation techniques (pluvial and damp compression), drained and undrained conditions, void ratio and effective normal stress on the results were investigated and comparatively analyzed for different displacement conditions. Details of the tests are summarized in Table 2.22.

Table 2.21. Physical properties of the tested sands (Sadrekarami and Olson, 2014)

Material	$D_{50}(mm)$	C_u	G_s	Void ratio		Particle size	Particle shape	Mineral	USCS
				e_{max}	e_{min}				
Ottawa (20/40) (clean)	0.538	1.32	2.63	0.679	0.391	medium	rounded	quartz and others	SP
Illinois river (clean)	0.507	2.30	2.63	0.757	0.464	fine-medium	rounded subrounded	quartz and others	SP
Mississippi river (silty)	0.091	6.05	2.65	1.038	0.563	fine	subrounded subangular	albite and others	SP

Table 2.22. Details of the ring shear and triaxial tests (Sadrekarami and Olson, 2014)

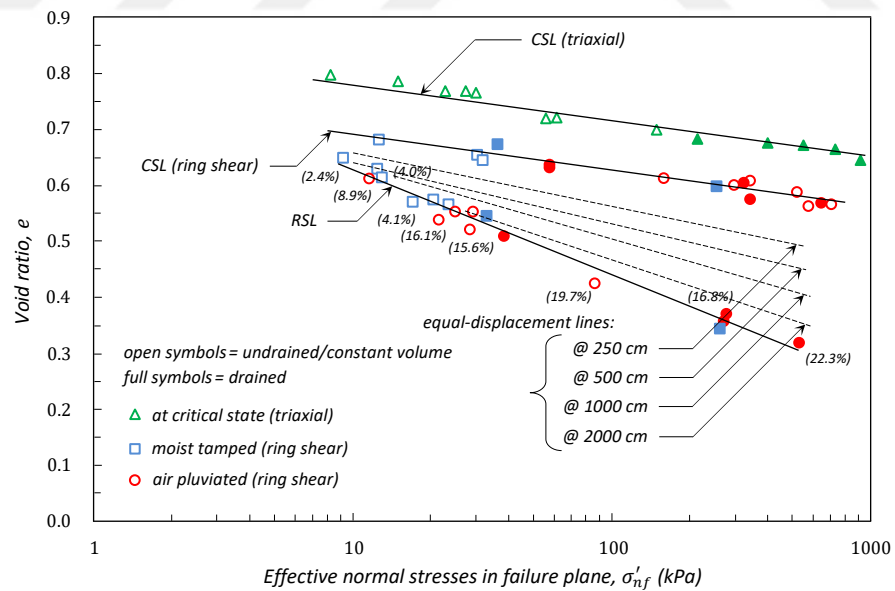
Test type	Dimensions of specimens(cm)			$D_r(\%)$	$\sigma'_n(kPa)$	Strain	
	r_{in}	r_{out}	h			rate(cm/dk)	level
Ring shear	20.3	27.0	2.6	56 - 88	28 - 728	18.6	> 10 m (Shear disp.)
Triaxial	5.08 (diameter)		10.16	60 - 93	85 - 773	0.127	%25 (Axial strain)

As a result of the study, it was seen that shear band formation and particle crushing are the important factors acting on ultimate (residual) state properties of granular materials. The researchers stated that materials reordered, rolled, and rearranged with negligible particle damage in critical state could be represented by the conventional critical state theory. Therefore, they stated that this theory will apply to the triaxial tests in this study where particle crushing was not encountered as well as other laboratory shear tests with limited displacement capacity (0.5 – 4 mm). The researchers reported that the soil that had a new particle size due to particle crushing in the shear band need great displacements to reach the critical state (Figure 2.35), which can be possible only with ring shear tests with large displacement capacities. Thus, a new residual state line (*RSL*) was defined for this state where the critical state line cannot be expressed with conventional theory. The researchers pointed out there were unique *CSL* and *RSL* lines for each sand and stated that they were

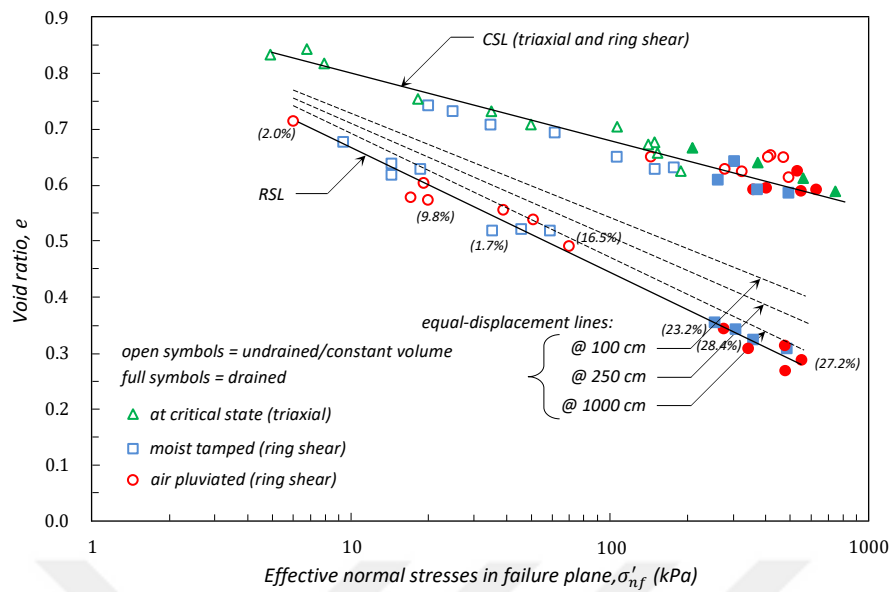
independent of specimen preparation methods, drainage conditions, stress path, initial effective normal stress, and void ratio (Figure 2.36).



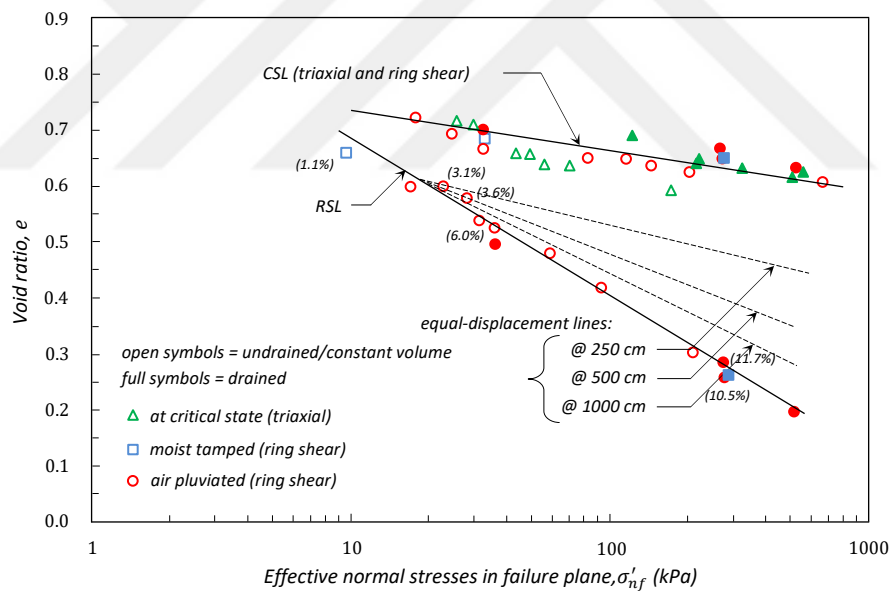
Figure 2.35. Specimens before and after ring shear test (from the shear band) (Sadrekarimi and Olson, 2010)



(a)



(b)



(c)

Figure 2.36. CSL and RSL lines of different sands: (a) Ottawa (20/40), (b) Illinois river sand, (c) Mississippi river sand (Sadrekarimi and Olson, 2014)

Noorzad and Zarinkolaei (2015) investigated the mechanical properties of fiber-reinforced sand soil and comparatively analyzed them. In the study, the relative density value was selected as 70%, the normal and confining pressure as 50, 100, 200, 400(kPa), the deformation level as 20%, the shear displacement rate as 1 mm/min for direct shear method and 0.35 mm/min for triaxial method; the fiber material lengths as 6, 12, 18 (mm), the ratio of fiber reinforcement weight to the weight of dry sand weight as $(W_f/W_s)(\%)$ 0 – 1. The material properties of uniform Babolsar sand and synthetic polypropylene fiber used in the study are given in Table 2.23 and Table 2.24, respectively.

Table 2.23. Material properties of Babolsar coast sand (Noorzad and Zarinkolaei, 2015)

Property	$D_{50}(mm)$	C_u	G_s	Void ratio		Particle size	Particle shape	Mineral	USCS
				e_{max}	e_{min}				
Value	0.19	1.7	2.74	0.86	0.58	fine	subrounded subangular	quartz and others	SP

Table 2.24. Material properties of polypropylene fiber (Noorzad and Zarinkolaei, 2015)

Property	G_s	Diameter (mm)	Length (mm)	Maximum tensile strength(MPa)	Melting temperature($^{\circ}C$)	Resistance to asides and alkalis	Color
Value	0.90	0.023	6, 12, 18	400	160-165	high	white

As a result of the study, higher peak strengths were obtained by the direct shear method in the unreinforced specimens, while by the triaxial method in the reinforced specimens. The researchers attributed this to the orientation of fiber reinforcement randomly placed within the soil. It was seen that the peak and ultimate strengths increased proportionally with the increase in fiber reinforcement length and concentration in both methods. It was observed that the strain at failure increased with increasing normal and confining pressure, fiber reinforcement concentration and length and this increase was more prominent in triaxial tests. On the other hand, it was seen that the fiber reinforcement increased ductility for all the methods, thus reducing brittleness, while it increased stiffness in the triaxial method but did not affect it in the direct shear method. The researchers stated that fiber reinforcement increased volumetric strain in the direct shear method but decreased it in the triaxial method, that it caused a slight increase in cohesion in the direct shear method but a significant increase in cohesion in the triaxial method, and that the failure envelope was linear for both methods.

The strength, stress-dilation and stiffness properties of well-graded sandy gravels were evaluated by Strahler et al. (2016a, 2016b) based on triaxial and plane strain methods and comparatively analyzed. The researchers compared their test data with the stress-dilation theories derived for various criteria and sandy soils and investigated their usability for well-graded sandy gravels. In the tests performed using Kanaskat sandy gravel ($D < 19.05 \text{ mm}$, $D_{50} = 6 \text{ mm}$, $C_u = 46$, subrounded grain shape, the main mineral of quartz) under drained conditions; the target relative density was selected as 65%, the shear strain rate as 0.05% per minute, the mean effective consolidation pressures (p'_c) as 10 – 1000(kPa) in the triaxial method and 28 – 172(kPa) in the plane strain method. As a result of the study, it was seen that the boundary conditions of various methods were highly effective on volumetric behaviors. Accordingly, the secant modulus (G_s) was obtained 1.5 times higher in the triaxial method (Figure 2.37), while in the plane strain method, the friction angle and the dilation angle were obtained 31% and 58% higher, respectively, than the other method.

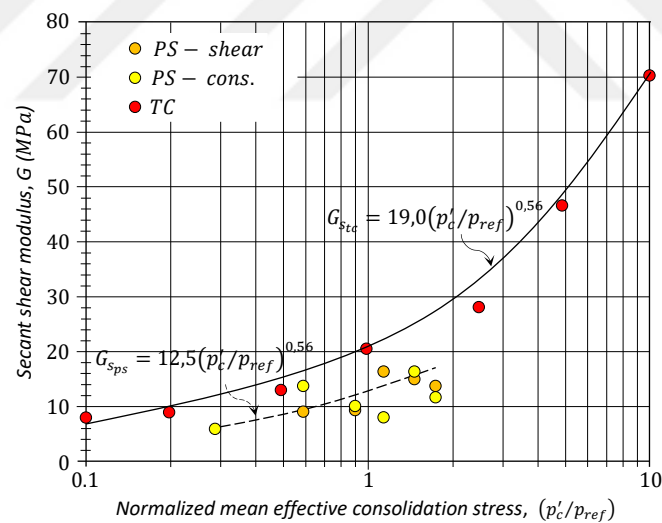


Figure 2.37. Initial shear modules for different stress paths ($\gamma_s = 0.05\%$, $p_{ref} = 101.3 \text{ kPa}$), (Strahler et al., 2016b)

When the failure criteria were compared, it was seen that Lade-Duncan's criterion (1973) was more consistent with the test results than Matsuoka-Nakai's criterion (1974). The researchers compared the relationships of the test data obtained with various empirical stress-dilation expressions (Figure 2.38 and Figure 2.39). In the evaluations, it was seen that Bolton's (1986) empirical stress-dilation relationship underestimated dilation size up to 22%

in average in well-graded sandy gravels and based on this relationship, the parameter (α) depending on the soil type and stress path was suggested as 1.08 and 0.58 for plane strain and triaxial state, respectively (Equation 2.87). The study where the approaches generally tended to underestimate concluded that the expressions developed in the literature might not apply to all soil and grading conditions.

$$\phi'_f = \phi'_{cv} + \alpha\psi_f \quad (2.87)$$

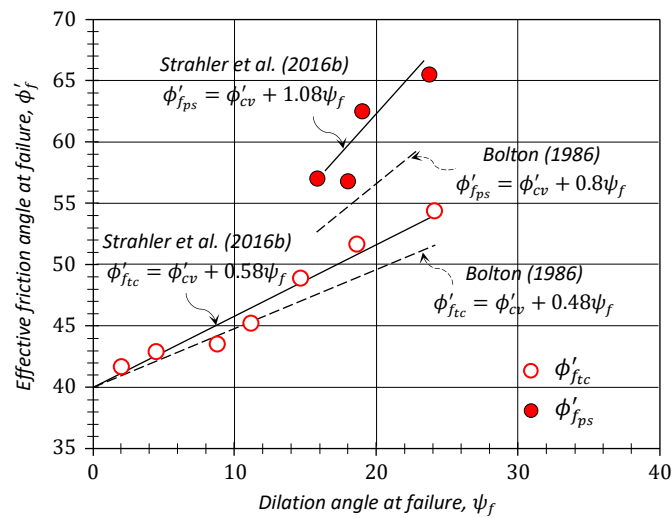


Figure 2.38. Comparison of effective friction and dilation angle (Strahler et al., 2016b)

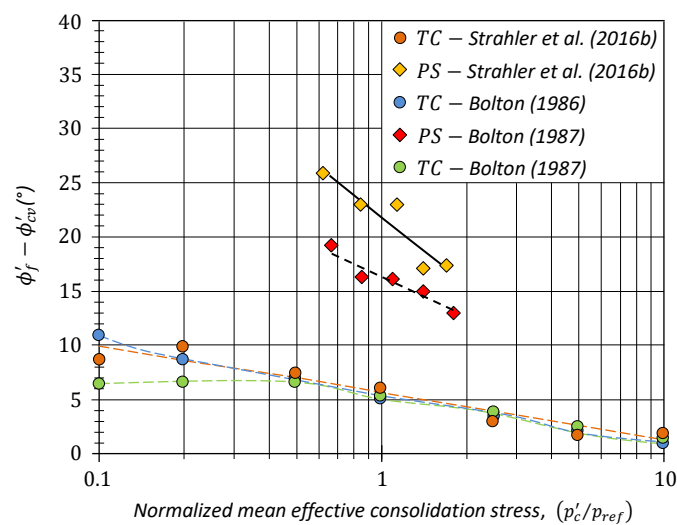


Figure 2.39. Comparison of the test results as a function of mean effective confining pressure with Bolton's (1986, 1987) approaches (Strahler et al., 2016b)

Dev et al. (2016) measured and comparatively analyzed the peak shear strength angles of plastic disc-added sands and fine-grained soils by triaxial and direct shear test methods. The researchers used uniform graded angular sand ($0.425 - 1.0 \text{ mm}$, $G_s = 2.67$, $C_u = 1.60$) and plastic disc ($D = 4.5 \text{ mm}$, $AR = 45$) as reinforcement in the tests where coarse-grained sands were used. In the study where all the tests were performed under drained conditions, the specimens ($B \geq 0.98$) prepared with a relative density of 65% and saturated with back pressure ($\geq 150 \text{ kPa}$) were consolidated under pressure of 50, 100, 200 (kPa) and sheared at a strain rate that was reevaluated within the obtained parameters based on Head's principle (1998). As a result of the study, greater strengths were obtained by the triaxial method in fine-grained soils and by the direct shear method in sands and it was seen that the plastic disc added to sands (10%) increased strength in the triaxial method but significantly decreased strength in the direct shear method (Table 2.25) and (Figure 2.40). This result is important since it shows that the addition of reinforcements to soils has different effects on strength properties depending on the test method.

Table 2.25. Effective shear strength angles from different methods (Dev et al., 2016)

No.	Soil	Effective shear strength angles ($^\circ$)		
		triaxial	direct shear	difference ($\phi'_{tc} - \phi'_{ds}$) $^\circ$
1	kaolin	29.5	21	8.5
2	IIT clay	28	20	8
3	silt	26.5	25.5	1
4	sand	42	44.5	-2.5
5	sand + plastic disc	45.5	35	10.5

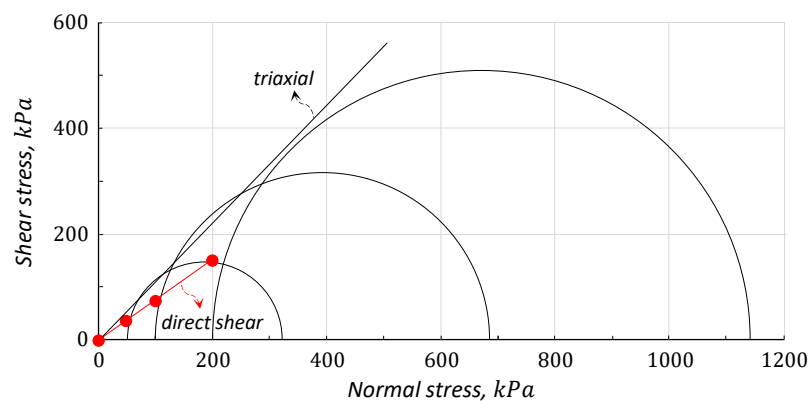


Figure 2.40. Failure envelopes of sands containing reinforcement from different methods (Dev et al., 2016)

Medzvieckas et al. (2017) used (simulated) Plaxis 3D software performing analyzes on the basis of the finite element method in order to evaluate the stress-strain states in sand specimens during the triaxial and direct shear tests. In the simulation analyses, Mohr-Coulomb model (assuming that soil shows linear elastic-perfectly plastic material behavior) was used, the strength (cohesion c , shear strength angle ϕ , dilation angle ψ) and strain (Elasticity module E , Poisson ratio ν) parameters of this model were obtained from a series of laboratory tests in which specimens prepared in dense form with angular fine sand materials were used (Table 2.26).

Table 2.26. Details of direct shear and triaxial tests (Medzvieckas et al., 2017)

Test type	Dimensions of specimens(mm)		e_0	σ'_n (kPa)	Strain	
	r	h			rate(mm/dk)	level
Direct shear	71.4	34.1	0.52	50-200	0.5	5 mm (shear disp.)
Triaxial	50	100	0.52	50-200	0.1	%14 (axial strain)

As a result of the study, it was seen that the peak and ultimate shear strength angles obtained by the direct shear method were 2.36° and 2.95° higher ($\phi'_{ds} - \phi'_{tc}$), respectively in the tests performed in laboratory setting. The researchers associated this difference with different stress-strain properties formed during the shear process. When the simulation analyses were evaluated, it was seen that in the direct shear method, the stresses in the shear plane were not equally distributed, and the shear stress and horizontal stress changed more than two and three times, respectively (Figure 2.41, Figure 2.42, Figure 2.43 and Figure 2.44); however, it was seen that in the triaxial method under uniform stress conditions, not only normal stress but also shear stress were effective on the shear strength of specimens (Figure 2.45, Figure 2.46 and Figure 2.47). The fact that the obtained analysis data were consistent with the laboratory test data and observations showed that such analyses can be used for practical purposes such as having preliminary information, understanding/evaluating the system behavior, etc.

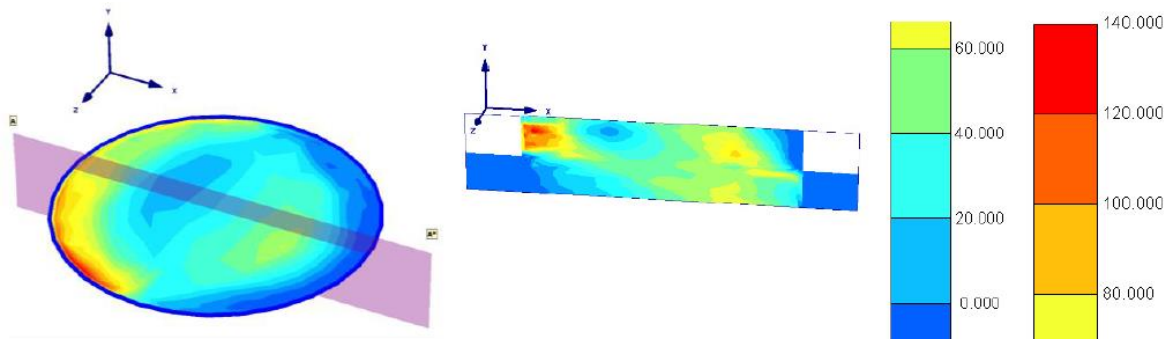


Figure 2.41. Mobilized shear strength distribution (kPa) in shearing plane and in $(A - A)$ cross section (Medzvieckas et al., 2017)

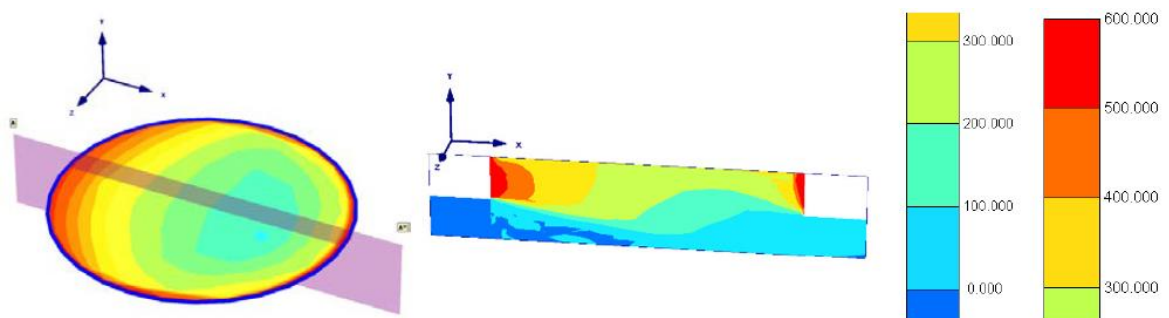


Figure 2.42. Displacement distribution $u_x (10^{-3}m)$ in shearing plane and in $(A - A)$ cross section (Medzvieckas et al., 2017)

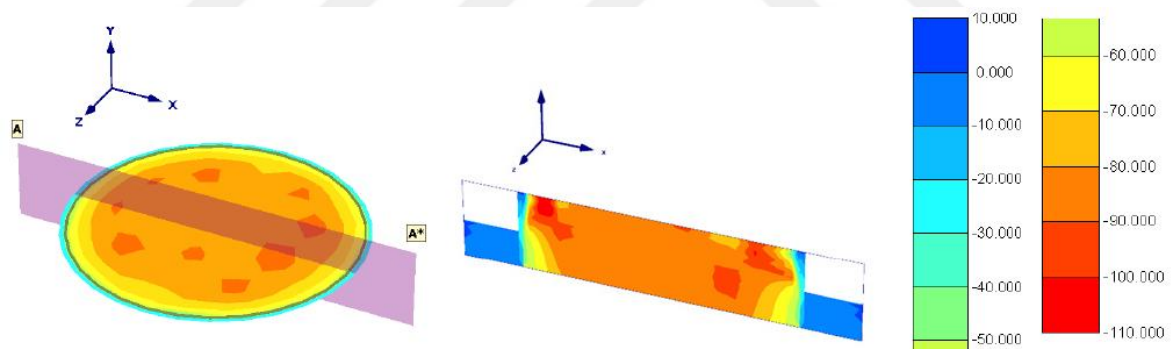


Figure 2.43. Distribution of vertical stresses $\sigma_y (kPa)$ after an initial compression phase in shearing plane and in cross section $(A - A)$ (Medzvieckas et al., 2017)

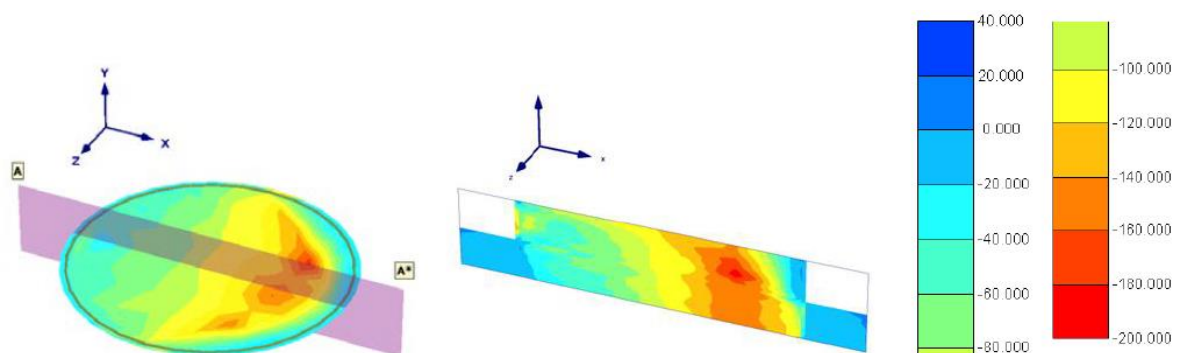


Figure 2.44. Distribution of vertical stresses $\sigma_y (kPa)$ at failure in shearing plane and in cross section $(A - A)$ (Medzvieckas et al., 2017)

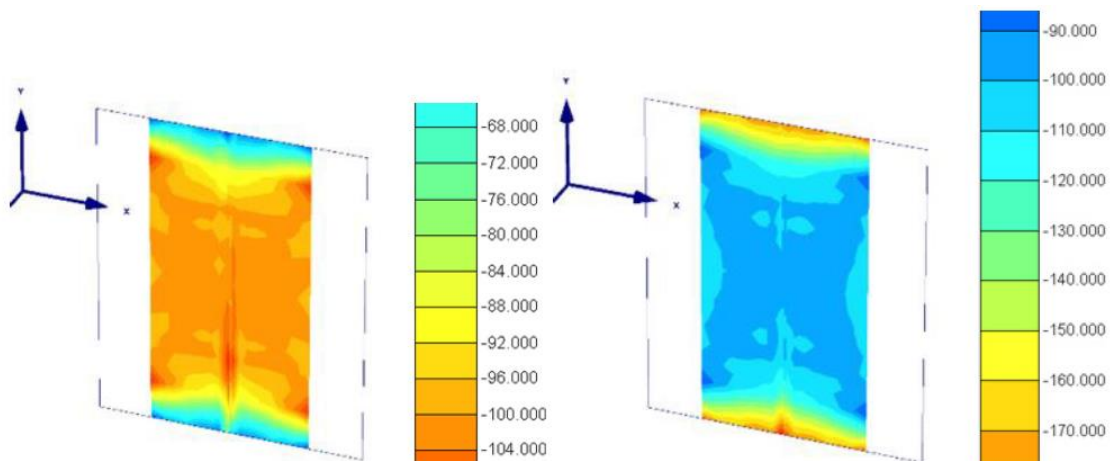


Figure 2.45. Distribution of horizontal stresses $\sigma_x(kPa)$ at confining pressure and failure phase (Medzvieckas et al., 2017)

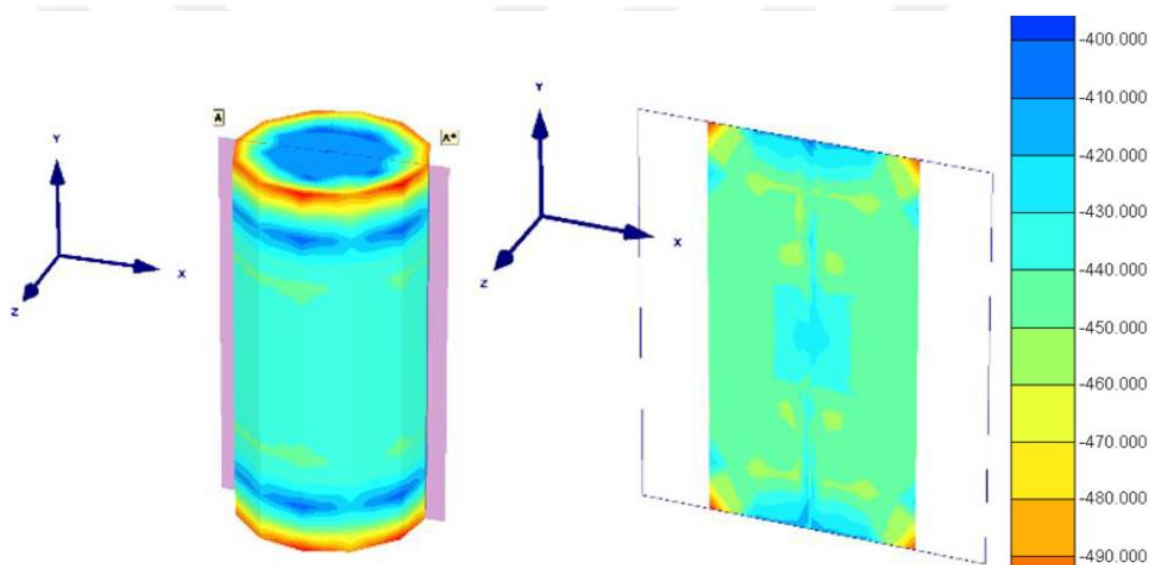


Figure 2.46. Distribution of horizontal stresses $\sigma_y(kPa)$ in the whole specimen and in cross section (A – A) at failure (Medzvieckas et al., 2017)

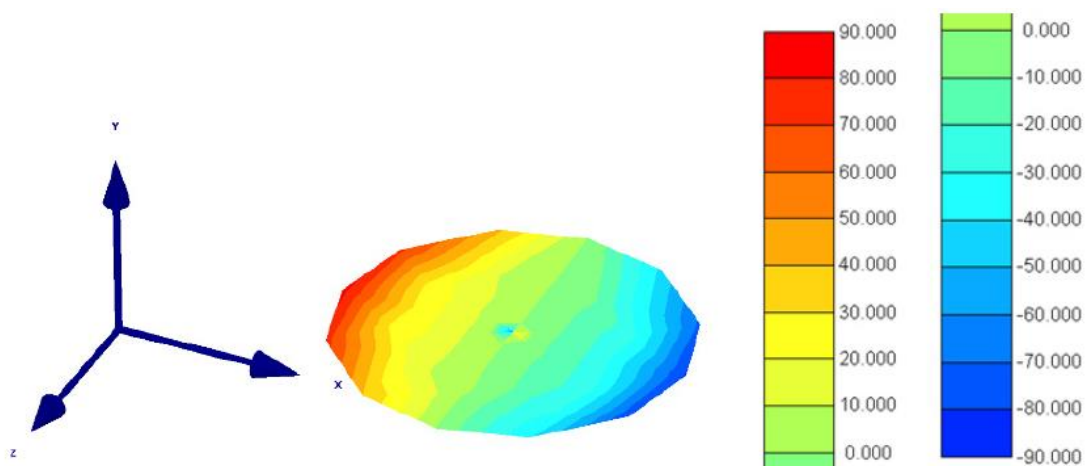


Figure 2.47. Distribution of shear stress $\tau_{xy}(kPa)$ under the cap at failure (Medzvieckas et al., 2017)

Hanna and Ayadat (2019) used the results of the empirical studies performed by Hanna and Massoud (1981) and Hanna (2001) when comparing the shear strength properties of sands obtained by different test methods. In these analyses, shear strength angle, dilatancy factor, particles interlocking, volumetric and axial strains were taken as the evaluation parameter and their effects on relative density or porosity were investigated. The researchers evaluated the results of these analyses on the basis of relative density, dilatancy factor, and particles interlocking and aimed various correlations for different test methods based on the flow rule (e.g., Rowe, 1962).

The researchers evaluated the results of empirical studies and stated that higher shear strength angles were obtained by the plane strain method for each void ratio and that this angle was lower at low porosity levels in the triaxial method and at high porosity levels in the direct shear method (Figure 2.48). When the volumetric and axial strains at failure (same porosity and confining pressure) were evaluated, they stated that as a result of test boundary conditions, the highest strains were observed with the triaxial method (Figure 2.49). They concluded that the test results of these two and other parameters were consistent with the literature data and can be used for analysis purposes.

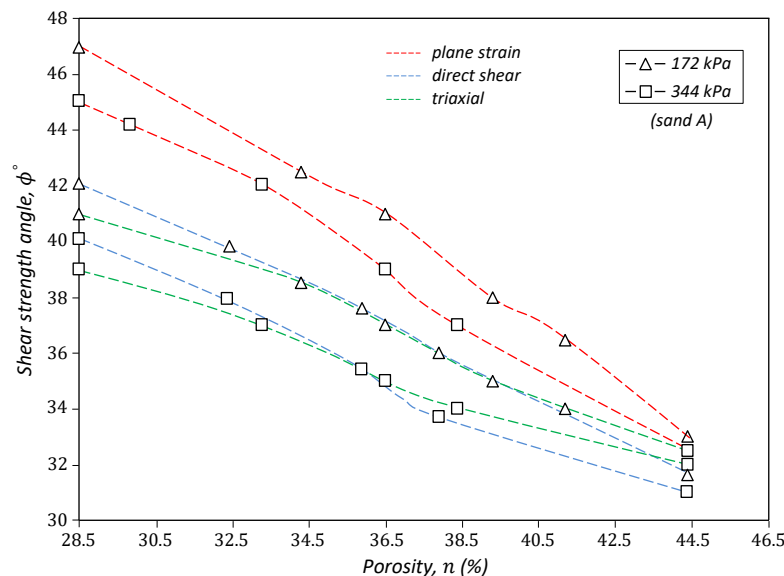


Figure 2.48. Peak shear strength angles from different methods, as a function of porosity (Hanna and Ayadat, 2019)

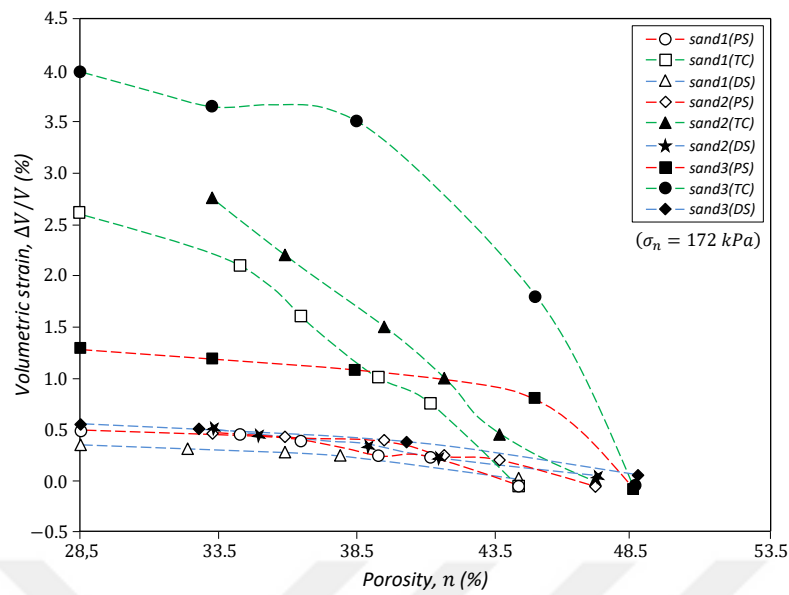


Figure 2.49. Effect of porosity on volumetric strains from different methods (Hanna and Ayadat, 2019)

Equation 2.89 was obtained by combining the expressions of Rowe (1962, 1969) in Equation 2.6, Equation 2.7, and Equation 2.18 with Equation 2.88 derived by Hanna (2011):

$$\tan \phi_{ps} \cos \phi_{cv} = \frac{(KD - 1)\sqrt{12D - 3D^2}}{4KD - KD^2 + 3D} \quad (2.88)$$

$$\tan \phi_{ds} = \frac{(KD - 1)\sqrt{12D - 3D^2}}{4KD - KD^2 + 3D} \quad (2.89)$$

Expression showing the relationship between the parameters of the stress-dilation relationship and the triaxial shear strength angle:

$$\sin \phi_{tc} = \frac{R - 1}{R + 1} = \frac{KD - 1}{KD + 1} \quad (2.90)$$

The following relationship was obtained between the triaxial method, and the direct shear method rearranged with Equation 2.89:

$$\sin \phi_{tc} = \frac{\overline{A}_1 \cdot \tan \phi_{ds}}{\overline{B}_1 \cdot \tan \phi_{ds} + \overline{C}_1} \quad (2.91)$$

The terms \overline{A}_1 , \overline{B}_1 and \overline{C}_1 in Equation 2.91 are constants that depend on dilation factor (D). These constants were expressed in terms of relative density (R_d) and defined as follows ($D = R_d + 1$):

$$\overline{A}_1 = 0.95(R_d + 3) \quad (2.92)$$

$$\overline{B}_1 = 1.9R_d \quad (2.93)$$

$$\overline{C}_1 = \sqrt{3}\sqrt{(1 + R_d)(3 - R_d)} \quad (2.94)$$

The procedure followed for the direct shear and triaxial method was applied for the plane strain and triaxial method and the following relationship was derived:

$$\tan \phi_{ps} \cos \phi_{cv} = \frac{\overline{A}_2 \sin \phi_{tc}}{\overline{B}_2 \sin \phi_{tc} + \overline{C}_2} \quad (2.95)$$

The researchers stated that the angle (ϕ_{cv}) in constant volume shear condition was equal for all the test methods ($\phi_{cv} = 30^\circ$ with 1% > error) and defined the dilation factor-dependant constants in terms of relative density:

$$\overline{A}_2 = \sqrt{3}\sqrt{(1 + R_d)(3 - R_d)} \quad (2.96)$$

$$\overline{B}_2 = -2R_d \quad (2.97)$$

$$\overline{C}_2 = R_d + 3 \quad (2.98)$$

3. SHEAR STRENGTH AND FAILURE CRITERIA OF SOILS

3.1. Introduction

“*Shear Strength*” is the most important engineering property of soils. This concept, which is defined as the maximum shear stress that occurs in the soil mass with the loading of soil medium and the soil can withstand along the shear surface, is used by geotechnical engineers in estimating the bearing capacity of foundations and in evaluating the stability of slopes and embankments, and the construction and design properties of retaining wall and various transportation structures.

In the first part of the section, the stress state in geotechnical applications is detailed, then the shear strength properties of sand soils and then the factors controlling these properties were discussed.

3.2. Stress State at a Point in Soil Mass

Soil mechanics is the application of laws of mechanics and hydraulics to sediments and other unconsolidated solid particles formed by the mechanical and chemical disintegration of rocks regardless of whether they contain organic substances (Terzaghi, 1943). Since soil is a particulate (grain) matter, it is voided (voids may be filled with water or air). Soil has specific characteristics such as heterogeneous structure, non-linear behavior, memory, non-linear stress-strain curves, physical and chemical interactions between components, which make its behavior so complicated. Due to this sophisticated structure of soil that cannot be modeled mathematically, it is assumed to be a homogeneous, isotropic, linearly elastic, and continuous material.

Stresses form on soil medium with the effects of self-weights of soil layers and external loads. When calculating these stresses, the special characteristics of soil mentioned above, and the assumptions used in continuum mechanics are taken into account to prevent possible uncertain complexities.

The stress vector acting on planes passing an infinitesimal soil mass is usually not perpendicular to the surface. The component of this inclined stress vector that is perpendicular to the plane section is called normal stress (compression or tensile) (σ), while its component within the plane is called shear stress (τ) (Figure 3.1).

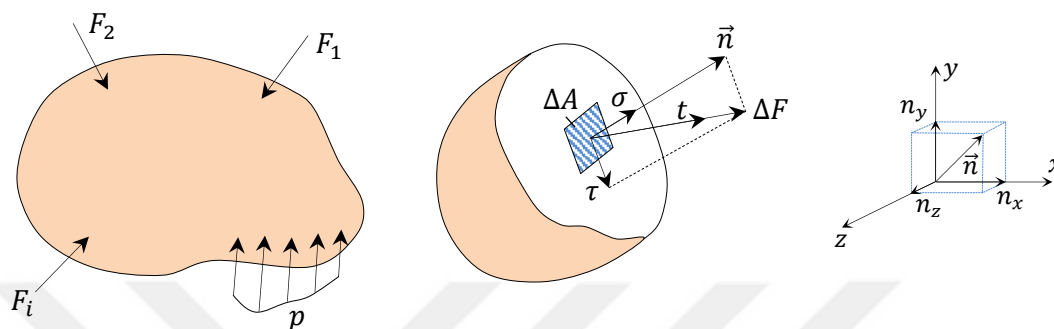


Figure 3.1. Stress definition of an infinitesimal soil that is exposed to external loads, around a point on any separated plane

The infinitesimal soil mass in Figure 3.1 is in equilibrium with external forces. In the section divided by the parting surface, the field element is represented by ΔA and the internal force acting on this element by ΔF . By approaching ΔA to zero, the stress vector was defined as in Equation 3.1 (Newton, 1686; Euler, 1757, 1771; Cauchy, 1823, 1827):

$$t^{\vec{n}} = \lim_{\Delta A \rightarrow 0} \frac{\Delta F}{\Delta A} = \frac{\partial F}{\partial A} \quad (3.1)$$

Infinite planes pass through a point. Among these planes, there are three special orthogonal planes. These planes on which only normal stresses act and thus there are no shear stresses are called principal stress planes. Normal stresses acting on the principal stress planes are also called principal stress. These stresses usually have different values (in order of magnitude, they are known as the major principal stress (σ_1), intermediate principal stress (σ_2) and the minor principal stress (σ_3)). Knowing the principal stresses at a point is important because stress state in all planes passing through that point would be learnt. In many problems in geotechnical engineering, it is assumed that the intermediate principal stress (σ_2) has no significant effect on failure. In such cases, the results are evaluated approximately by considering the two-dimensional stress condition.

Figure 3.2a shows the general stress components acting on infinitesimal soil element at any depth that is arranged with axes in soil medium. If a very fine soil mass in XZ plane is under the effect of forces in the same plane, stresses perpendicular to this plane do not form or form at negligible levels. In such cases, *plane stress state* assumption is adopted because it is adequate and makes the calculations simple. This assumption is useful for many geotechnical engineering applications (Figure 3.2b).

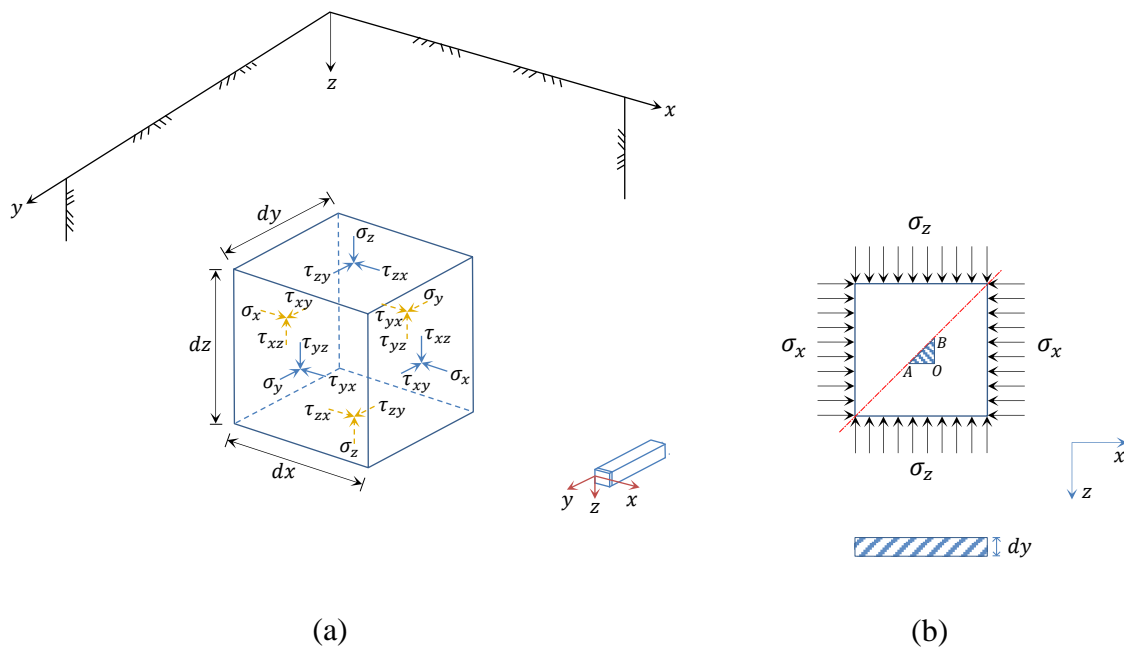


Figure 3.2. (a) Stress components of infinitesimal soil element, (b) Representative stress state reduced to two dimensions

When finding transformation equations for the plane stress state, the triangle prism in Figure 3.3a can be used. Because the most of forces used in geotechnical engineering are pressure, pressure forces and stresses are taken as positive when selecting the sign direction. Although the sign direction of shear stress is arbitrarily selected, the study of Merry and Lawton (2012) showed that for geotechnical engineering applications, taking the opposite direction of clockwise, which is generally accepted in conventional construction mechanics, as positive is important, which because meets static equilibrium conditions, especially for graphical solution of problems (Figure 3.3b).

By transforming the principal stresses acting on the triangle prism in Figure 3.3c into force, projection equations are obtained in ξ, η directions.

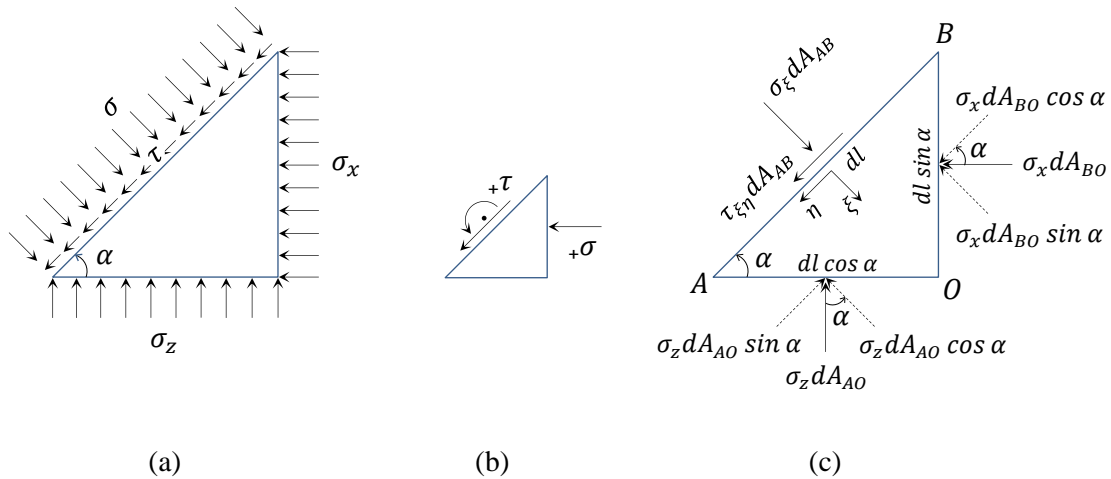


Figure 3.3. (a) Stresses acting on the triangle element, (b) Positive sign directions, (c) Separation of principal stresses in XZ plane into components

Prism thickness dy was considered and it was assumed that it was loaded with σ_x, σ_z stresses in orthogonal direction. Under this loading condition, vertical stress (σ_ξ) and shear stress ($\tau_{\xi\eta}$) on the inclined plane were obtained with force-balance equations written in ξ and η directions from

$\sum F_\xi = 0$ condition:

$$\sigma_\xi dA_{AB} - (\sigma_z dA_{AO} \cos \alpha) - (\sigma_x dA_{BO} \sin \alpha) = 0$$

$\sum F_\eta = 0$ condition:

$$\tau_{\xi\eta} dA_{AB} - (\sigma_z dA_{AO} \sin \alpha) + (\sigma_x dA_{BO} \cos \alpha) = 0$$

When these equations are simplified, the following relations are obtained for transformation equations:

$$\sigma_\xi = \sigma_z \cos^2 \alpha + \sigma_x \sin^2 \alpha \quad (3.2)$$

$$\tau_{\xi\eta} = (\sigma_z - \sigma_x) \sin \alpha \cos \alpha \quad (3.3)$$

The transformation equations can be also expressed differently using the following trigonometric expressions:

$$\begin{aligned} \cos^2 \alpha - \sin^2 \alpha &= \cos 2\alpha ; \cos^2 \alpha = \frac{1}{2}(1 + \cos 2\alpha) \\ \sin^2 \alpha &= \frac{1}{2}(1 - \cos 2\alpha) ; 2 \sin \alpha \cos \alpha = \sin 2\alpha \end{aligned}$$

Hence, the expressions in Equation 3.2 and Equation 3.3 can be transformed to the following forms, respectively:

$$\sigma_{\xi} = \frac{\sigma_z + \sigma_x}{2} + \frac{\sigma_z - \sigma_x}{2} \cos 2\alpha \quad (3.4)$$

$$\tau_{\xi\eta} = \frac{(\sigma_z - \sigma_x)}{2} \sin 2\alpha \quad (3.5)$$

If the equations above are squared, summed side by side and their angle-dependent terms (α) are simplified:

$$\left(\sigma_{\xi} - \frac{\sigma_z + \sigma_x}{2} \right)^2 + \tau_{\xi\eta}^2 = \left(\frac{\sigma_z - \sigma_x}{2} \right)^2 \quad (3.6)$$

The relation in Equation 3.6 is obtained. If the stresses in the planes defined with ξ and η directions are known, we obtain a circle with a radius of $r = \left(\frac{\sigma_z - \sigma_x}{2} \right)$ and its center at $(\sigma_M, 0), \sigma_M = \left(\frac{\sigma_z + \sigma_x}{2} \right)'$:

$$(\sigma - \sigma_M)^2 + \tau^2 = r^2 \quad (3.7)$$

If the relation above is drawn at an axis set of which horizontal axis is σ , and vertical axis is τ , as in Figure 3.4, stresses in all planes passing through a point can be shown by a simple circle called *Mohr's Circle* (Culmann, 1866; Mohr, 1882).

σ_z and σ_x are the principal stresses acting on principal planes, as mentioned before. The major principal stress was taken as σ_z , the minor principal stress as σ_x , assuming $\sigma_z = \sigma_1$ and $\sigma_x = \sigma_3$:

$$\sigma_\xi = \frac{\sigma_1 + \sigma_3}{2} + \frac{\sigma_1 - \sigma_3}{2} \cos 2\alpha \quad (3.8)$$

$$\tau_{\xi\eta} = \frac{(\sigma_1 - \sigma_3)}{2} \sin 2\alpha \quad (3.9)$$

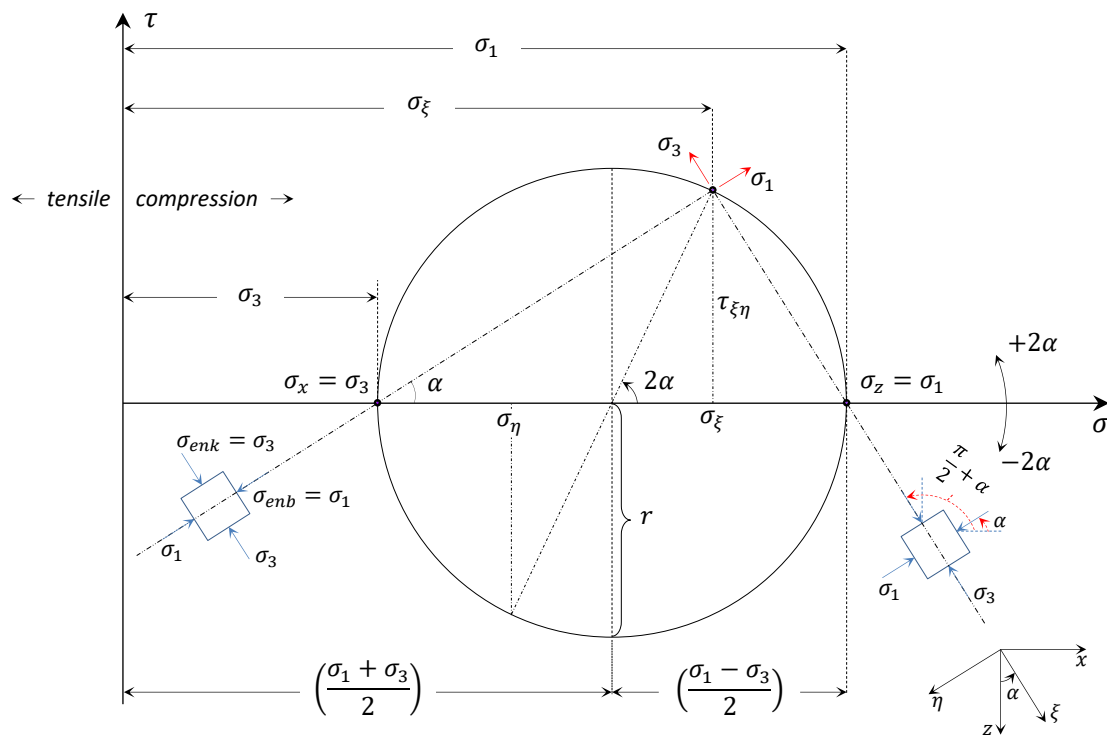


Figure 3.4. Mohr's stress circle for plane stress condition

3.3. Mohr-Coulomb Failure Criterion

In engineering, it is essential to know the strength properties of materials under stress. For this purpose, to describe failure or yielding, many criteria, particularly St. Venant (1837), Rankine (1843), Maxwell (1856), Tresca (1864), Beltrami (1885) were developed. Most of these criteria are not suitable for very special materials such as soil. And most of the criteria applicable to soil are not sufficient for every case. However, the most used one is Mohr-Coulomb's (1900) failure criterion with a simple and easy-to-understand mathematical and physical statement.

The results of the study, which was performed by Coulomb, a military engineer in the French army, to investigate the causes of failures that occurred in fortifications built against the British with whom they were in the colonial race, made the first major scientific contribution in understanding the soil behavior. Coulomb (1773) expressed the shear strength of soils as the sum of cohesion and friction components and defined this hypothesis with a linear relationship on the basis of total stress, as follows:

$$s = \tau_f = c + \sigma_f \tan \phi \quad (3.10)$$

Where, τ_f defines the shear strength of soil; σ_f , defines the total normal stress acting on shear plane; c and ϕ , which are the shear strength parameters defined on the basis of total stress, indicate apparent cohesion and shear strength angle of soil (internal friction angle), respectively.

Coulomb, in his theory, assumed that failure occurred along a plane with shear and mathematically expressed that its position could be determined by "*Maximum and Minimum Principles (Nova Method)*" (Leibniz, 1684); calculated the stress occurred in the shear plane using the laws of rigid body mechanics (Amontons, 1699 friction law; Musschenbroek, 1729 cohesion law) for solid and rock, for the first time. Contrary to this theory where shear stress is taken as the essential element in failure, Mohr (1900) demonstrated that failure is caused not only by shear stress or normal stress but also the critical combination of these acting together on the plane and generalized the theory. According to Mohr, who assumed that the intermediate principal stress (σ_2) has no effect on shear strength, failure occurs when shear

stress, as a function of normal stress, increases and becomes equal to shear strength in failure plane:

$$\tau_f = f(\sigma_f) \quad (3.11)$$

Mohr failure envelope represents the high-grade curve. In most geotechnical applications, taking the normal shear stress ($\sigma - \tau$) relationship as linear does not give results with sufficient accuracy. If the Mohr curve is taken linear and the relation is expressed with Coulomb parameters, then the Mohr-Coulomb failure criterion is obtained (Figure 3.5).

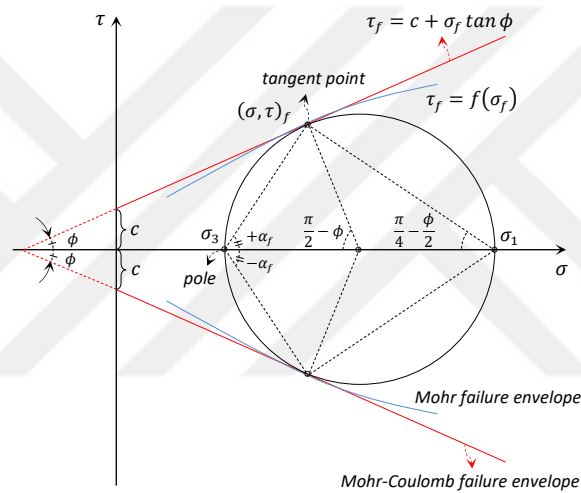


Figure 3.5. Mohr's diagram and failure envelopes

Although the Mohr-Coulomb theorem was used in various geotechnical applications during that period, it became important with the effective stress concept suggested by Terzaghi (1924, 1925). Terzaghi, in this theory, stated that the shear strength is formed only by grains, and other phases of soil (water and air) have no contribution to the strength and defined the concept "*effective stress*" to distinguish the stresses carried by the grains and the water.

$$\tau_f = c' + (\sigma_f - u_f) \tan \phi' \quad (3.12a)$$

$$\tau_f = c' + \sigma_f' \tan \phi' \quad (3.12b)$$

Where, effective normal stress in shear plane at failure is σ_f' , pore water pressure (neutral stress) is u_f , and shear strength parameters relative to effective stresses are c' and ϕ' .

Figure 3.6 shows the Mohr's circle showing the effective stress conditions at the time when soil failed, in other words, reached plastic equilibrium.

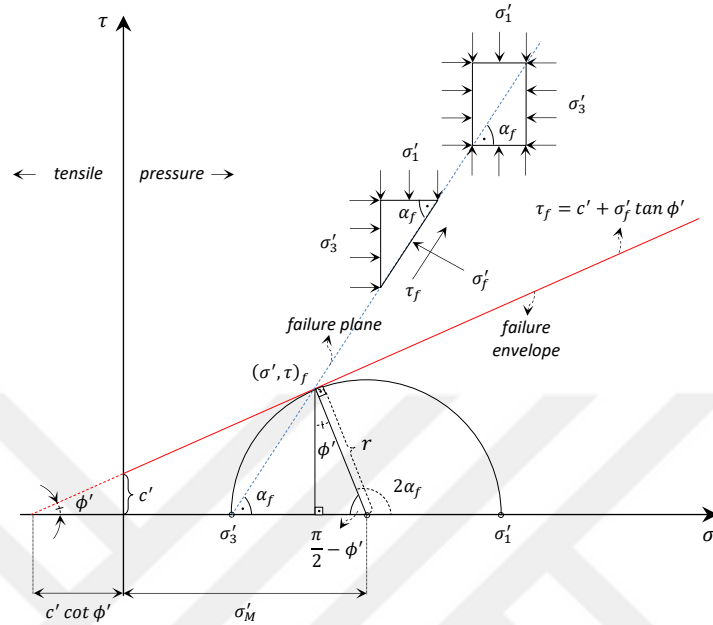


Figure 3.6. Failure state according to Mohr-Coulomb criterion

The geometric relationship between the effective shear strength angle and the angle of the failure plane with the principal axis ($\pi/2 - \phi' = \pi - 2\alpha_f$) is as in Equation 3.13:

$$\alpha_f = \frac{\pi}{4} + \frac{\phi'}{2} \quad (3.13)$$

The mathematical expression of the Mohr-Coulomb criterion can be obtained with the radius of the Mohr's circle and its distance from center to origin. In Figure 3.6, if $\sin \phi' = r / (c' \cot \phi' + \sigma'_M)$ is considered, the parameters ϕ' and c at failure can be written as follows:

$$\sin \phi' = \frac{\frac{1}{2}(\sigma'_1 - \sigma'_3)}{c' \cot \phi' + \frac{1}{2}(\sigma'_1 + \sigma'_3)} = \frac{(\sigma'_1 - \sigma'_3)}{(\sigma'_1 + \sigma'_3 + 2c' \cot \phi')} \quad (3.14)$$

$$c' = \frac{\sigma'_1(1 - \sin \phi') - \sigma'_3(1 + \sin \phi')}{2 \cos \phi'} \quad (3.15)$$

The expressions in Equation 3.14 and Equation 3.15 are combined and Equation 3.16 is obtained:

$$\left(\frac{\sigma'_1 - \sigma'_3}{2}\right) - \left(\frac{\sigma'_1 + \sigma'_3}{2}\right) \sin \phi' - c' \cos \phi' = 0 \quad (3.16)$$

By rearranging the expression in Equation 3.16, the following relationship can be written between the effective principal stress and shear strength parameters:

$$\sigma'_1(1 - \sin \phi') - \sigma'_3(1 + \sin \phi') - 2c' \cos \phi' = 0 \quad (3.17)$$

The statement above is re-expressed in terms of the major and minor effective principal stresses and associated with the shear strength parameter:

$$\sigma'_1 = \sigma'_3 \left(\frac{1 + \sin \phi'}{1 - \sin \phi'} \right) + 2c' \left(\frac{\cos \phi'}{1 - \sin \phi'} \right) \quad (3.18)$$

$$\sigma'_3 = \sigma'_1 \left(\frac{1 - \sin \phi'}{1 + \sin \phi'} \right) - 2c' \left(\frac{\cos \phi'}{1 + \sin \phi'} \right) \quad (3.19)$$

Equation 3.18 and Equation 3.19 are rearranged using the following trigonometric expressions:

$$\frac{1 + \sin \phi'}{1 - \sin \phi'} = \tan^2 \left(\frac{\pi}{4} + \frac{\phi'}{2} \right); \quad \frac{1 - \sin \phi'}{1 + \sin \phi'} = \tan^2 \left(\frac{\pi}{4} - \frac{\phi'}{2} \right)$$

$$\frac{\cos \phi'}{1 - \sin \phi'} = \tan \left(\frac{\pi}{4} + \frac{\phi'}{2} \right); \quad \frac{\cos \phi'}{1 + \sin \phi'} = \tan \left(\frac{\pi}{4} - \frac{\phi'}{2} \right)$$

Hence, the following relations are obtained for the major (Equation 3.20) and minor (Equation 3.21) effective principal stresses:

$$\sigma'_1 = \sigma'_3 \tan^2 \left(\frac{\pi}{4} + \frac{\phi'}{2} \right) + 2c' \tan \left(\frac{\pi}{4} + \frac{\phi'}{2} \right) \quad (3.20)$$

$$\sigma'_3 = \sigma'_1 \tan^2 \left(\frac{\pi}{4} - \frac{\phi'}{2} \right) - 2c' \tan \left(\frac{\pi}{4} - \frac{\phi'}{2} \right) \quad (3.21)$$

The shear strength parameters in these practical relations that allow expressing the Mohr-Coulomb failure criterion in terms of effective principal stresses can be simplified according to the soil characteristics.

3.4. Stress-Strain Behavior of Sands

The shear strength parameters of soils (c, ϕ) take different values for different drainage and loading conditions (in the same soil). This shows that the shear strength parameters are the terms representing certain conditions, rather than a physical property of soil.

Cohesion that is the component of shear strength from normal stress is defined as molecular attractive force between the same kinds of materials. This concept, which is the adaption of tensile force to soils in the rigid body mechanics, is used in two different ways; Coulomb's (1773) "apparent cohesion" definition that is related to the absorption effect of void water pressure, not related with geotechnical engineering applications except for name similarity, and Hvorslev's (1936a) "true cohesion" definition that is a function of soil water content without effective stress.

Clean sands, gravels and non-plastic silts constitute cohesionless soil group. Materials in this group show no cohesion or negligible cohesion ($0 - 2 \text{ kPa}$)_{max} in dry state or under water (cementation, negative void water pressure, etc.), except for some exceptional cases. Then, the expressions in Equation 3.10 and 3.12 defined for general soils can be simplified as follows ($c = 0$).

$$\tau_f = \sigma_f \tan \phi \quad (3.22)$$

$$\tau_f = \sigma'_f \tan \phi' \quad (3.23)$$

The second equation is more essential because the shear strength of soils is mainly formed by intergranular contact surface action.

A cohesionless soil such as sand derives its shear strength from friction. This term takes into account the common effect of the interlocking effect and the shear and rolling friction formed by the relative motion of grains. Rowe (1962) evaluated this relationship on the basis of volume change (Reynolds, 1885), Lee and Seed (1967) defined a new component formed by the crushing of grains at high confining pressures. These relationships are schematically shown in Figure 3.7 and Figure 3.8.

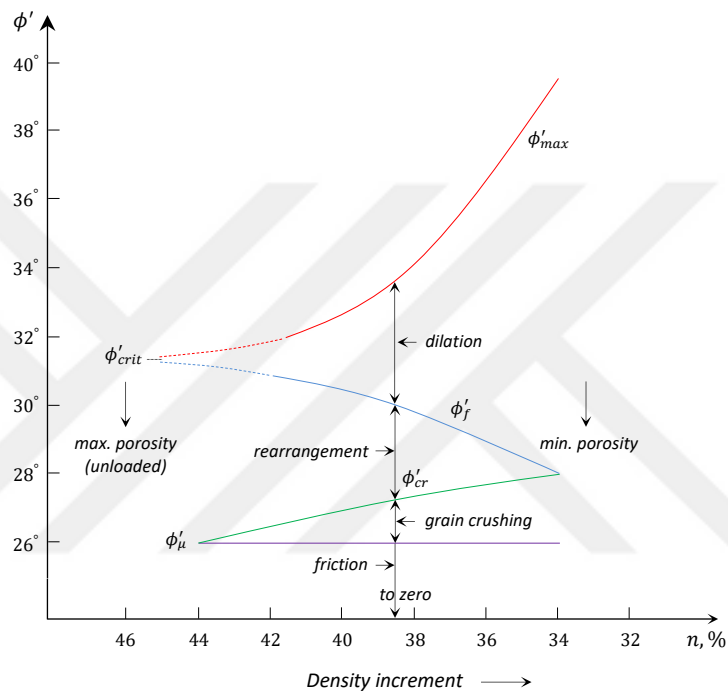


Figure 3.7. Shear strength components of sand (based on porosity) (Rowe, 1962; Lee and Seed, 1967)

In Figure 3.7, the components of effective friction angle ϕ'_{max} : $\phi'_f = (\phi'_{max} - \text{dilation})$ indicates rearrangement, ϕ'_{cr} crushing, ϕ'_{μ} mineral friction. ϕ'_{crit} is the effective critical friction angle.

Reynolds, who was mostly known for his studies on fluid mechanics, defined a dimensionless number to characterize the flow regime of viscous liquids, evaluated the studies of various researchers including (Reynolds, 1883); Navier (1822), Cauchy (1823), Poisson (1831), St. Venant (1843), Stokes (1845) on the dynamic behavior characteristics of liquids, and applied the phenomenon of volume increase observed in viscous materials under pressure to grained (granular) materials.

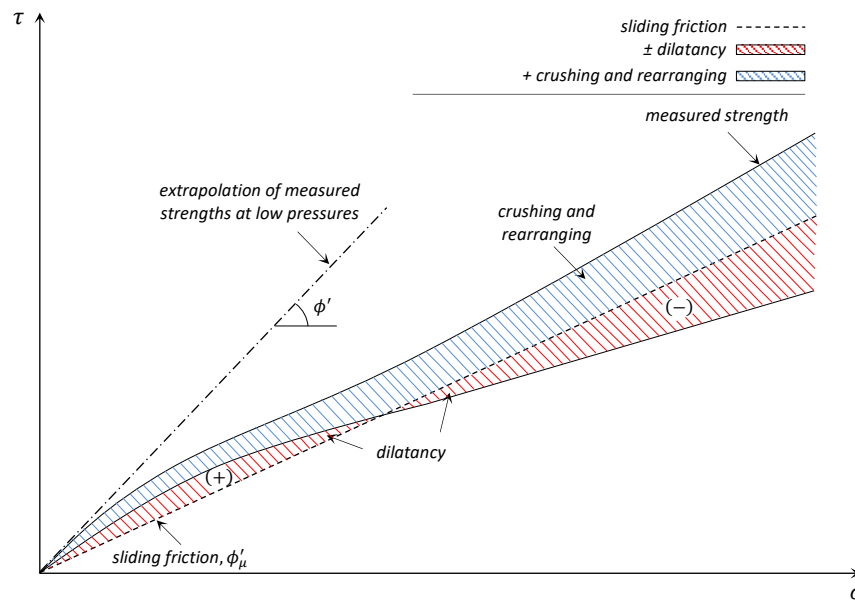


Figure 3.8. Mohr failure envelope components of sand at high confining pressures (Lee and Seed, 1967)

When granular materials are sheared by force, they undergo volume change. Reynolds (1885) defined this as compression for loose sands and as dilation for dense sands. Reynolds, who attributed the volume change in properly arranged rigid spheres at the time of shearing to the initial arrangement of the spheres, showed that the shear stresses of the spheres being subjected to strain might act differently from the direction of application. The concept of dilation is important because it successfully explains the stress, strain, and strength behaviors of granular materials.

The study performed by Reynolds with ideal rigid spheres assumed smooth showed that contrary to what was known until then, the shear strength depends on not only friction between spheres but also the volume change. Terzaghi (1920) was the first researcher who used this concept in soil mechanics applications and defined the conventional soil pressure theories, which did not consider volume change even in soils containing granular materials (Coulomb, 1773; Rankine, 1857), as outmoded.

Reynolds compared the strain properties of sands put in a water-proof canvas bag in dry and saturated conditions and thus did not measure the effect of density difference on strength properties when defining the phenomenon of dilation. Casagrande (1936) measured

the strength properties of materials with different densities and defined the concept of critical void ratio (e_{crit}), thus the subject could be investigated deservedly. Casagrande, in his study whose results are presented in Figure 3.9, stated that the volume (void ratio) of loose sand specimens decreased with the increasing shear stresses in a series of direct shear tests performed under drained conditions, while the volume of dense sand specimens slightly decreased in the beginning and then increased; and empirically showed the critical void ratio at which the void ratio was theoretically equal for both cases after a certain strain level under a constant normal stress. However, for dynamic conditions, this relationship was first noted by Castro (1969), his student, with undrained triaxial tests (stress controlled).

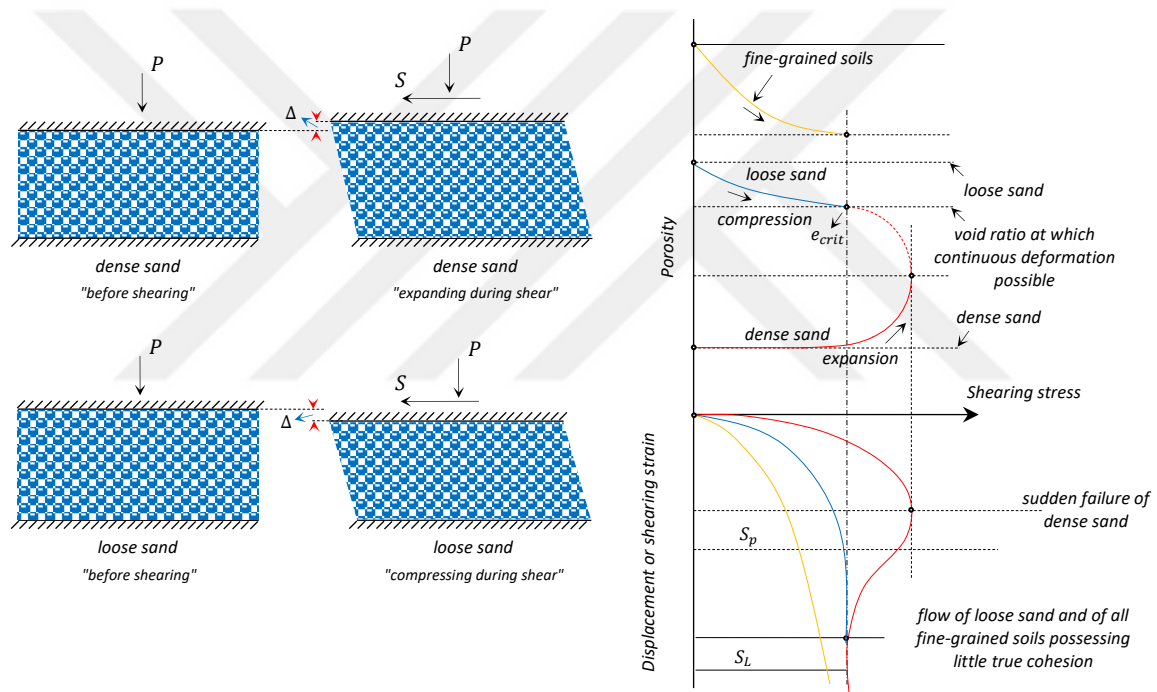


Figure 3.9. Effect of shearing force on the volume of soils (Casagrande, 1936)

In Figure 3.9, shear stress is represented by S , normal pressure in the shear plane by P , volume change by Δ , constant shear stress by S_L , and the greatest shear stress by S_p .

The first mechanical definition of the concept of dilation was suggested by Taylor (1948). Taylor, in his study, investigated the friction-dilation effect on dense sands using the results of a series of direct shear tests performed with Ottawa sand. Thus, the components of the strength of granular soils were separated for the first time. Taylor described the friction

term with the resistance between grains during shear distortion, while the dilation term with the work performed for volume increase during this distortion. This concept suggested by Taylor was first formulated by Bishop (1950) and is given with Schofield's (1998) presentation as below:

$$\tau \partial x = (\mu \sigma' \partial x) + (\sigma' \partial y) \quad (3.24)$$

The relation above representing the work performed at peak strength may be arranged with " $\sigma' dx$ " and expressed as follows:

$$\tau / \sigma' = (\mu) + (\partial y / \partial x) \quad (3.25)$$

Where, shear strength is represented by τ , effective normal stress by σ' , friction coefficient by μ , horizontal direction by x , and vertical direction by y .

The relationship of ∂x representing the shear distortion with ∂y as a measure of volume change in the vertical direction is important because it shows the interlocking level of sand. Accordingly, the strength at the greatest value of $\partial y / \partial x$ expression represents the peak, while the ratio $\partial y / \partial x$ approaching to zero with the increasing ∂x expression shows the strength is "critical" represented only the friction term.

The study of Taylor is important because it explained the phenomenon of dilation using the energy principles for the first time. After Taylor, other researchers including Skempton and Bishop (1950), Bishop (1954), Newland and Allely (1957), et al. made various contributions to this subject however, their methods were technically incorrect because they took into account only the effect of required energy (external work) to overcome the strength of granular soil. Unlike the previous researchers, Rowe (1962) took into account internal work, thus developed the first stress-dilation model based on minimum energy rate. Hence:

$$\frac{\sigma'_1}{\sigma'_3} = \left(1 + \frac{\partial v}{\partial \varepsilon_1}\right) \tan^2 \left(\frac{\pi}{4} + \frac{\phi_u}{2}\right) \quad (3.24)$$

Where, σ'_1 and σ'_3 represent the major and minor effective principal stress, respectively; v volumetric unit strain, and ε_1 the major principal stress. Using the relations of energy consumption during the shear of granular materials, the relationships between effective principal stress ratio and strain increment rates in the principal stress direction are obtained for triaxial compression, triaxial tensile and plane strain test methods (Rowe, 1962, 1969; Rowe et al., 1964).

It is essential to accurately define dilation, which is the ratio of plastic volumetric strain increment to plastic deviator strain increment, for the estimation of stress-strain behaviors of soils (Mitchell and Soga, 2005). After this leading study of Rowe (1962) who gave dilation as a function of stress ratio and expressed the strength properties of soils in terms of volume change, many important studies have been conducted on this subject by various researchers, particularly Cornforth (1964), Lee and Seed (1967), Roscoe and Burland (1968), Vesic and Clough (1968), Bishop (1971), de Jong (1976), Bolton (1986), Houlsby (1991), Vaid and Sasitharan (1992), Wan and Guo (1998), Salgado et al. (2000), Chakraborty and Salgado (2010), Lau and Bolton (2011), Sadrekarimi and Olson (2011), Zhao et al. (2013), Strahler et al. (2015, 2018), Guida et al. (2019). This section reveals the relationship between strength parameters and explains the study of Bolton (1986) that made a great contribution to this subject.

Combining the strength and dilation data of 17 different sands evaluated based on axisymmetric or plane strain at different density and confining pressure, Bolton (1986) investigated the relationship between the peak effective shear angle and the peak dilation rate (maximum dilation angle), the variation of dilation with respect to effective stresses, and the effect of both relative density and particle crushing on the behavior properties of sands. Bolton (1979, 1986, 2018) stated that the effective shear strength angle (ϕ') varied by stress and density is of great importance for engineers, summarized different types of shear test behaviors as follows, and mentioned that various theoretical models were developed within these principles:

1. A certain sand soil has only one ultimate (residual) internal friction angle (ϕ'_r), regardless of its initial density. In other words, ϕ'_r is independent of initial density and confining pressure.

2. The sands that are initially dense have higher peak strength (τ_p) than their ultimate strengths (τ_r). The sands that have reached this strength reach the critical density with the increasing volume as a result of thin failure zones formed due to the increased strain (δ). The strength and strain parameters of a typical direct shear test for a highly dense specimen (e.g., $D_r = 95\%$) can be compared as follows.

$$\tau_p \gg \tau_r \quad , \quad \phi'_p \gg \phi'_r \quad , \quad \delta_p \ll \delta_r$$

3. The sands that are initially loose remain at a constant ultimate strength level without reaching peak strength with the increasing strain. Thus, the specimen volume decreases, its density increases, and the strength is fixed at a certain critical void ratio. The critical strength at this moment should not be considered different from the ultimate strength.
4. The peak shear strength angle of dense soils depends on the dilation rate (Figure 3.10).

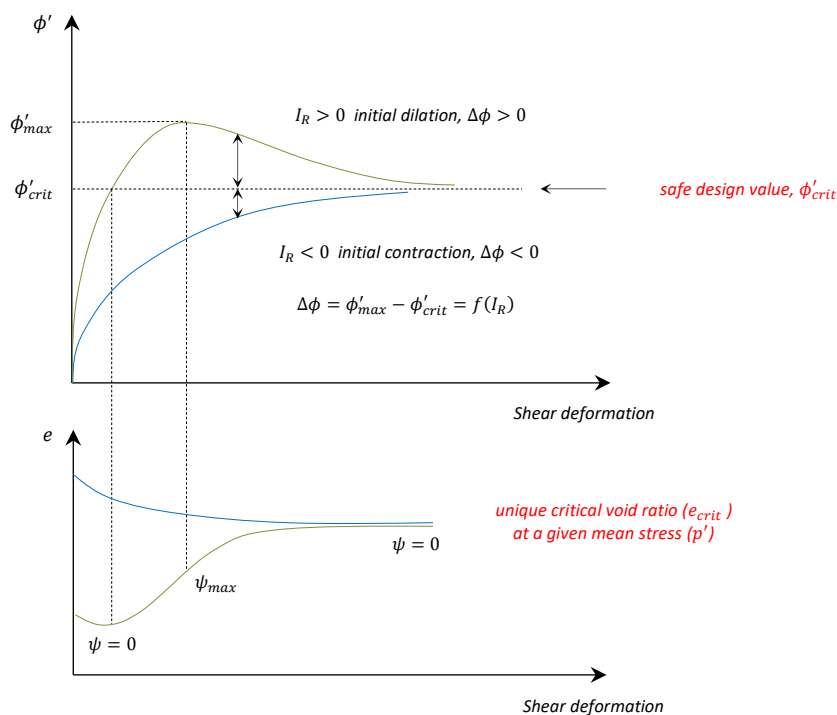


Figure 3.10. Contribution of dilation to internal friction (Bolton, 2018)

5. Although sand soils do not show a general dilation property, they have grains that interlock to each other with friction if they are forced to relative motion.

$$\phi'_{crit} \gg \phi'_\mu$$

6. Crushing of dense sands as a result of high stresses to which they are exposed reduces their dilation properties but increases their shear strengths. In other words, dense sands behave like loose sands.

Newland and Allely (1957) evaluated the friction-dilation relationship of granular soils (Taylor, 1948) with the relative strain of plates in the course of shearing and explained the interface with a simple saw blades model (Figure 3.11). This model was based on the fact that when the macro plane of shearing is horizontal, sand is sheared along a series of inclined micro planes that are parallel to each other (at the dilation angle of this rough inclined plane with horizontal). Bolton (1979, 1986) showed the relationships between the strength parameters of the model, as given in Equation 3.25 and Equation 3.11.

$$\phi' = \phi'_{crit} + \psi \quad (3.25)$$

In Equation 3.25, the term (ϕ') is the sum of critical friction angle (ϕ'_{crit}) and dilation component (ψ) representing the interlock degree.

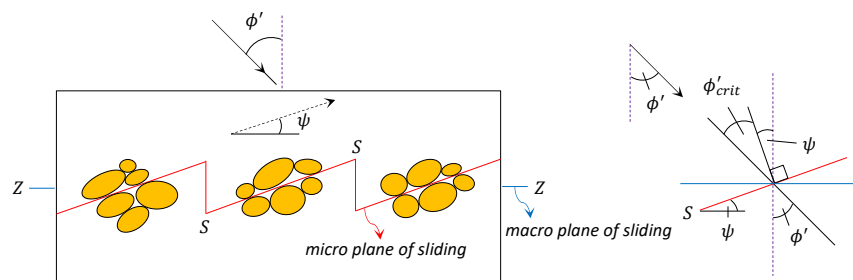


Figure 3.11. Illustration of dilation behavior with saw blades model (Bolton, 1979, 1986)

The concept of critical state is important in better understanding the friction behavior of soil. When a soil (granular) is sheared, it reaches the ultimate critical state with a single

stress ratio on the shear plane (Equation 3.26). The critical void ratio at that moment (on the shear zone) is a logarithmic function of stresses (Bolton, 1979).

$$\tan \phi'_{crit} = \frac{\tau}{\sigma'} \quad (3.26)$$

The initial void ratio decreases with the increasing strain (at constant effective normal stress, σ') in loose sands, while it increases and remains at a critical value (e_{crit}) that is independent from shear stresses in dense sands. All these relationships between void ratio (volume) and stresses are represented by an envelope called the critical state line (CSL) (Figure 3.12). Because this concept represents the stress state at failure, it is important, but it does not explain the peak strengths of dense sands (Schofield and Wroth, 1968; Bolton, 1979).

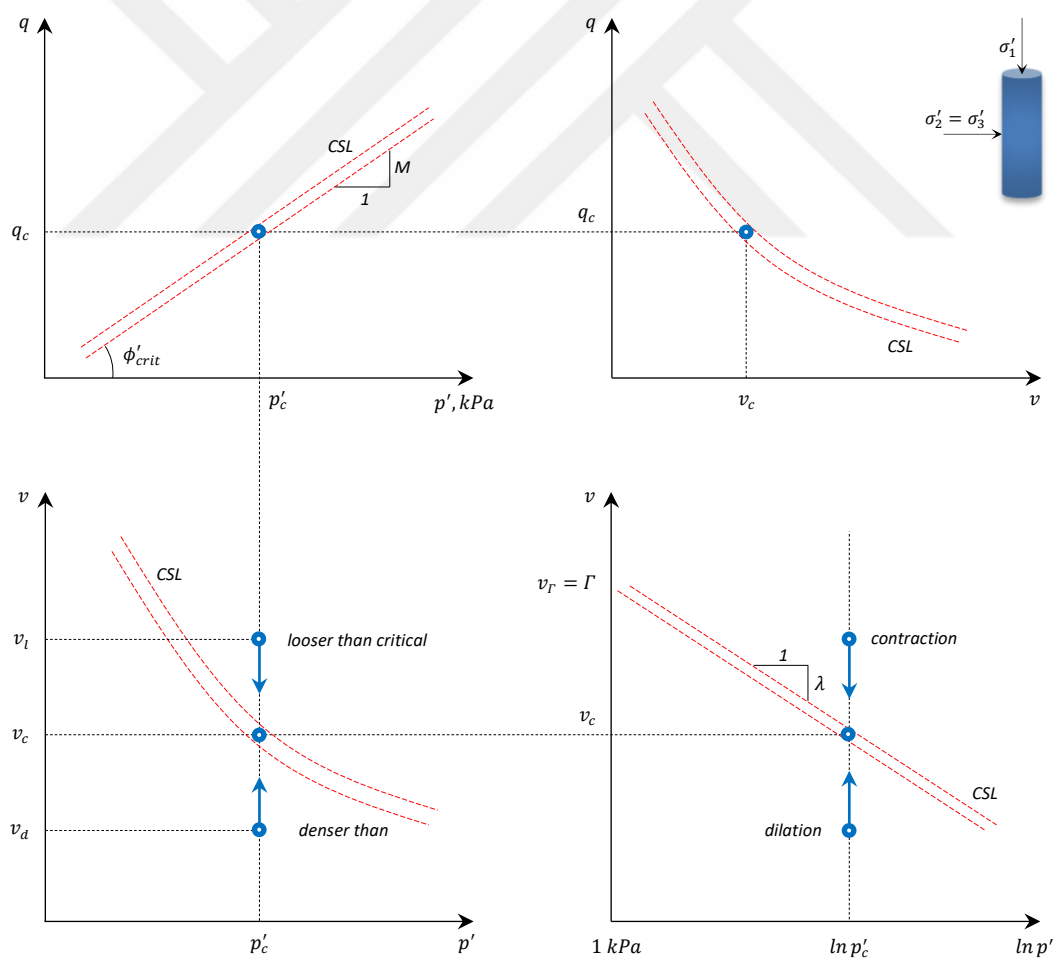


Figure 3.12. Critical state lines at q', p', v space (Schofield and Wroth, 1968; Bolton, 1979; Wood, 1990; Jefferies and Been, 2016)

In Figure 3.12, deviatoric stress is represented by q , critical deviatoric stress by q_c , mean effective normal stress by p' , critical mean effective normal stress by p'_c , critical effective shear strength angle by ϕ'_{crit} , CSL slope at $q:p'$ space (soil-specific material (friction) constants (M, Γ, λ)) by

$$M = (q/p') = f[\sin(\phi'_{crit})] (6 \sin \phi'_{crit}) / (3 - \sin \phi'_{crit}) = (q) / \exp((\Gamma - v) / (\lambda)),$$

specific volume (soil volume containing one unit of solid matter) by $v = (1 + e)$, loose specific volume by v_l , critical specific volume by v_c , dense specific volume v_d , specific volume of soil corresponding to CSL at $p' = 1.0 \text{ kPa}$ by $v_r = \Gamma = v + \lambda \ln p'$, CSL slope at $v: \ln p'$ space by λ .

Shearing of sands at constant volume ($\psi = 0$) occurs at ϕ'_{crit} , exceeding ϕ'_μ , depending on grain roughness, angularity, eccentricity, gradation, mineralogy, and other factors. For smooth quartz sands, these expressions are about $\phi'_\mu \approx 10^\circ$ (Senetakis et al., 2010) and $\phi'_{crit} \approx 33^\circ$ (Bolton, 1986). This difference between the components of effective internal friction angle forms the basis of the part of the subject discussed so far.

With the crushing of granular materials under high stresses, ψ decreases, while ϕ'_{crit} remains almost constant. For such stress conditions in which the grain crushing is effective, compression is observed in dense sands, dilation is observed at low stresses. For loose sands, compression is observed even under low stresses. Bolton (2018) showed this logarithmic relationship between stress and density based on volumetric changes in Figure 3.13.

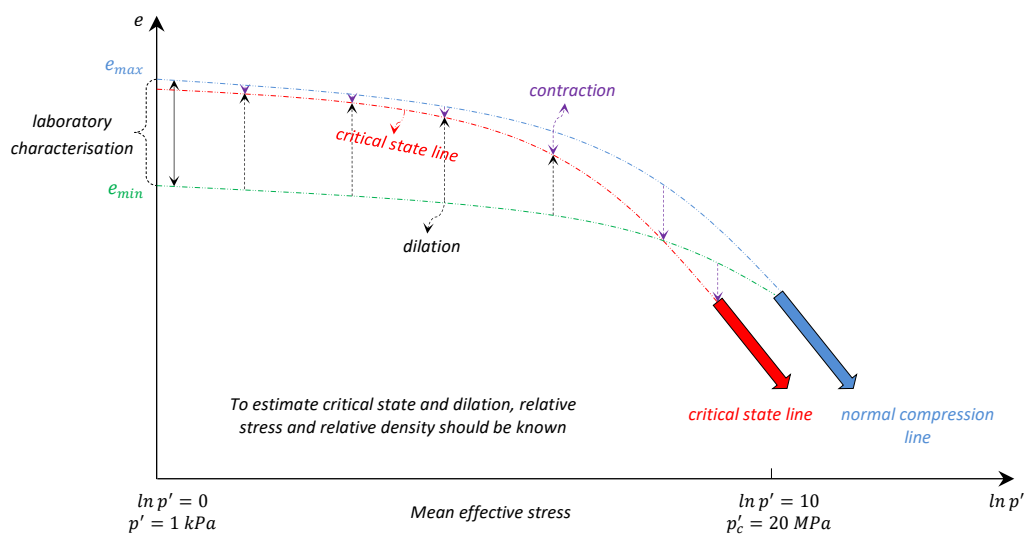


Figure 3.13. Variation of dilation and critical state line at $p' - e$ space (Bolton, 2018)

Bolton (1986), in his study as detailed in the previous paragraphs, observed that the peak shear strengths of sands correspond to the peak dilation rate and derived a new equation in consistent with Rowe's (1962) stress-dilation theory by including the concept of critical state in this relationship.

$$\phi' = \phi'_{crit} + 0.8\psi_{max} \quad (3.27)$$

Bolton noted the relationship of the component of dilation rate with the parameter related to relative density ($I_D = D_r/100$, $0 \leq I_D \leq 1$) and the mean effective stress at failure ($p' = (\sigma'_1 + \sigma'_2 + \sigma'_3)/3$) and defined a new relative dilation index ($I_R, I_R \geq 0$) on the basis of density to explain this:

$$I_R = I_D(Q - \ln p') - R \quad (3.28)$$

The expression p' in Equation 3.28 was normalized with atmosphere pressure ($p_a = 1 \text{ atm} \approx 100 \text{ kPa}$). This equation p'_{crit} becomes the following form at special stress conditions like ($I_R = 0$):

$$\ln p'_{crit} = Q - \frac{R}{I_D} \quad (3.29)$$

Where, Q and R represent the fit parameters depending on the characteristic of sand. These parameters were calculated as $Q = 10$ and $R = 1$ for quartz-based sands. Hence, Equation 3.28 is written as follows:

$$I_R = I_D(10 - \ln p') - 1 \quad (3.30)$$

When Equation 3.27 and Equation 3.28 are written in terms of A_ψ , which is a variable coefficient depending on soil type and stress path, and generalized, the following relationship is obtained:

$$\phi' - \phi'_{crit} = A_\psi I_R = A_\psi [I_D(Q - \ln p') - R] \quad (3.31)$$

The relative dilation index in Equation 3.31 takes a value between $0 \leq I_R \leq 4$ for general conditions. When this parameter is negative ($-$), this indicates a volume decrease in very loose sands or high-pressure conditions; however, when it is $I_R > 4$, this indicates over dilation. On the other hand, the coefficient A_ψ takes 5 for the plane strain state and 3 for the triaxial strain state. The expression applicable to both strain states is as follows:

$$I_R = \frac{(-\partial\varepsilon_v/\partial\varepsilon_1)_p}{0.3} = \frac{\phi' - \phi'_{crit}}{A_\psi} \quad (3.32)$$

Because the expression of dilation rate at failure $(-\partial\varepsilon_v/\partial\varepsilon_1)_p$, whose terms were already defined, show numerically insignificant differences from the results obtained from other relative dilation index relation above, Equation 3.32 is considered as an alternative relation.

One of the most important concepts used to explain the strength and dilation properties of sands is relative crushability index of grains (I_{CR}):

$$I_{CR} = \ln \frac{\sigma'_{CR}}{\sigma'} \quad (3.33)$$

The stress terms in Equation 3.33 can be expressed with p'_{cr} and p' in the axisymmetric tests. The relationship of the crushability parameter with the relative dilation index is as follows:

$$I_R = I_D I_{CR} - 1 \quad (3.34)$$

Equation 3.34 becomes the following form in critical state ($I_R = 0$):

$$\ln \frac{\sigma'_{CR}}{\sigma'_{crit}} = \frac{1}{I_D} \quad (3.35)$$

The expression σ'_{CR} in Equation 3.35 is about 20 MPa for quartz sands (5 MPa for carbonated sands, 80 MPa for quartz silt). The expressions mentioned in this section can be better understood by understanding Figure 3.13 suggested by Bolton.

Another important consideration is the slope of Mohr-Coulomb strength envelope. The shear strength of soils is a function of normal stress to which they are exposed. In case where normal stress is zero, the shear strength of soils is zero, but it increases with the increasing normal stress. However, this increase is not linear due to the reasons mentioned in the previous section (Figure 3.14).

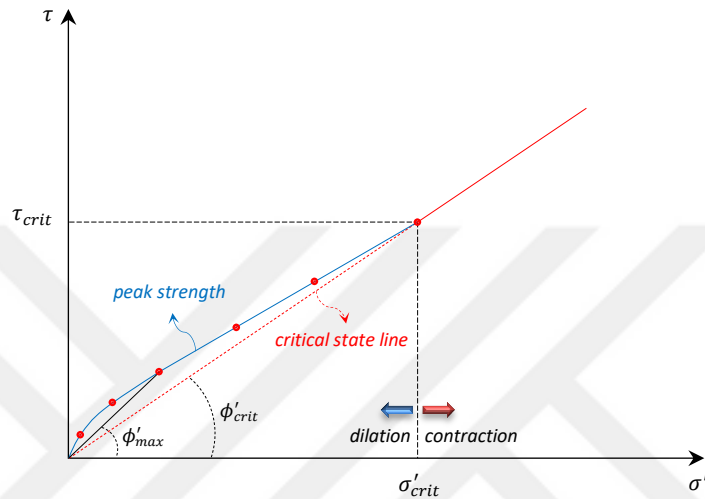


Figure 3.14. Non-linear strength envelope of sand soil (Bolton, 2018)

As is seen in Figure 3.14, a high internal friction secant angle (ϕ'_{sec}) is obtained at low confining pressures, while a low internal friction angle is obtained at high confining pressures. Bolton suggested the following relation to accurately explain this reverse, non-linear complex relationship between the variables:

$$\left(\frac{\tau_{max}}{\tau_{crit}}\right) = \left(\frac{\sigma'}{\sigma'_{crit}}\right)^{\beta} \quad (3.36)$$

β in Equation 3.36 represents a coefficient depending on the expression I_D defined for the plane strain state ($\beta \approx 1 - 0.14I_D$). The relationship between internal friction angles for the same loading method is expressed as $\phi_{max} = \phi_{crit} + 5 [I_D \ln(\sigma'_{crit}/\sigma') - 1]$.

This section provides information about the strength properties of sands under static-drained loading conditions. Undoubtedly, the strength properties have big differences under undrained loading conditions (with the presence of void water pressure) without volume

change. On the other hand, understanding of the strength properties of fine-grained soils is so complicated due to the extreme causes mentioned in the first section. However, the strength and strain behaviors of soils at cycle loading conditions are evaluated with different concepts and criteria.

3.5. Factors Acting on the Shear Strength of Sands

As detailed in the previous section, the strength of sands depends on the distortion of grains and relative motions between them. This relationship where friction is the main determinant is controlled by various factors such as *soil state, nature and properties of soil grains, and environmental factors*. In this section, the main factors acting on the shear strength of sands were mentioned and supported by schematic illustrations to better understand the relationship between them.

Soil state includes various parameters such as void ratio or relative density, confining pressure, storage condition of the soil, cementation, and aging. Undoubtedly, the most important parameter affecting the shear strength property of sands is void ratio. Shear strength decreases with the increasing void ratio, and vice versa. The most important concept in explaining this phenomenon in sands is the effect of dilation. Therefore, the peak shear strength of sand depends on its dilation capacity, while the critical shear strength value is independent of density (Figure 3.10). Another important factor affecting the strength of sands is confining pressure. Because high confining pressures will reduce dilation, the peak shear strength angle will also decrease. Figure 3.13 and Figure 3.14 are important in explaining this. The current deposition status of sand grains is another important parameter acting on the soil behavior. This effect is limited in clean sands, but it is significant if they have fine grains. Cementation may occur with the presence of various cementation agents, especially in sands deposited in the marine environment. Very strongly cemented sands behave like rocks; however, relatively poor cemented sands can be evaluated on the same basis as other uncemented sands. However, the main consideration here is the true cohesion component that can be formed by cementation at any level. The aging parameter is related to the strength and rigidity properties of deposited sands that vary by time. The formation of this phenomenon is explained with dynamic loads or long-term physical, chemical or

microbiological mechanisms between grains during various improvement (dynamic compaction, etc.) activities in the field.

Nature and properties of soil grains include various parameters such as the mineralogical origin of grains, the shape and roughness of grains, and grain diameter distribution. Mineralogy directly affects the strength properties of soil. Sand grains usually consist of quartz mineral that is very hard and resistant to high pressure. The friction between sand grains composing of this mineral is a function of grain size (Figure 3.15). The presence of water increases friction in some minerals depending on surface roughness while, it reduces friction in mica group ($\phi_{\mu(mica)} \leq 15^\circ$) minerals such as naturally cracked muscovite, biotite, phlogopite, and chlorite. The friction angles of mineral surfaces under saturated conditions are presented in Table 3.1.

Table 3.1. Friction angles between mineral surfaces (under saturated conditions) (Procter and Barton, 1974)

<i>Mineral</i>	<i>Test type</i>	ϕ'_μ (°)
<i>quartz</i>	<i>particle-particle</i>	26
<i>feldspar</i>	<i>particle-plane</i>	37
<i>zircon</i>	<i>particle-plane</i>	23
<i>hornblende</i>	<i>block on block</i>	31
<i>calcite</i>	<i>block on block</i>	33
<i>anthracite</i>	<i>block on block</i>	31
<i>chalk</i>	<i>block on block</i>	30
<i>muscovite</i>	<i>along cleavage faces</i>	13
<i>biotite</i>	<i>along cleavage faces</i>	7
<i>phlogopite</i>	<i>along cleavage faces</i>	9
<i>chlorite</i>	<i>along cleavage faces</i>	12

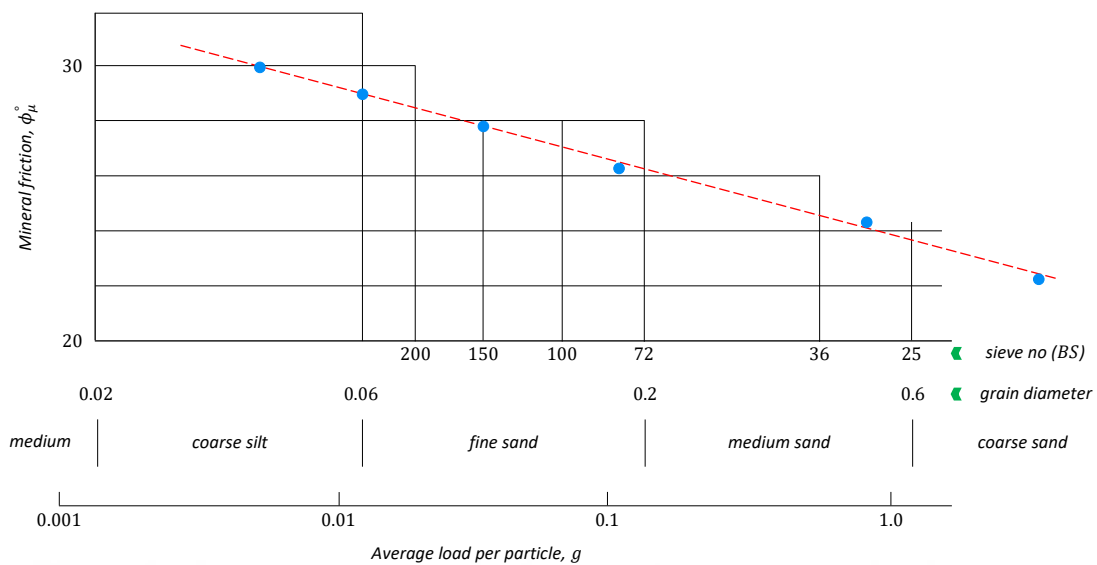


Figure 3.15. Friction angle envelope of quartz sands as a function of grain size (Rowe, 1962)

Another important factor acting on the strength properties of sands is the grain shape. Soils composing of angular (irregular angle) grains due to the high interlocking effect have larger shear strength than soils having round grains. However, the fact that angular grains have a higher failure potential than round grains at high confining pressures is the opposite of low stress conditions in terms of contribution to strength. On the other hand, the strength increases with the increasing grain surface roughness, but the presence of water slightly limits this contribution. The grain distribution properties of sands are among the most important factors acting on strength. Because well-graded sands contain grains of many different sizes, they have a more compact structure as compared to poorly graded sands. Since this will reduce compressibility and thus increase interlocking, it allows obtaining larger shear strength values.

Environmental factors include various parameters such as water content and test type. Because the presence of water causes a lubricating effect on sands, it will reduce shear strength, even slightly. However, as mentioned previously, the strength properties of cracked or brittle materials under low or high stresses are more affected by water. The evaluations made based on the axisymmetric or plane strain principles are another important factor acting on the results of shear strength. The test properties ensure to obtain larger strength values as a function of density on the basis of plane strain. The comparison of this relationship is the main subject of the thesis.

In addition to those mentioned above, there are other factors acting on the shear strength of soils, such as shear rate, grain size, over consolidation, capillary effect, presence of fine materials, etc. In general, some factors are overlooked because their contribution on strength cannot be measured exactly, or they have a limited effect.

The schematic illustration in Figure 3.16 as modified by Holtz et al. (2011), who associated the correlations presented by Casagrande (1936), Means and Parcher (1963), and NAVFAC (1986) under axisymmetric stress conditions on the basis of effective friction angle, dry density, and soil classification, is very helpful in evaluating the strength characteristics of cohesionless soils.

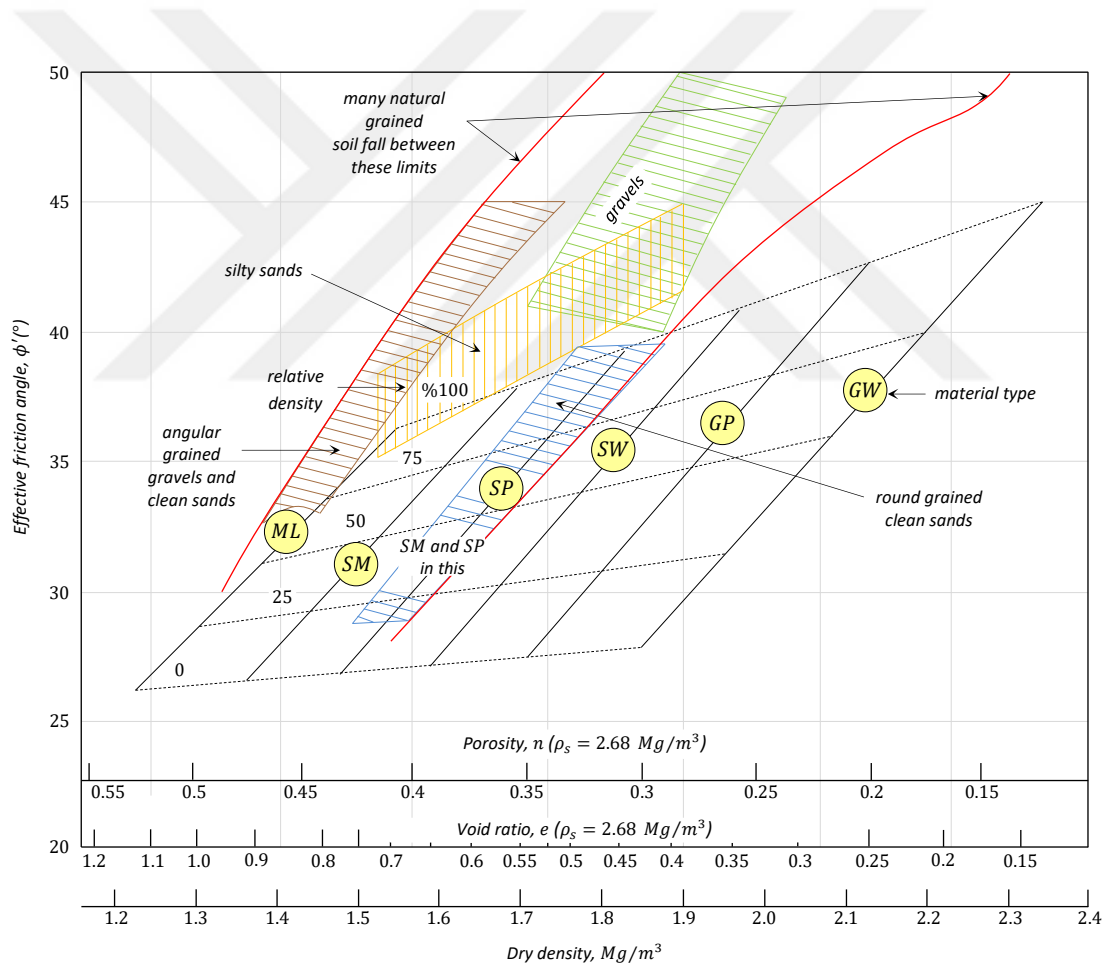


Figure 3.16. Relationship between effective friction angle, dry density, and soil classification (Holtz et al., 2011)

4. MATERIAL AND METHOD

4.1. Introduction

Various test methods with different characteristics can be used to determine the shear strength of the soil. The method, sand and reinforcement are the main factors affecting the test results. The primary aim of this study is to measure the effect of direct shear, triaxial shear and ring shear test methods on unreinforced samples and associate them to the plane strain method. The ultimate aim of this study; on the other hand, is to investigate the contribution of the fiber material to the test results and to make a comparative analysis between the test methods. In order to achieve these goals, a total of 1203 experiments were conducted. Details of the experiments are given in Table 4.1.

The properties of the sand and reinforcement used in the study are defined in Section 4.2. The details of the test procedure and study program are presented in Section 4.3. In Section 4.4, direct shear, triaxial shear and ring shear test methods are introduced, and some more details are given.

Table 4.1. Number of tests performed in the study

Test Type	Standardization tests		Actual tests	
	Unreinforced	Reinforced	Unreinforced	Reinforced
Direct shear	144	180	42	66
Triaxial	108	120	42	66
Ring shear	120	156	42	66
Particle size distribution	5	-	2	-
Specific gravity	5	-	3	-
Maximum density	5	-	5	-
Minimum density	5	-	5	-
Compaction characteristics	5	5	3	3
Total	397	461	144	201
Grand Total	1203			

4.2. Material Specifications

In the literature review part of this study, it was seen that sand and geosynthetic reinforcement material were quite effective on the test results of different methods. For this reason, we decided to choose the materials with specific standards to avoid testing limitations for the test results, to have more significant comparisons, and for many other purposes.

4.2.1. CEN Standard Sand

The European Community countries apply certain standards for a series of products such as cement in order to remove international trade barriers. For this purpose, the CEN Technical Committee (CEN/TC 51), formed by CEN (Comité Européen de Normalisation), standardized the CEN sand by developing the ISO/R 679:1968 norm (1987) with some additions and regulations in the following years (1994, 2005, 2016).

The "CEN Standard Sand" produced by Limak Cement Factory in accordance with TS EN 196-1 was used in the thesis study (Figure 4.1). Since the particle size distribution of the CEN reference sand defined in the TS EN 196-1 standard does not exist in nature, the CEN standard sand can only be produced industrially in the specified criteria (TSE, 2016). Raw sand, which is brought wet to the production facility after a series of mineralogical tests, is dried and transferred to vibratory silos together with unprocessed some other dry sand. Then, the sieving process is continued until the sands transferred to a series of sieves arranged on top of each other with sieve openings varying between 0.08 – 2.00 (*mm*), and the amount of material passing through each sieve is 0.5 *g/min*. At the end of the sieving process, the samples taken from each sieve are stored in separate storage areas. These samples in different fractions are collected in sand mixers in accordance with the standard amounts and packed in polyethylene bags of 1350 ± 5 grams. The produced sand is delivered after undergoing a series of tests in order to control the relevant standards during/after production by the manufacturer and independent inspection institutions.



Figure 4.1. CEN standard sand produced in accordance with TS EN 196-1

CEN reference sand is a clean, natural silica sand containing at least 98% proportion of silica (silicon dioxide) even in the finest fractions, its particles are generally isometric and rounded to subrounded in shape, without coarse sand. The ratio of mass loss to dry sand mass (moisture content) after drying at 105 – 110 °C degrees until it reaches a constant mass is less than 0.2%.

A series of tests were carried out in accordance with the ASTM standards to determine the index and some engineering properties of CEN standard sand. The data to be obtained from these tests are essential for measuring strength and strain properties. Therefore, the tests were repeated with the utmost care, in accordance with the standards, paying attention to keeping the deviations between the results within the criteria specified in the standards.

Particle size distribution plays an important role in understanding the behavior of granular soils. In the tests carried out in accordance with ASTM D6913/D6913M-17 standard, the material was sieved mechanically, followed by a time-adjusted automatic sieve shaker, before a series of sieve sets were arranged in decreasing sieve openings from top to bottom. At the end of the test, the remaining soil mass in each sieve was weighed and the percentage of soil passed was calculated accordingly. The particle size distribution (granulometry) curve of the obtained CEN standard sand is shown in Figure 4.2.

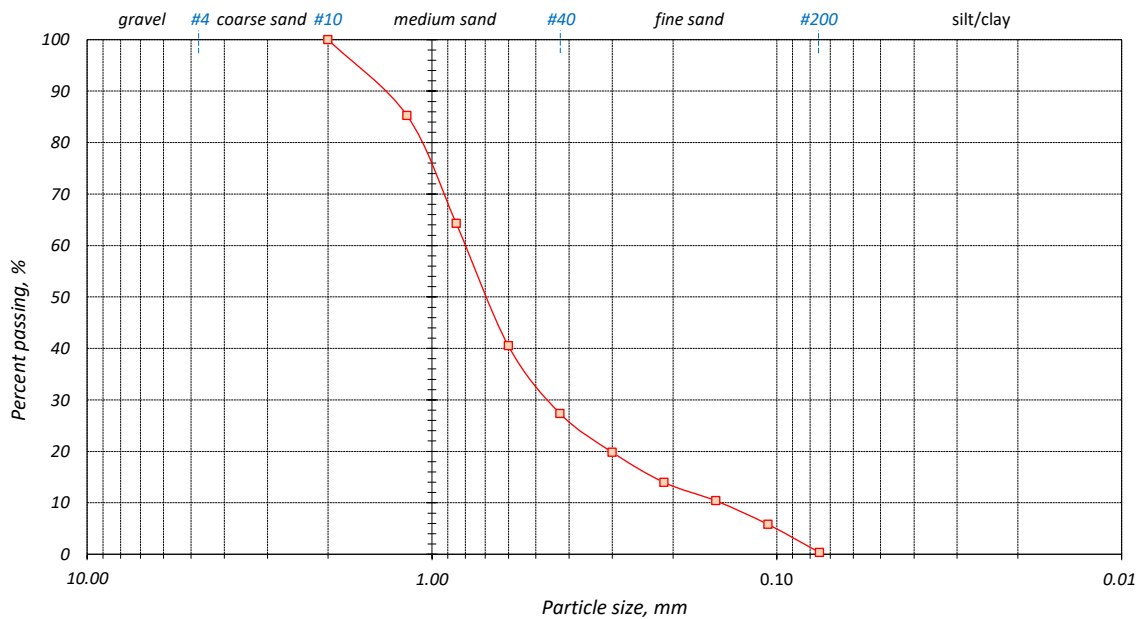


Figure 4.2. The particle size distribution (granulometry) curve of the CEN standard sand

The particle size of CEN standard sand varies between $D = 0.08 - 2$ (mm). This range classifies CEN standard sand as medium-fine particle size sand in terms of *USCS* standards (Figure 4.3). The fact that it is $D_{max} = 2$ mm was one of the most important reasons for choosing this sand, enabling correct comparisons (testing criteria) among the results obtained from the test methods.

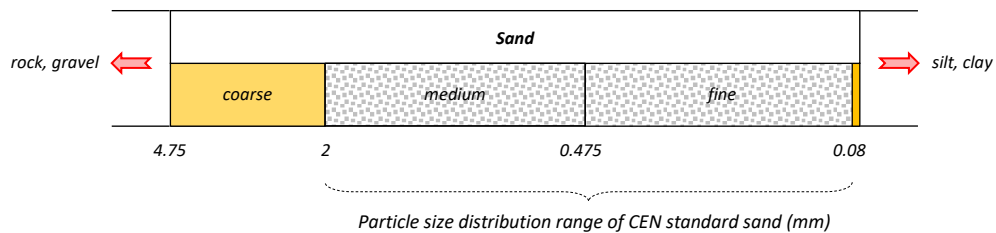


Figure 4.3. Particle size distribution range of CEN standard sand (*USCS*)

The density index (relative density) is the most important parameter influencing the engineering behavior of granular soil, as detailed in Section 3.5. This parameter is important as it characterizes the stacking state of granular soil as the degree of density. It should be noted that this concept, first introduced by Terzaghi (1925), is a definition rather than a natural feature of granular soil. Therefore, it cannot be used alone as a safe design criterion. The density index is defined as a function of (I_d) void ratio as in Equation 4.1 (Figure 4.4):

$$I_d = f(e) \quad (4.1)$$

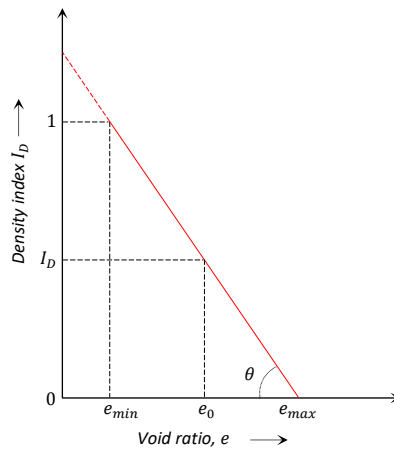


Figure 4.4. Relationship between density index and void ratio (Venkatramaiah, 2018)

Using the linear relationship of the parameters in Figure 4.4 with the help of trigonometric functions, the following equation is obtained:

$$I_d = \frac{e_{max} - e}{e_{max} - e_{min}} \quad (4.2)$$

The above equation can also be written as in Equation 4.6 and Equation 4.7, respectively, in terms of dry density and unit weight using the following void ratio expressions:

$$e = \frac{\rho_w \times G_{s\,ort}}{\rho_d} - 1 \quad (4.3)$$

$$e_{min} = \frac{\rho_w \times G_{s\,ort}}{\rho_{d\,max}} - 1 \quad (4.4)$$

$$e_{max} = \frac{\rho_w \times G_{s\,ort}}{\rho_{d\,min}} - 1 \quad (4.5)$$

Here, the density of water at 20°C is represented by ρ_w (1.0 Mg/m^3), and the average specific weight of the soil with $G_{s\,ort}$.

$$I_d = \frac{1/\rho_{d \min} - 1/\rho_d}{1/\rho_{d \min} - 1/\rho_{d \max}} \quad (4.6)$$

$$I_d = \left(\frac{\gamma_{d \max}}{\gamma_d} \right) \frac{\gamma_d - \gamma_{d \min}}{\gamma_{d \max} - \gamma_{d \min}} \quad (4.7)$$

In the above equations, the maximum void ratio for the minimum density case is e_{\max} , the minimum dry density or unit weight is $\rho_{d \min}$, $\gamma_{d \min}$, respectively; for the highest density case the minimum void ratio is e_{\min} , the maximum dry density or unit weight is $\rho_{d \max}$, $\gamma_{d \max}$, respectively; void ratio, dry density and unit weight of the soil in its natural or investigated state are symbolized by e , ρ_d , γ_d , respectively.

The density index parameters are obtained by laboratory tests. An absolute measurement cannot be achieved, since the results obtained from the tests depend on the person who conducts the tests, the unique structure of the granular soil, possible testing errors and similar factors. Therefore, it would be more meaningful to define the concept in question as an index feature.

The $\rho_{d \max}$ and $\rho_{d \min}$ values of CEN standard sand in the maximum and minimum density conditions were determined according to the principles in ASTM D4253-16 and ASTM D4254-16 standards, respectively. For the maximum density case, the sand soil was placed in thin layers in a (2830 cm^3) mold of known volume by applying a vibrator and compaction energy from the top. Some water (lubrication effect) was added with each material placed in the mold in order to compact the particles better (with min. void). This step was carried out with the utmost care so that the forces applied in compaction do not cause particle breakage. Since it is known that granular materials cannot be compacted at the 100% level due to their structure, the tests were repeated five times for the consistency of the results (within 2%). At the end of each test, the dry mass in the mold was calculated by weighing the sand material part with a known total dry mass outside the mold, and the $\rho_{d \max}$ value was obtained from the ratio of this mass to the maximum dry sample volume (Equation 4.8). In the min. density case, the sand soil was slowly poured into the mold of the same volume used in the calculation of the maximum dry density, without any compaction energy, without vibration, in a spiral motion with the help of a funnel from a height of 13 mm

approximately. For the above-mentioned reasons, the tests were repeated five times for the consistency of the results (within 1%). The $\rho_{d \min}$ value was calculated from the ratio of the dry mass in the mold to the dry sand volume (Equation 4.9). Table 4.2 shows the results of all these tests.

$$\rho_{d \max} = \frac{M_s}{V} \quad (4.8)$$

$$\rho_{d \min} = \frac{M_s}{V} \quad (4.9)$$

In the above equations, the mass of the dry soil in the mold is defined as M_s , and its volume as V ($\gamma_d = 9.807\rho_d, kN/m^3$).

Table 4.2. Maximum and minimum dry density test results of CEN standard sand

Dry density (Mg/m ³)	Tests				
	1	2	3	4	5
$\rho_{d \min}$	1.57	1.57	1.56	1.56	1.57
$\rho_{d \max}$	1.79	1.81	1.78	1.79	1.80

The *specific gravity* is the ratio of the density of the particles that make up the soil to the density of the distilled water at 20°C. It is important to precisely define this concept, which is directly related to most soil properties. The specific gravity of soil particles can be calculated using the following equation:

$$G_s = \frac{\rho_s}{\rho_{w,t^\circ}} = \frac{M_s G_{w,t^\circ}}{M_s - M_{pws,t^\circ} + M_{ps,t^\circ}} \quad (4.10)$$

Here, specific gravity is G_s , specific gravity (at °C) is $G_{w,t}$, particle density is ρ_s , water density (at °C) is $\rho_{w,t}$, dry particle mass is M_s , the total mass of pycnometer, water, and particle (at °C) is $M_{pws,t}$, the total mass of pycnometer and water (at °C) is $M_{ps,t}$.

The specific gravity of the CEN standard sand was determined based on the principles of the ASTM D854-14 standard. The pycnometer cup (500 mL) was calibrated

for different temperature values by slowly filling it with distilled water, deaired up to the lower surface mark level of the meniscus. The water in the calibrated pycnometer was emptied to about one-third level, and then, 100 grams of dry sand was carefully poured into it (with the aid of a funnel) without any grain loss. The sample, in which partial vacuum was applied, was boiled for approximately 15 minutes and left to cool in an airtight environment (by vacuuming occasionally). The cooled pycnometer cup was carefully filled with de-aerated distilled water up to the meniscus lower line and its mass was weighed. In this highly sensitive test, the absolute temperature values at the beginning and end of the test must be taken into account. The results of the tests repeated three times are given in Table 4.3.

Table 4.3. Specific gravity test results of CEN standard sand

Specific gravity (20°C)	Tests		
	1	2	3
G_s	2.64	2.64	2.64
$G_{s\ ort}$	2.64		

Compaction characteristic is another important concept required to prepare a sample. With the increasing water content of cohesionless soils, capillary forces occur among the particles. After reaching a certain bottom point (point of lowest density), the soil becomes completely saturated (the dry density of granular soil reaches a certain peak) as the apparent cohesion forces disappear with increasing water content. After this point, the dry density of the soil decreases again with increasing water content.

Compaction characteristics of CEN standard sand were determined in accordance with the ASTM D7382-20 standard. The sand sample was mixed thoroughly for each added amount of water and compacted in three layers with the help of a vibratory compactor. At the end of the test, the collar attached to the mold was removed and the sample surface was leveled very precisely. The weighed mold was removed, and some soil was taken for the water content (ASTM D2216-19). All these processes were continued until reaching the optimum water content. The same procedure was performed for fiber-added samples as well. Test results showed that fiber additive at a certain concentration ($v_f = V_f/V = 0.3\%$) did not affect the water content but decreased the dry density (Figure 4.5).

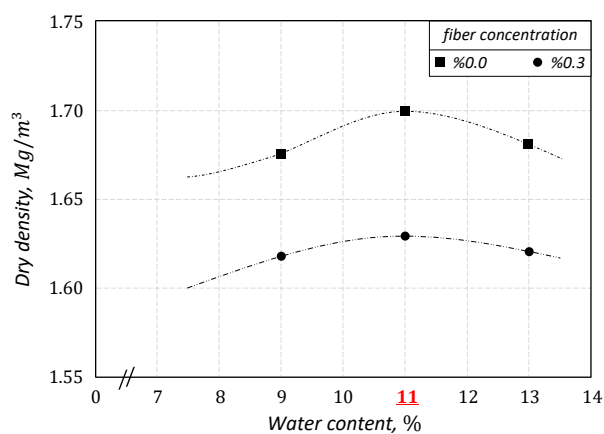


Figure 4.5. Compaction curves of CEN standard sand

The index properties of the CEN standard sand obtained as a result of the tests are presented in detail in the table below (Table 4.4).

Table 4.4. Index properties of CEN standard sand

Property	$D_{50}(mm)$	C_u	C_c	G_s	Void ratio		Particle size	Particle shape	Mineral	USCS
					e_{max}	e_{min}				
Value	0.70	6.5	2.04	2.64	0.69	0.46	fine-medium	rounded subrounded	quartz	SW

The particle structure, surface topography and composition of the CEN standard sand were visualized with the help of Scanning Electron Microscope (SEM) of different sizes (Figure 4.6).

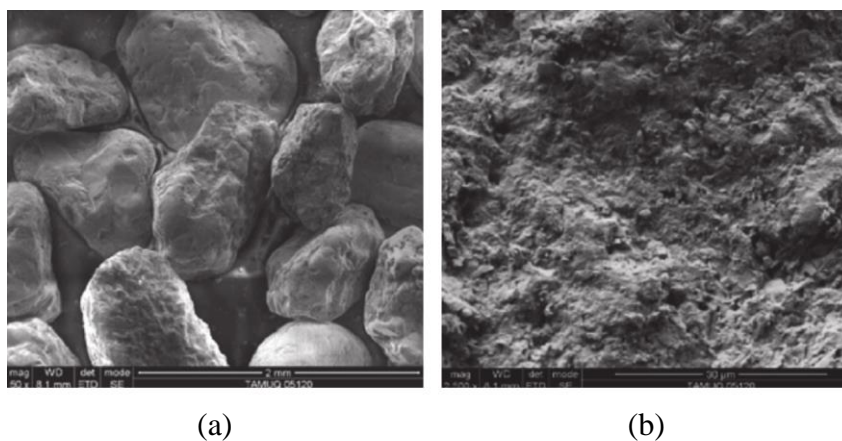


Figure 4.6. SEM outputs of CEN standard sand: (a) 50X, (b) 2500X

The SEM outputs are very important for the tests on granular materials, especially for the micro-level examinations. In this thesis study, it was used as an auxiliary source in order to check the particle crushing effect in the shear band. Other properties of CEN standard sand and X-Ray Fluorescence (XRF) analysis results are given in Table 4.5.

Table 4.5. Other properties of CEN standard sand

<i>Parameter</i>	<i>Value</i>
<i>water absorption (%), TS EN 1097-6</i>	<i>0.2</i>
<i>fineness modulus (%), TS EN 12620</i>	<i>2.65</i>
<i>sand flowing (s), TS EN 933-6</i>	<i>28</i>
<i>water content (%), TS 1900-1/T4</i>	<i><0.2</i>
<i>loss on ignition (950 °C), TS EN 196-2</i>	<i>0.16</i>
<i>chloride content (ppm)</i>	<i><50</i>
<i>silica content (%SiO₂)</i>	<i>98.05</i>
<i>alumina content (%Al₂O₃), ISO 29581-2</i>	<i>0.54</i>
<i>iron content (% Fe₂O₃), ISO 29581-2</i>	<i>0.07</i>
<i>phosphate content (% P₂O₅), ISO 29581-2</i>	<i>0.03</i>
<i>titanium content (%TiO₂)</i>	<i>0.02</i>

4.2.2. Fiber reinforcement

It is desirable for soil to have properties suitable for its intended use. However, this expectation can rarely be met in nature. For this reason, various stabilization methods are applied without additives (mechanical, drainage, etc.) and with additives (chemical, geosynthetic, etc.) in order to achieve the desired qualities of the engineering properties of the soil. Geosynthetic is one of these methods, it is a solution that has been developing, diversifying, and expanding its application area for decades due to its easy applicability, high performance, and cost-efficiency. In this thesis, a discrete polymeric material, which has an important place in geosynthetics and is applied by embedding into the soil, was used as a reinforcement element.

STRUX[®] 90/40 synthetic macro fiber produced by GCP Applied Technologies company was used as the fiber material (Figure 4.7). Dimensions of this standard fiber are given in Figure 4.8, and other technical specifications are given in Table 4.6.



Figure 4.7. Standard STRUX[®] 90/40 synthetic macro fiber

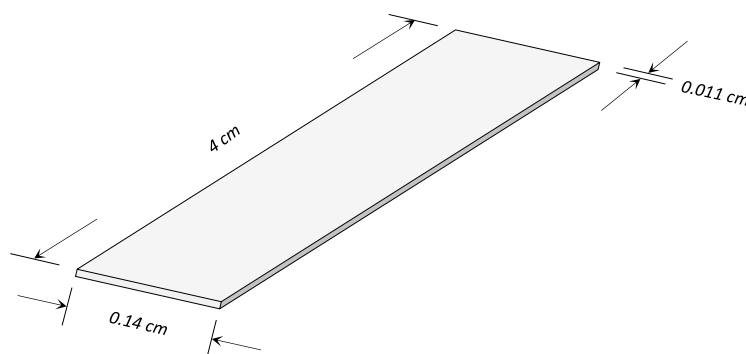


Figure 4.8. Dimensions of standard STRUX[®] 90/40 fiber

Table 4.6. Technical specifications of standard STRUX[®] 90/40 fiber (GCP, 2020)

<i>Properties</i>	<i>Value</i>
<i>class</i>	<i>synthetic macro fibers</i>
<i>material</i>	<i>polyolefin (blend of polypropylene and polyethylene)</i>
<i>standard dimensions</i>	<i>rectangular prism (4 cm x 0.14 cm x 0.011 cm)</i>
<i>nominal length and equivalent diameter</i>	<i>4 - 0.043 cm</i>
<i>nominal aspect ratio</i>	<i>~ 90</i>
<i>specific gravity</i>	<i>0.92</i>
<i>modulus of elasticity</i>	<i>9.5 GPa</i>
<i>tensile strength</i>	<i>620 MPa</i>
<i>melting point</i>	<i>160 °C</i>
<i>ignition point</i>	<i>590 °C</i>
<i>alkali, acid and salt resistance</i>	<i>high</i>
<i>absorption</i>	<i>none</i>
<i>color</i>	<i>gray</i>

Polyolefin (Koerner, 2012), the most common polymer used in the manufacture of geotextiles, can be defined as thermoplastic elastomer materials formed by the polymerization of unsaturated hydrocarbons (olefin (or alkene)). This polymer material, which is widely used in different fields today, is used as an additive material for various civil engineering products and especially for concrete production. The first systematic use of this material for geotechnical engineering was the filtration design of Terzaghi and Casagrande. Figure 4.9 shows the historical background of the polymer material.

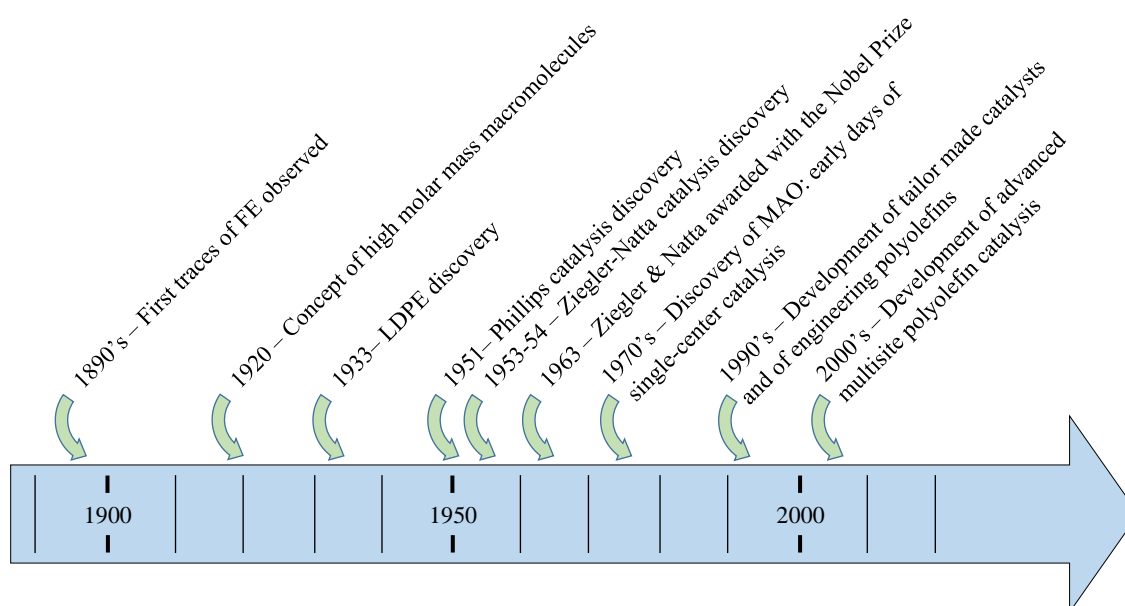


Figure 4.9. Historical development process of polyolefin (Sauter et al., 2017)

4.3. Test Procedure and Study Program

The most important stage of a test is the preparation of the sample in accordance with certain standards and "*with proper conditions*". This makes it much more important to prepare samples that will represent the field conditions for important and special materials such as soil, and then to choose and apply the appropriate test methods for the purpose.

In the first part of the section, the sample preparation method and application principles used in the thesis study are provided in detail, then the selection of the test parameters and the application details of the study program are given.

4.3.1. Sample preparation method and application principles

The methods used in the preparation of test samples significantly affect the mechanical (such as strength and dilation) and other types of behavior of the soil. Fiber reinforcement materials added to the soil make this issue more critical in terms of representing the field conditions. In particular, the effect of fiber reinforcement orientation on the engineering properties of the soil has been frequently discussed in recent studies (Michalowski and Čermák, 2002; Diambra et al., 2007; Michalowski, 2008; Ibraim et al., 2010; Soriano et al., 2017). The main discussion here is about the existence of an anisotropic strength, since the fiber is in the same direction, generally in a near-horizontal orientation while the sample is being prepared.

In the literature, for the fiber-reinforced soil samples, the "*Moist tamping*" method presented by Ladd (1978) is the most preferred method. This method has advantages such as not requiring too much special equipment, easy application, preventing flotation and segregation formations of fiber reinforcement, homogeneous distribution of fiber reinforcement, and providing density control. However, the most disadvantageous characteristic of this method is the presence of the above-mentioned horizontal fiber reinforcement orientation in the prepared composites. In order to eliminate this disadvantage, vibration support was provided in the thesis study (especially for high density levels).

Preparation of the test sample includes mixing and formation stages. In the mixing stage, the dry sand material weighed for each density value was mixed with approximately $w_{opt} = 11\%$ ratio of deaired distilled water obtained by measuring the compaction characteristics detailed in the previous section. After the wet sand was mixed well in the sample crucible, it was transferred to angular inner trays and portioned. Then, the fiber reinforcement at 0.3% concentration was distributed very carefully and evenly to the sand material formed and mixed again until a homogeneous composite sample was obtained. The carefully prepared samples were transferred to the test reservoir and the formation phase was started. Undoubtedly, the correct planning and implementation of this stage is the most important part of the whole process. Since the height effect for placing the prepared sample in the test reservoir is important, the initial height was taken as a basis for each test method. In line with the height ($h < 25 \text{ mm}$) specified by Ladd, the sample was placed in the test reservoir as equal layers with regular checks. A very low energy level was applied for all density levels in order to avoid anisotropy caused by the placement of the fiber reinforcement. The selected number of layers and energy level were easily applied for the formation of very low density, low density and medium density sand, and vibration support for high density sand made the process very practical. Thus, it was observed that the fiber reinforcement was randomly distributed in all directions rather than in a single direction in the composite sample formed. Since it is known that the test results depend on the person performing the test, it is important that all tests are carried out by a single expert who has theoretical and practical knowledge of the subject, if possible.

The fiber reinforcement concentration of the composite formed (v_f) is defined as the ratio of the fiber reinforcement volume (V_f) to the total volume (V):

$$v_f = \frac{V_f}{V} \times (\%100) \quad (4.11)$$

The density of the fiber-reinforced composite can be evaluated based on three different principles. The first principle is to evaluate the fiber reinforcement as solid; the second principle is to evaluate the fiber reinforcement as the void volume, and the third principle is to accept dry density equal for the samples with and without fiber additive. In the thesis study, the first principle, the details of which are presented below, was preferred

for the most ideal comparisons by preserving the fiber reinforcement concentration and the total mass of the composite:

$$e = \frac{V_v}{V_s + V_f} = \frac{V_{vs} + V_{vf}}{V_s + V_f} \quad (4.12)$$

$$\gamma_d = \frac{W_s + W_f}{V_s + V_f + V_v} = \frac{W_s(1 + w_f)}{V_s + V_f + V_v} \quad (4.13)$$

In the above equations, e refers to void ratio, V_v refers to void volume, V_s refers to particle volume, V_{vs}, V_{vf} refer to void volume caused by particle and fiber reinforcement, respectively, γ_d refers to dry unit volume weight, w_f refers to the ratio of fiber reinforcement mass to dry sand mass, W_s, W_f refer to particle weight and fiber reinforcement weight, respectively. Equation 4.14 can be obtained by combining Equation 4.12 and Equation 4.13:

$$e = \left(\frac{1 + w_f}{\gamma_d} \right) \frac{G_s G_f \gamma_w}{G_f + G_s w_f} - 1 \quad (4.14)$$

In terms of volume, w_f and the material weights in the composite corresponding to the target e and v_f were calculated as follows¹:

$$w_f = \frac{(1 + e)v_f G_f}{(1 + e)(G_f - G_s)v_f + G_s} \quad (4.15)$$

$$W_f = \left(\frac{V}{1 + e} \right) \frac{G_s G_f w_f \gamma_w}{w_f G_s + G_f (1 - w_f)} \quad (4.16)$$

$$W_s = \left(\frac{V}{1 + e} \right) \frac{G_s G_f (1 - w_f) \gamma_w}{w_f G_s + G_f (1 - w_f)} \quad (4.17)$$

The expression ($v = 1 + e$) in Equation 4.14 can be defined in terms of specific volume as follows:

$$v = \left(v_s + v_f \frac{G_s w_f}{G_f} \right) \frac{G_f}{G_f + G_s w_f} \quad (4.18)$$

¹ When using this principle, the void volumes of high-density reinforced composites should be checked. If these volume values are insufficient, the other principles mentioned above should be used "for the whole study".

In Equation 4.18, the specific gravity of the particle and fiber reinforcement is G_s , G_f , respectively, and the specific volumes of composite, particle and fiber reinforcement are symbolized with v , v_s , v_f , respectively, and defined as in Equation 4.19:

$$v = \frac{V}{V_s + V_f} ; v_s = \frac{V_{v_s} + V_s}{V_s} ; v_f = \frac{V_{v_f} + V_f}{V_f} \quad (4.19)$$

In order to make the above statements clearer to understand, the phase diagrams representing the fiber reinforced situation are given in Figure 4.10. When the soil is mixed with fiber reinforcement, some void volumes are stolen by the fiber material with the effect of electrical forces (Diambra et al., 2010; Wood, 2013). This situation, which is also valid for the plant roots-soil relationship, which is also noticed by observations made with electron microscopy, is important for understanding the behavior of soils with additive materials such as fiber or pozzolana under strain and for structural modeling strategies. Therefore, it was deemed appropriate to add this component to the above equations.

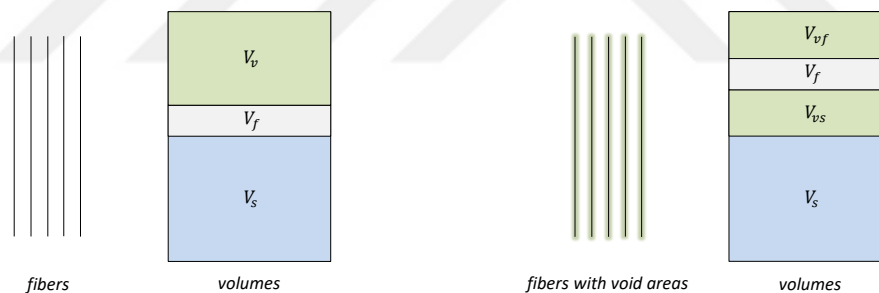


Figure 4.10. Phase diagram for fiber reinforced samples

4.3.2. Selection of test parameters and study program

In order to make a comparative analysis of different test methods, certain standards were used in the selection of the materials and the application of the test procedure. For the selection of the standards, the specific limitations and properties of the test methods and the literature review on the subject were taken into consideration. In addition to the principles mentioned above, the representativeness of real field conditions was taken into account for the selection of the test parameters.

The thesis study was carried out with and without fiber reinforcement. As fiber reinforcement, macro type material was selected due to the fact that it better reflects the workability, applicability, and mechanical effect of fiber with sand matrix. $v_f = 0.3\%$ level was chosen as it was seen that meaningful comparisons could not be made with very low and very high percentage levels of fiber reinforcement concentration. The fiber aspect ratio was chosen as $a_r = 11.25:1$ due to the restrictive effects of the ring shear test. Thus, the orientation effect of the fiber reinforcement mentioned in Section 4.3.1 was minimized.

In the selection of normal or confining stress, $\sigma_{n,c} = 50, 100, 200$ (kPa) values were selected in the range (near the surface) encountered in most geotechnical structures in practice. Another important factor in this selection was the correct representation of the Mohr-Coulomb failure envelope.

It was detailed in Section 3.5 that density is the most important factor affecting the engineering properties of the granular soil. In order to compare the effect of this parameter on the mechanical properties of the test methods, it is necessary to examine it in a wide range. Therefore, density values were selected as $I_D \approx 20\%$, $I_D \approx 40\%$, $I_D \approx 60\%$, and $I_D \approx 80\%$ for very low density, low density, medium density, and high density, respectively.

In line with the parameters detailed above, all tests were carried out carefully with the same sensitivity to sample preparation, placement, and other factors. In order to achieve the most accurate measurements, the tests of the samples without additives were repeated three times, and the tests of the samples with reinforcement were repeated five times due to the extra properties of the fiber reinforcement. On the other hand, the tests of high-density samples were repeated five times for the samples without additives and seven times for the fiber-reinforced samples due to their formation. Thus, a total of 324 tests were carried out, 126 for the samples without additives and 198 for the fiber reinforced samples, the details of which are given in Table 4.7. The results of each data group were evaluated separately, combined with MATLAB® (R2020b) software, and analyzed according to these principles. In Table 4.7, samples without fiber reinforcement are coded with (U), fiber-reinforced samples are coded with (R), direct shear test is coded with (DS), triaxial shear test is coded with (TX) and ring shear test is coded with (RS).

Table 4.7 Test Program

<i>Test Code</i>	v_f (%)	$\sigma_{n,r}$ (kPa)	I_D (%)	<i>Test Code</i>	v_f (%)	$\sigma_{n,r}$ (kPa)	I_D (%)
DS20-050-U-1	0,0	50	20	DS40-200-U-2	0,0	200	40
DS20-050-U-2	0,0	50	20	DS40-200-U-3	0,0	200	40
DS20-050-U-3	0,0	50	20	DS40-200-R-1	0,3	200	40
DS20-050-R-1	0,3	50	20	DS40-200-R-2	0,3	200	40
DS20-050-R-2	0,3	50	20	DS40-200-R-3	0,3	200	40
DS20-050-R-3	0,3	50	20	DS40-200-R-4	0,3	200	40
DS20-050-R-4	0,3	50	20	DS40-200-R-5	0,3	200	40
DS20-050-R-5	0,3	50	20	DS60-050-U-1	0,0	50	60
DS20-100-U-1	0,0	100	20	DS60-050-U-2	0,0	50	60
DS20-100-U-2	0,0	100	20	DS60-050-U-3	0,0	50	60
DS20-100-U-3	0,0	100	20	DS60-050-R-1	0,3	50	60
DS20-100-R-1	0,3	100	20	DS60-050-R-2	0,3	50	60
DS20-100-R-2	0,3	100	20	DS60-050-R-3	0,3	50	60
DS20-100-R-3	0,3	100	20	DS60-050-R-4	0,3	50	60
DS20-100-R-4	0,3	100	20	DS60-050-R-5	0,3	50	60
DS20-100-R-5	0,3	100	20	DS60-100-U-1	0,0	100	60
DS20-200-U-1	0,0	200	20	DS60-100-U-2	0,0	100	60
DS20-200-U-2	0,0	200	20	DS60-100-U-3	0,0	100	60
DS20-200-U-3	0,0	200	20	DS60-100-R-1	0,3	100	60
DS20-200-R-1	0,3	200	20	DS60-100-R-2	0,3	100	60
DS20-200-R-2	0,3	200	20	DS60-100-R-3	0,3	100	60
DS20-200-R-3	0,3	200	20	DS60-100-R-4	0,3	100	60
DS20-200-R-4	0,3	200	20	DS60-100-R-5	0,3	100	60
DS20-200-R-5	0,3	200	20	DS60-200-U-1	0,0	200	60
DS40-050-U-1	0,0	50	40	DS60-200-U-2	0,0	200	60
DS40-050-U-2	0,0	50	40	DS60-200-U-3	0,0	200	60
DS40-050-U-3	0,0	50	40	DS60-200-R-1	0,3	200	60
DS40-050-R-1	0,3	50	40	DS60-200-R-2	0,3	200	60
DS40-050-R-2	0,3	50	40	DS60-200-R-3	0,3	200	60
DS40-050-R-3	0,3	50	40	DS60-200-R-4	0,3	200	60
DS40-050-R-4	0,3	50	40	DS60-200-R-5	0,3	200	60
DS40-050-R-5	0,3	50	40	DS80-050-U-1	0,0	50	80
DS40-100-U-1	0,0	100	40	DS80-050-U-2	0,0	50	80
DS40-100-U-2	0,0	100	40	DS80-050-U-3	0,0	50	80
DS40-100-U-3	0,0	100	40	DS80-050-U-4	0,0	50	80
DS40-100-R-1	0,3	100	40	DS80-050-U-5	0,0	50	80
DS40-100-R-2	0,3	100	40	DS80-050-R-1	0,3	50	80
DS40-100-R-3	0,3	100	40	DS80-050-R-2	0,3	50	80
DS40-100-R-4	0,3	100	40	DS80-050-R-3	0,3	50	80
DS40-100-R-5	0,3	100	40	DS80-050-R-4	0,3	50	80
DS40-200-U-1	0,0	200	40	DS80-050-R-5	0,3	50	80

Table 4.7. Test Program (Continued)

<i>Test Code</i>	v_f (%)	$\sigma_{n,r}$ (kPa)	I_D (%)	<i>Test Code</i>	v_f (%)	$\sigma_{n,r}$ (kPa)	I_D (%)
DS80-050-R-6	0,3	50	80	TX20-100-R-4	0,3	100	20
DS80-050-R-7	0,3	50	80	TX20-100-R-5	0,3	100	20
DS80-100-U-1	0,0	100	80	TX20-200-U-1	0,0	200	20
DS80-100-U-2	0,0	100	80	TX20-200-U-2	0,0	200	20
DS80-100-U-3	0,0	100	80	TX20-200-U-3	0,0	200	20
DS80-100-U-4	0,0	100	80	TX20-200-R-1	0,3	200	20
DS80-100-U-5	0,0	100	80	TX20-200-R-2	0,3	200	20
DS80-100-R-1	0,3	100	80	TX20-200-R-3	0,3	200	20
DS80-100-R-2	0,3	100	80	TX20-200-R-4	0,3	200	20
DS80-100-R-3	0,3	100	80	TX20-200-R-5	0,3	200	20
DS80-100-R-4	0,3	100	80	TX40-050-U-1	0,0	50	40
DS80-100-R-5	0,3	100	80	TX40-050-U-2	0,0	50	40
DS80-100-R-6	0,3	100	80	TX40-050-U-3	0,0	50	40
DS80-100-R-7	0,3	100	80	TX40-050-R-1	0,3	50	40
DS80-200-U-1	0,0	200	80	TX40-050-R-2	0,3	50	40
DS80-200-U-2	0,0	200	80	TX40-050-R-3	0,3	50	40
DS80-200-U-3	0,0	200	80	TX40-050-R-4	0,3	50	40
DS80-200-U-4	0,0	200	80	TX40-050-R-5	0,3	50	40
DS80-200-U-5	0,0	200	80	TX40-100-U-1	0,0	100	40
DS80-200-R-1	0,3	200	80	TX40-100-U-2	0,0	100	40
DS80-200-R-2	0,3	200	80	TX40-100-U-3	0,0	100	40
DS80-200-R-3	0,3	200	80	TX40-100-R-1	0,3	100	40
DS80-200-R-4	0,3	200	80	TX40-100-R-2	0,3	100	40
DS80-200-R-5	0,3	200	80	TX40-100-R-3	0,3	100	40
DS80-200-R-6	0,3	200	80	TX40-100-R-4	0,3	100	40
DS80-200-R-7	0,3	200	80	TX40-100-R-5	0,3	100	40
TX20-050-U-1	0,0	50	20	TX40-200-U-1	0,0	200	40
TX20-050-U-2	0,0	50	20	TX40-200-U-2	0,0	200	40
TX20-050-U-3	0,0	50	20	TX40-200-U-3	0,0	200	40
TX20-050-R-1	0,3	50	20	TX40-200-R-1	0,3	200	40
TX20-050-R-2	0,3	50	20	TX40-200-R-2	0,3	200	40
TX20-050-R-3	0,3	50	20	TX40-200-R-3	0,3	200	40
TX20-050-R-4	0,3	50	20	TX40-200-R-4	0,3	200	40
TX20-050-R-5	0,3	50	20	TX40-200-R-5	0,3	200	40
TX20-100-U-1	0,0	100	20	TX60-050-U-1	0,0	50	60
TX20-100-U-2	0,0	100	20	TX60-050-U-2	0,0	50	60
TX20-100-U-3	0,0	100	20	TX60-050-U-3	0,0	50	60
TX20-100-R-1	0,3	100	20	TX60-050-R-1	0,3	50	60
TX20-100-R-2	0,3	100	20	TX60-050-R-2	0,3	50	60
TX20-100-R-3	0,3	100	20	TX60-050-R-3	0,3	50	60

Table 4.7. Test Program (Continued)

<i>Test Code</i>	v_f (%)	$\sigma_{n,r}$ (kPa)	I_D (%)	<i>Test Code</i>	v_f (%)	$\sigma_{n,r}$ (kPa)	I_D (%)
TX60-050-R-4	0,3	50	60	TX80-100-R-6	0,3	100	80
TX60-050-R-5	0,3	50	60	TX80-100-R-7	0,3	100	80
TX60-100-U-1	0,0	100	60	TX80-200-U-1	0,0	200	80
TX60-100-U-2	0,0	100	60	TX80-200-U-2	0,0	200	80
TX60-100-U-3	0,0	100	60	TX80-200-U-3	0,0	200	80
TX60-100-R-1	0,3	100	60	TX80-200-U-4	0,0	200	80
TX60-100-R-2	0,3	100	60	TX80-200-U-5	0,0	200	80
TX60-100-R-3	0,3	100	60	TX80-200-R-1	0,3	200	80
TX60-100-R-4	0,3	100	60	TX80-200-R-2	0,3	200	80
TX60-100-R-5	0,3	100	60	TX80-200-R-3	0,3	200	80
TX60-200-U-1	0,0	200	60	TX80-200-R-4	0,3	200	80
TX60-200-U-2	0,0	200	60	TX80-200-R-5	0,3	200	80
TX60-200-U-3	0,0	200	60	TX80-200-R-6	0,3	200	80
TX60-200-R-1	0,3	200	60	TX80-200-R-7	0,3	200	80
TX60-200-R-2	0,3	200	60	RS20-050-U-1	0,0	50	20
TX60-200-R-3	0,3	200	60	RS20-050-U-2	0,0	50	20
TX60-200-R-4	0,3	200	60	RS20-050-U-3	0,0	50	20
TX60-200-R-5	0,3	200	60	RS20-050-R-1	0,3	50	20
TX80-050-U-1	0,0	50	80	RS20-050-R-2	0,3	50	20
TX80-050-U-2	0,0	50	80	RS20-050-R-3	0,3	50	20
TX80-050-U-3	0,0	50	80	RS20-050-R-4	0,3	50	20
TX80-050-U-4	0,0	50	80	RS20-050-R-5	0,3	50	20
TX80-050-U-5	0,0	50	80	RS20-100-U-1	0,0	100	20
TX80-050-R-1	0,3	50	80	RS20-100-U-2	0,0	100	20
TX80-050-R-2	0,3	50	80	RS20-100-U-3	0,0	100	20
TX80-050-R-3	0,3	50	80	RS20-100-R-1	0,3	100	20
TX80-050-R-4	0,3	50	80	RS20-100-R-2	0,3	100	20
TX80-050-R-5	0,3	50	80	RS20-100-R-3	0,3	100	20
TX80-050-R-6	0,3	50	80	RS20-100-R-4	0,3	100	20
TX80-050-R-7	0,3	50	80	RS20-100-R-5	0,3	100	20
TX80-100-U-1	0,0	100	80	RS20-200-U-1	0,0	200	20
TX80-100-U-2	0,0	100	80	RS20-200-U-2	0,0	200	20
TX80-100-U-3	0,0	100	80	RS20-200-U-3	0,0	200	20
TX80-100-U-4	0,0	100	80	RS20-200-R-1	0,3	200	20
TX80-100-U-5	0,0	100	80	RS20-200-R-2	0,3	200	20
TX80-100-R-1	0,3	100	80	RS20-200-R-3	0,3	200	20
TX80-100-R-2	0,3	100	80	RS20-200-R-4	0,3	200	20
TX80-100-R-3	0,3	100	80	RS20-200-R-5	0,3	200	20
TX80-100-R-4	0,3	100	80	RS40-050-U-1	0,0	50	40
TX80-100-R-5	0,3	100	80	RS40-050-U-2	0,0	50	40

Table 4.7. Test Program (Continued)

<i>Test Code</i>	v_f (%)	$\sigma_{n,r}$ (kPa)	I_D (%)	<i>Test Code</i>	v_f (%)	$\sigma_{n,r}$ (kPa)	I_D (%)
RS40-050-U-3	0,0	50	40	RS60-200-R-1	0,3	200	60
RS40-050-R-1	0,3	50	40	RS60-200-R-2	0,3	200	60
RS40-050-R-2	0,3	50	40	RS60-200-R-3	0,3	200	60
RS40-050-R-3	0,3	50	40	RS60-200-R-4	0,3	200	60
RS40-050-R-4	0,3	50	40	RS60-200-R-5	0,3	200	60
RS40-050-R-5	0,3	50	40	RS80-050-U-1	0,0	50	80
RS40-100-U-1	0,0	100	40	RS80-050-U-2	0,0	50	80
RS40-100-U-2	0,0	100	40	RS80-050-U-3	0,0	50	80
RS40-100-U-3	0,0	100	40	RS80-050-U-4	0,0	50	80
RS40-100-R-1	0,3	100	40	RS80-050-U-5	0,0	50	80
RS40-100-R-2	0,3	100	40	RS80-050-R-1	0,3	50	80
RS40-100-R-3	0,3	100	40	RS80-050-R-2	0,3	50	80
RS40-100-R-4	0,3	100	40	RS80-050-R-3	0,3	50	80
RS40-100-R-5	0,3	100	40	RS80-050-R-4	0,3	50	80
RS40-200-U-1	0,0	200	40	RS80-050-R-5	0,3	50	80
RS40-200-U-2	0,0	200	40	RS80-050-R-6	0,3	50	80
RS40-200-U-3	0,0	200	40	RS80-050-R-7	0,3	50	80
RS40-200-R-1	0,3	200	40	RS80-100-U-1	0,0	100	80
RS40-200-R-2	0,3	200	40	RS80-100-U-2	0,0	100	80
RS40-200-R-3	0,3	200	40	RS80-100-U-3	0,0	100	80
RS40-200-R-4	0,3	200	40	RS80-100-U-4	0,0	100	80
RS40-200-R-5	0,3	200	40	RS80-100-U-5	0,0	100	80
RS60-050-U-1	0,0	50	60	RS80-100-R-1	0,3	100	80
RS60-050-U-2	0,0	50	60	RS80-100-R-2	0,3	100	80
RS60-050-U-3	0,0	50	60	RS80-100-R-3	0,3	100	80
RS60-050-R-1	0,3	50	60	RS80-100-R-4	0,3	100	80
RS60-050-R-2	0,3	50	60	RS80-100-R-5	0,3	100	80
RS60-050-R-3	0,3	50	60	RS80-100-R-6	0,3	100	80
RS60-050-R-4	0,3	50	60	RS80-100-R-7	0,3	100	80
RS60-050-R-5	0,3	50	60	RS80-200-U-1	0,0	200	80
RS60-100-U-1	0,0	100	60	RS80-200-U-2	0,0	200	80
RS60-100-U-2	0,0	100	60	RS80-200-U-3	0,0	200	80
RS60-100-U-3	0,0	100	60	RS80-200-U-4	0,0	200	80
RS60-100-R-1	0,3	100	60	RS80-200-U-5	0,0	200	80
RS60-100-R-2	0,3	100	60	RS80-200-R-1	0,3	200	80
RS60-100-R-3	0,3	100	60	RS80-200-R-2	0,3	200	80
RS60-100-R-4	0,3	100	60	RS80-200-R-3	0,3	200	80
RS60-100-R-5	0,3	100	60	RS80-200-R-4	0,3	200	80
RS60-200-U-1	0,0	200	60	RS80-200-R-5	0,3	200	80
RS60-200-U-2	0,0	200	60	RS80-200-R-6	0,3	200	80
RS60-200-U-3	0,0	200	60	RS80-200-R-7	0,3	200	80

4.4 Test Systems and Application Details

The first recorded work on measuring the frictional resistance of a material belongs to Da Vinci (1493). Da Vinci suggested that there is a linear relationship between friction force and normal force, and Amontons (1699) made important contributions to the subject in the upcoming period. Coulomb (1773) used this phenomenon for the first time in soil mechanics applications.

Coulomb investigated the shear strength of the soil, which he defined by adding the cohesion component to the friction term, in a mechanism similar to the direct shear method with the relative motion of two rigid plates relative to each other, and Collin (1846) systematized this approach experimentally for the first time. In the following years, researchers such as Leygues (1885), Goodrich (1904), Bell (1915), and Krey (1926) made important contributions to the development of the direct shear method. However, the test system took its final modern form with the stress-controlled study of Terzaghi and Casagrande (1932) and strain-controlled study of Gilboy (1936).

The researchers mostly preferred test systems that represent axisymmetric loading conditions in order to eliminate the disadvantages of both the field conditions and the direct shear method. For this purpose, Westerberg (1921) first used the system developed by Adams and Nicholson (1900) (with σ_3 metal sheath) and later by Kármán (1910, 1911) (with σ_3 water pressure) to determine the strength properties of rocks for soil tests. Terzaghi (in Vienna) and his student Casagrande (in Massachusetts) developed the first modern style triaxial test systems (1930). Terzaghi's students in Europe (Rendulic, 1933; Buisman, 1934; Kjellman, 1936; et al.) and the USA (Jürgenson, 1934; Stanton and Hveem, 1934; Housel, 1936; et al.) contributed significantly to the optimization of these developed systems for soil mechanical practice.

In order to improve the limited strain properties of direct shear and triaxial shear methods, Terzaghi together with his students in Europe designed the ring shear test instrument that allows high strain levels (Gruner and Haefeli, 1934; Hvorslev, 1936b, 1937, 1939; Tiedemann, 1937; Haefeli, 1938; et al.). At that time, when the foundations of contemporary soil mechanics were laid, this more sophisticated method was not preferred

because researchers generally focused on the peak strength properties of the soil. However, later on, the importance of final strength in geotechnical engineering applications was understood (Skempton, 1964; De Beer, 1967; Kenney, 1967; et al.) and this method became quite popular after the seventies in order to reach the strain levels representing field conditions. A lot of studies were carried out for the development of methods and test equipment (La Gatta, 1970; Bishop et al., 1971; Bromhead, 1979).

In the next section, the systems used in the study of direct shear, triaxial shear and ring shear test methods, with the historical background above, will be introduced and the application principles for each method will be presented in detail.

4.4.1. Direct shear test

It is the first test used to measure the strength properties of the soil. In this test type, square or circular samples are placed inside the shear box consisting of two rigid plates and consolidated under a vertical normal load, which represents the conditions of the sample in the field. The consolidated samples are sheared at a constant shear strain speed that will not generate pore water pressure under the consolidation loading. During shearing, one of the plates is kept fixed while the other plate is loaded with shear force. The reaction force measured by the load cell represents the shear strength of the soil, which resists this increased force until the sample fails. Vertical and horizontal strains are obtained by means of displacement measurement tools on the test system. The general design of the test system is shown in Figure 4.11.

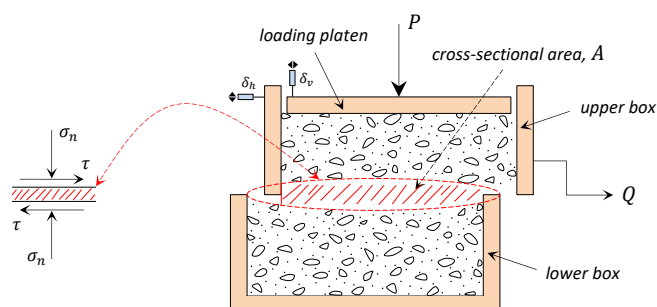


Figure 4.11. Schematic section diagram of the direct shear test (Wood, 2009)

The major principal stress on the shear plane during the consolidation phase is represented by the applied normal stress, and the minor principal stress is represented by the earth pressure at rest. Principal stress cannot be obtained directly since the shear axes formed on this plane during shear will rotate. However, this type of stress on the rotating principal planes can be obtained with the help of the Mohr-Coulomb failure envelope as in Figure 4.12.

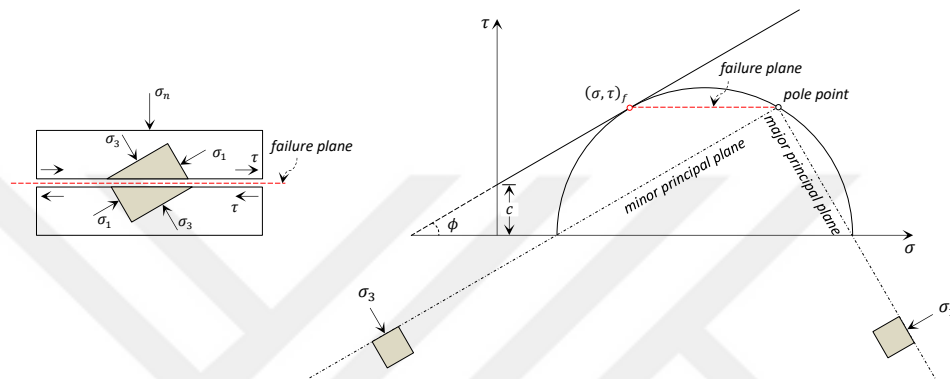


Figure 4.12. Representation of stress states on the shear plane with Mohr's circle (Taylor, 1948)

When a shear force is applied to the soil, the shear plane area decreases accordingly. This decrease causes an increase in the normal stress force affecting the soil sample. While this is often ignored for practical purposes, it must be taken into account in such comparative analyses that require precise measurements. In the calculations of this study, it was seen that the related phenomenon affects the shear strength parameters between $0.5^\circ - 2.5^\circ$ as a function of the normal force and especially the joint effect of the relative density. For this reason, the notion of corrected area was taken into account when evaluating the results of the study. Accordingly, normal and shear stress expressions are calculated using the following relations:

$$\sigma'_n = \frac{P}{A_c} \quad (4.20)$$

$$\tau = \frac{Q}{A_c} \quad (4.21)$$

In the above equations, P refers to normal load, Q refers to horizontal load, and A_c refers to corrected cross-sectional area of the sample. This area can be defined as Equation 4.22 for circular shear boxes:

$$A_c = A_o K \quad (4.22)$$

$$K = \frac{2}{\pi} \left[\cos^{-1} \left(\frac{\delta_h}{D} \right) - \frac{\delta_h}{D} \sqrt{1 - \left(\frac{\delta_h}{D} \right)^2} \right] \quad (4.23)$$

Here, A_o refers to initial area, K refers to correction factor, D refers to diameter of shear box, and δ_h refers to horizontal displacement. The schematic representation of the corrected cross-sectional area is presented in Figure 4.13.

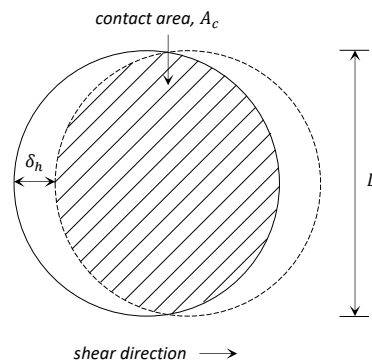


Figure 4.13. Dynamic shear area diagram of circular shear box

Due to the limitations of the direct shear test such as forcing the sample to be sheared along a predetermined plane, non-uniform stress-strain distribution on the shear plane, failure to control drainage, non-verified degree of saturation, effect of boundary conditions of the shear box etc., the researchers should be careful about directly using the results obtained; the results should be supported by other laboratory tests. On the other hand, this test has become a standard practice especially for measuring the engineering properties of coarse-grained soil types due to its advantages such as being quite simple, inexpensive, and easy to apply.

Direct shear tests were carried out with the EL26-2114/01 series digital direct/final shear apparatus manufactured by ELE International as a soil test equipment (Figure 4.14). The fact that it has a microprocessor-controlled driver system and a touch keyboard input with an LCD screen makes the device highly functional. The device can be used for square and circular samples and is strain-controlled. In this study, a circular shear box with a diameter of 63.5 mm was used (Figure 4.15), and the depth of the sample was chosen as 25 mm. On the other hand, the apparatus was designed in a way that the ratio of the load on the load hanger to the load affecting the sample to be 1:10. Displacements during both consolidation (K_0 conditions) and shear were measured with linear variable differential transformers (LVDT) (ELE 27-1689, ELE 27-1697), while shear stresses were measured with S-Type high-capacity load cells (ELE 27-1561) (Figure 4.16). Records obtained from the physical systems (real-world phenomena) can be evaluated by transferring them to the computer system by means of data collection systems and signal converter systems (ELE GDU 8, RS 232C, ELE DS7.3). The test apparatus supports numerous technical standards including ASTM, AASHTO, BSI and ISO. In this study, the ASTM D3080/D3080M-11 standard was used in order to facilitate the use of the circular shear box and to be compatible with other test methods. The general features of the direct shear apparatus and other auxiliary equipment are summarized in Table 4.8.



Figure 4.14. Direct shear apparatus manufactured by ELE International (26-2114/01)

Table 4.8. Specifications of direct shear test apparatus (ELE, 2015, 2019)

<i>Specifications</i>	<i>Value</i>
<i>maximum specimen size</i>	<i>square $\leq 100 \text{ mm}^2$ diameter $\leq 63.5 \text{ mm}$</i>
<i>speed range</i>	<i>0.00001 - 9.99999 mm/min</i>
<i>maximum shear travel</i>	<i>12.5 mm</i>
<i>maximum design shear force</i>	<i>5 kN</i>
<i>maximum design normal load</i>	<i>1000 kg</i>
<i>vertical load</i>	<i>10.0 kN using 10:1 lever ratio</i>
<i>travel range of displacement transducers</i>	<i>15 mm</i>
<i>supply voltage (s)</i>	<i>115/230 V AC, 50/60 Hz, single phase</i>
<i>power consumption</i>	<i>26W - 1.6A - T</i>
<i>weight (approximate)</i>	<i>82 kg</i>
<i>approximate dimensions (L x W x H)</i>	<i>320 x 1135 x 1260 mm</i>

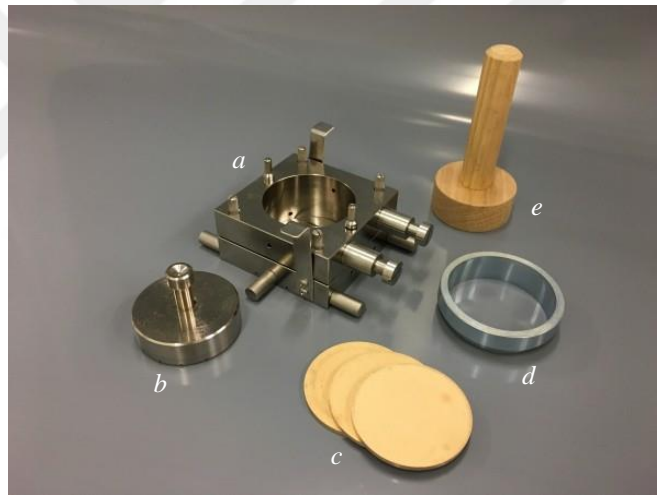


Figure 4.15. Auxiliary equipment of the circular shear box: (a) Shear box, (b) Loading pad, (c) Porous plate, (d) Specimen cutter, (e) Specimen extrusion (26-2213)

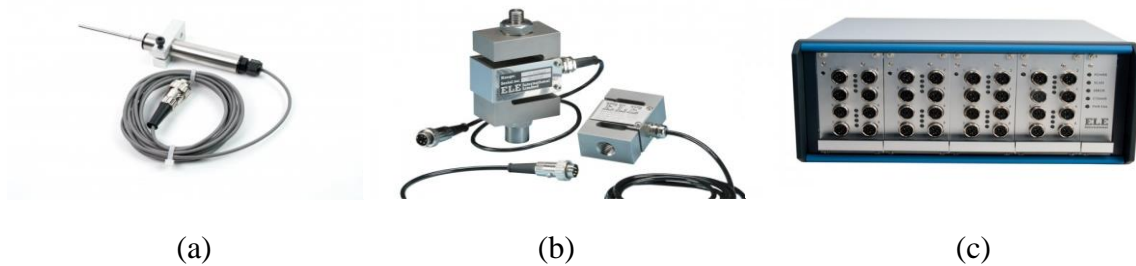


Figure 4.16. System tools used in the study: (a) LVDT, (b) Load cell, (c) Data acquisition unit

After the procedures, the details of which are given in Section 4.3, the tests were started (Figure 4.17). At this stage, first, the lower and upper two separate rigid parts were mounted to each other with the help of lifting and connecting screws, and the shear box was installed. The shear box was fixed by placing it in the test reservoir on the apparatus. Then, a porous plate was placed on the base plate at the bottom of the box, the sample was placed with the target density in accordance with the principles mentioned in Section 4.3, and a porous plate was placed on it. Finally, the loading pad was closed, and the equipment was prepared for the test. Then, the final preparations of the test apparatus were completed by checking the vertical and horizontal transducers, load cell, vertical normal load, and so forth. Since the test was planned to be carried out in drained conditions, the reservoir was filled with water and left for enough time for the sample to be saturated. After the preparation was completed, the sample was left for consolidation (Figure 4.18). After the consolidation, the connection screws were removed, and the plates were separated from each other with the help of lifting screws. Since this operation forms the shear plane, it can directly affect the test results; therefore, this step is very important (effect of gap size). As a result of a series of tests conducted specifically for this study, it was seen that the range should be accepted as 3.5 mm. The method used to determine this range should be re-evaluated for each study, as many factors such as the dimensions of the shear box, the properties of the soil material ($L_D/D_{50} = 90$) play an important role in this regard. This determined range was maintained in all direct shear tests. On the other hand, since the vertical elevation difference between the plane on which the shear force was applied and the sample shear plane can cause moments, the effect of the eccentric loading condition in which these rotations would occur on the strength properties was also investigated (effect of lever arm). Accordingly, it was observed that there was a difference of 0.2° between the heights that are commonly used and recommended in the ASTM D3080/D3080M-11 standard, which affected the shear strength parameters (5 mm). Although this difference is negligible for practical applications, in this comparison study, it was taken into account by adhering to the height recommended in the standards. Since it was aimed to obtain not only the peak strength but also the ultimate strength in the tests, shearing was continued until the relative lateral displacement reached 100%. The constant shear strain rate was chosen as 1 mm/min for all tests. After the test was completed, the shear box was removed from the reservoir and disassembled, and some material was taken from the shear plane to determine the water content at the end of the test (Figure 4.19). It was seen that the obtained water content (18 – 20%) were compatible with

the literature data for the drainage tests in saturated conditions. Finally, the measured strength parameters were re-evaluated using all relevant correction factors.

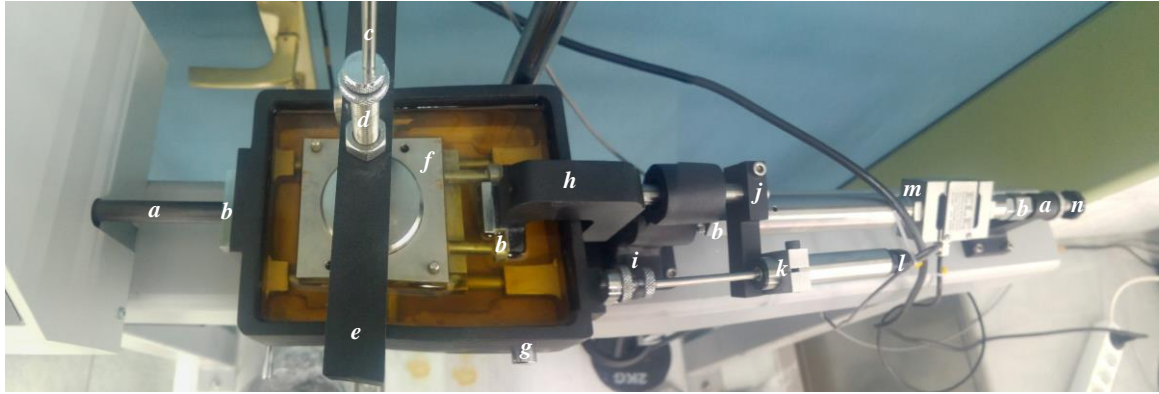
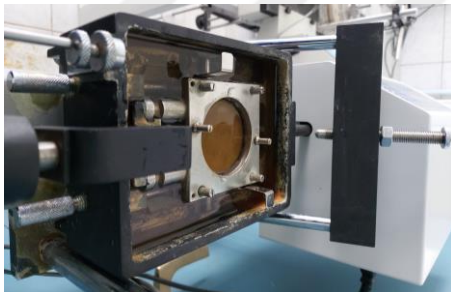
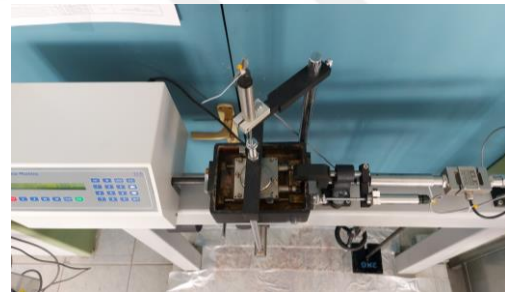


Figure 4.17. General view of the direct shear apparatus from the top profile: (a) Loading shaft, (b) Train of components, (c) Vertical displacement transducer, (d) Load pin, (e) Loading yoke, (f) Shear box, (g) Drain plug, (h) Swan neck, (i) Locking screw, (j) Swan neck guide shaft arm, (k) Split bracket, (l) Horizontal displacement transducer, (m) Load cell, (n) Load cell adjustment lever



(a)



(b)

Figure 4.18. Pre-test procedure: (a) Sample preparation, (b) Consolidation stage

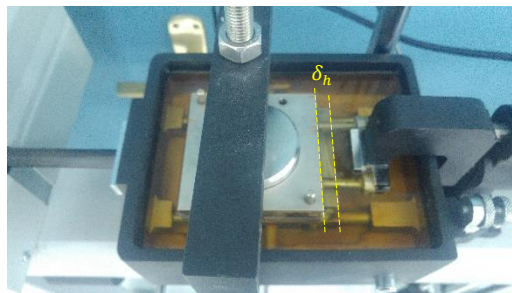


Figure 4.19. Post-test procedure: Shear completion and disassembly of the shear box

4.4.2. Triaxial shear test

It is the most common test type used to determine the strength properties of the soil. This test, the details of which were first described by Bishop and Henkel (1957), is based on the principle of shearing cylindrical samples under a hydrostatic pressure load with increased stress (deviator stress) in the vertical direction. The most important advantages of this test type are that it is suitable for all soil types and that the soil can represent the field loading/drainage conditions. With this test, in which the shear strength parameters can be obtained in three different ways (UU-CU-CD) based on the loading and drainage conditions, the relevant definitions can be expressed in terms of total stress or effective stress.

In this study, a consolidated-drained (CD) type triaxial shear test was used. The CD test is based on the consolidation of the saturated sample, which is subject to drainage, under a constant confining pressure, and sheared by the deviator stress, which is increased at a rate low enough not to generate pore water pressure. Effective stress can be expressed as total stress in this test type since excess pore water pressure is not generated in this test. It is suitable to be used for situations where slopes, strength structures, foundations, excavations need to be analyzed for a long time (such as negative pore water pressure situation that may occur). The schematic diagram of the test method is given in Figure 4.20.

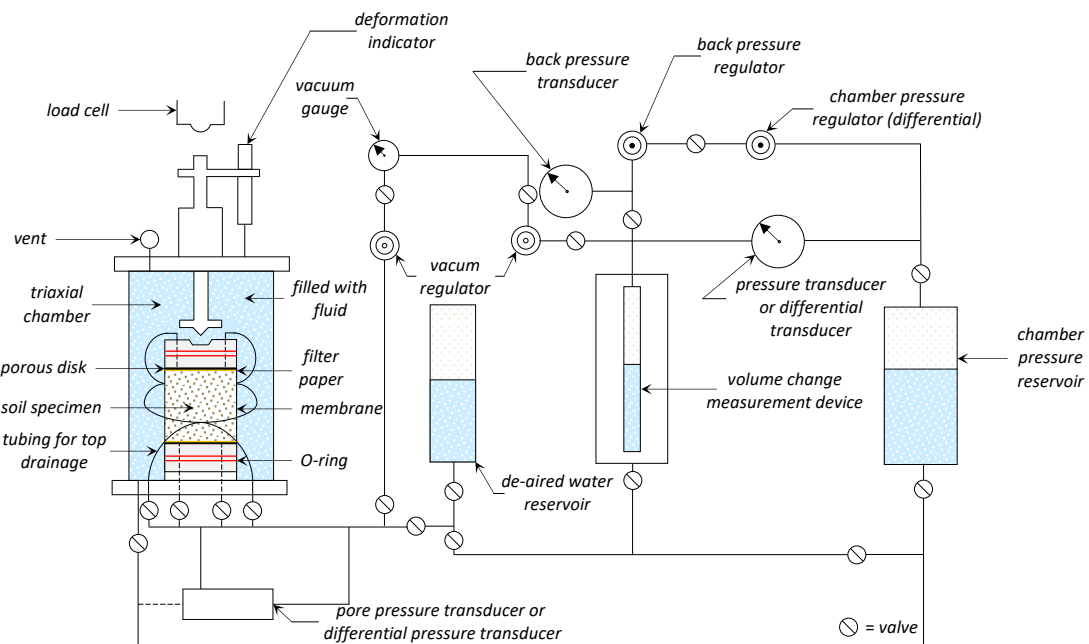


Figure 4.20. Schematic diagram of consolidated drained triaxial apparatus (ASTM, 2020)

Since detailed information and visuals about the triaxial shear method for understanding the general stress conditions of the soil have been presented in Section 3, they are not presented in this section again.

In contrast to direct shear and ring shear tests, which are based on stress on the shear plane, principal stress is used in the triaxial tests. This situation makes the interpretation of triaxial test results very difficult. Some assumptions must be made in order to overcome this procedural difference among the test methods and to carry out comparative analyzes in a meaningful way. In this context, using the relationship in Figure 3.6 for the triaxial test, the following equations representing the stress state at failure can be obtained:

$$\sigma' = \frac{\sigma'_1 + \sigma'_3}{2} - \frac{\sigma'_1 - \sigma'_3}{2} \sin \phi' \quad (4.24)$$

$$\tau = \sigma' \tan \phi' = \frac{\sigma'_1 - \sigma'_3}{2} \cos \phi' \quad (4.25)$$

As in the direct shear test, the cross-sectional area of the soil sample changes during the triaxial shear test. This area is defined as following for the saturation, consolidation, and shear stage as a function of height and volumetric strain. For the saturation and consolidation stage:

$$H_{co} = H_o - \Delta H_{co} \quad (4.26)$$

$$V_{co} = V_o - \Delta V_{co} \quad (4.27)$$

$$A_{co} = \frac{V_{co}}{H_{co}} = \frac{V_{co} - \Delta V_{sat}}{H_{co} - \Delta H_{sat}} \quad (4.28)$$

Here, the initial height and volume of the sample are represented by H_o and V_o , the post-consolidation sample height and volume by H_{co} and V_{co} , respectively, the change in sample height and volume at the end of consolidation by ΔH_{co} and ΔV_{co} , respectively, the change in the total height and volume of the sample at the saturation phase by ΔH_{sat} and $\Delta V_{sat} = 3V_o(\Delta H_{sat}/H_o)$, respectively.

At the end of the consolidation, the density of the sample is re-evaluated using the following:

$$\gamma_{dco} = \frac{W}{V_{co}} \quad (4.29)$$

$$e_{co} = \frac{G_s \gamma_w}{\gamma_{dco}} - 1 \quad (4.30)$$

For drainage tests, the mean cross-sectional area at the shear stage (A_c) can be defined as follows²:

$$A_c = \frac{V_{co} - \Delta V_\varepsilon}{H_{co} - \Delta H_\varepsilon} = \frac{V_{co}}{H_{co}} \frac{1 - \frac{\Delta V_\varepsilon}{V_{co}}}{1 - \frac{\Delta H_\varepsilon}{H_{co}}} = A_{co} \frac{1 - \varepsilon_v}{1 - \varepsilon_h} \quad (4.31)$$

Here, the height and volume changes during shear until any strain level are represented by ΔH_ε and ΔV_ε , respectively, and axial strain and volumetric strain are represented by ε_h and ε_v , respectively.

The results obtained from the triaxial test systems depend on many factors due to the complicated structure of the system. For practical purposes, in most standard studies, these factors may be partially ignored, but in this comparative study, all factors were considered to make a meaningful comparison. Accordingly, the deviator stress (σ_d) can be defined as:

$$\sigma_d = (\sigma'_1 - \sigma'_3) = \frac{P}{A_c} S_c = \frac{F + T + \sigma'_3 (A_c - A_p)}{A_c} - \sigma'_3 \quad (4.32)$$

Here, P refers to applied axial load, S_c refers to system correction constant representing hydrostatic lift pressure, piston friction and other effects, F refers to load transmitted to the

² La Rochelle et al. (1988), Zhang and Garga (1997) and other researchers stated that A_c can be defined in different formats depending on factors such as the type and nature of the soil and membrane, strain level, failure pattern and shear band formation, drainage status, and additive materials. In this study, it was assumed that the sample was strained in a vertical circular cylindrical form in accordance with ASTM D7181-20.

piston, T refers to load transmitted from components such as piston weight and loading head, and A_p refers to area of the loading piston.

Using the expressions in Equations 4.29 and 4.30, it was seen that the sample void ratio decreased by 0.7% at the saturation stage and by 1.8% at the end of consolidation, while the decrease in the void volume was more limited in fiber reinforced samples. On the other hand, it was observed that the shear strength angles of the corrected area decreased by 3.1° - 5.4° depending on the confining pressure, sample void ratio, fiber reinforcement and test method. Finally, it was determined that the deviator stress decreased by an average of 25% regardless of the fiber reinforcement and test method. All these results show the effect of the correction parameters on the results obtained from the highly complicated triaxial test systems.

Some limiting factors can be listed as major disadvantages of this test type. For example; ultimate (residual) strength parameters cannot be determined due to the limited displacement capacity of the triaxial shear test, the instruments of the test system are quite complicated and expensive, drainage tests take relatively longer time compared to other shear tests, and although the test sample is consolidated in isotropic conditions, the actual field conditions are usually anisotropic, stress distribution in the sample is not uniform due to the limiting effect of the base pedestal and the top cap, resulting in different unit shortenings along the sample body. On the other hand, this test type also has some important advantages. For example, controlling drainage conditions, direct measurement of volumetric changes and pore water pressure, uniform stress on the shear plane, being able to identify the stress paths of the field in the laboratory environment, and unlike other shear tests, the failure occurs in the weakest plane. Despite its disadvantages, this test type is the most preferred test type today, due to its important features such as better representation of the field conditions compared to other shear tests, being suitable for all soil types and determining the shear strength parameters at the desired quality.

Triaxial shear tests were carried out under strain control with the EL25-3516/01 series digital shearing apparatus produced by ELE International as a soil test equipment (Figure 4.21). The fact that it has a microprocessor-controlled driver system and a touch keyboard input with an LCD screen makes the device highly functional. In the tests, different sizes of base adapters (ELE 25-4166) and suitable caps (upper adapter) are used to provide

base, suction pressure and drainage (ELE 25-5430). Granular samples prepared with the support of a two-part vacuum mold in a latex membrane (Figure 4.22) are tested in triaxial plexiglass cells (ELE 25-4047) that can withstand a maximum of 1700 kPa pressure and are designed to carry only water pressure. Deaired water obtained by vacuuming the water circulated in the tank reservoir by the deaired water apparatus is used for the test (ELE 25-1833/01). The volume change in the triaxial system is automatically measured by the volume change unit (transducer) with electrical signals produced in proportion to the volume of the displaced water (ELE 27-1641). Axial vertical displacement is measured with a 50 mm capacity transducer (LVDT) (ELE 27-1617), while axial load is measured by a load ring with 50 kN maximum load capacity (ELE 78-0860). Another important equipment of the test system is the oil/water constant pressure units. These units with a pressure capacity of 1700 kPa are used in confining and back pressure applications (ELE 26-1800/01). A panel that functions as a universal pump and pressure indicator is provided for controlling and monitoring the pressure in the system (ELE 26-1880). Three different pressure transducers with 1700 kPa capacity are used to measure cell, pore water and back pressure (ELE 27-1633). Records obtained from the physical system can be evaluated by transferring them to the computer system by means of data acquisition systems and signal converter systems. Although this test system supports many standards, the ASTM D7181-20 standard was preferred in the study due to its compatible nature both with the auxiliary equipment and with other test methods. The visuals of the measuring apparatus used in the test are given in Figure 4.23, and the technical specifications of the system are summarized in Table 4.9.



Figure 4.21. Triaxial shear panel manufactured by ELE International (25-3516/01)

Table 4.9. Specifications of triaxial shear test apparatus (ELE, 1993, 2019)

<i>Specifications</i>	<i>Value</i>
<i>capacity</i>	<i>compression 50 kN tension 10 kN</i>
<i>speed range</i>	<i>0.00001 - 9.99999 mm/min</i>
<i>maximum axial travel</i>	<i>25 mm</i>
<i>maximum vertical clearance</i>	<i>910 mm</i>
<i>minimum vertical clearance</i>	<i>305 mm</i>
<i>horizontal clearance</i>	<i>364 mm</i>
<i>platen travel</i>	<i>100 mm</i>
<i>platen diameter</i>	<i>133 mm</i>
<i>supply voltage (s)</i>	<i>115/230 V AC, 50/60 Hz, single phase</i>
<i>power consumption</i>	<i>0.3/0.15A - T</i>
<i>weight (approximate)</i>	<i>90 kg</i>
<i>approximate dimensions</i>	<i>500 x 500 x 1470 mm</i>

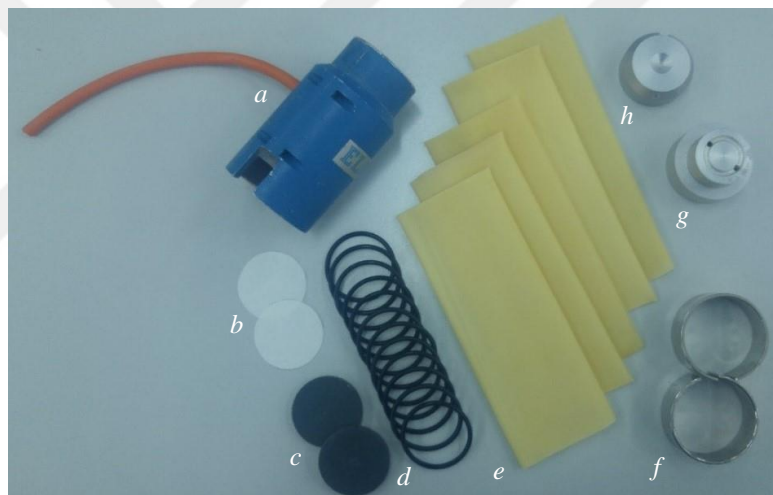


Figure 4.22. Auxiliary equipment of the triaxial shear test: (a) Two-part vacuum split mold, (b) Filter Disc, (c) Porous plate, (d) O-ring, (e) Membrane, (f) Membrane placing tool, (g) Base adapter, (h) Porous top cap

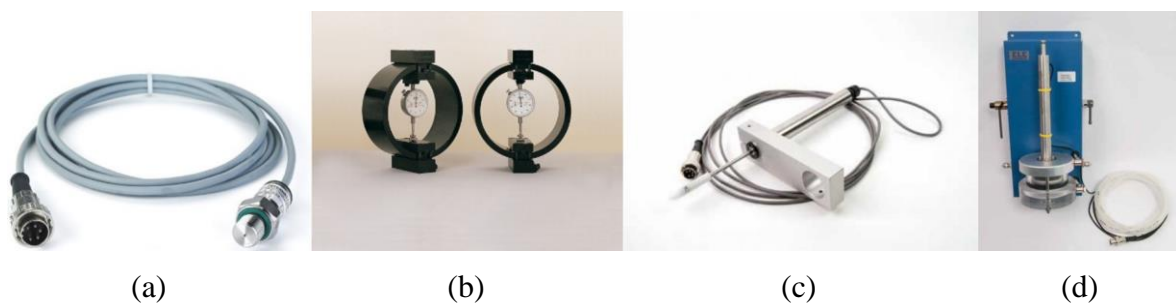


Figure 4.23. System tools used in the study: (a) Pressure transducer, (b) Clamped boss load ring, (c) LVDT, (d) Volume change unit

After the procedures, the details of which are given in Section 4.3, the tests were started. The methods to be used in the test phase vary greatly based on the material properties of the soil. Two-part vacuum split molds are used for the preparation of samples consisting of granular materials such as sand. These molds are attached to the outer surface of the latex membrane ($t_m = 0.6 \text{ mm}$, $E_m = 1400 \text{ kPa}$) placed on the base adapter with O-rings. By applying suction pressure with the help of a vacuum device, the membrane is stretched until the sample is completely placed in the mold. At this stage, a porous plate was placed in the membrane at the bottom, the filter disc was placed on top of it, and the sample with the target density was placed on top of it in accordance with the principles mentioned in Section 4.3. A filter disc was placed on the sample again, a porous plate was placed on it, and finally a top cap with a nylon tube was placed on it, and the membrane was fixed with O-rings. In order for the prepared sample ($D = 50 \text{ mm}$, $H = 100 \text{ mm}$) to stand, approximately -20 kPa suction pressure was applied from the universal vacuum panel. This pressure was relieved after the mold was removed, the cell was placed, the displacement and load transducers were adjusted, and the cell was filled with deaired water.

Another important step of the triaxial test is the saturation of the sample. In this procedure, which was carried out according to the ASTM D7181-20 standard, the saturation of the sample was controlled by the Skempton's (1954) pore pressure coefficient (B). Here B is the ratio of the change in confining pressure ($\Delta\sigma_3$) to the change in pore water pressure (Δu)

$$B = \frac{\Delta u}{\Delta\sigma_3} \quad (4.33)$$

In the test, the confining pressure and the back pressure were increased gradually until the desired saturation level ($0.95 \leq B$). The preferred increment value for the confining pressure and back pressure was selected as 50 kPa , and the pressure difference between them as 10 kPa . These values are in compliance with the pressure range values recommended by ASTM D7181-20. The volume change unit performs the supply of water used in saturation of the sample and the measurement of the amount of water. Therefore, this equipment must be filled with enough water and positioned according to the test standards before the test. Another important point to be mentioned in this regard is that the porous stones must be cleaned and saturated with deaired distilled water before the test. In this way,

the mobility of the water in the sample will be easier and the volume change unit will be able to make more reliable measurements. After the sample reached the desired saturation level, the consolidation phase was started. Unlike the saturation phase, the volume change unit was arranged to absorb water from the sample in this phase. The test system was adjusted to the desired constant confining pressure (50, 100, 200 kPa) and the sample was consolidated isotropically. The amount of water displaced in both the saturation and consolidation stages is very important as it is equal to the change in soil volume.

After the consolidation was completed, the shear phase was initiated for the triaxial test. At this stage, the drainage valves were left open, and the axial shear strain speed was chosen as low (1 mm/min) in order to prevent pore water pressure. In the apparatus loading takes place in a bottom-up manner. The deviator stress was increased at a constant speed, and the test was continued until the strain level reached the apparatus capacity ($\epsilon_a = 25\%$). Upon completion of the test, the triaxial cell was disassembled and some material was taken to measure the water content of the tested sample. The resulting water content (17 – 19%) is important both in terms of being compatible with the literature data for the tests with drainage of sands in saturated conditions and proving the consistency of the saturation and consolidation stages applied in this study. Details of the test system and its stages are shown in Figure 4.24 and Figure 4.25.

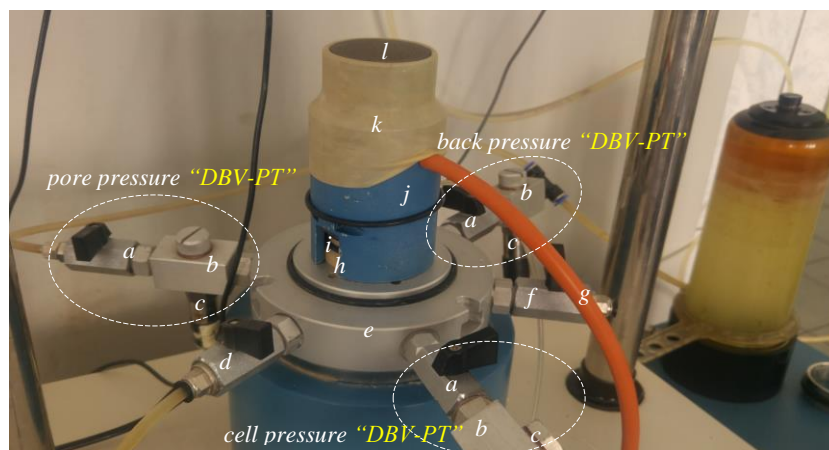


Figure 4.24. Other details of the sample setup and system valves for the triaxial test: (a) Drain/pressure valve, (b) De-airing Block, (c) Pressure transducer, (d) Cell water supply valve, (e) Cell base, (f) Suction pressure application valve, (g) Membrane vacuum line, (h) Base adapter, (i) O-ring, (j) Two-part vacuum split mold, (k) Membrane, (l) Porous plate



(a)



(b)



(c)



(d)



(e)



(f)

Figure 4.25. Stages of the triaxial shear test: (a) Preparing the sample, (b) Removing the mold, (c) Filling the cell with water, (d) Saturating the sample, (e) Consolidation stage, (f) Shear stage

4.4.3. Ring shear test

Ring shear is another important test type used to directly measure the strength properties of the soil. In this test, samples placed in the reservoir of a ring-shaped shear box consisting of two rigid plates at a target density are consolidated (by saturation) under a predetermined vertical normal load by means of a torsion beam (top cap). Consolidated samples are sheared at constant shear strain speed (with drainage) low enough not to generate pore water pressure (0.01 mm/min until peak, 1 mm/min after peak). During shearing, one of the platens is kept fixed while the other platen is loaded with torque (torsion) force. The resisting reaction force (measured by the load cells through the A-B ring arms), which is increased until the sample fails, represents the shear strength of the soil. The strains are obtained from the angular displacement of the torque movement, which can be followed by the transducer vertically and by the graduated scale on the test reservoir horizontally. The general arrangement of the ring shear test apparatus is shown in Figure 4.26.

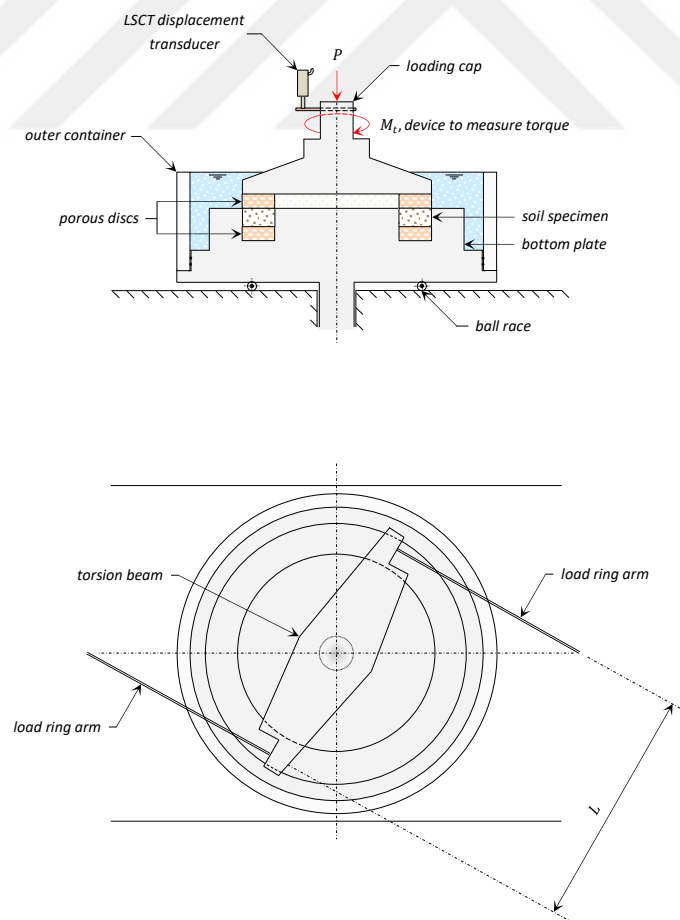


Figure 4.26. General view of ring shear test apparatus (Type B) (BS, 1990; ISO, 2018)

In contrast to the triaxial test, in the ring shear test, the samples are consolidated under anisotropic stress conditions (K_0). The direction of the principal stresses occurring in the shear plane during consolidation changes by rotating during shearing (σ_1 , $0^\circ \leq \delta \leq 90^\circ$)³, so the stress can be defined as in Figure 4.12 (in a form similar to the direct shear test). Undoubtedly, the style in which the ring shear test apparatus was produced, and the procedure used in its application are the most decisive factors for this definition.

In the ring shear tests, the stresses on the shear plane are not uniform. Bishop et al. (1971) used Hvorslev's (1936b) mean radius concept in order to eliminate this deficiency and stated that results with sufficient accuracy could be obtained with the uniform acceptance of the plane. Bromhead (1979); on the other hand, stated that in addition to this concept, reducing the sample thickness limits the stress difference on the shear plane, so uniform acceptance is sufficient only for certain soil types. This assumption is also accepted in standards such as BS 1377, BS EN ISO 17892, ASTM D6467, and ASTM D7608 and is based on the evaluation of the ring shear test results. Accordingly, the effective vertical (normal) stress, the average shear stress and the effective shear strength angle are expressed as:

$$\sigma'_n = \frac{P}{\pi(R_2^2 - R_1^2)} \quad (4.34)$$

$$\tau = \frac{3(F_1 + F_2)L}{4\pi(R_2^3 - R_1^3)} \quad (4.35)$$

$$\tau/\sigma'_n = \tan \phi' = \frac{3L(F_1 + F_2)(R_2^2 - R_1^2)}{4P(R_2^3 - R_1^3)} \quad (4.36)$$

In the above equations, R_1 and R_2 refer to inner and outer radius, respectively, F_1 and F_2 refer to forces measured on load ring A and B , and L refers to torque arm length (Figure 4.27). The details of the derivation of Equation 4.35 are given in footnote 4⁴, and the free-body diagram of the shear band of the stresses defined above is shown in Figure 4.28.

³ The major principal stress is σ_1 , the angle between the σ_1 direction and the vertical is represented by δ .

⁴ Moment = $\tau \times$ sample area \times moment arm $\rightarrow \int_0^{2\pi} R d\theta \int_{R_1}^{R_2} \tau \times R dR = \frac{L}{2} \times (F_1 + F_2) \rightarrow 2\pi \times \tau \left[\frac{R^3}{3} \right]_{R_1}^{R_2} = \frac{L}{2} \times (F_1 + F_2) \rightarrow 2\pi \times \tau \left[\frac{R_2^3}{3} - \frac{R_1^3}{3} \right] = \frac{L}{2} \times (F_1 + F_2) \rightarrow \frac{2}{3}\pi \times \tau [R_2^3 - R_1^3] = \frac{L}{2} \times (F_1 + F_2) \rightarrow \tau = \frac{3(F_1 + F_2)L}{4\pi(R_2^3 - R_1^3)}$

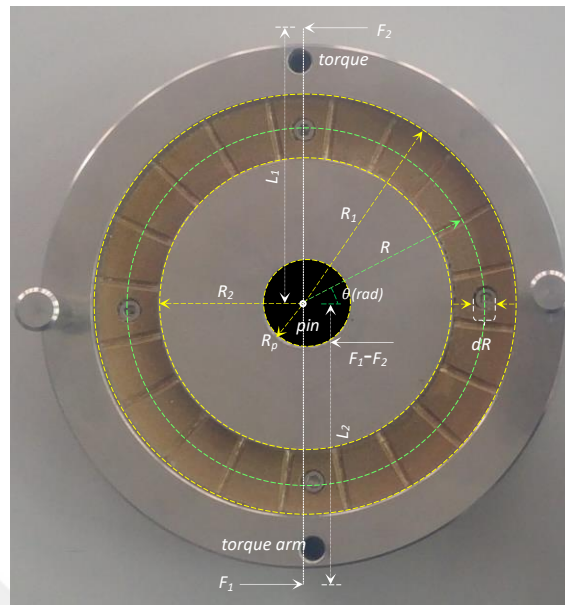


Figure 4.27. Plan view of bottom platen, center pin and torque arms of ring shear test apparatus (Type B)

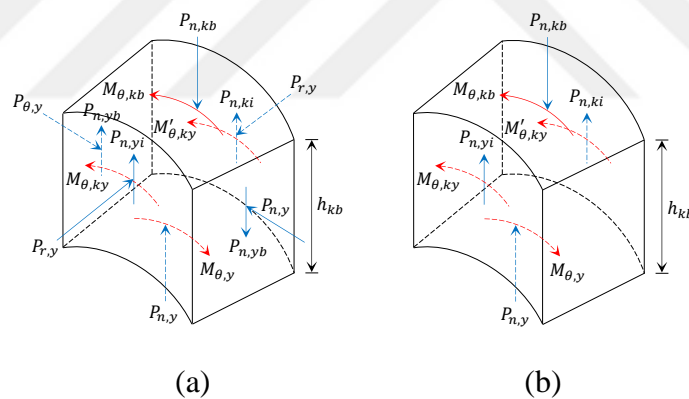


Figure 4.28. Stress state of the shear band in the ring shear test: a) Resultant of forces, b) Unbalanced forces (*Detailed explanations of notation representation can be found in Sadrekarimi's study (2009).*)

The relationship between the angular displacement (θ) and mean linear displacement (d_l) is as follows:

$$d_l = \left(\frac{\theta \times \pi}{180}\right) \left(\frac{R_1 + R_2}{2}\right) \tag{4.37}$$

Since the area of the shear plane did not change during the test, no correction expression was used for this area. On the other hand, some factors may cause errors in test results. For example, wall friction, rebound of the sand, friction between the rings and the top plate as a result of material extrusion, errors in force measurement (friction of unequal load arms with central pin), tendency of the top head to transfer non-uniform stress distribution. Bromhead (1979) stated that these effects may vary based on the shear speed, sample depth, soil type and ring shear type. He reported that the friction of the central pin is more important for coarse grained soil types ($1.18 \text{ mm} > D_m$) to be used in the device he developed. Accordingly, the torque error (M_e) can be obtained with the following equation:

$$M_e = (F_1 - F_2)\mu R_p \quad (4.38)$$

In the above equation, R_p refers to the pin radius and μ refers to the friction between the central pin and the platen. For Bromhead type (Type B) ring shear apparatus, this value should be accepted as $R_p = 5 \text{ mm}$, in case of lubrication of the tool it should be accepted as $\mu = 0.1$.

All procedures and details described herein apply only to coarse-grained soil types. Undoubtedly, different parameters and correction expressions must be used for fine-grained soil types, which have very different material properties.

This test type has some disadvantages as well. For example, non-uniformity of stress-strain distributions on the shear plane, friction caused by the wall, rebound effect for granular materials, potential release of the test sample towards out of the reservoir, the complex procedure required for tests without drainage, and shearing along a predetermined plane. However, due to some advantages, it is the preferred test method for determining the ultimate strength, which is an intrinsic property of soils. Examples of these advantages can be listed as shearing samples at desired displacement levels (unlimited), stable cross-sectional area of the shear plane during the test, functional structure, the less amount of sample required for the test (therefore, it provides the opportunity for rapid drainage and consolidation)⁵, being suitable for all types, classes, and properties of soil.

⁵ Applicable to Bromhead type ring shear test apparatus.

Ring shear tests were carried out with a torsion Bromhead type VJT5600A/01 series digital shearing apparatus manufactured by VJTech Limited as a soil test equipment (Figure 4.29). The microprocessor-controlled driver system and the LCD-screened control panel on the device make it highly functional. Dimensions of the sample confined radially between concentric rings: $100 \times 70 \times 5$ (mm) (outer diameter, inner diameter, depth, respectively) (Figure 4.30); the ratio of the load on the load hanger to the load acting on the sample was designed as 1:10. In this system, circular shear displacement is provided by a microprocessor-controlled stepper motor through a gearbox drive. Torque force resisting the force transmitted to the bottom base of the sample box is measured by S-Type high-capacity load cells (VJTS0364) thanks to the A and B arms placed orthogonally to the head collars; and vertical displacements during consolidation (K_0 conditions) and shear are measured with linear strain converter transducers (LSCT) (VJT0270). Records obtained from the physical system can be evaluated by transferring them to the computer system by means of data collection systems and signal converter systems (VJT-USB-RS232, VJT-csRING). The test apparatus complies with many standards including ASTM, BS, and ISO. In this study, the modified ASTM D6467-13^{e1} standard was used in order to make meaningful comparisons with other test methods. The visuals of the transducer interface and measuring devices used in the test are presented in Figure 4.31, and the technical specifications of the system are summarized in Table 4.10.



Figure 4.29. Ring shear test system (VJT5600A/01) manufactured by VJ Tech Limited

Table 4.10. Specifications of the ring shear test apparatus (VJTech, 2018)

<i>Specifications</i>	<i>Value</i>
<i>maximum specimen size</i>	$100 \times 70 \times 5 \text{ mm}$ $A = 40 \text{ cm}^2, V = 20 \text{ cm}^3$
<i>speed range</i>	$0.0001 - 900 \text{ }^\circ/\text{min}$
<i>maximum shear stress</i>	1000 kPa
<i>maximum design normal load</i>	1000 kPa
<i>vertical load</i>	10.0 kN using 10:1 lever ratio
<i>travel range of displacement transducer</i>	10 mm
<i>supply voltage (s)</i>	$90/240 \text{ V AC}, 50/60 \text{ Hz}, \text{ single phase}$
<i>power consumption</i>	$26\text{W} - 1.6\text{A} - T$
<i>power consumption</i>	105 kg
<i>approximate dimensions (L x W x H)</i>	$1335 \times 380 \times 1400 \text{ mm}$

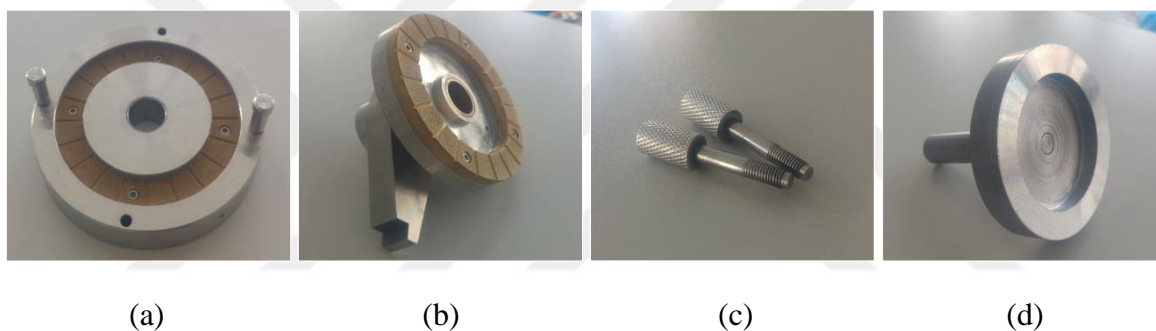


Figure 4.30. Auxiliary equipment of ring shear box: (a) Specimen container and lifting handle (bottom part), (b) Bronze porous torsion beam (top cap, modified type), (c) Clamping screws, (d) Circular tamping tool

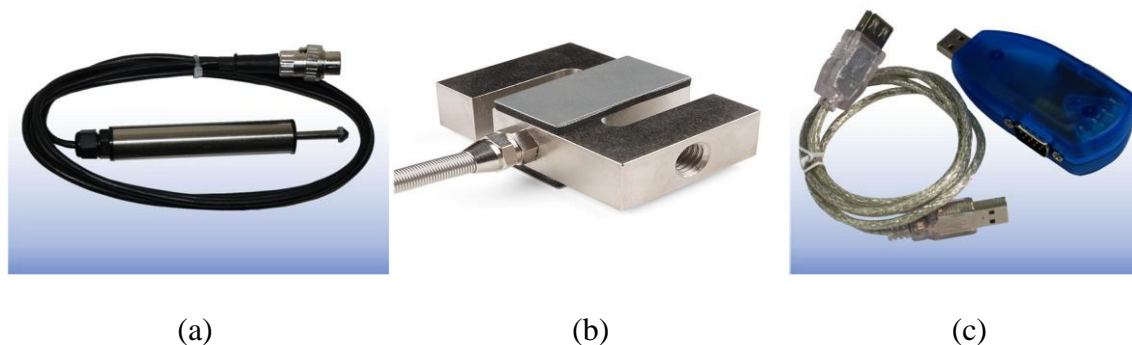


Figure 4.31. System tools used in the study: (a) LSCT, (b) Load cell, (c) Converter interface

After the procedures, the details of which are given in Section 4.3, the setup phase was started for the test system. At this stage, first, the soil material with target density was placed in the sample box with a bronze porous inner bottom. Loss of material in placements (even very small amounts), fiber orientation (for reinforced samples), or deviation in sample depth required more care than other test methods as they would change the target density due to the unique nature of sample dimensions. After the formation process, the sample box (bottom part) on which the lifting screws were mounted was placed in the ring shear cell and fixed to the cell by means of clamping screws. An appropriate amount of synthetic vacuum grease was used to reduce friction between the central pin and the ring shear box. After the lubrication, the torsion beam (top cap) was carefully placed on the sample box and the angular indicator was reset (Figure 4.32). Then, A and B load arms, which measure the resistance of the soil against shear (they must be the same as the coordinated values), were placed orthogonally to the top head and their joints were fixed. Finally, the load hanger, dead loads to be placed on the weight hanger, the loading beam and the locking screw were adjusted, the vertical displacement transducer was placed, and the reservoir was filled with water. Thus, the setup for the test system was completed and the testing phase was started.

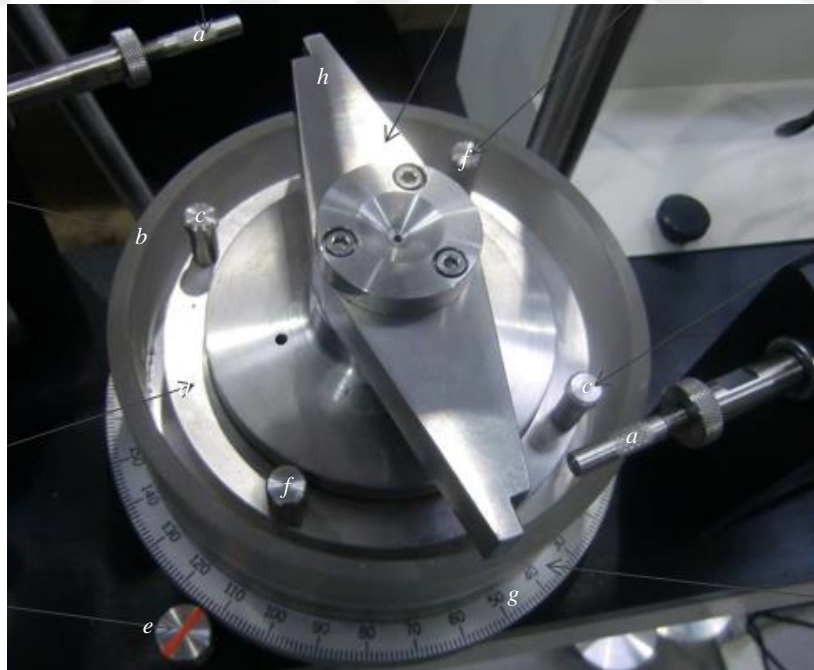
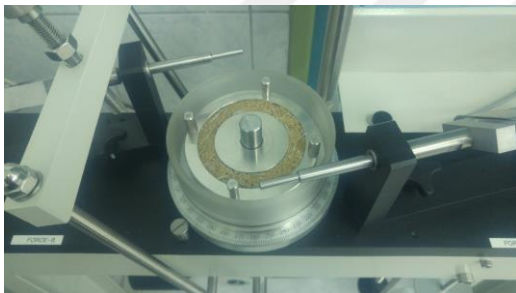


Figure 4.32. Details of ring shear box: (a) Load ring arm, (b) Water chamber, (c) Lifting handle, (d) Specimen container, (e) Angular indicator, (f) Clamping screw, (g) Graduated scale, (h) Torsion beam (top cap)

In the testing phase, the samples were first consolidated under various vertical loads (50, 100, 200 kPa) (Figure 4.33). The granular structure of the samples and the low sample depth reduced the consolidation duration considerably. After this process was completed, the shear phase was initiated, and the samples were sheared at constant strain speed (consistent with the angular velocity, $1.348^\circ/min$) at which their ultimate strengths could be obtained. Here, the reason why the consolidation loads, and angular strain rates were chosen low was to prevent material extrusion, which is one of the most important limiting features of the ring shear tests. These principles were kept the same (for all) in a linear order to make meaningful comparisons with other test methods. After the test was completed, the ring shear box was removed from the reservoir and disassembled, and some material was taken from the shear plane to determine the water content at the end of the test (Figure 4.34). It was seen that the obtained water content (17 – 20%) were compatible with the literature data for the drainage tests in saturated conditions. Finally, the measured strength parameters were re-evaluated using all relevant correction factors.



(a)



(b)

Figure 4.33. Pre-shear procedure: (a) Sample preparation, (b) Consolidation stage



(a)



(b)

Figure 4.34. Post-shear procedure: (a) Material extrusion ($\delta_r \approx 1 m$), (b) Disassembly of the ring shear box

5. RESULTS AND DISCUSSION

5.1. Introduction

Part 2 covers the comprehensive literature review about the thesis subject, Part 3 covers the theoretical and applied knowledge about the strength and strain properties of sand, Part 4 covers the materials and the method used in the study, the detailed presentation regarding the testing apparatus. This part comprehensively evaluates, compares, and analyzes the direct shear, triaxial pressure, and ring shear test results.

Mechanical properties of soil can be measured in different quantities based on the test method. This difference is related to the stress conditions exposing the test sample, such as the limit conditions of strain, principal stress (Figure 5.1), and failure plane orientations, in particular (Figure 5.2).

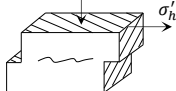
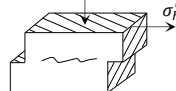
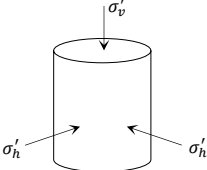
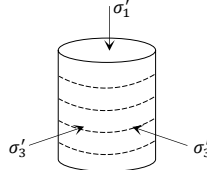
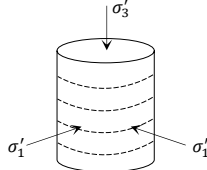
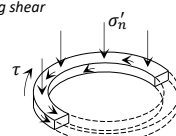
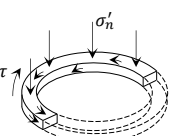
Apparatus	Orientation of major principle stress		
	$\alpha = 0^\circ$	$0^\circ < \alpha < 90^\circ$	$\alpha = 90^\circ$
Direct shear (shear box) 	N/A		N/A
Triaxial 	 Triaxial compression	N/A	 Triaxial extension
Ring shear 	N/A		N/A

Figure 5.1. Specimen stress, deformation and boundary conditions for the test methods used in the study (N/A: Not Applicable) (O'Kelly, 2015)

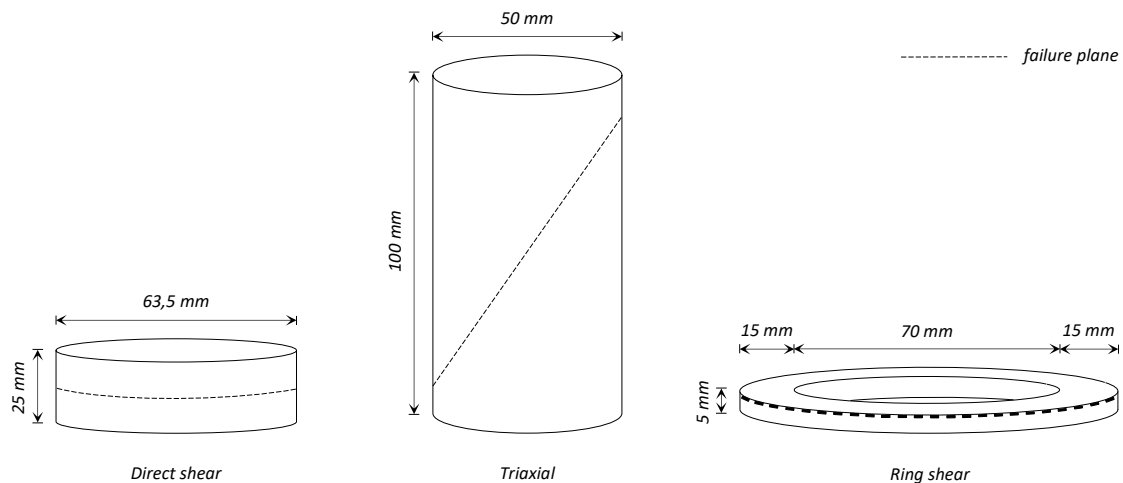


Figure 5.2. Scaled test specimens for the direct shear, triaxial and ring shear apparatus

Related details as explained in Part 4:

- In the shearing tests, shearing is done on a soil pre-determined while triaxial tests are managed with failure plane soil properties and structure.
- In the shearing tests, principal stress orientations and magnitudes cannot be known since they continuously change during strain loading, however, principal stress orientations do not change in the triaxial tests in the during the test.
- The magnitude of the intermediate and minor principal stress is not known based on the applied vertical load and soil properties in the shearing tests, but they are known in triaxial tests.
- Various stress distributions occur across the failure plane during the process of shearing the test sample depending on the strain conditions. This difference in the stress distributions is managed with the main factors such as the soil property, geometry, the confining that was applied, and normal pressure (Saada and Townsend, 1981). Since the effect of non-uniform stress distributions on the properties of shear strength and its measure to this effect cannot be precisely determined, researchers indicated that shear strength measurement is required to be evaluated on average (Sowers, 1964).

When comparing the results of the test methods, the above-mentioned distinctive properties should be taken into consideration.

Part 5.2, Part 5.3, and Part 5.4 present the results of the direct shear, triaxial, and ring shear test methods, respectively. And Part 5.5 presents the comparative analysis of these methods' results.

5.2. Direct Shear Test Results

Part 4 covers theory belonging to the direct shear test method, mathematical model, operating procedure, the introduction of the test apparatus, and other related details. This part comprehensively evaluated and analyzed the shear strength results obtained from the direct shear tests and results belonging to the soil parameters on various bases.

The direct shear test is a translational shearing test allows the shear strength parameters to be obtained directly on a forced plane of the soil. Related soils used in the defining of the soil behavior belonging to this test were analyzed using Mohr-Coulomb failure criteria based on the shear stress occurring according to the normal stresses affecting the shearing plane.

Direct shear tests detailed in Part 4 were done in four different densities from very loose to dense, in three different normal (vertical) stress force loading, in constant shear strain rate, in a single volumetric fiber concentration, and drained conditions using the standard circular shear box. Round (rounded shaped) grained standard sand was used for matrix and macro fiber with discrete structure was chosen as a reinforcement. This study included 108 direct shear tests in total as 45 and 63 repetitive tests for unreinforced and fiber-reinforced tests, respectively.

In the first part of the section, shear strength parameters belonging to the unreinforced and reinforced samples were evaluated while the results of volumetric strains were examined in the second part.

5.2.1. Stress-strain relationship

The shear strength of the soils depends on the load they are exposed to ($\sigma' \tan \phi$). In addition to the previous studies indicating this load to have a significant effect in higher values (Terzaghi and Peck, 1948; Roberts and de Souza, 1958; Bishop, 1966; Lee and Farhoomand, 1967; Lee and Seed, 1967; Marsal, 1967; Vesic and Clough, 1968; Miura and Yamanouchi, 1973; Hardin, 1985; Lade and Yamamuro, 1996), many recent studies indicate that very low loading conditions also have a significant effect for the shear strength of the soils (Ponce and Bell, 1971; Stroud, 1971; Fukushima and Tatsuoka, 1984; Sture et al., 1998; Fannin et al., 2005; Lancelot et al., 2006; Chakraborty and Salgado, 2010; Lehane and Liu, 2013; Giampa and Bradshaw, 2018; Rousé, 2018). Of course, it would be more correct to evaluate the work done by soil grains as triggering failure with their relative movements, in other words, the energy capacity done with the volume strain of the soils.

As it is explained in Part 3.2 in detail, soils are nonlinear materials showing a significant degree of nonelastic (plastic) strains under the applied loads. These materials' stress-strain relationship curve initially represented an elastic area for a very limited area and later a plastic area after proportionality (yield) limit with the increasing strains. This curve stress level representing the stress-strain properties of the soil depends on the stress level, pore water pressure, material properties, stress and strain increase orientation, and parameters detailed in Part 3.5 (Lade, 1972; Rahman and Ülker, 2018; Fernandes, 2020). Part 4 presents the comprehensive presentation of these parameters.

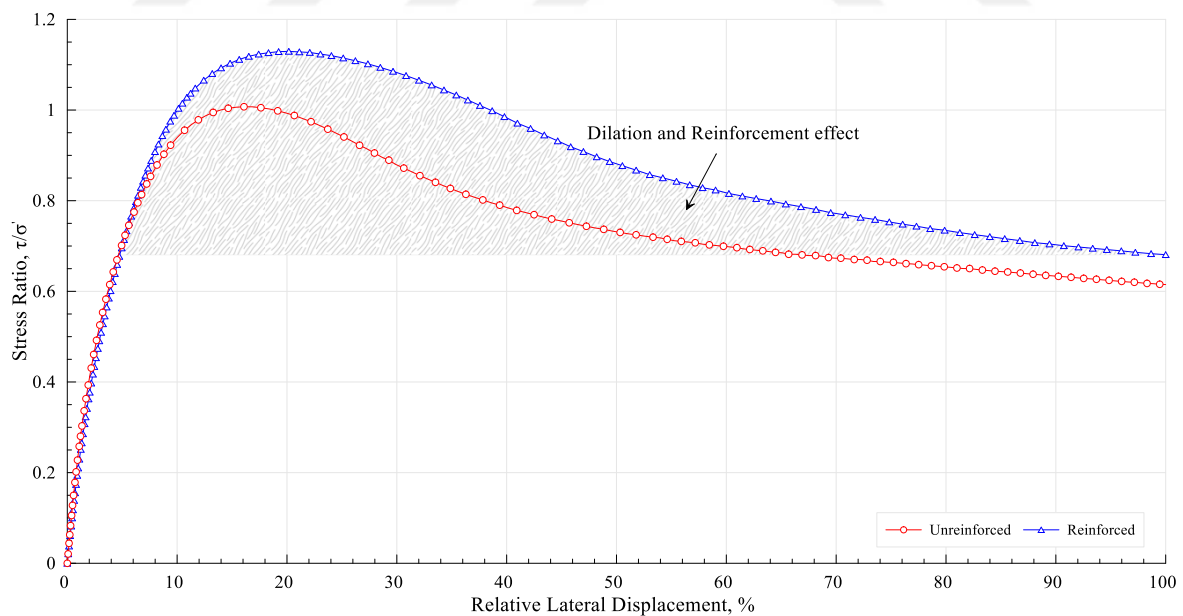
Granular soils exposed to the constant load and shearing strain have various stress-strain curves according to the initial conditions (void ratio, stress level, drainage, etc.). The most significant factor in this difference is the distortion of grains and the relative movement of grains, which are related to each other. During the strain process, changes based on stress differences occur in the soil due to the various mechanisms. These changes are controlled with the effective stress and volumetric change capacity of the grains. All these factors are directly related to the frictional resistance controlling the grain contact points and inner kinematics limitations related to the changes in the soil structure. Part 3.4 presents the details regarding the subject.

Stress-strain behaviors of soils are usually determined with direct shear or triaxial test methods. Correlating the shear stresses (or principal stress difference) corresponding to shear (or axial) strain with the strain-controlled tests yields typical curves similar to those in Figure 5.3. The stress-strain curve of soil is evaluated under three different stages. The first section is a multi-energy area where failure has not occurred yet, stress values increase linearly in even very few strains and are controlled with environmental factors. Strength, in this area, is obtained by friction causing grains to re-locate such as friction of grain and mineral, the rotation of grains against each other, grain rolling friction. Here, in the continuation of this first part assumed to be elastic area, it is being proceeded to the second stage named plastic area. This transition point between the first and second parts is called proportionality limit (yield). The second part is controlled with mechanical and multi-energy. At this stage, big volume strains emerged by affecting from grain locking contributing to the strength of granular soils quickly reach to the peak point of the soil, therefore, it causes failure. The capacity of the grain locking phenomenon that is valid for the dense sands is a function of the void ratio. Strain hardening being effective due to exceeding the proportionality limit continues until the peak stress point and then stress softens and it proceeds to the third stage, which is when it reaches the critical stress value where shearing occurs. At this stage, stress value exceeds a flow condition with the increasing strains and reach gradually to an asymptotic value, which is a critical state. This area where stress softening occurs is controlled with mechanical energy, and in the second stage, interlocking between effective grains loses its effects after failure and goes back to the frictional forces that are effective in the first stage. In this situation, the strain will continue in constant stress and volume.

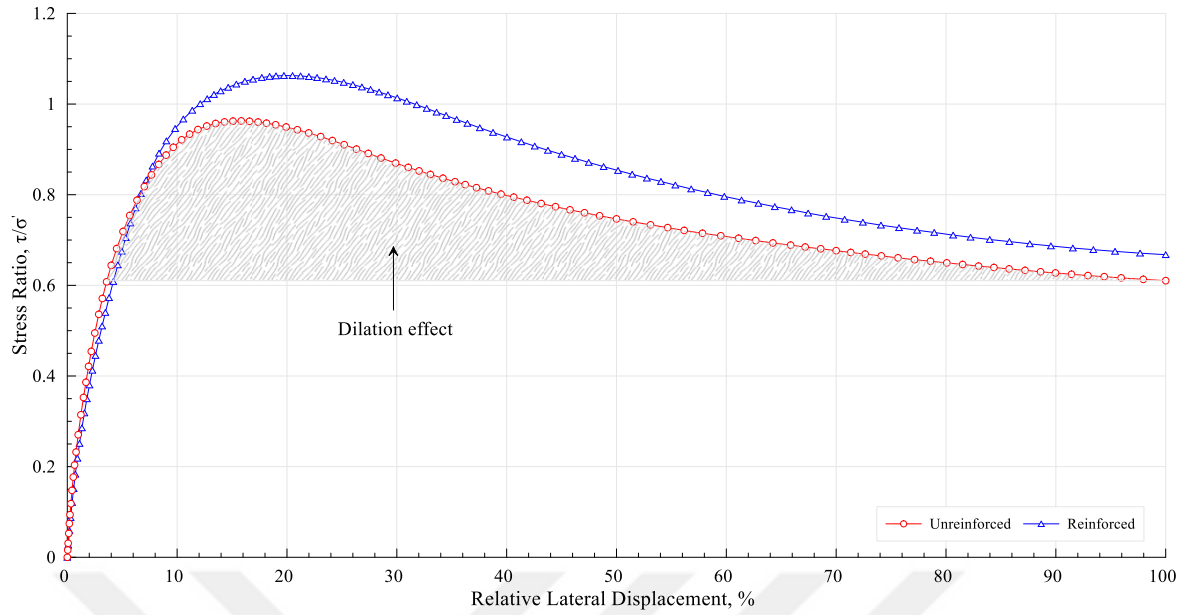
Although the above process is used for the densely packed sands, the failure organization is different in sands with loose density. Grains that want to locate more densely will become closer to each other with the starting of strain and the void ratio between grains will reduce. At this stage, friction contributions for densely packed sands are also valid for the loose sands. Soil assumed to elastically behave in the beginning, starting from very few strains will show hardening behaviors in all series with the increasing strains. Volume change in these density does not show a tendency to strain softening and brittleness tends to contraction throughout the straining process.

Figure 5.3 presents stress ratio-strain curves belonging to the ($\sigma'_n = 50, 100, 200 \text{ kPa}$) densely packed ($e_0 = 0.50$) unreinforced and reinforced composites under the various consolidation loadings. Related six curves (three unreinforced and three reinforced) have the aforementioned strain process and the same tendency for the dense sands. In the drawing of the stress-strain curves, the relationship of stress ratio-relative lateral strain has been taken into consideration. The main aim of using the stress ratio parameter obtained with normalizing shear stress with normal stress (τ/σ'_n) is to see the effect of normal stress on shear strength more clearly, follow the contribution of reinforcement to the strength more effectively, see the becoming clear of peak points in a narrower stress range instead of a very large one and prevent the possible stress/pressure faults in the sophisticated tests, in particular.

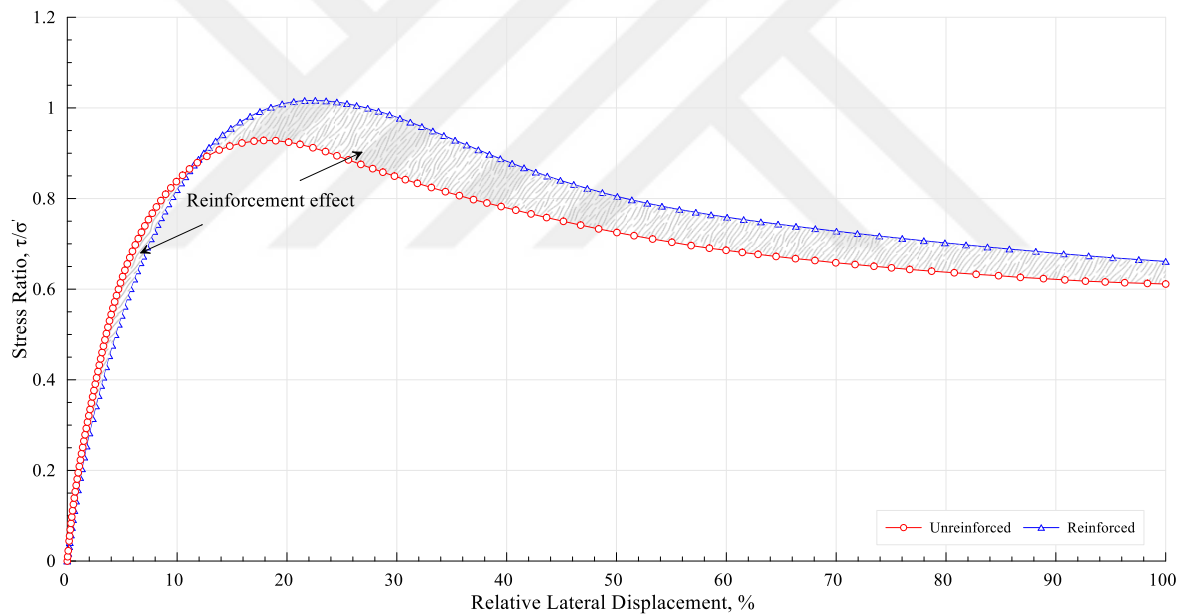
Figure 5.3a presents 50 kPa curves belonging to the unreinforced and reinforced composites sheared under the normal load. Curves, where stress-strain curves are in the same tendency, show that reinforcement and geometrical interference are the main determinant factors.



(a)



(b)



(c)

Figure 5.3. The stress ratio - Relative lateral displacement relationship for direct shear ($e_0 = 0.50$): (a) 50 kPa, (b) 100 kPa, (c) 200 kPa

The greatest stress ratio of the unreinforced samples is 1.007 while this ratio has been increased to 1.129 in the peak value of the reinforced samples. Although small reinforcement concentration was used in this study, its effect on the strength increment was found to be 1.121 which was striking. The greatest stress ratio in all the test series was reached on this density and normal stress loading. This is because of the freedom of the

dilation parameter. The increase in the critical strength showed a similar trend to the peak, however, changes in the reinforcement orientation within the composite remained limited with the increasing strain.

Figure 5.3b shows the test curves of the unreinforced and reinforced composites in which normal stress is chosen to be 100 kPa . Stress-strain curves 50 kPa show similar characters with normal stress loading while a decrease is seen in the contribution of the peak and critical stress ratios and reinforcement to the strength of the composite. This decrease is related to the increase in the suppression on the geometrical interference (interlocking) in the peak state and the effect of this suppression on the reinforcement orientation.

Figure 5.3c presents the stress ratio-strain curves of the 200 kPa , which is the greatest normal stress chosen in the study. In this stress condition which transfers the load to the sample two times and four times more than the other normal stresses, lower peak and critical stress ratios were obtained. This result is significant in terms of showing the fact that as the normal/confining pressure increases, interlocking between grains and the effect of reinforcement to the composite reduces. In this series, in which the high density was tested in particular, the related effect became clearer. When compared with the 50 kPa , the effect of normal stress on the reinforcement contribution was found to be 26% on average for the peak and critical stress ratios.

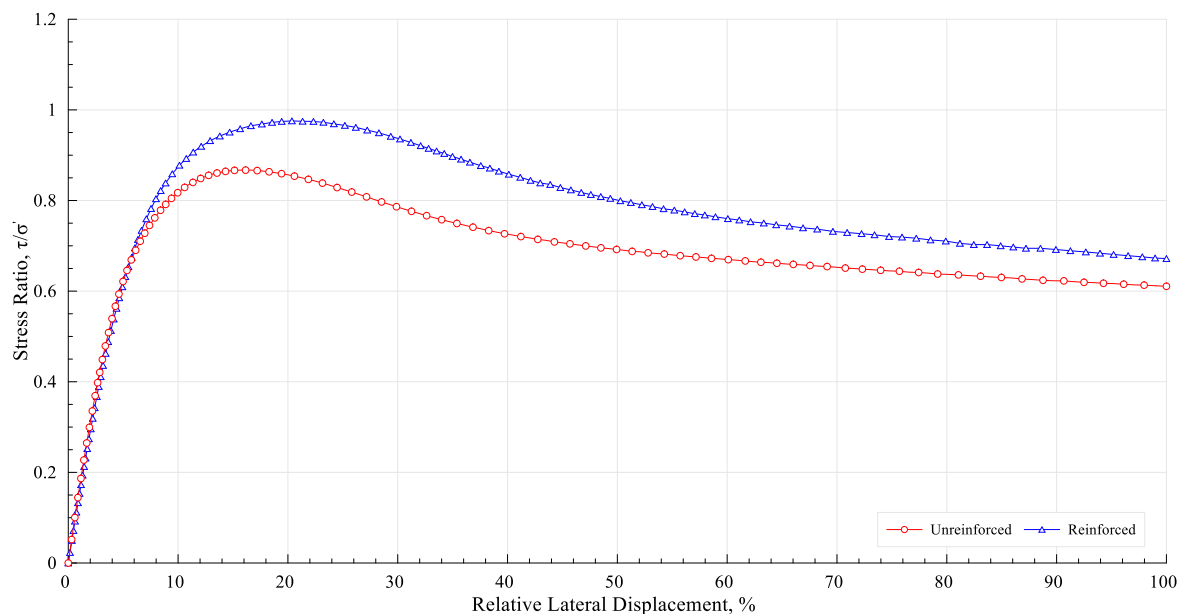
Figure 5.4 presents the strain curves belonging to the samples tested in the various normal stress of the medium-densely packed ($e_0 = 0.55$) sands. This part examined the effect of normal stresses on the medium packed unreinforced or reinforced samples, and their comparisons about other density situations were described at the end of the part.

Depending on the decreasing geometrical interference capacity of the medium densely packed sands, densely packed sands had quite lower stress ratios. The peak stress ratio was found to be 0.893 for the unreinforced situation while this ratio reached to 1.006 in the reinforced situation. This result is significant in terms of showing that reinforcement material increased the geometrical interference capacity. As the stress load increased, the geometrical interference capacity of the soil decreased, and reinforcement had a contribution to the peak strength for the 100 and 200 kPa at the ratio of 1.112. Lastly, decreasing ratio

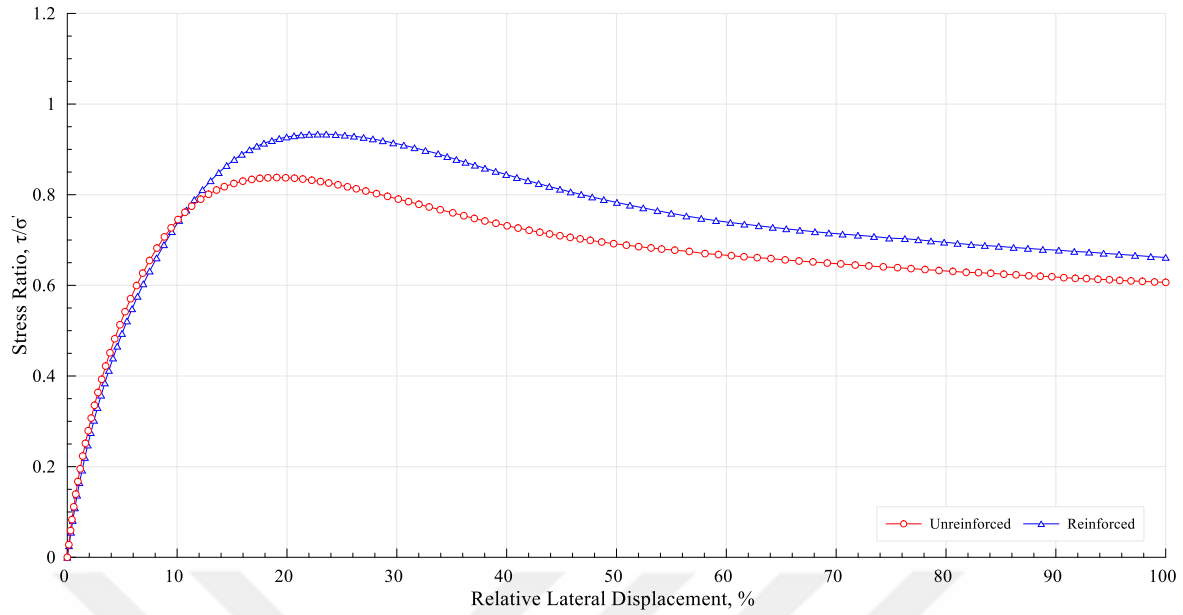
from peak to the strength for medium-dense sands, and it was found that reinforced sands had affected by the unreinforced sands 10% more. This finding proved that the aforementioned geometrical interference capacity of the soil increased with reinforcement.

Figure 5.5 presents the stress-strain curves ($e_0 = 0.60$) of the loosely packed sands. In this density level in which geometrical interference capacity decreased compared to other dense sands, reinforcement's contribution to the peak strength increment happened at the level of 1.30. This strange relationship can be explained by the fact that the frictional force between the more densely packed sand grains (grain - grain) was more than the one between reinforcement-grain friction. The typical value of the mineral friction angle for the quartz sand was found to be 26° (Procter and Barton, 1974), these tests found this value to be 21° for the reinforcement. The friction relationship between grain and reinforcement should be evaluated within this scope. Another significant factor for the occurrence of this paradox is undoubtedly the cohesion formed in the existence of reinforcement. The effect of cohesion on the shear strength has been evaluated in the subsequent parts under a separate headline.

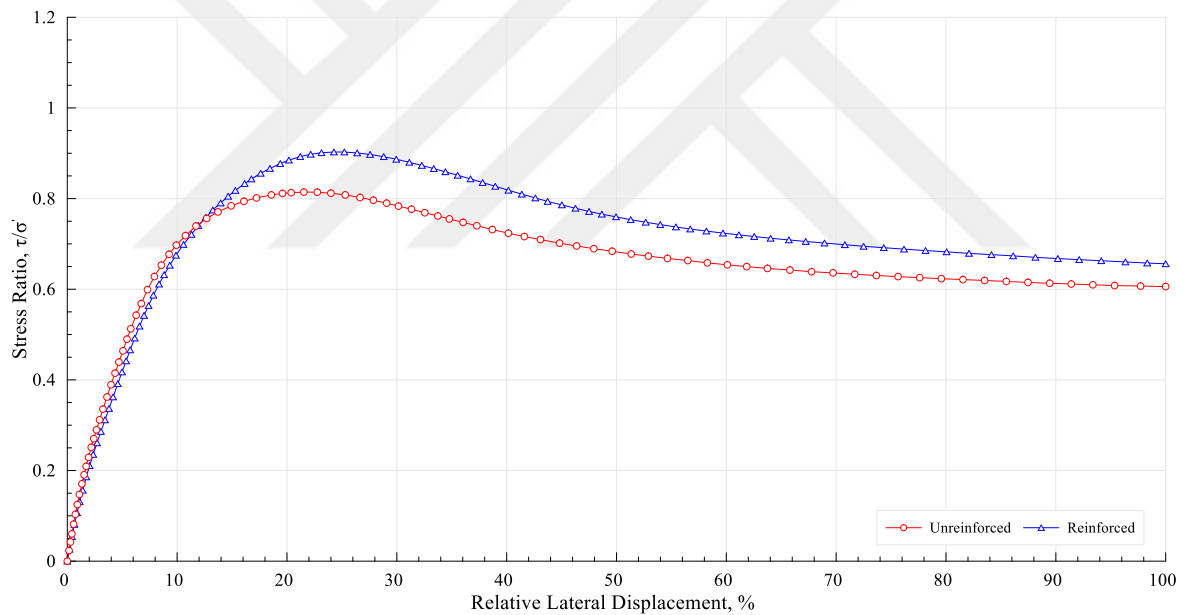
As in the other density levels, increasing normal stress caused the reinforcement's effect on peak and critical strength to partially decrease. The most significant factor in this decrease is the suppression of geometrical interference capacity mentioned above in detail.



(a)



(b)

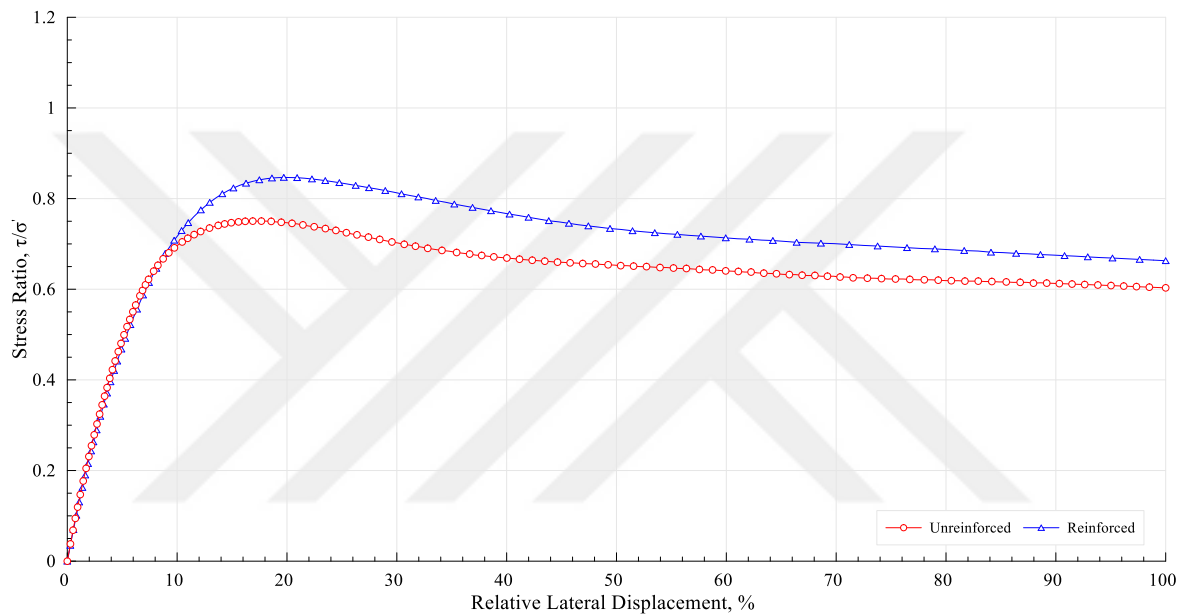


(c)

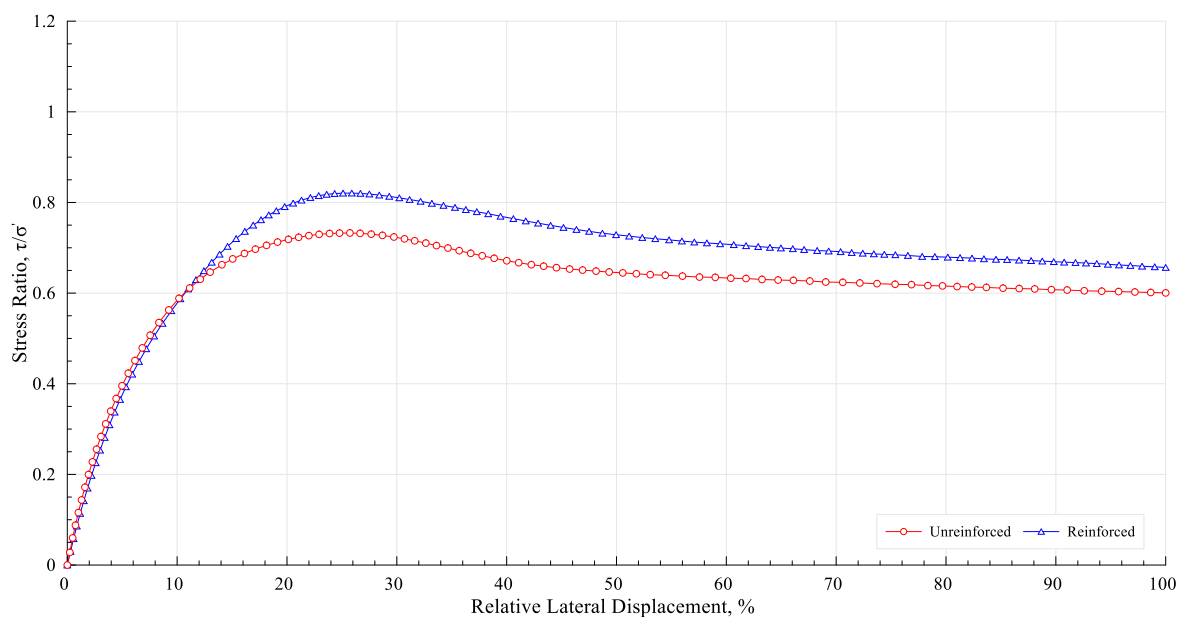
Figure 5.4. The stress ratio - Relative lateral displacement relationship for direct shear ($e_0 = 0.55$): (a) 50 kPa, (b) 100 kPa, (c) 200 kPa

When the loss of strength at the critical state which is reached by strain softening after peak and where the stress ratio remained constant is investigated, it was observed that the unreinforced samples decreased with the ratio of 1.716 while reinforced samples decreased with the ratio of 1.644, according to $e_0 = 0.55$. This result is significant since it directly supports the strength concept mentioned in the previous paragraphs.

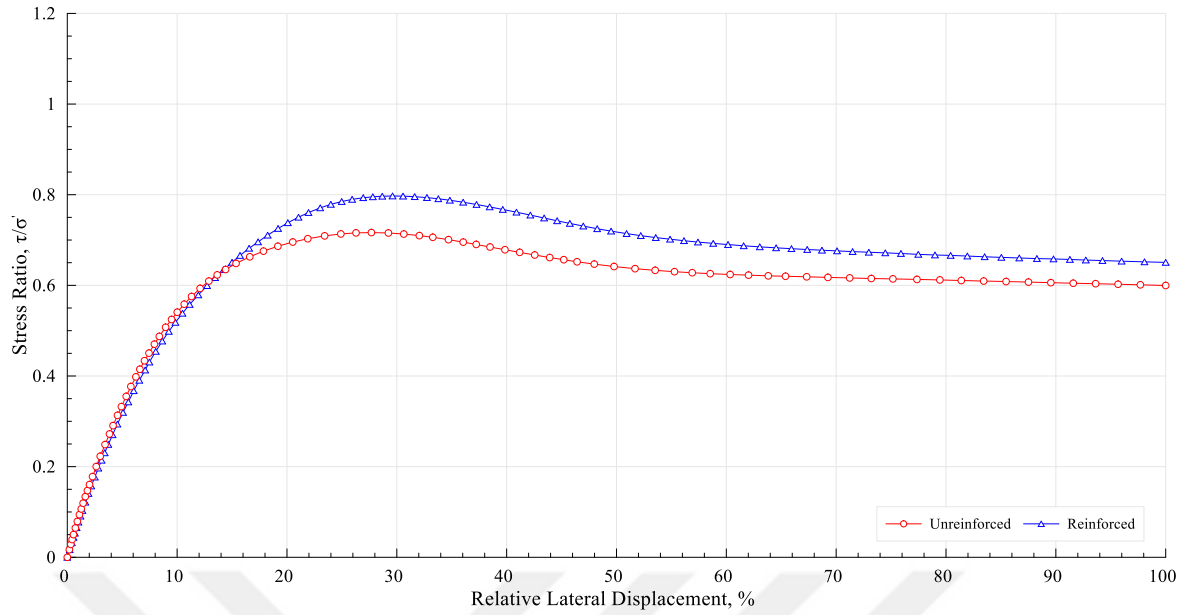
Figure 5.6 shows stress-strain curves belonging to very loose ($e_0 = 0.65$) samples tested under various normal stresses. When examining these curves, the most significant factor drawing attention was the fact that the ratio of strength loss ratio during the critical level of peak stress ratio was found to be 1.042 – 1.015, and 1.083 – 1.043 for the normal stress in the lowest and the greatest unreinforced and reinforced samples, respectively. This result indicated that increasing geometrical interference capacity with reinforcements was affected by the strain-softening more after the peak.



(a)



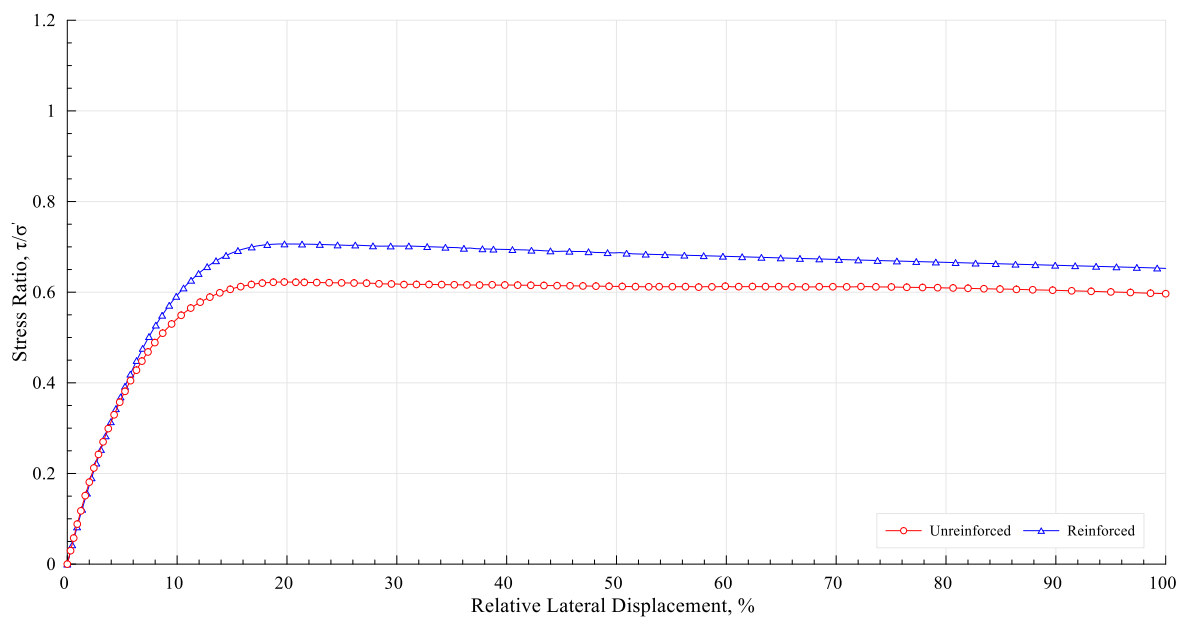
(b)



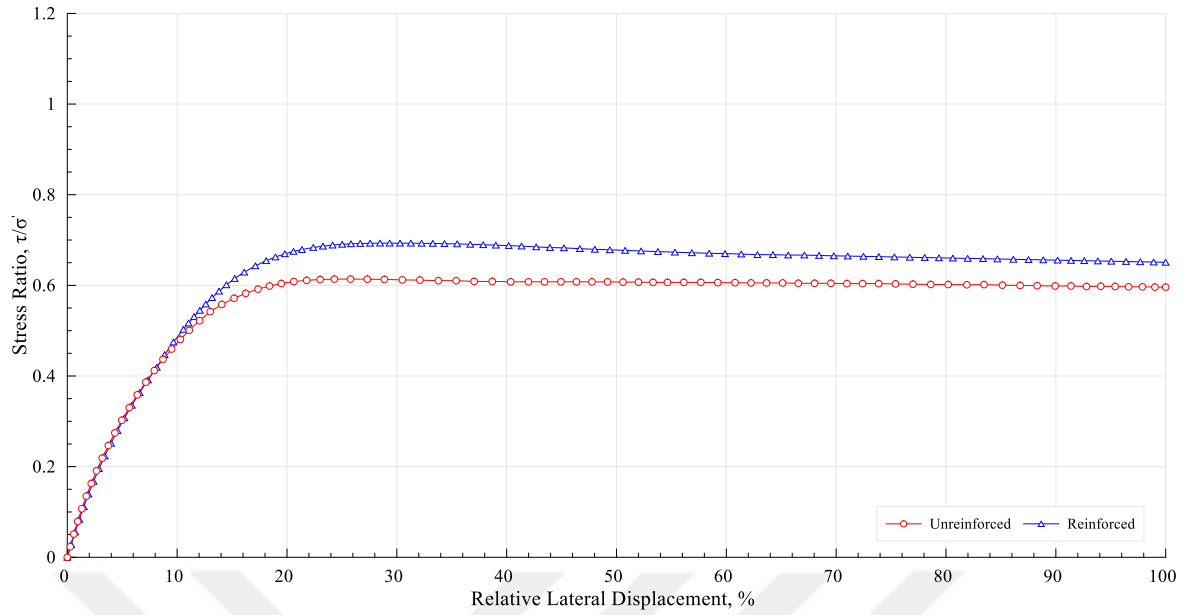
(c)

Figure 5.5. The stress ratio - Relative lateral displacement relationship for direct shear ($e_0 = 0.60$): (a) 50 kPa, (b) 100 kPa, (c) 200 kPa

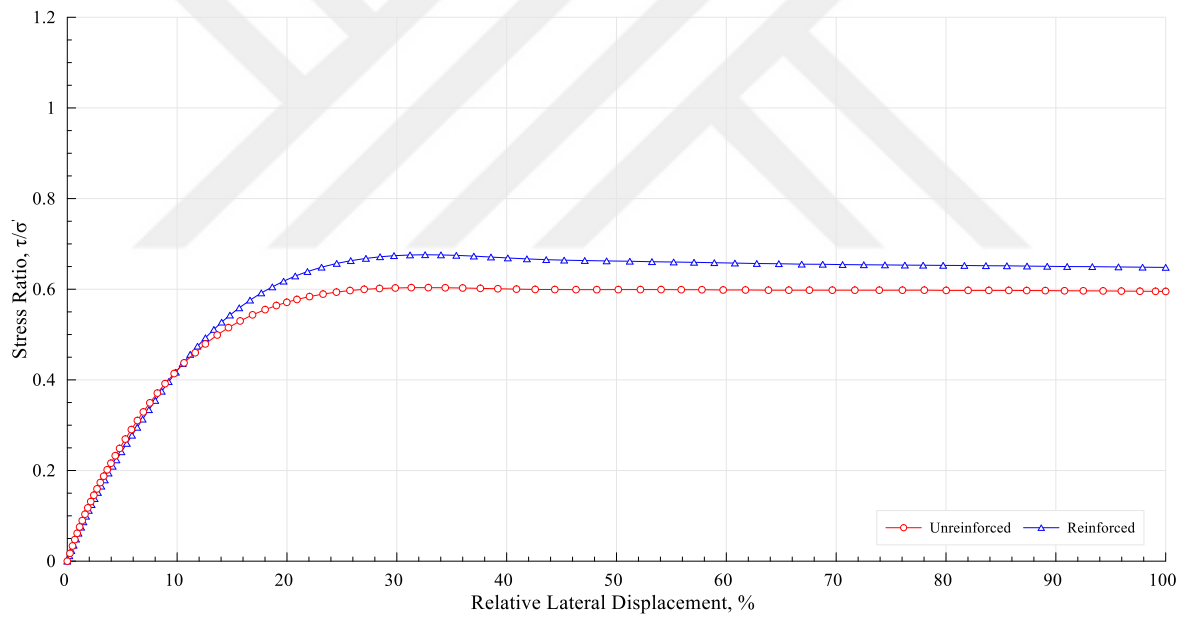
In other words, this result is significant in terms of indicating the different effects of reinforcement on the peak and critical strength. When the stress ratios were compared, higher values were obtained in the lowest stress condition (50 kPa) as in other densities. However, these values remained lower compared to the denser samples.



(a)



(b)



(c)

Figure 5.6. The stress ratio - Relative lateral displacement relationship for direct shear ($e_0 = 0.65$): (a) 50 kPa, (b) 100 kPa, (c) 200 kPa

Strength increase had a tendency close to linear as a function of normal stress. Another significant result obtained about $e_0 = 0.65$ was that reinforcement contributed to the peak and critical strengths relatively more than the other densities. The main reasons for this situation were stated in the evaluation done for the loose sands. This result is significant in

terms of the fact that reinforcements are very effective in the improvement of the engineering properties of the loose soils.

The void ratio of the quartz-predominant sands ranges from greatest effective stress ratios to 0.5 – 1 as a function of the normal stress (Sack, 1960; Horn and Deere, 1962). This range is compatible with the results obtained for the direct shear tests. It is not possible to talk about such a range for the composite samples in the case of reinforcement. The main reason for this is reinforcement material's being able to be controlled with various variables such as the type, class, acceptance principle, concentration, aspect ratio, smoothness, length, orientation, mechanical properties of the reinforcement. In this present study, the greatest stress ratios for the composite samples were obtained between the range of 1.129 and 0.676 (Figure 5.7e). Previous studies indicated that effective critical state stress ratios of quartz-weighted sands that are the rounded - subrounded grain shaped mineral content changed within the range of 0.57 – 0.67 (typically 0.65) (Rowe, 1962; Koerner, 1970; Bolton, 1986). This range is in accordance with the test results. It is not possible to talk about such a range for effective critical state stress ratio in composite samples due to the aforementioned reasons. Effective critical state stress ratios obtained from this study ranges between 0.648 – 0.681 (Figure 5.8e). In soil mechanics, although theoretically, there is only one effective critical state friction angle for each sand independent of the initial density, this is not valid in the presence of reinforcements. For instance, differences such as compression method, compression compaction energy in the composites prepared by the only operator with the same reinforcement and same reinforcement concentration, and even the different orientations in the composite of the discrete reinforcement do not allow a unique effective critical state stress ratio for reinforcement.

The peak effective (τ_p/σ'_n) and critical effective state stress ratios (τ_{cs}/σ'_n) as a function effective normal stress (σ'_n), initial void ratio (e_0), volumetric reinforcement concentration (v_f) are given in Figure 5.7 and Figure 5.8. The greatest effective stress ratios are compared by choosing the effective normal stress parameter in Figure 5.7a, Figure 5.7b, and Figure 5.7c. Of the figures in which the greatest effective stress ratios are obtained in the lowest effective normal stress (50 kPa) loading, σ'_n increased and so τ_p/σ'_n ratio gradually decreased. On the other hand, the presence of reinforcements increases the value

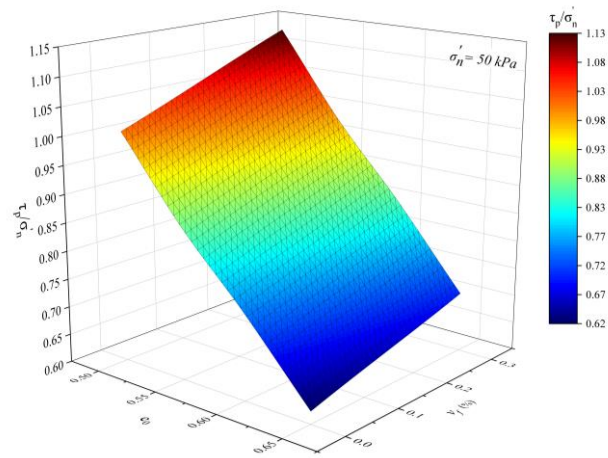
of τ_p/σ'_n in a distinct way. The reason for this increment is the geometrical interference phenomenon mentioned in the previous section. Initial void ratio is one of the most significant parameters affecting the ratio of τ_p/σ'_n . Related curves indicated that decreasing the void ratio causes the τ_p/σ'_n value to increase significantly. This increase is in a linear relationship from very loose to dense. Here, choosing σ'_n and e_0 ranges in a limited range have a significant role in this study.

The effect of the reinforcement concentration on the greatest effective stress ratio and its measurement depending on the density and normal stress of this effect was shown in Figure 5.7d, Figure 5.7e, and Figure 5.7f. The same unit scale was used for the significant comparisons of the unreinforced (Figure 5.7d) and reinforced (Figure 5.7e) states. Therefore, the effect of reinforcements' existence on τ_p/σ'_n becomes clear. On the other hand, three-dimension images were used to see the contribution ratio (v_{fr}) of reinforcement to the strength for both situations, the common effect of σ'_n and e_0 parameters. Accordingly, effect of reinforcements on the τ_p/σ'_n caused e_0 to increase and σ'_n to decrease, which are presented in Figure 5.7f. The main reason for this difference in the v_{fr} ratio is due to the fact that friction capacity's being affected if the grains of reinforcements added to the sand matrix are forced to relatively move.

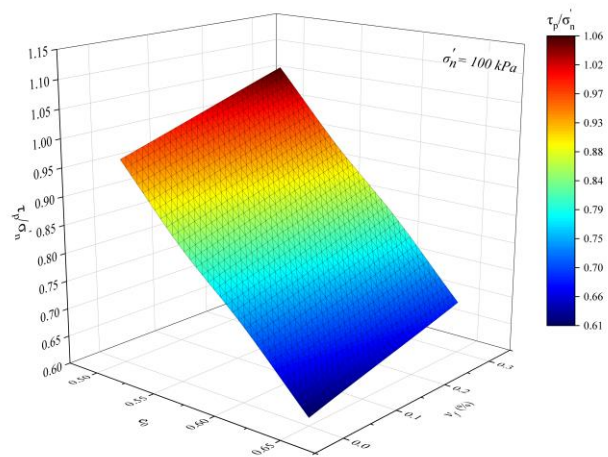
Figure 5.8 presents images regarding the relationship of critical effective stress ratio (τ_{cs}/σ'_n), σ'_n , e_0 to the reinforcement for the direct shear tests. Figure 5.8a, Figure 5.8b, and Figure 5.8c show that higher σ'_n cause a bit lower τ_{cs}/σ'_n , and in the case of reinforcements, this difference becomes clear. Images explaining this situation are shown in Figure 5.8d and Figure 5.8e. When examining the v_{fr} parameter, results similar to the peak situation were obtained; however, the effect of σ'_n and e_0 remained a little in the limited levels. This situation is directly related to the geometrical interference and orientation of the reinforcement in critical situations.

The main subject of this thesis is the research of the strength properties of the soils in different strain modes, therefore, this thesis will not explain the details about the parameters controlling the soil strength (Part 3) and the effect of reinforcement on the granular soils. To further research this effect for direct shear tests, the following studies can

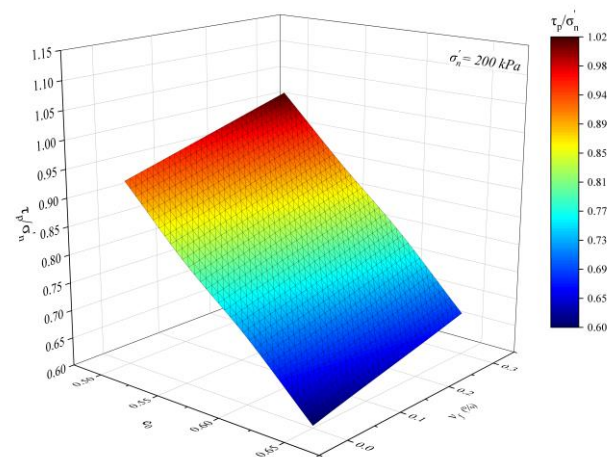
be looked at: Gray and Ohashi (1983), Arteaga (1989), Yetimoğlu and Salbaş (2003), Ibrahim and Fourmont (2006), Sadek et al., (2010), Falorca and Pinto (2011), Punetha et al., (2017).



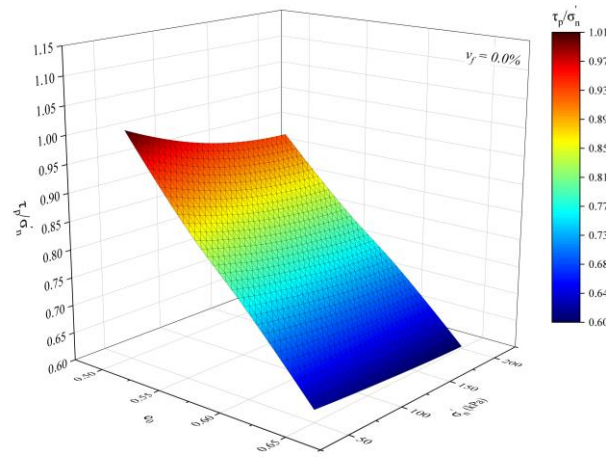
(a)



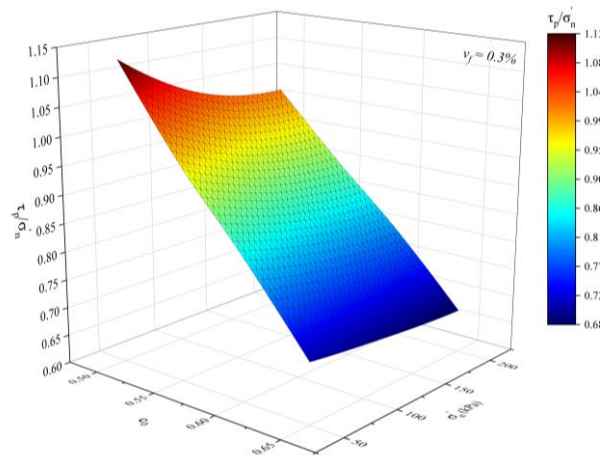
(b)



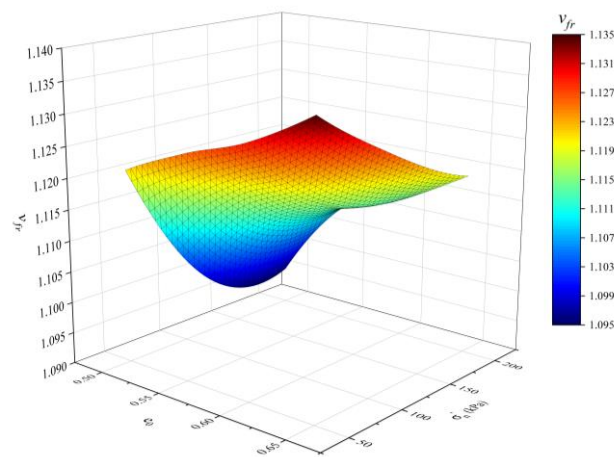
(c)



(d)

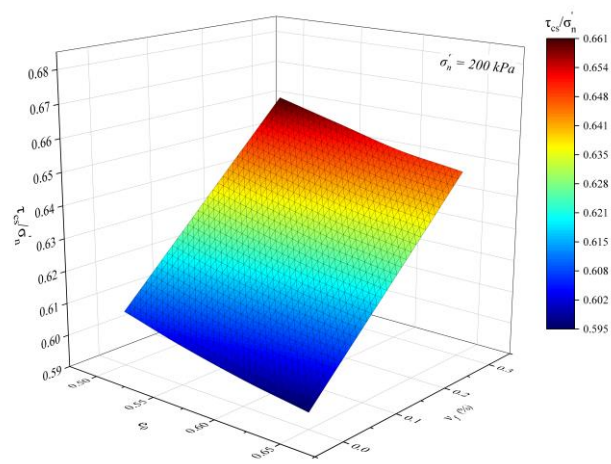
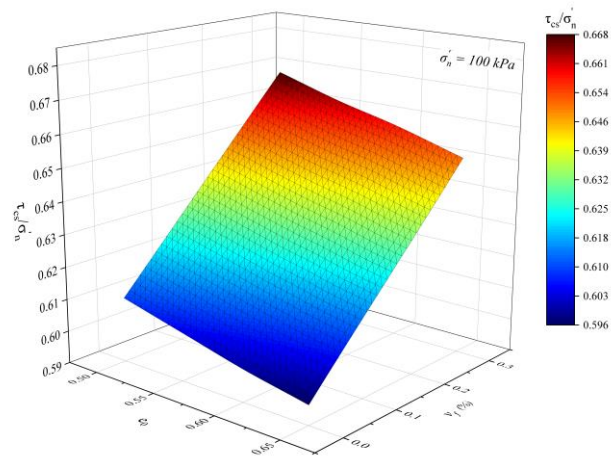
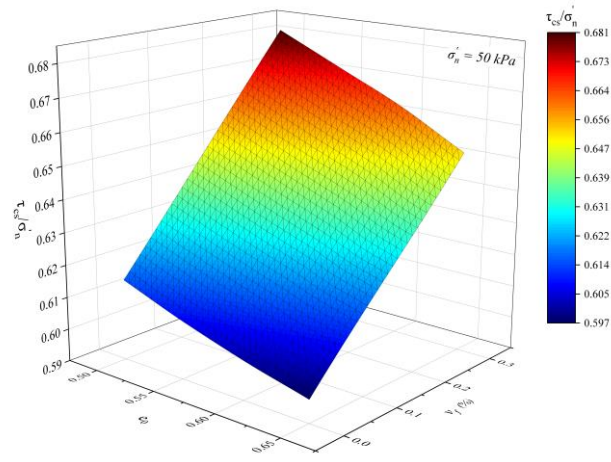


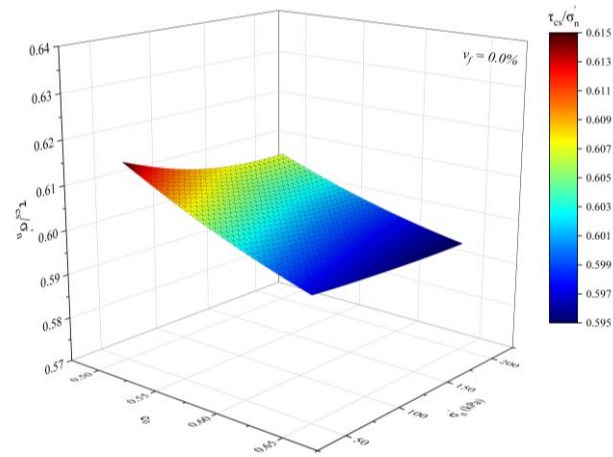
(e)



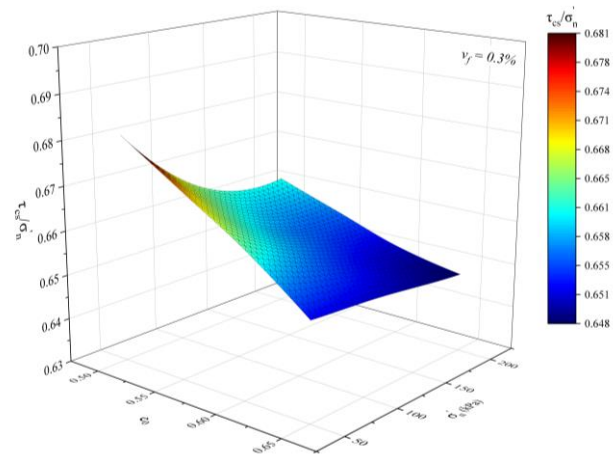
(f)

Figure 5.7. Effect of effective normal stress (σ'_n), initial void ratio (e_0) and volumetric reinforcement concentration (v_f) on the peak effective stress ratio for the direct shear tests (τ_p/σ'_n): (a) $\sigma'_n = 50 \text{ kPa}$, v_f - e_0 , (b) $\sigma'_n = 100 \text{ kPa}$, v_f - e_0 , (c) $\sigma'_n = 200 \text{ kPa}$, v_f - e_0 , (d) $v_f = 0.0\%$, σ'_n - e_0 , (e) $v_f = 0.3\%$, σ'_n - e_0 , (f) v_{fr} , σ'_n - e_0

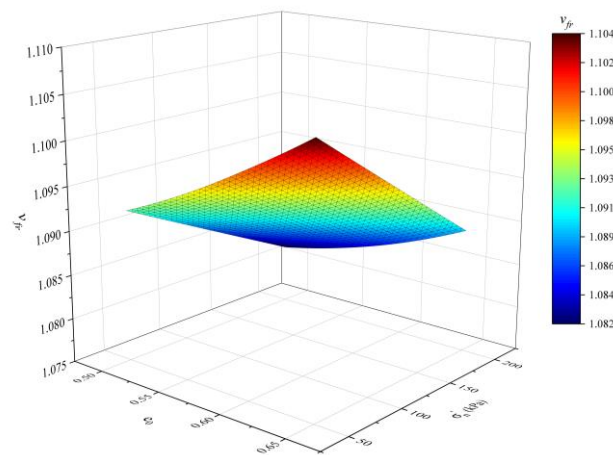




(d)



(e)



(f)

Figure 5.8. Effect of effective normal stress (σ'_n), initial void ratio (e_0) and volumetric reinforcement concentration (v_f) on the critical state stress ratio for the direct shear tests (τ_{cs}/σ'_n): (a) $\sigma'_n = 50 \text{ kPa}$, v_f - e_0 , (b) $\sigma'_n = 100 \text{ kPa}$, v_f - e_0 , (c) $\sigma'_n = 200 \text{ kPa}$, v_f - e_0 , (d) $v_f = 0.0\%$, σ'_n - e_0 , (e) $v_f = 0.3\%$, σ'_n - e_0 , (f) v_f , σ'_n - e_0

5.2.2. Shear strength parameters

Coulomb (1776) defined the shear strength of the soils with friction angle (ϕ) and cohesion (c) terms and stated it terms of total stress. Mohr published his own graphic management method using Cullmann's graphic method in three-dimension stress analysis (Mohr, 1882) and developed his famous theory by defining the failure of material in shear stress as a function of normal stress in the subsequent studies (Mohr,1900). In other words, failure of material happens not only due to the effect of greatest shear stress or greatest normal stress but due to the critical common combination of these. Later, this method was compounded with Coulomb theory and used in the soil mechanics practices. Terzaghi (1925), with his effective stress concept, carried the Mohr-Coulomb criteria one step further. Part 3 presents detailed information about the subject.

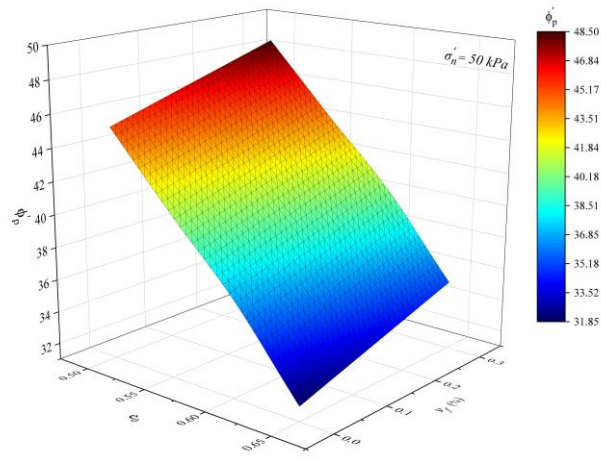
Mohr-Coulomb failure equation (Equation 3.12) defined in effective stress for general soils converts into Equation 3.23 for granular sands (clean) such as sand. Part 3 presents detailed information about this subject. The most significant subject to be known here is that friction angle and cohesion are not internal properties of the grains forming the soil mass. These parameters take different values based on the loading conditions (drainage, consolidation, load, etc.) Therefore, it will be a better approach to define these as an appointed coefficient or mathematical expression to state the soil friction.

The first section of the part will discuss the test results belonging to the effective friction angles and in the later sections, effective cohesions generated with reinforcements will be examined.

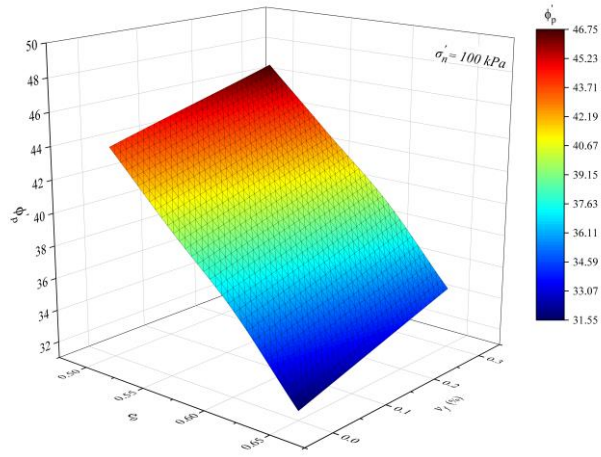
Results for peak effective (ϕ'_p) and critical state effective (ϕ'_{cs}) friction angle as a function of effective normal stress (σ'_n), initial void ratio (e_0) and volumetric reinforcement concentration (v_f) are presented in Figure 5.9 and 5.10 in detail. The friction angle of cohesionless soil is controlled by kinetic friction (ϕ'_μ) and geometrical interference ϕ'_g . These frictional components are directly affected by the internal factors of particle mineral structure and composition, particle shape, particle diameter distribution and void ratio, and external factors such as effective-normal stress, loading mode, stress traces, drainage conditions, saturation, and anisotropy.

As seen in Figure 5.9, it was observed that with the decrease in the initial void ratio and effective normal stress, there was a linear increase in the peak effective friction angle with a decreasing rate. The main reason for this increase is the linking of the particles to each other more closely compared to the initial condition due to the increasing strain and the effect of the effective normal stress load on this linking. It was observed that the σ'_n value of ϕ'_p angle obtained from the lowest and the highest initial void ratio was between $11^\circ - 13^\circ$, depending on the normal stress. This range is consistent with the interval presented by Bolton (1986), Kulhawy and Mayne (1990). When the effect of the presence of reinforcement on ϕ'_p is examined, it is seen that similar to the unreinforced state, ϕ'_p shows a linear increase with a decreasing ratio. This increase rate (v_{fr}) has remained limited depending on the increasing geometrical interference. When the effect of the presence of reinforcement on e_0 and σ'_n is examined, the increase in e_0 and decrease in σ'_n increased the contribution to strength. The fact that the ratio between the greatest and lowest increase rates being 1.042 is important in terms of showing the effect of e_0 and σ'_n .

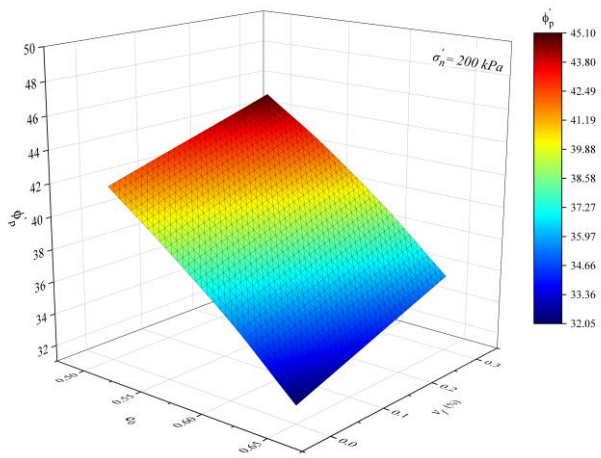
In Figure 5.10, the effect of reinforced and unreinforced samples for e_0 and σ'_n conditions were investigated for the effective critical state friction angle. As seen from figures, ϕ'_{cs} scatters within a narrow band for both reinforced and unreinforced states. The main reason for this is the absence of geometrical interference in critical state. In this situation where the particle movement in a constant σ'_n load develops unilaterally, the value of friction angle is controlled with kinetic and rolling friction. The increase in the scattering in the presence of reinforcement is related to the orientation of the randomly distributed reinforcement in the sand matrix and different heterogeneities occurring in the composite. Another finding obtained from the experiment results is that the contribution of the reinforcement to strength is less in critical state compared to peak state. The main reason for this is that the new position of the reinforcement is in the direction of shearing. Since the direct shear experiment devices have limited shearing strain capacities, there is a suspicion with regard to the permanent strengths of fine-grained soils. Although a very little volumetric reinforcement concentration was chosen in the study, critical state being affected by this fact makes it more critical for the sands.



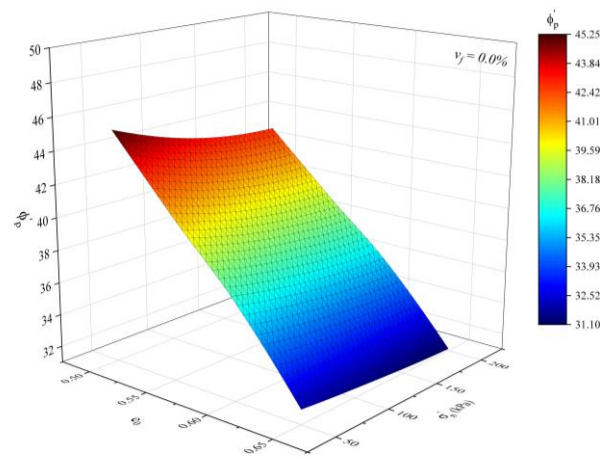
(a)



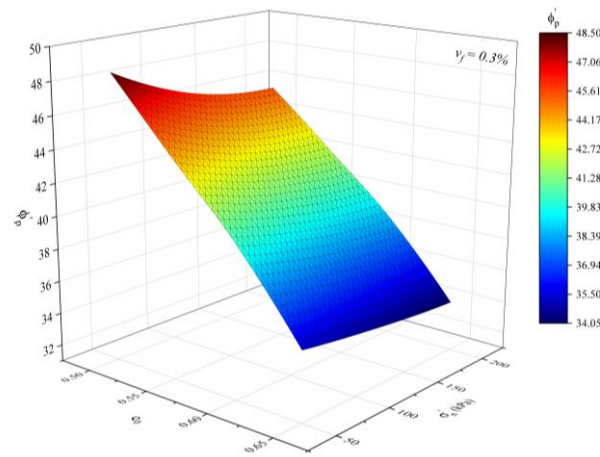
(b)



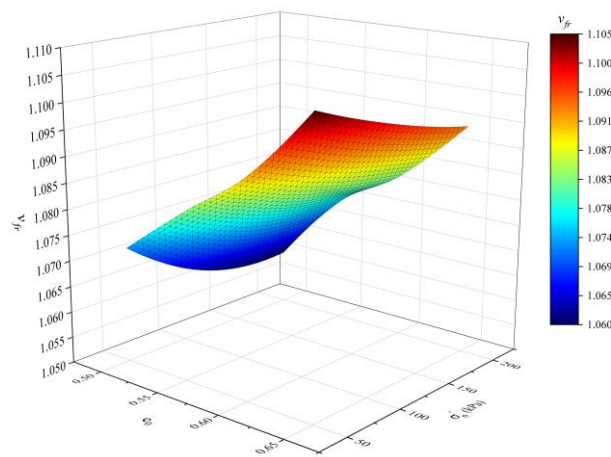
(c)



(d)

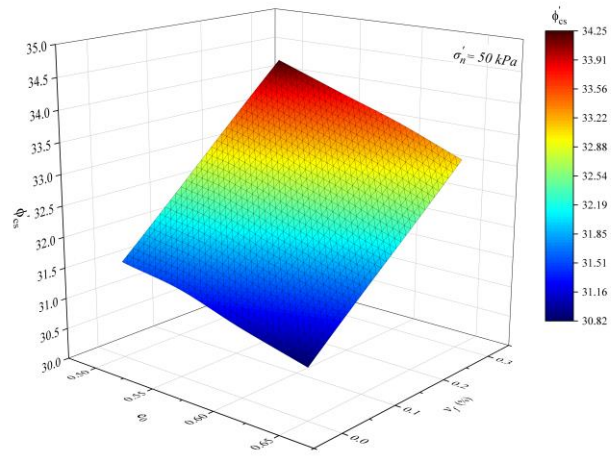


(e)

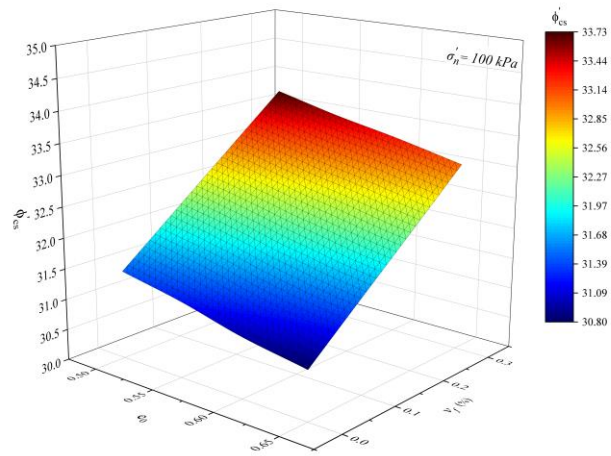


(f)

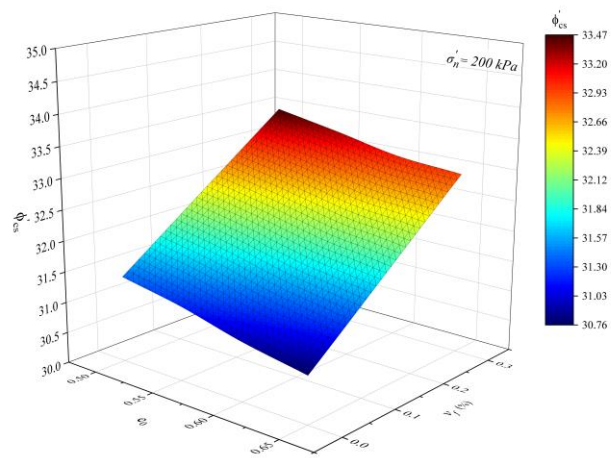
Figure 5.9. Effect of effective normal stress (σ'_n), initial void ratio (e_0) and volumetric reinforcement concentration (v_f) on the peak effective friction angle (ϕ'_p) in direct shear tests: (a) $\sigma'_n = 50 \text{ kPa}$, v_f - e_0 , (b) $\sigma'_n = 100 \text{ kPa}$, v_f - e_0 , (c) $\sigma'_n = 200 \text{ kPa}$, v_f - e_0 , (d) $v_f = 0.0\%$, σ'_n - e_0 , (e) $v_f = 0.3\%$, σ'_n - e_0 , (f) v_{fr} , σ'_n - e_0



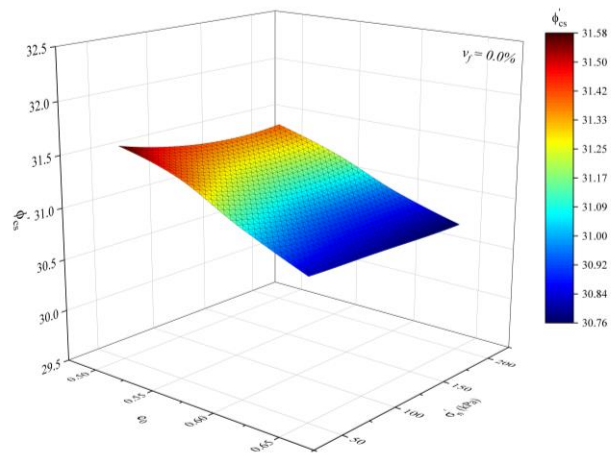
(a)



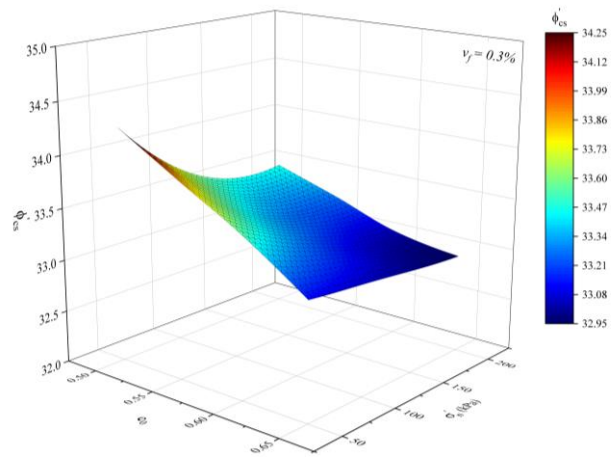
(b)



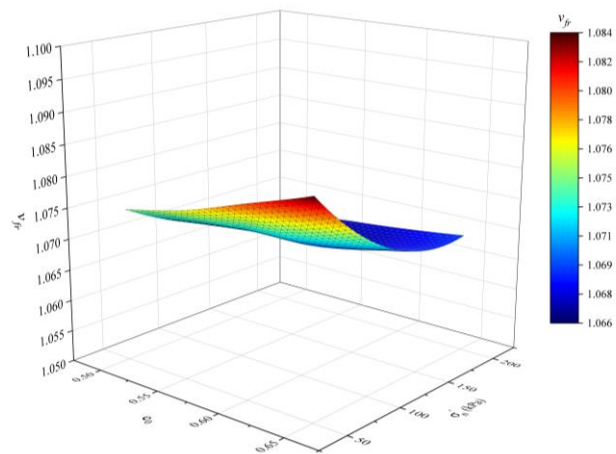
(c)



(d)



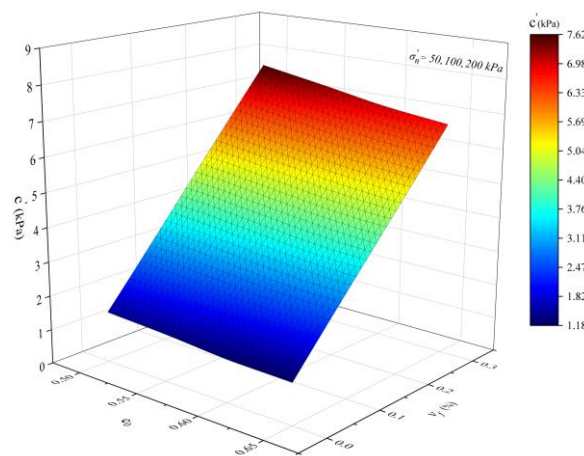
(e)



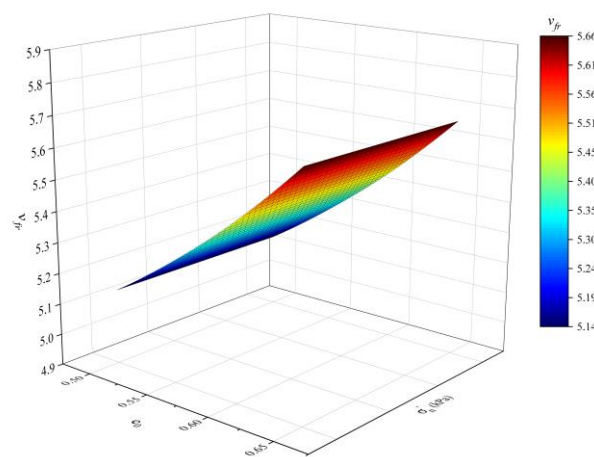
(f)

Figure 5.10. Effect of effective normal stress (σ'_n), initial void ratio (e_0) and volumetric reinforcement concentration (v_f) on the critical state friction angle (ϕ'_{CS}) in direct shear tests: (a) $\sigma'_n = 50 \text{ kPa}$, v_f - e_0 , (b) $\sigma'_n = 100 \text{ kPa}$, v_f - e_0 , (c) $\sigma'_n = 200 \text{ kPa}$, v_f - e_0 , (d) $v_f = 0.0\%$, σ'_n - e_0 , (e) $v_f = 0.3\%$, σ'_n - e_0 , (f) v_{fr} , σ'_n - e_0

Figure 5.11 shows the effect of void ratio and the presence of reinforcement on the cohesion parameter. Accordingly, while low cohesion values are obtained for unreinforced state in the direct shear tests, it was seen that the presence of reinforcement increased these values to a certain extent. Theoretically, it is known that sands do not have cohesion. However, due to the presence of reinforcement and cementation, sands reach to a significant cohesion level. First studies regarding the increase in the shear strength properties of sands by producing cohesion were conducted by Vidal (1969) and Schlosser and Long (1974). Researchers put forward various relations (regarding soil pressure) for the prediction of the magnitude by suggesting that geosynthetics produced pseudo-cohesion.



(a)



(b)

Figure 5.11. Effect of initial void ratio (e_0) and volumetric reinforcement concentration (v_f), on cohesion parameter (c') in direct shear tests: (a) v_f - e_0 , (b) v_{fr}

5.2.3. Volumetric strains

Cohesionless soils are first contracted and then dilated with increasing strain. This relative displacement shown by the grain during the shearing phase is the basis of the shear strength. Therefore, it is necessary to look at the issue from the aspect of volume change in order to understand the issue of the shear strength of the soil.

The absence of dilation in test equipment with sufficient deformation capacity applies only to the loosest packed sand. The presence of dilation should be mentioned for all other levels of density. As can be seen in Figure 5.12, with the increasing void ratio and normal stress, the level of contraction of the soil for both reinforced and unreinforced situations increased, while the dilation capacity decreased significantly. When the effect of reinforced presence on contraction and dilation was examined, it was seen that it reduced the contraction capacity compared to the situation without reinforcement and increased the dilation capacity. Another important finding is that the presence of reinforcement increases the volumetric strain capacity of the soil by absorbing the shear load. From all these findings, it is understood that the shear strength of the sand soils cannot be described only by the effective angle of friction, but also depends on the contraction-dilation feature.

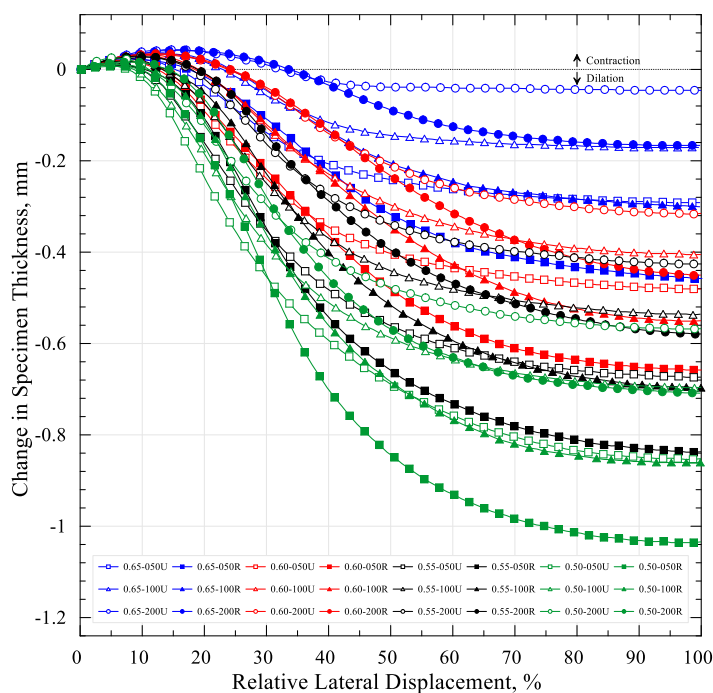


Figure 5.12. Volumetric strain curves obtained from direct shear tests

5.3. Triaxial Test Results

Triaxial test is a sophisticated test providing the saturation of the soil sample under the effect of constant confining pressure, consolidation of it under isotropic conditions (hydrostatic stress state), and then obtaining shear strength parameters by axially loading it with the help of a piston. It allows the correct representation of loading conditions in which soil exposed/will expose to (simulation of loading scenario), more effective control, and definition of the stress marks. In this method in which stress in the failure plane cannot be directly measured (free shear plane), the related shear strength parameters (to which it is related to normal stress in a linear way) are defined with Mohr-Coulomb failure criteria.

The aim of the study is to make a comparative analysis by measuring the shear strength via various parameters, therefore, all determinants used in the shearing tests were applied within the triaxial test method in the same way. Accordingly, triaxial tests detailed in Part 4 were performed under drained conditions with strain-controlled in four different densities from very loose to very dense, under the effect of three different isotropic confining (radial, cell) pressure, in the constant axial strain rate and a single volume fiber concentration. Rounded shaped standard sand was used for matrix and macro fiber with discrete structure was chosen as a reinforcement. This study included 108 drained triaxial tests (CD type) in total as 45 and 63 repetitive tests for unreinforced and reinforced tests, respectively. Part 4 covers theory belonging to the drained triaxial test method, mathematical model, operating procedure, the introduction of the test apparatus, and other related details.

In the first part of the section, the shear strength parameters of the unreinforced-reinforced samples were comprehensively evaluated and analyzed differently than the shearing tests while the results of volumetric strains were examined in second part.

5.3.1. Stress-strain relationship

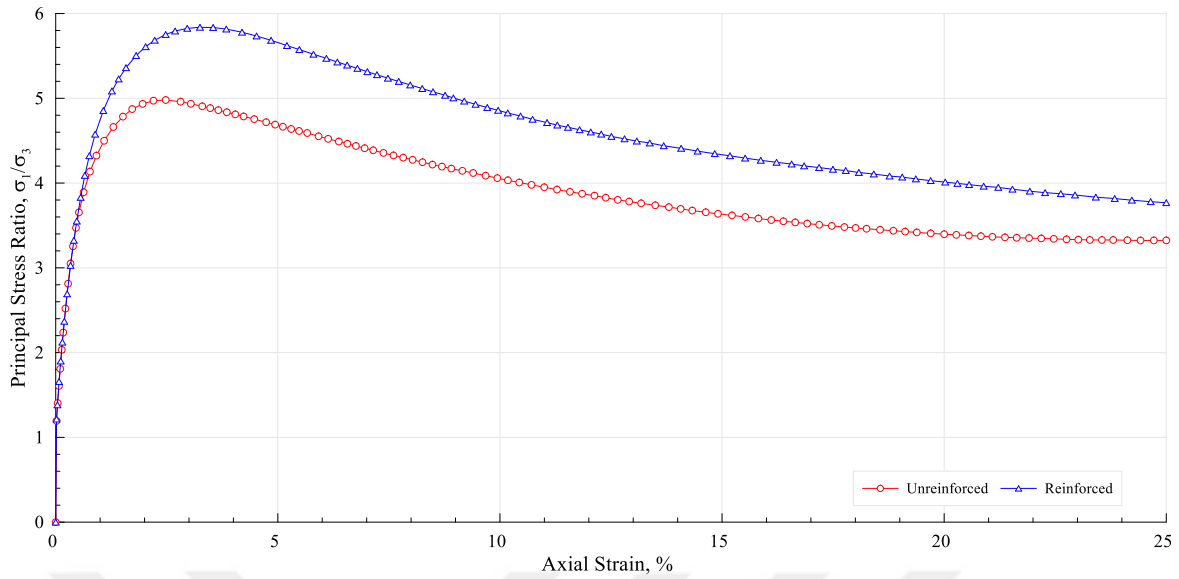
Failure in the drained triaxial tests is defined in three different essentials:

1. Maximum principal stress ratio: $(\sigma_1/\sigma_3)_{\text{pik}}$ & $(\sigma'_1/\sigma'_3)_{\text{pik}}$
2. Maximum principal stress difference: $(\sigma_1 - \sigma_3)_{\text{pik}}$ & $(\sigma'_1 - \sigma'_3)_{\text{pik}}$
3. A certain unit strain: $\tau = [(\sigma_1 - \sigma_3)/2]$ & $[(\sigma'_1 - \sigma'_3)/2]$

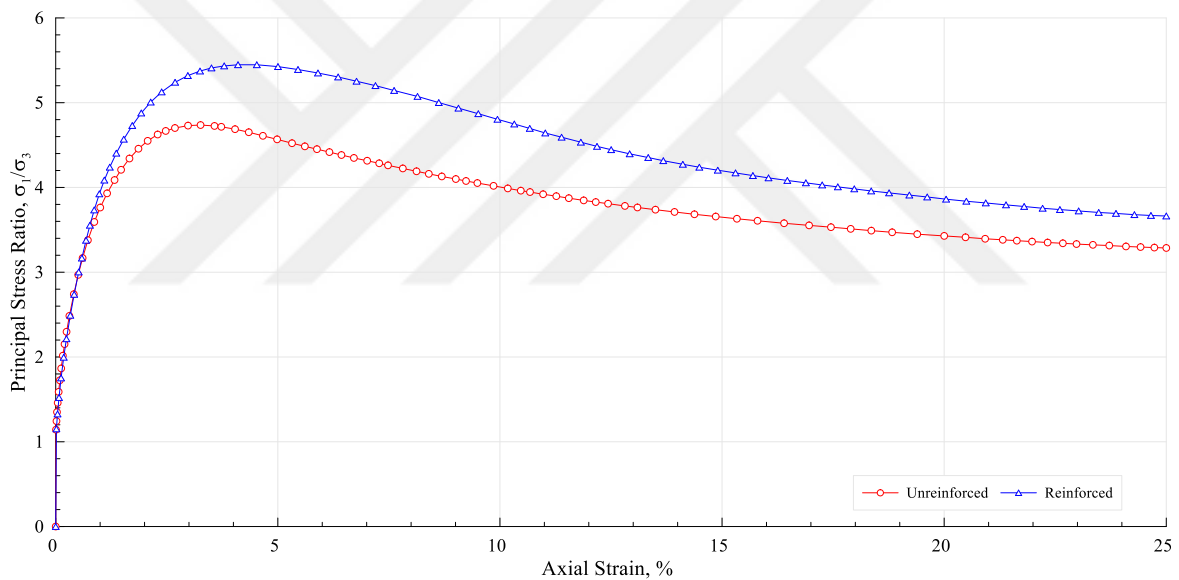
A quasi of the normalized phenomenon used in the definition of failure in the direct shear tests were applied for the triaxial tests. Accordingly, total axial stress (major principal stress: $\sigma_1 = \sigma_3 + \Delta_d$ (Δ_d : Principal stress difference), confining pressure (minor principal stress: σ_3) was normalized as it was defined in the first item. Part 5.2.1 explains the superiorities belonging to the choosing of this demonstration in which the strength-strain relationship is clearly seen in detail.

Figure 5.13 presents stress-strain curves belonging to the densely packed unreinforced and reinforced composites under the effect of isotropic ($\sigma'_c = 50, 100, 200 \text{ kPa}$) confining pressure ($e_0 = 0.50$). In the drawing of the stress-strain curves, the relationship of principal stress ratio-axial strain has been taken into consideration. The effect of chosen confining pressures on the related density index was categorized under three different graphics for the unreinforced and reinforced samples.

Figure 5.13 presents graphics showing that principal stress ratios are decreasing with the increasing confining pressure. The decreasing ratio between the greatest and lowest confining pressures for the peak strength was found to be 1.094 and 1.123 for reinforced and unreinforced samples, respectively. This ratio for critical strength was found to be 1.014 and 1.045 for unreinforced and reinforced samples, respectively. The main reason for this severe difference between peak and critical values is the grain freedom which is reached as a result of the strain-softening of the samples with the high density. Another striking factor for the dense soil is losses in the energy area in which principal stress ratio-strain curves with the tendency to lean by going towards the re-arrangement from the point where the dilation rate of the grains is high are found to be effective in the very low volumetric reinforcement concentration used in this study. This effect of reinforcement has been found to be in a similar tendency for the strain mode in the studies such as Gray and Maher (1989), Al-Refeai (1991), Ranjan et al., (1994). The following parts include more detailed evaluations about this subject.



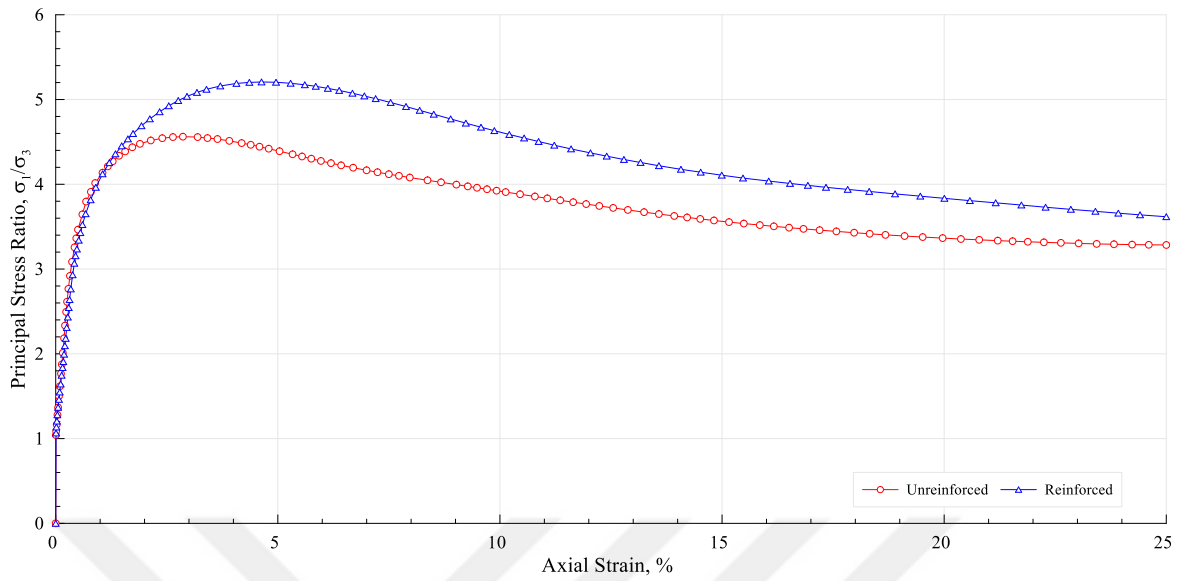
(a)



(b)

Figure 5.14 shows the curves belonging to the effective stress ratio-axial strain relationships of the medium packed ($e_0 = 0.55$) sands. Curves seem to be in similar trends but in the lower levels with ($e_0 = 0.50$) in the ranges in which brittle behavior is effective. This is because grains are required to do less work for their relative movements.

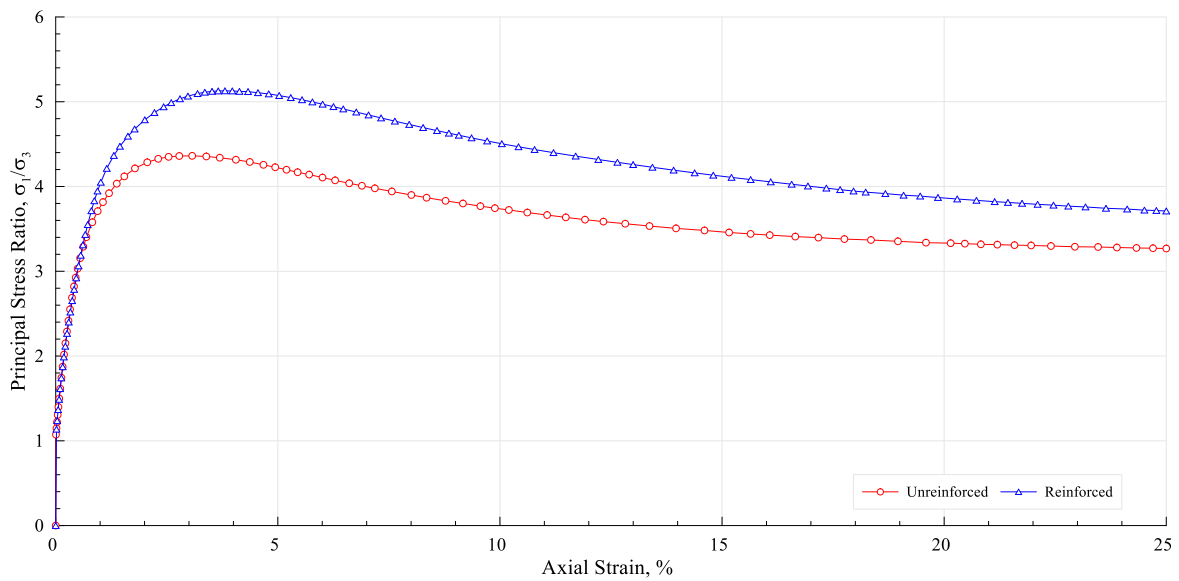
Reinforcements are clearly seemed to affect the strength loss with increasing strain for all the effective confining pressures. This loss is a property that is wanted for geotechnical practices; however, it makes it nearly impossible to research some geotechnical practices that are interested in the reinforcements' post-peak relationships through triaxial tests.



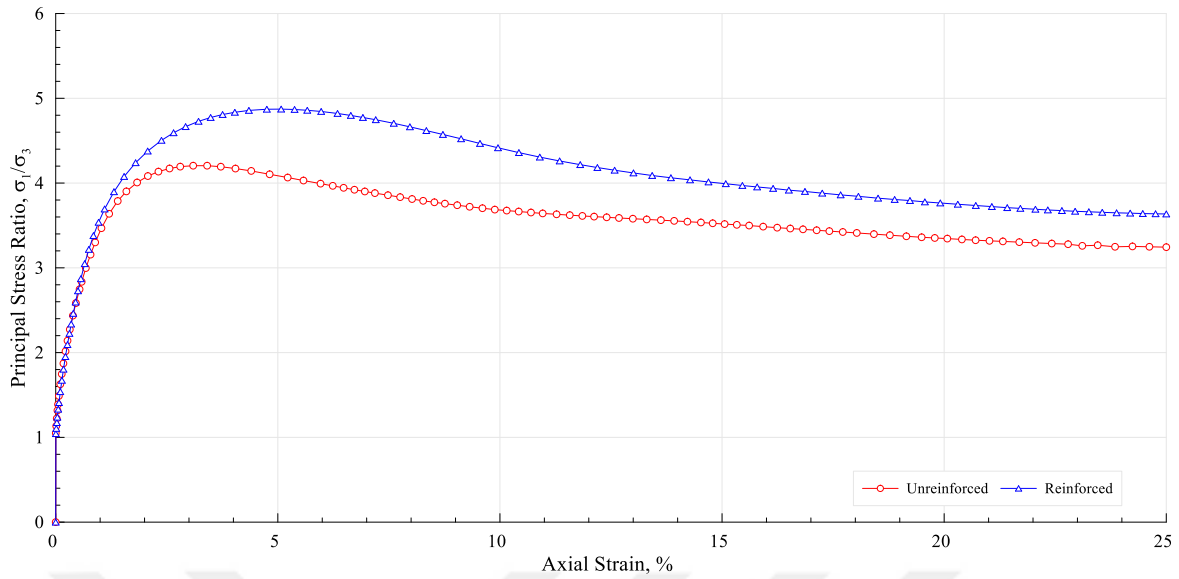
(c)

Figure 5.13. Principal stress ratio - Axial strain relationship for triaxial ($e_0 = 0.50$): (a) 50 kPa, (b) 100 kPa, (c) 200 kPa

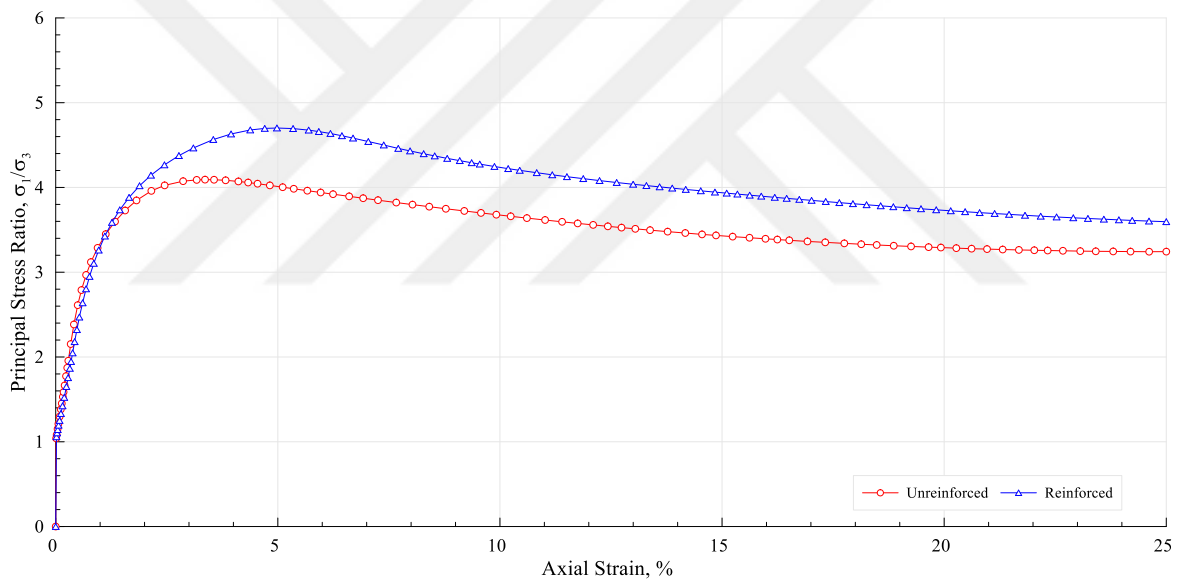
When the curves for $e_0 = 0.55$ are examined, it is seen that greater effective principal stress ratios are obtained for 50 kPa and that this effect gradually decreases with increasing confining pressure.



(a)



(b)

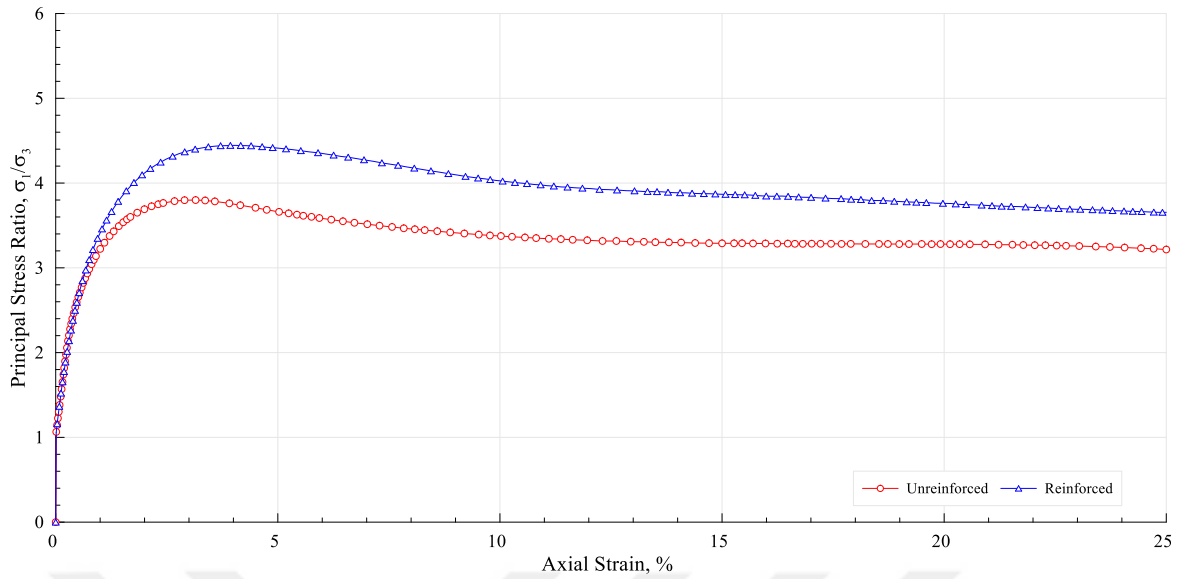


(c)

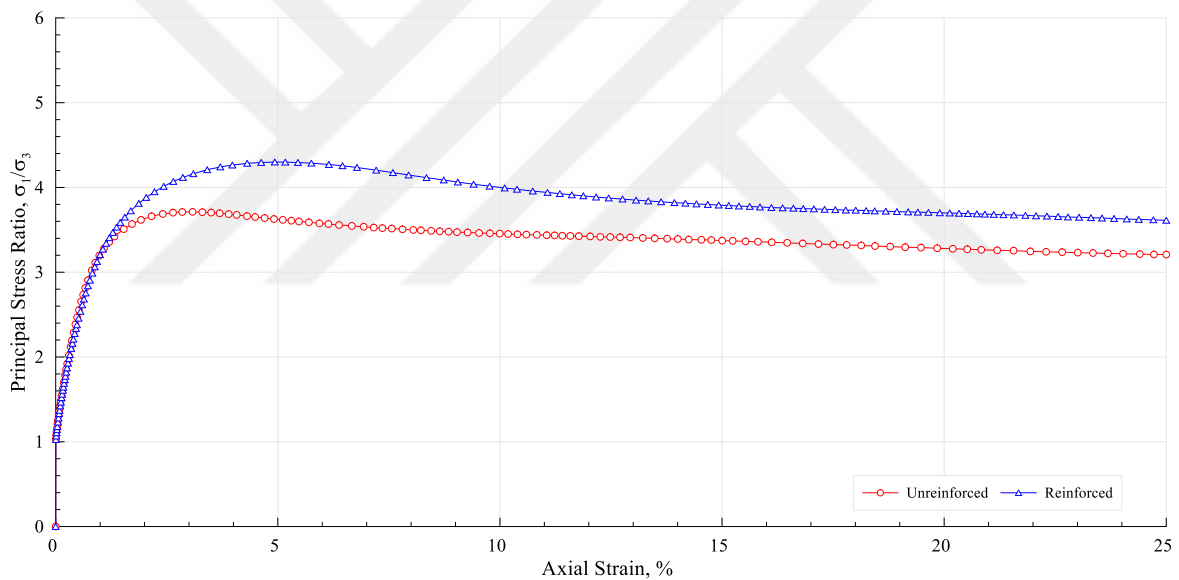
Figure 5.14. Principal stress ratio - Axial strain relationship for triaxial ($e_0 = 0.55$): (a) 50 kPa, (b) 100 kPa, (c) 200 kPa

As a function of normal stress, reinforcements' effect on these curves decreases with the increasing confining pressure. The main reason for this is that friction emerging with the reinforcement-grain relationship remained lower compared to the grain-grain relationship.

Figure 5.15 shows effective principal stress ratio-axial strain curves belonging to the unreinforced and reinforced samples prepared ($e_0 = 0.60$) in loose density.

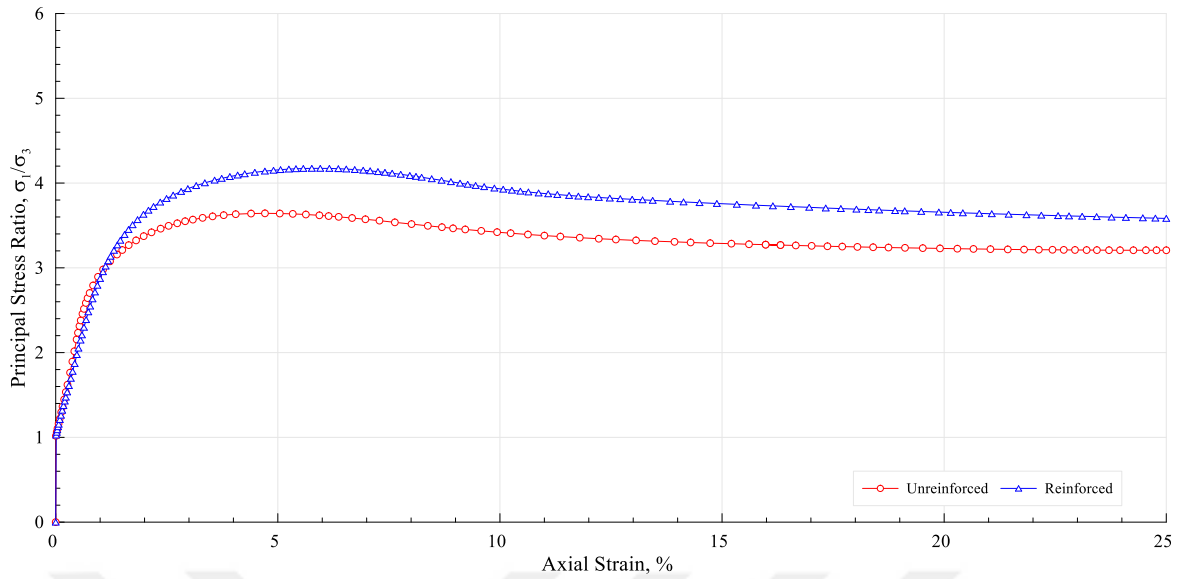


(a)



(b)

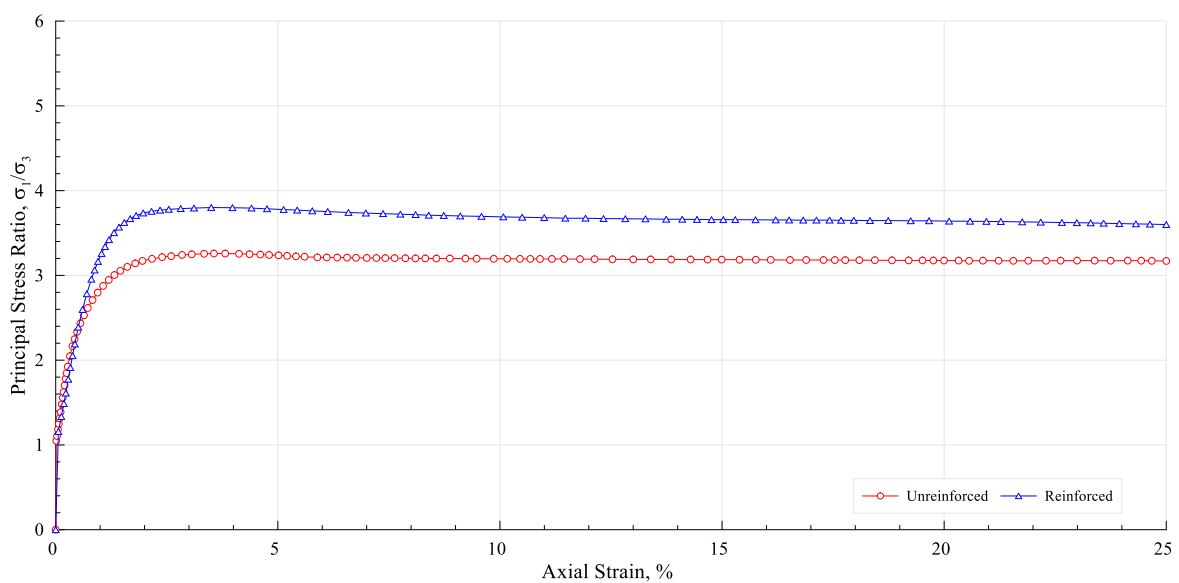
With the increase in the initial void ratio, effective principal stress ratios of the reinforced and unreinforced soils decreased compared to the above situations with less voids. This decrease has been seen to be more in the greatest effective stress ratios compared to the effective critical stress ratios. But, in the case of the reinforcements, this effect affected the low effective confining pressures (50 *kPa*) more as a function of the greatest effective stress ratios. On the other hand, 50 *kPa* when examining the effect of effective confining pressure on the reinforcements, normalized greatest (τ_p/σ'_c) and critical (τ_{cs}/σ'_c) stress ratios were found to be incremented in ratios of 1.138 and 1.123 ratios, respectively.



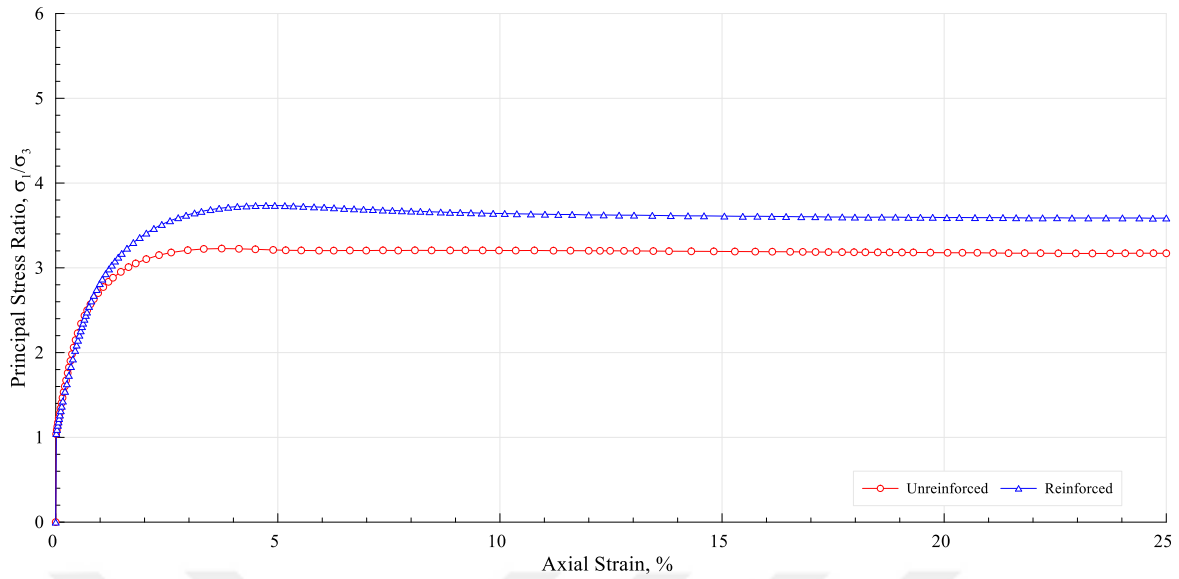
(c)

Figure 5.15. Principal stress ratio - Axial strain relationship for triaxial ($e_0 = 0.60$): (a) 50 kPa, (b) 100 kPa, (c) 200 kPa

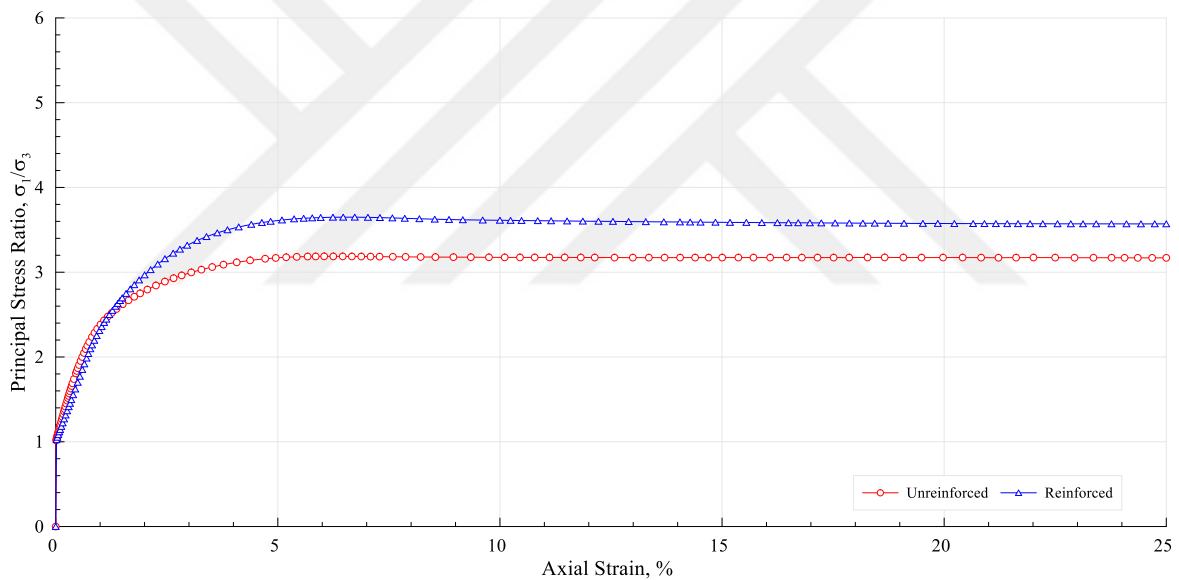
Figure 5.16 shows the curves belonging to the effective principal stress ratio-axial strain relationship of the loosely packed sands ($e_0 = 0.65$). With the increasing void ratio, greater strains have required the decrease in the necessary level of void ratio for the failure of grain sequences. Reinforcements increased this strain level that is necessary for failure as seen in the below figures.



(a)



(b)



(c)

Figure 5.16. Principal stress ratio - Axial strain relationship for triaxial ($e_0 = 0.65$): (a) 50 kPa, (b) 100 kPa, (c) 200 kPa

When these relationships are taken as an effective stress angle parameter, it is seen that grains lose less energy in the failure locations under the smaller confining pressures.

As detailed in Part 4.4.2, triaxial tests are used in the measurement of the shear strength of the soils due to their various benefits. Arteaga (1989) who searched the effect of reinforcements on the strength properties of soils observed that the triaxial test method both

represents the reinforced soils better and provides more significant results. This situation has been realized by many researchers and the effect of reinforcements on shear strength or other mechanical properties of the soil was researched with the triaxial tests.

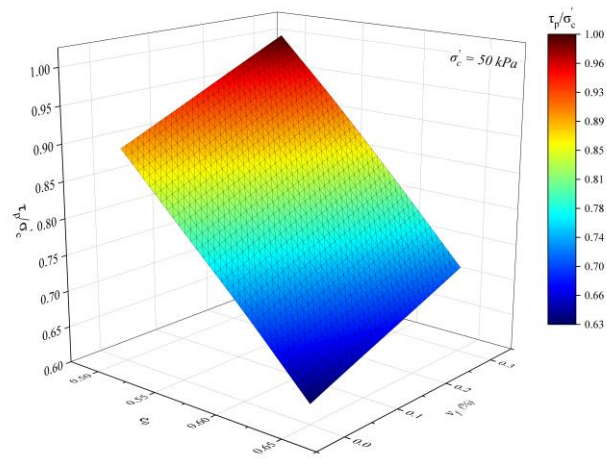
The aim of the study was the comparative analysis of the shear strength for the various strain modes, that is why the concept of effective stress ratio was used instead of the effective principal stress in the analysis of triaxial tests. The relationship between the peak (τ_p/σ'_c) and critical effective strain ratio (τ_{cs}/σ'_c) as a function of effective normal stress (σ'_c), initial void ratio (e_0) and volume reinforcement (v_f) concentration are shown as three-dimensional images in Fig. 5.17 and Fig. 5.18, respectively. Figure 5.16 presents that the peak effective stress ratios are within the ranges given in the previous section for the quartz sand. Images in the Figure 5.17a, Figure 5.17b, and Figure 5.17c in which σ'_c is taken as a parameter indicate that increasing the confining pressure four times the $e_0 = 0.50$ caused the decreased ratio of τ_p/σ'_c value to be 1.071 for unreinforced state and 1.087 for reinforced state. This ratio decreases for both states in case of the higher void ratios. The main reason for this is that strength depends on the rolling resistance created by grains' pushing each other due to increasing void ratio's forcing grains to move towards the shearing orientation. Terzaghi et al. (1996) state that this resistance has quite a limited friction angle like only 5 – 6 degrees. Figure 5.17d and Figure 5.18e show that reinforcements are taken as a parameter. Figures show that reinforcement contributes to the strength for each of the e_0 and σ'_c . This is because reinforcement material placed in the soil decreases the movement capacity of the grains according to themselves and causes better geometrical interference and so improves mechanical properties. The contribution of reinforcement to the strength is understood better when evaluated as in Figure 5.17f e_0 and within the scope of the grain-reinforcement relationship as the common function of σ'_c as mentioned above.

Figure 5.18 presents the relationship of the parameters belonging to the critical effective state with confining pressure (σ'_c), initial void ratio (e_0), and reinforcement (v_f). Strength properties of the sands in the critical state are theoretically provided with kinetical friction, pushing and rearrangement friction. This situation indicates that obtained τ_{cs}/σ'_c values will be within a narrow bandwidth. This study indicated that reinforcements increased this bandwidth range in the ratio of 1.06 for triaxial tests. This much increase happens in

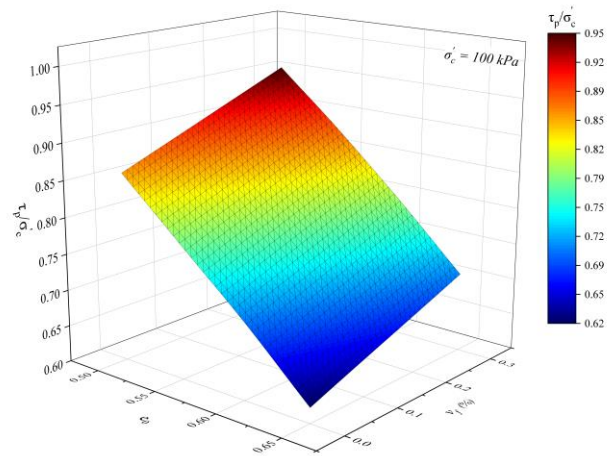
very low reinforcement concentration reveals itself as a kinematic strain hardening depending on the higher reinforcement concentration or properties of the reinforcement material in various orientations.

Figure 5.18a, Figure 5.18b, and Figure 5.18c' de σ'_c shows the effect of the chosen parameter τ_{cs}/σ'_c on void ratio and reinforcement. For the unreinforced and reinforced state, the greatest τ_{cs}/σ'_c values were reached in the low confining pressures for the low initial void ratio. When the effect of reinforcements on the τ_{cs}/σ'_c were examined, e_0 was found to be more effective than σ'_c . Undoubtedly, this situation is directly related to the resistance forces emerging within the grains of the reinforcement in the composite exposed to strain. Another significant matter is that τ_{cs}/σ'_c the stress range τ_p/σ'_c showed in Figure 5.18d and Figure 5.18f for unreinforced and reinforced states, respectively had a very low level of change when compared to Figure 5.17d and Figure 5.17f drew in the same scale. The mechanism mentioned above is the fundamental reason for this phenomenon.

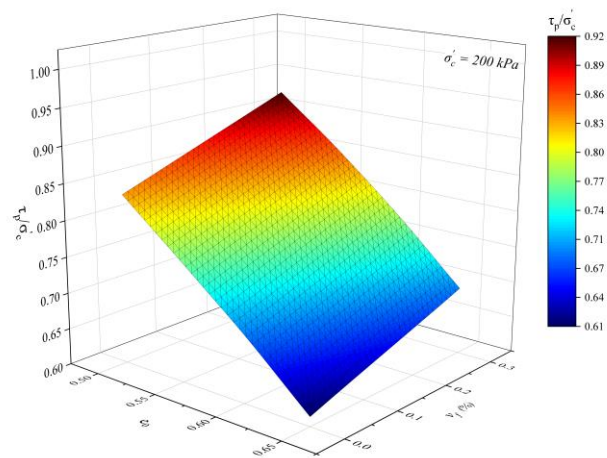
Testing of strength and strain properties of the reinforced soils for various drainage or loading conditions with the triaxial method is common due to the aforementioned methods. The use of this test method becomes more critical both to ensure enough reinforcement orientation and to develop a more effective relationship with sand matrix especially when discrete random distributed macro or microfiber geosynthetics. In accordance with the ultimate aim of this thesis study, enough information has been given here. Researchers who are interested in the subject can benefit from the Gray and Al-Refeai (1986), Maher and Gray (1990), Ranjan et al., (1996), Michalowski and Zhao (1996), Zornberg (2002), Michalowski and Čermák (2002, 2003), Consoli et al., (2007), Diambra et al., (2010), dos Santos et al, (2010), Diambra and Ibrahim (2015) et al. which used triaxial test for the more comprehensive study.



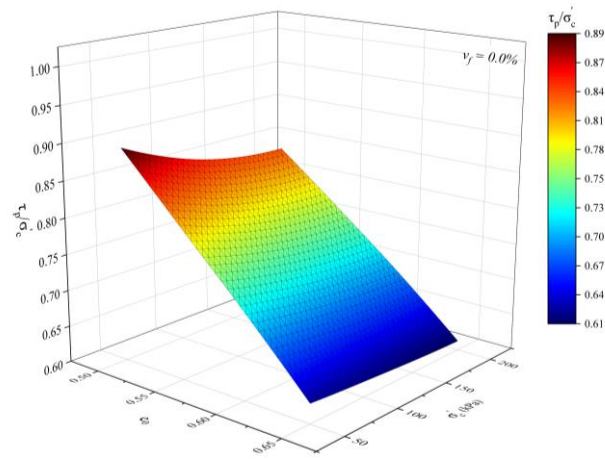
(a)



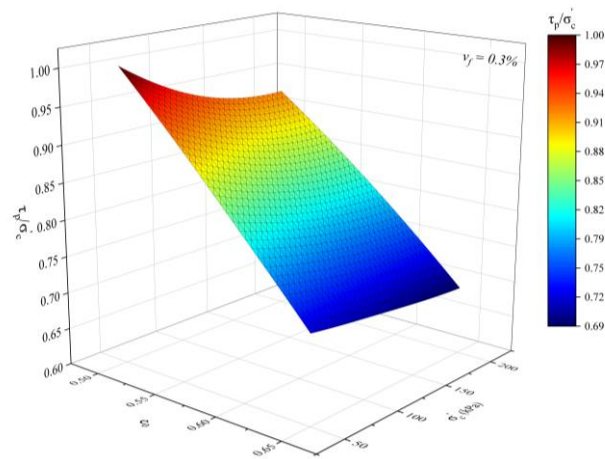
(b)



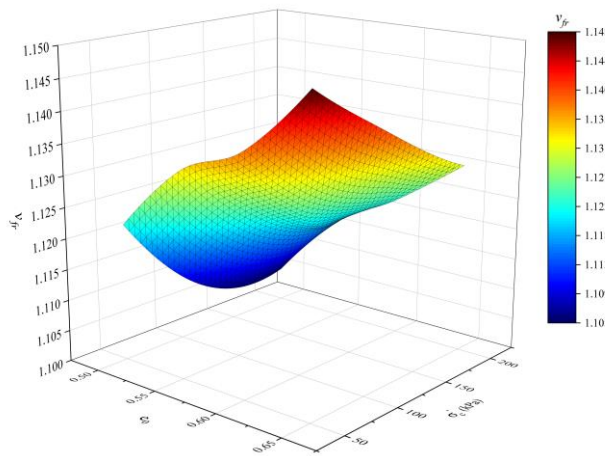
(c)



(d)

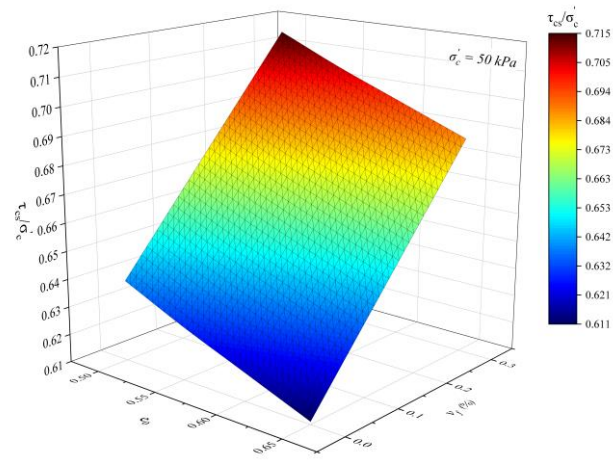


(e)

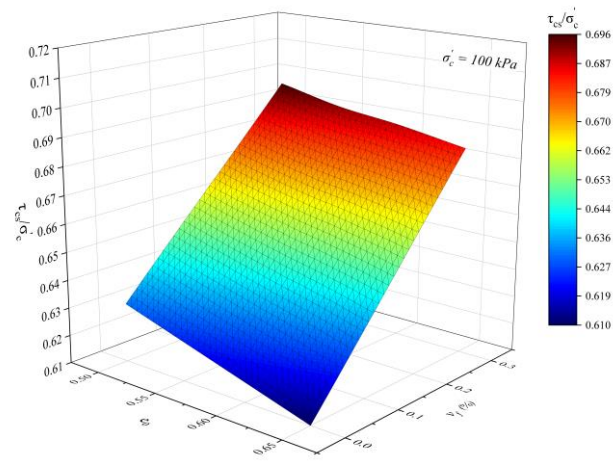


(f)

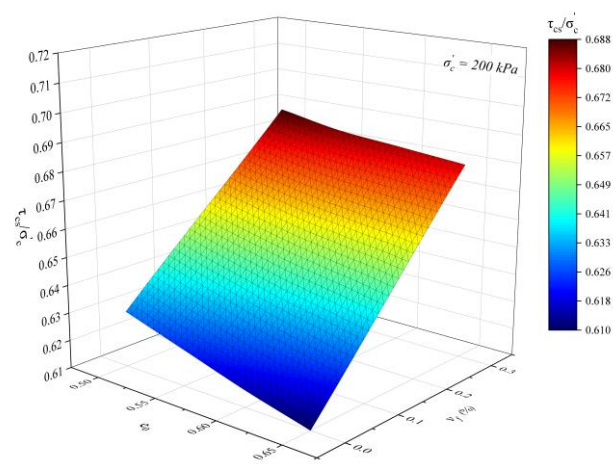
Figure 5.17. Effect of effective cell pressure (σ'_c), initial void ratio (e_0) and volumetric reinforcement concentration (v_f) on the peak effective stress ratio for the triaxial tests (τ_p/σ'_c): (a) $\sigma'_c = 50 \text{ kPa}$, v_f - e_0 , (b) $\sigma'_c = 100 \text{ kPa}$, v_f - e_0 , (c) $\sigma'_c = 200 \text{ kPa}$, v_f - e_0 , (d) $v_f = 0.0\%$, σ'_c - e_0 , (e) $v_f = 0.3\%$, σ'_c - e_0 , (f) v_{fr} , σ'_c - e_0



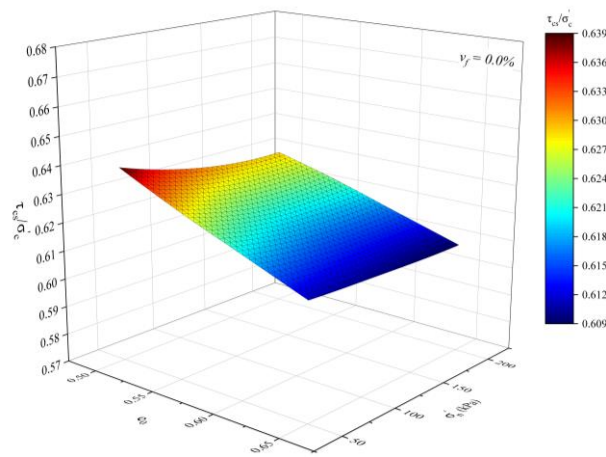
(a)



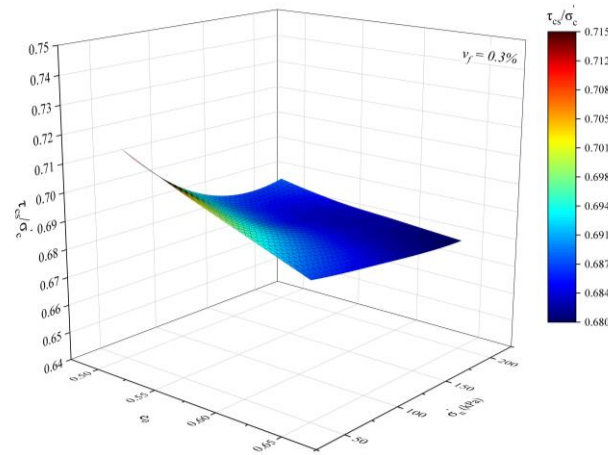
(b)



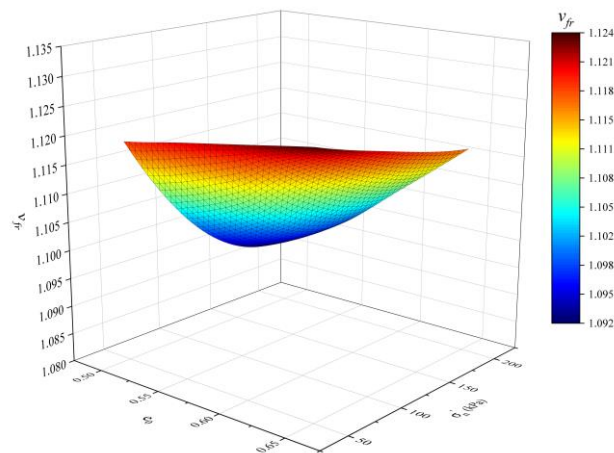
(c)



(d)



(e)



(f)

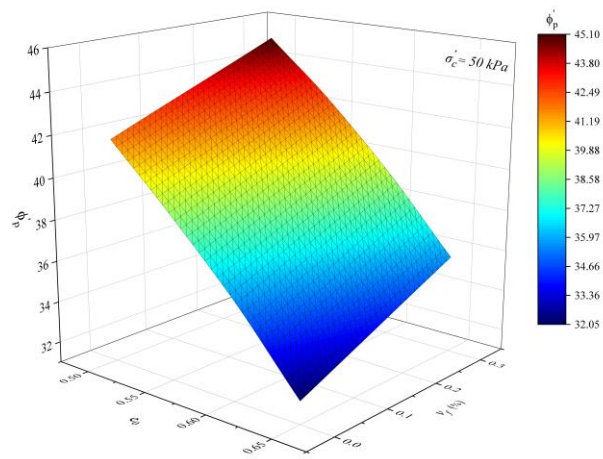
Figure 5.18. Effect of effective cell pressure (σ'_c), initial void ratio (e_0) and volumetric reinforcement concentration (v_f) on the critical state stress ratio for the triaxial tests (τ_{cs}/σ'_c): (a) $\sigma'_c = 50 \text{ kPa}$, v_f - e_0 , (b) $\sigma'_c = 100 \text{ kPa}$, v_f - e_0 , (c) $\sigma'_c = 200 \text{ kPa}$, v_f - e_0 , (d) $v_f = 0.0\%$, σ'_c - e_0 , (e) $v_f = 0.3\%$, σ'_c - e_0 , (f) v_{fr} , σ'_c - e_0

5.3.2. Shear strength parameters

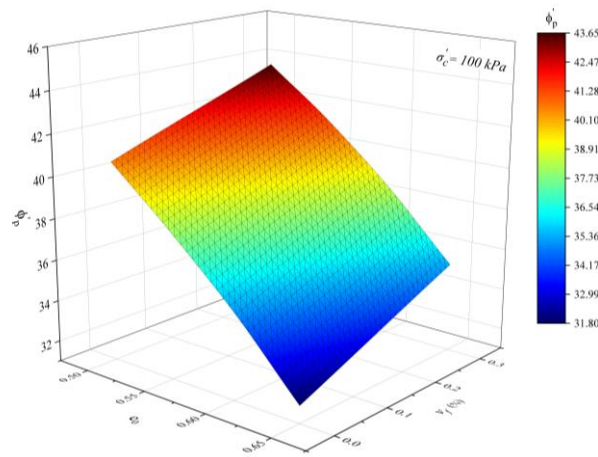
Triaxial experiment is a preferable method in obtaining shear strength parameters due to its superiorities mentioned in Chapter 4. In fact, this method has widely been used in the general diagrams of the frictional angles of soils (e.g., Meyerhof, 1956; Means and Pacher, 1963; Terzaghi and Peck, 1967; Peck et al., 1974; Schmertmann, 1978; Villet and Mitchell, 1981; NAVFAC, 1982). In the first chapter, the results of the peak and critical effective frictional angles and in the last chapter, the results of cohesion parameter have been comparatively analyzed for both unreinforced and reinforced states.

Results regarding the relation between the peak effective internal friction angle, confining pressure (σ'_c) and initial void ratio (e_0) were given in Figure 5.19. In the triaxial experiment, since the particles tend to volumetric strain instead of interlocking, the difference between the greatest and lowest (ϕ'_p) values were found as 10° in unreinforced state, and 11° in reinforced state. This difference is significant due to showing that the presence of reinforcement has a greater effect on the peak effective frictional angle compared to critical state. This is despite the well-known fact that the presence of reinforcement limits the reorientation of the particles after peak. In spite of the fact that a very low reinforcement concentration was used in the thesis, its great effect on ϕ'_p value shows a better operation of reinforcement and sand combination in the triaxial tests. This effect is observed to be higher with the increase in void ratio and decrease in the effective confining pressure. The main reason for this is that the particles are initially far from each other in the loose samples and that they are forced to work together by laying a bridge between them with the help of reinforcement. There is no need to such a reaction in conditions where the void ratio is low, therefore the contribution of reinforcement to strength remains limited.

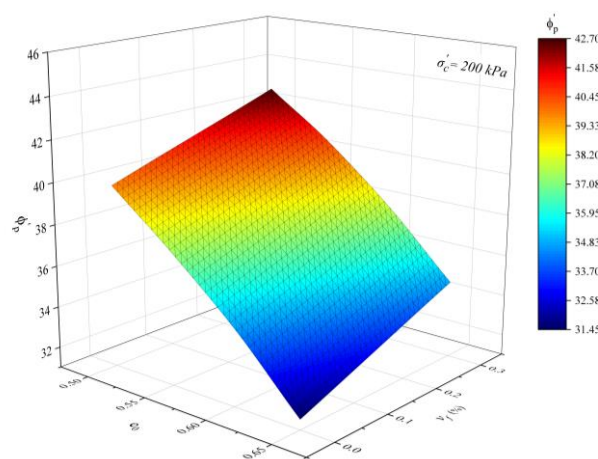
Results regarding the effective critical state frictional angle are given in Figure 5.20. Since the triaxial experiment has a limited capacity, it is very difficult for the principal stress difference to touch the critical band (particularly in the presence of reinforcement). Experiment results show that the critical state that is thought to be independent from the initial void ratio is critically affected by the friction angle in the presence of reinforcement. The main reason for this is that the reinforcement orientation is not completed on the plane of failure.



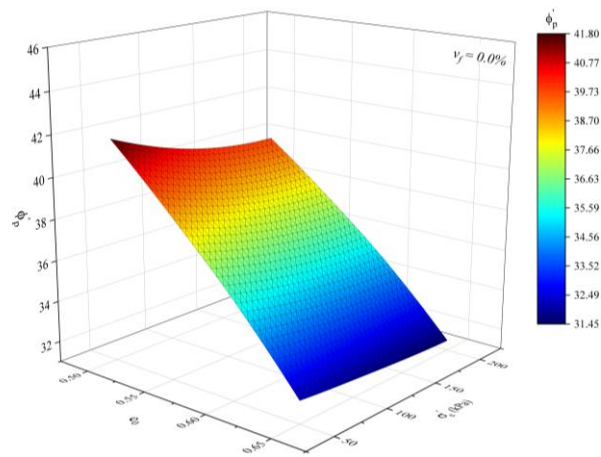
(a)



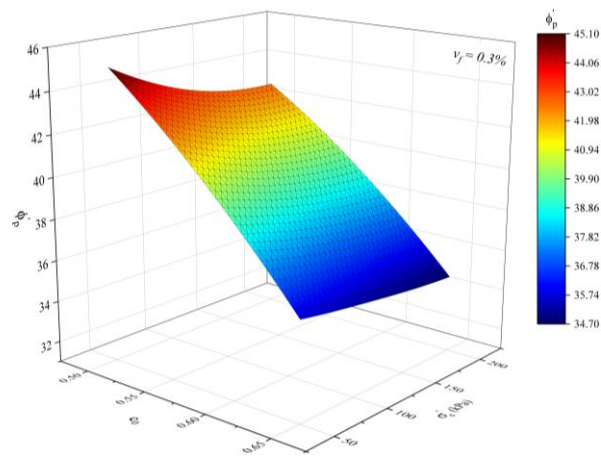
(b)



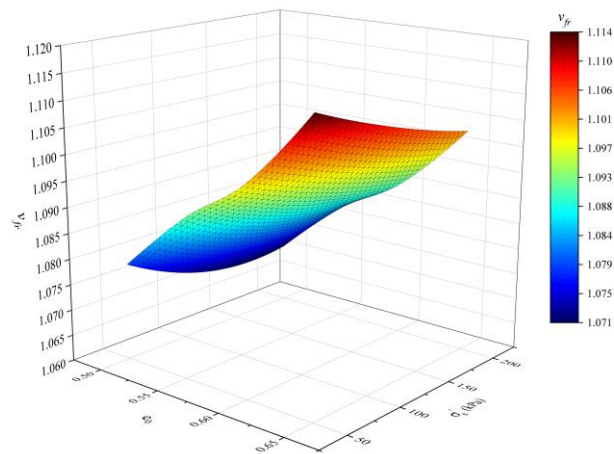
(c)



(d)

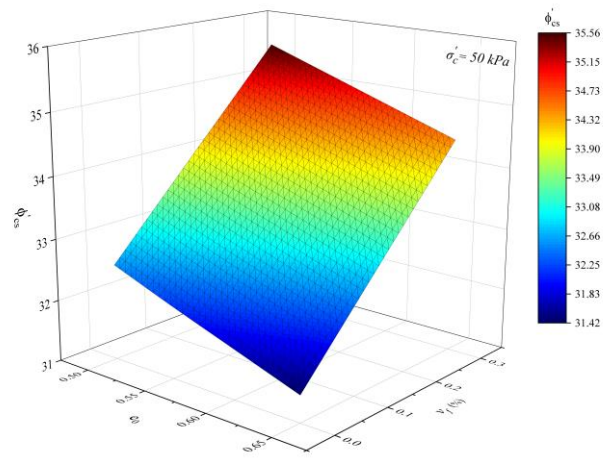


(e)

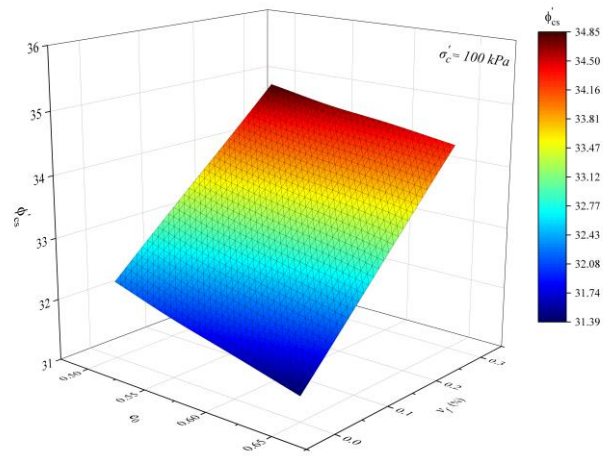


(f)

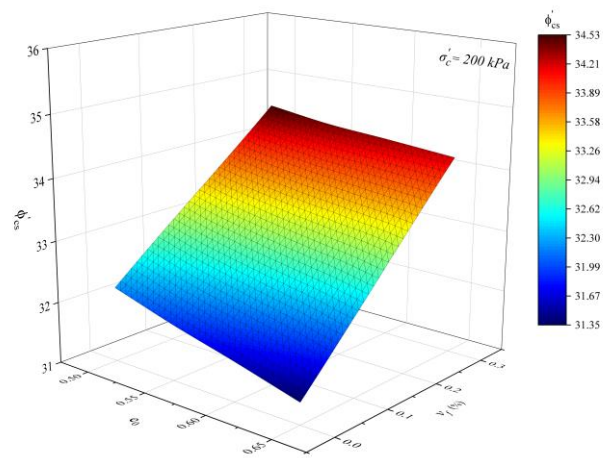
Figure 5.19. The effect of effective all around pressure (σ'_c), initial void ratio (e_0) and volumetric reinforcement concentration (v_f) on the effective peak friction angle (ϕ'_p) for triaxial tests: (a) $\sigma'_c = 50 \text{ kPa}$, v_f - e_0 , (b) $\sigma'_c = 100 \text{ kPa}$, v_f - e_0 , (c) $\sigma'_c = 200 \text{ kPa}$, v_f - e_0 , (d) $v_f = 0.0\%$, σ'_c - e_0 , (e) $v_f = 0.3\%$, σ'_c - e_0 , (f) v_{fr} , σ'_c - e_0



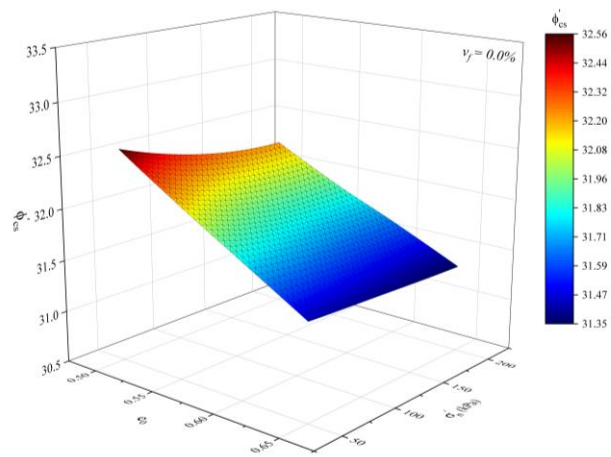
(a)



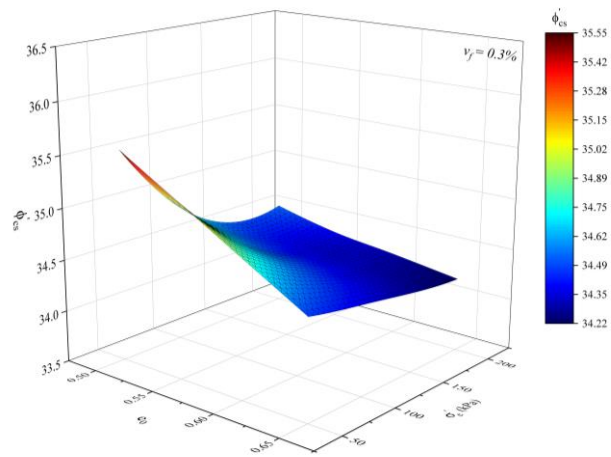
(b)



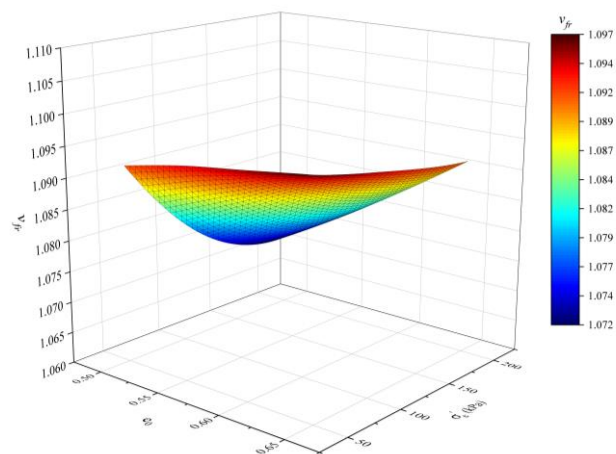
(c)



(d)



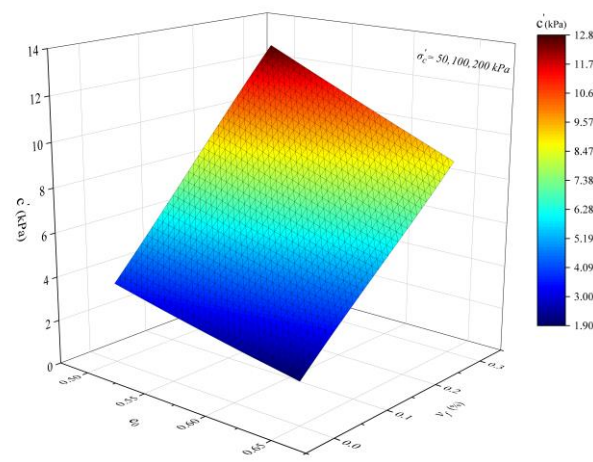
(e)



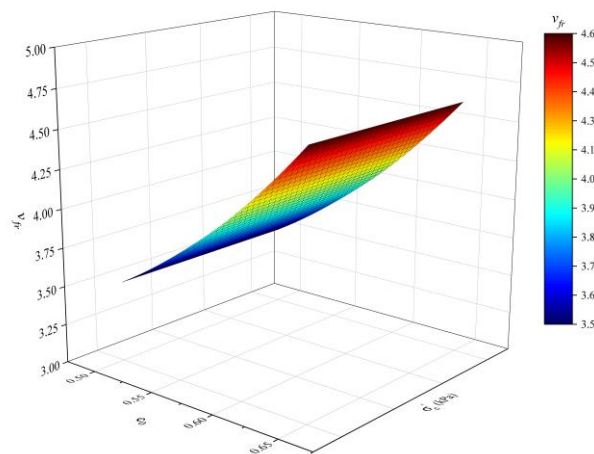
(f)

Figure 5.20. The effect of effective all around pressure (σ'_c), initial void ratio (e_0) and volumetric reinforcement concentration (v_f) on the critical state friction angle (ϕ'_{cs}) for triaxial tests: (a) $\sigma'_c = 50 \text{ kPa}$, v_f - e_0 , (b) $\sigma'_c = 100 \text{ kPa}$, v_f - e_0 , (c) $\sigma'_c = 200 \text{ kPa}$, v_f - e_0 , (d) $v_f = 0.0\%$, σ'_c - e_0 , (e) $v_f = 0.3\%$, σ'_c - e_0 , (f) v_{fr} , σ'_c - e_0

Figure 5.21 shows the experiment results regarding the effective cohesion parameter (c'). As seen from the figures, while c' value is in low level in the unreinforced states, its contribution increases in the presence of reinforcement. This increase is related to the electrostatic forces between the particles and the membrane surfaces. Bringing in the cohesion property to the sands taking its strength from friction has been a popular research topic these days. In fact, while geosynthetic and pozzolana materials had been commonly used in the past, today, biological living things such as bacteria, microbes, algae are being used for the purpose of cementation.



(a)



(b)

Figure 5.21. The effect of initial void ratio (e_0) and volumetric reinforcement concentration (v_f) on cohesion parameter (c') in triaxial tests: (a) v_f - e_0 , (b) v_f - r

5.3.3. Volumetric strains

Triaxial tests are generally preferred to measure the volumetric strain of the soils more accurately. This is because the amount of water entering and leaving the sample in triaxial tests is a measure of volumetric strains. This feature is the main reason for choosing this method in the theoretical (Bishop, 1954; Rowe, 1962; Schofield and Wroth, 1968) or experimental (Roscoe, 1970; Bolton, 1986; Collins et al., 1992) examination of the stress-dilatation relationships of soils.

Volumetric strain curves obtained from triaxial tests are shown in Figure 5.22. When the curves are examined, it is seen that the volumetric strains for both the reinforced and unreinforced states vary significantly as a function of the void ratio and confining pressure. Undoubtedly, this finding is important in terms of being the cause of the effects of the void ratio and confining pressure on the shear strength parameters. The difference between the initial contraction levels is related to the different initial positions of the grains. The main thing here is to see that the necessary mechanical energy that passes the grains into the dilation phase is a measure of the strength and strain characteristics of the soils.

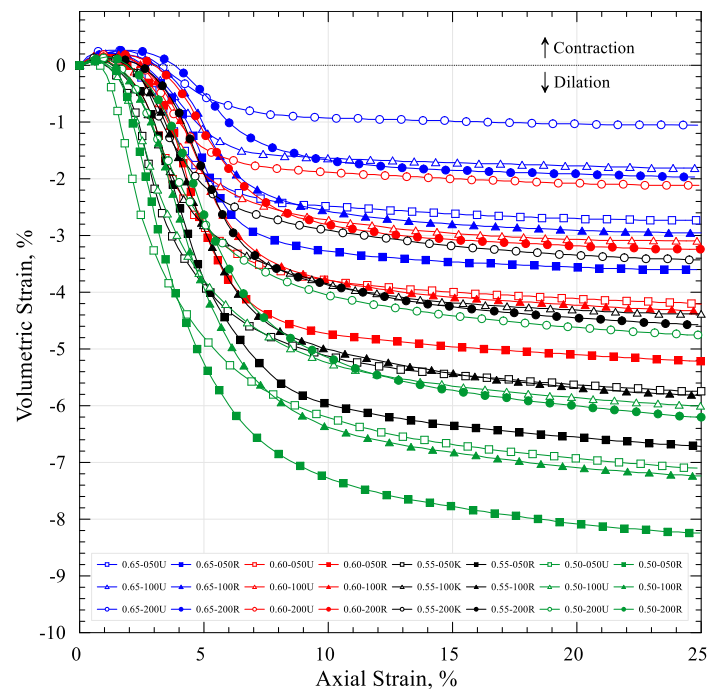


Figure 5.22. Volumetric strain curves obtained from triaxial tests

5.4. Ring Shear Test Results

Ring shear test is a significant shearing test used in the examination of the shear strength and stress-strain behaviors of the soils. What is making significant this test is that even though the limited strain levels of the other laboratory tests, it is possible to reach a nearly limitless level of strain, and therefore it can reach the permanent strength parameters of the soils in a certain approximation. Part 4 includes detailed information regarding the relevant test method.

The ring shear test required the continuous improvement of the shear parameters by eliminating the hardships such as wall friction, potential soil extrusion, nonuniform stress, and strain distribution (Scarlett and Todd, 1969; Stark and Eid, 1993; Tika et al., 1996). Meehan et al. (2007) state that the above-mentioned inadequacies will be minimized by using the Bromhead type of the modified bronze porous torsion beam. Due to the superiority to other test tools, Meehan et al. (2007) used the ring shear test tool on the suggested level. Shear strength parameters belonging to the test method are obtained through Mohr-Coulomb failure criteria relating any effective normal stress affecting any plane during failure (σ'_n) to shear strength (τ) (σ'_n and τ parameters' affecting any plane with its critical combination, $\tau_f = f(\sigma)$).

Aiming to conduct a comparative analysis of the shear strength parameters with various test methods, this thesis study used the empirical procedure chosen for the direct shear and triaxial method for the ring shear test, as well. Accordingly, ring shear tests which were explained in detail in Part 4 were performed in four different intensities from loose to dense representing the unreinforced and reinforced density index, in three different effective normal stress force loading, in a single volumetric reinforcement concentration and modified Bromhead type ring shear test tool with bronze porous and torsion beam. To minimize the effect of restrictive factors on the peak strength properties, the test sample was sheared in two different angular strain rates until reaching the peak and after the peak. These strain rates chosen for the ring shear tests in the analysis of unreinforced and reinforced sands were compatible with the Novosad (1964), Hunger and Morgenstern (1984), Sassa (2000) studies. Isometrical and rounded to subrounded shaped clean standard sand were used for matrix and macro fiber with discrete structure was chosen as a reinforcement. This study performed 45

ring shear tests for the unreinforced samples and 63 for the fiber-reinforced composite samples, 108 in total.

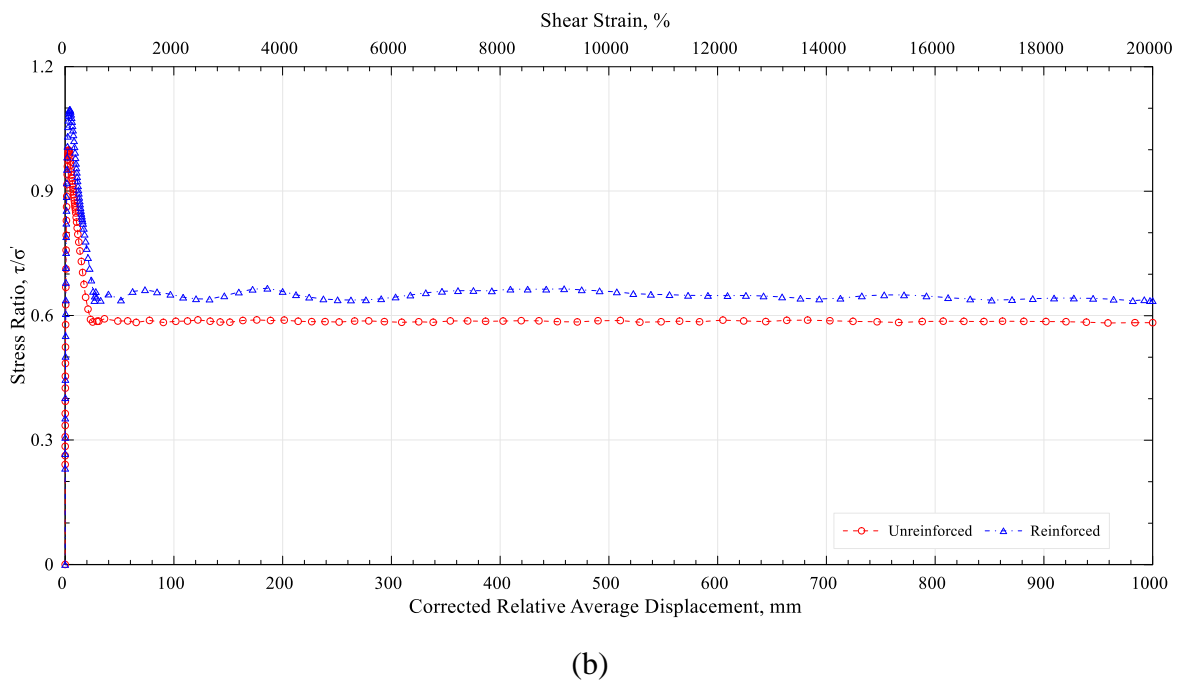
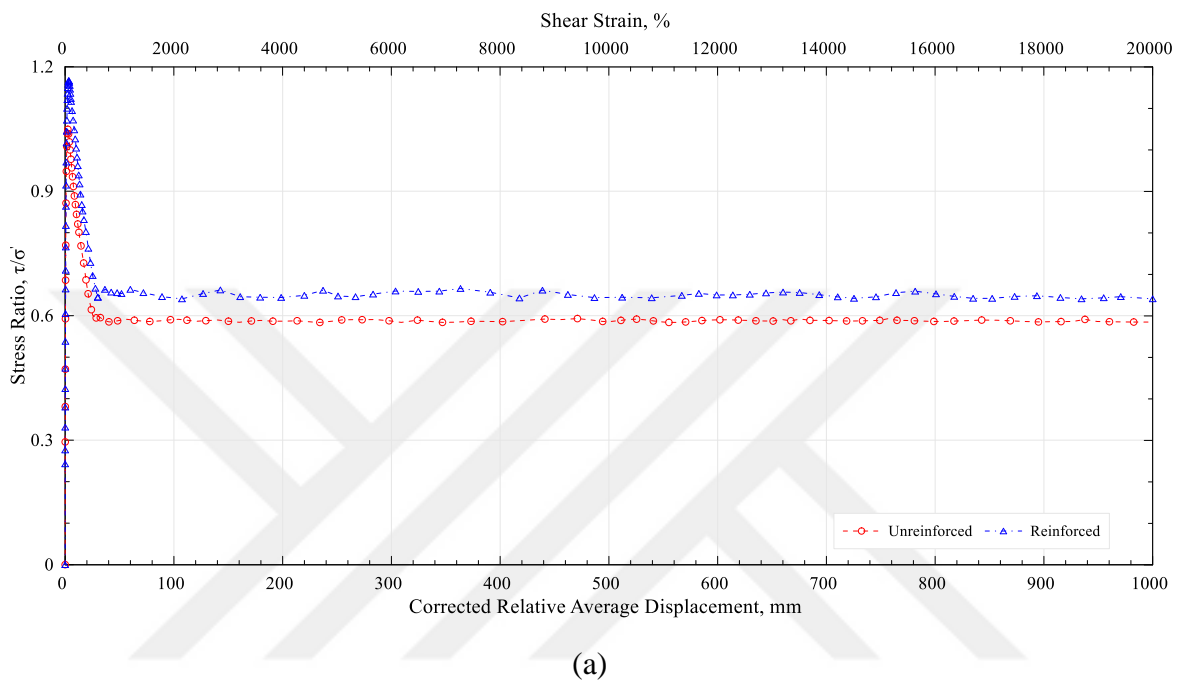
In this section where the results of the ring shear test method presented, in the first part the shearing strength properties in the continuation volumetric strains were discussed and comparative analysis were conducted.

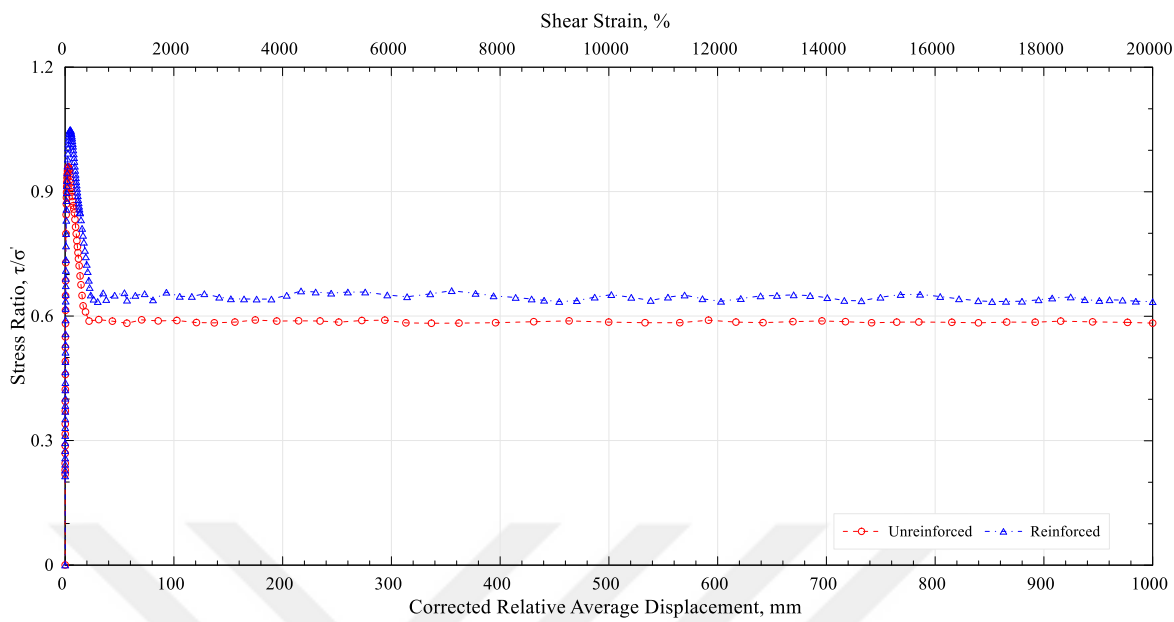
5.4.1. Stress-strain relationship

Failure of the sands in the ring shear method is defined with stress ratio normalized with effective normal stress and strain level in which the sample has been failed or shearing stress has been constant. Ring shear test is a kind of direct shear test, which is why the effective stress ratio concept chosen due to its advantage in the direct shear test (τ/σ'_n) has been used for this method.

Figure 5.23 presents stress displacement/strain curves belonging to the densely packed ($e_0 = 0.50$), unreinforced, and reinforced composites ($\sigma'_n = 50, 100, 200 \text{ kPa}$) under the effect of three different normal stress. Effective stress ratio-shear displacement/strain curves are similar to the curves obtained from direct shear and three axial test methods. What is making this similarity different is the scaling effect causing displacement levels to reach to $1m$. Of the related figures, the peak τ/σ'_n is seen for both unreinforced and reinforced state and the lowest σ'_n is seen in the (50 kPa). This situation is due to the friction's emerging between the surfaces due to the two-dimension resistance grains shown in the constant cross-sectional area and the geometrical interference's being inversely proportional with the increasing σ'_n . Another factor drawing attention in the figures is the difference in the τ_{cs}/σ'_n values occurring in the critical strength area. The reason for this is the sand extrusion out of the ring shear box as a result of the angle increasing shear strain rate after the obtained τ_p/σ'_n value. With the extrusion of sand, grains on the shear band try to redirect. Thus, stress occurs in the wall surfaces and at the center. This mechanism is the indicator of the material out to be continued. Especially, in the case of reinforcements, this effect is clearly seen to be more as understood from the figures.

Figure 5.24 presents ($e_0 = 0.55$) effective stress ratio-shear displacement/strain relationships belonging to the medium sands. When examined the effect of σ'_n for reinforced and unreinforced samples grains were found to be more sensitive to the σ'_n as a result of the decreasing energy losses.

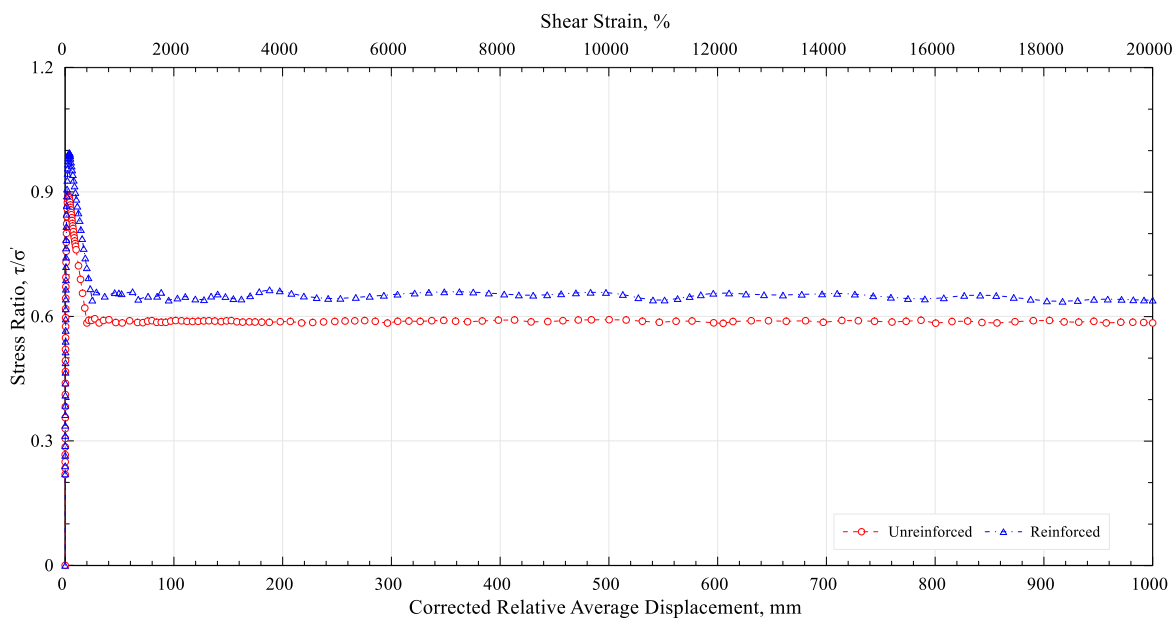




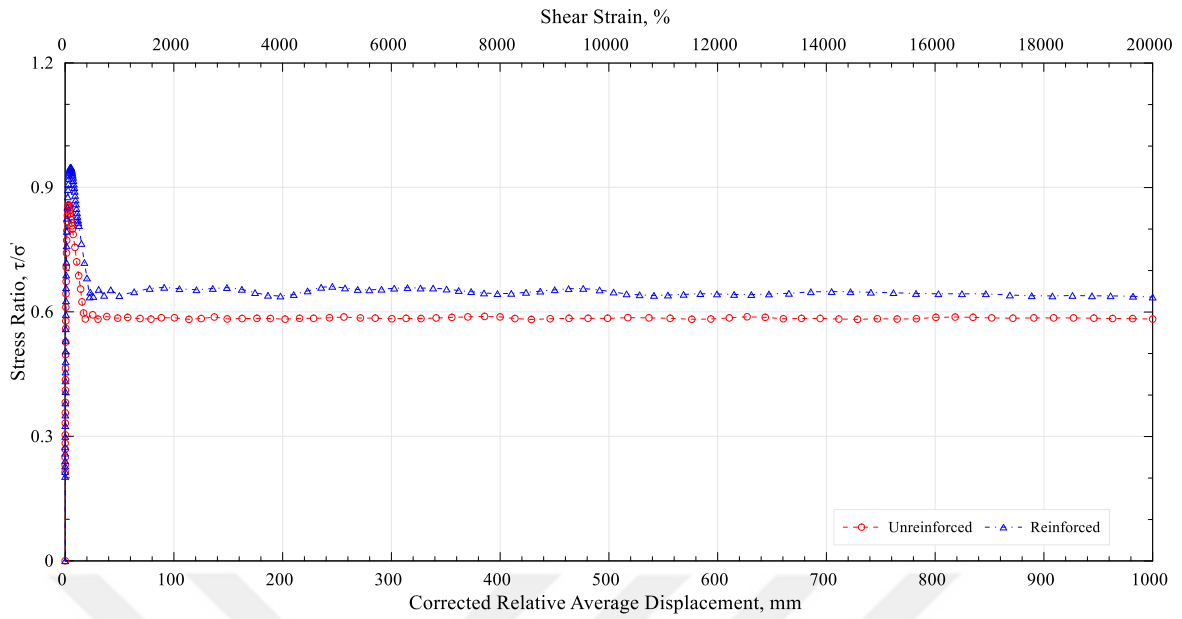
(c)

Figure 5.23. The stress ratio - Shear displacement relationship for ring shear ($e_0 = 0.50$):
 (a) 50 kPa, (b) 100 kPa, (c) 200 kPa

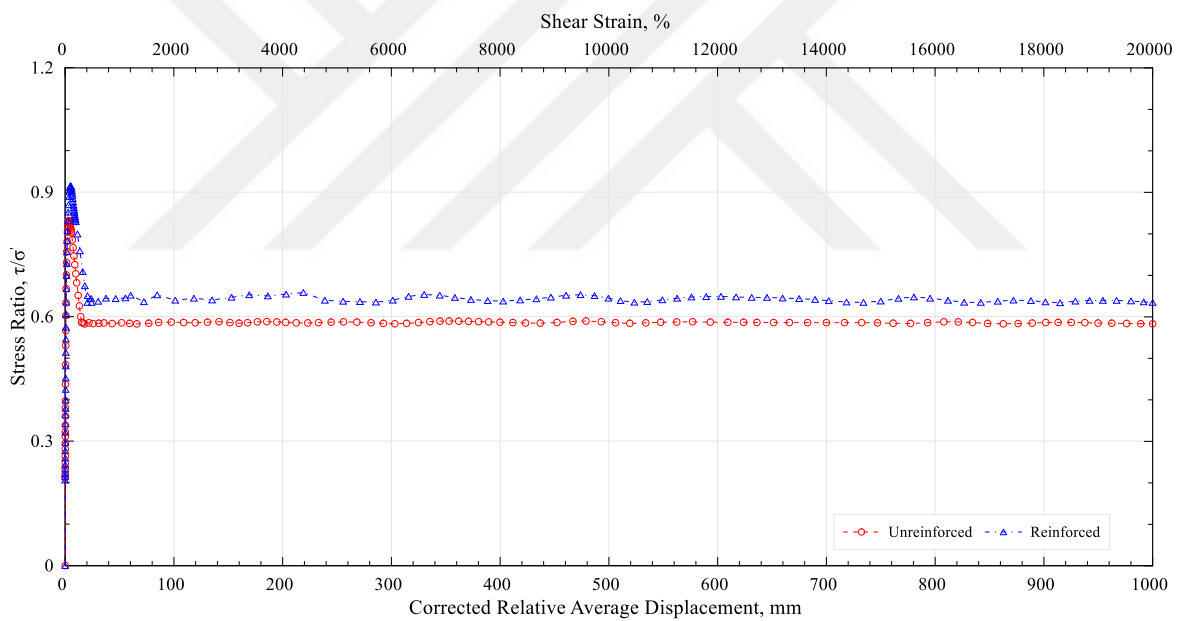
When examining the behavior after peak, the change in the effective stress ratio was seen to be more limited compared to $e_0 = 0.50$ in the increasing void ratio.



(a)



(b)

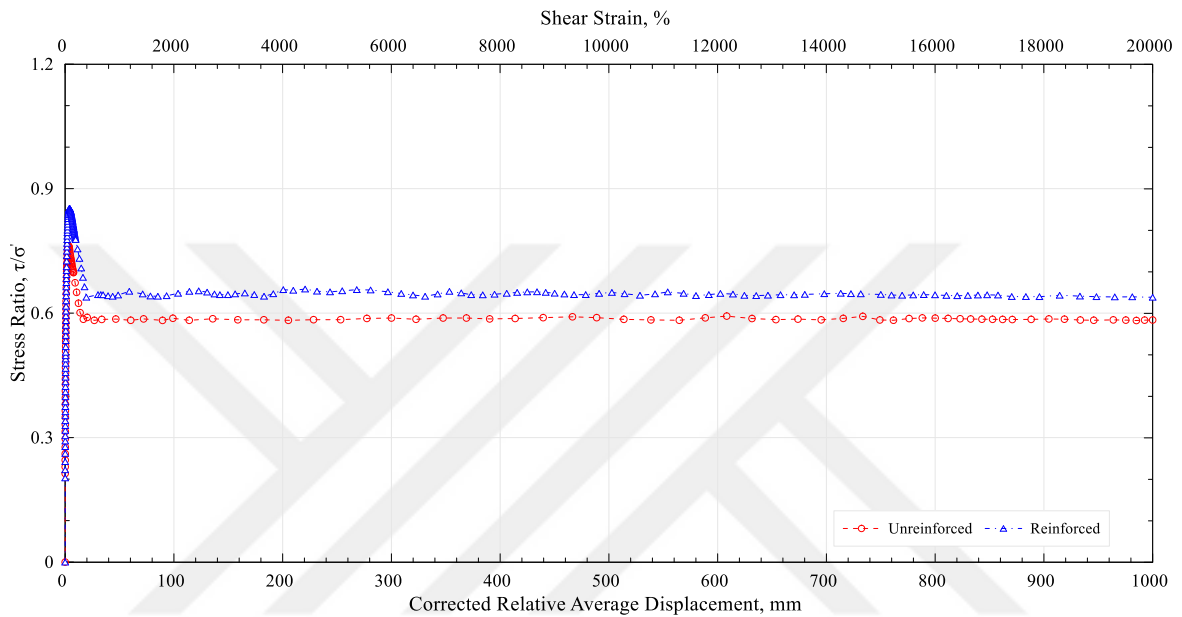


(c)

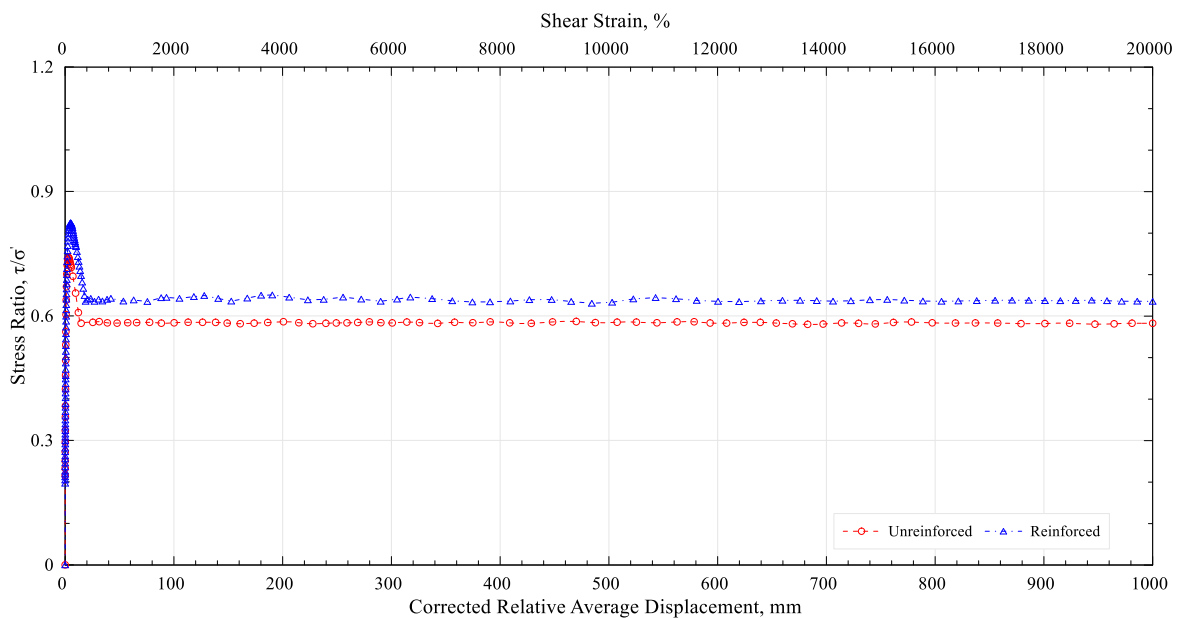
Figure 5.24. The stress ratio - Shear displacement relationship for ring shear ($e_0 = 0.55$):
 (a) 50 kPa, (b) 100 kPa, (c) 200 kPa

Figure 5.25 shows the effective stress ratio-shear displacement/strain curves in loosely packed ($e_0 = 0.60$) unreinforced and reinforced samples. With the effect of increasing the initial void ratio, the contribution of reinforcement to the strength had been more even though lower τ_p/σ'_n and τ_{cs}/σ'_n ratios were obtained for the densely and medium

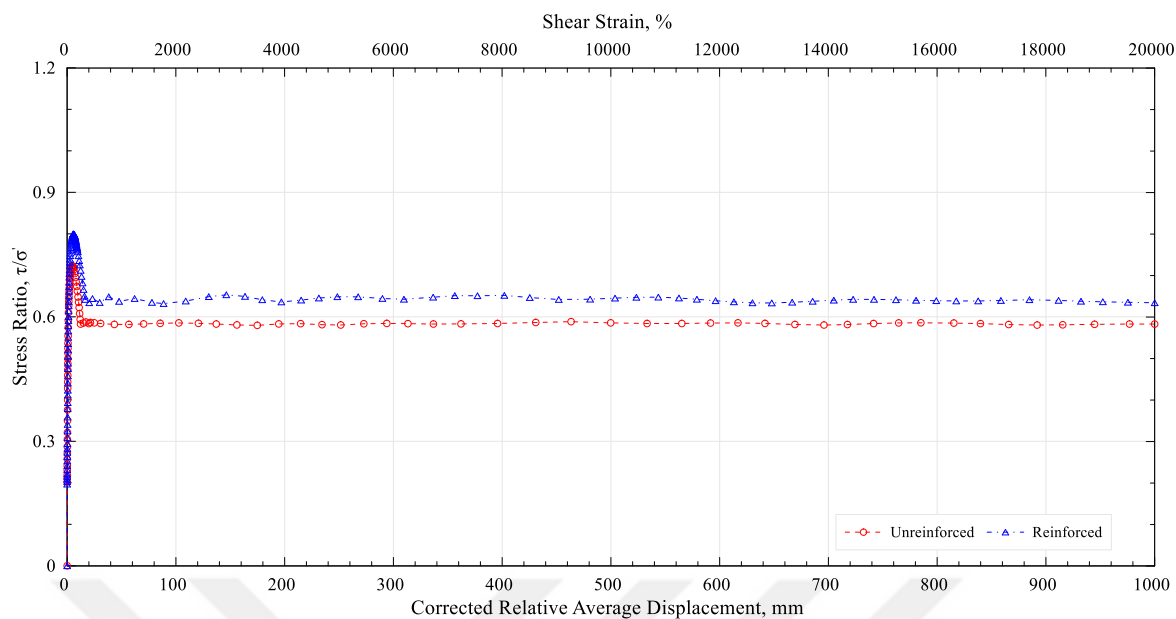
packed samples. The reason for this is that loose samples work better with materials to create this kind of tensile stress for reaching a denser form. Therefore, grains closing each other create a denser structure based on their previous subjects and necessary shear strength for the failure. Undoubtedly, this situation is the desired thing in the improvement of strength properties of the loose sands, especially liquefaction.



(a)



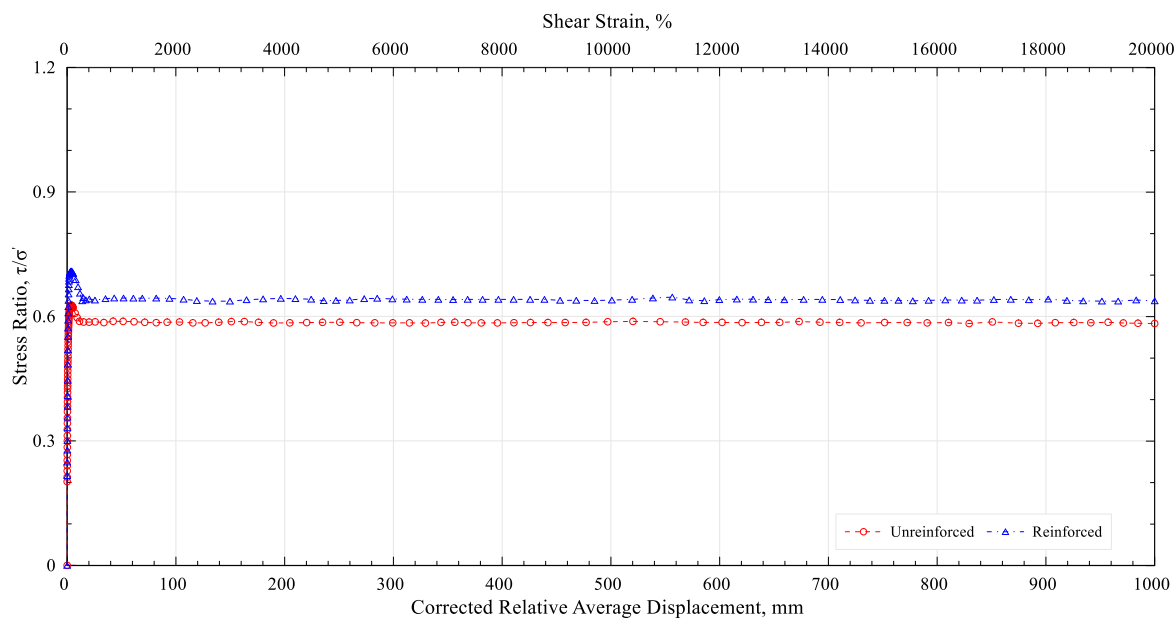
(b)



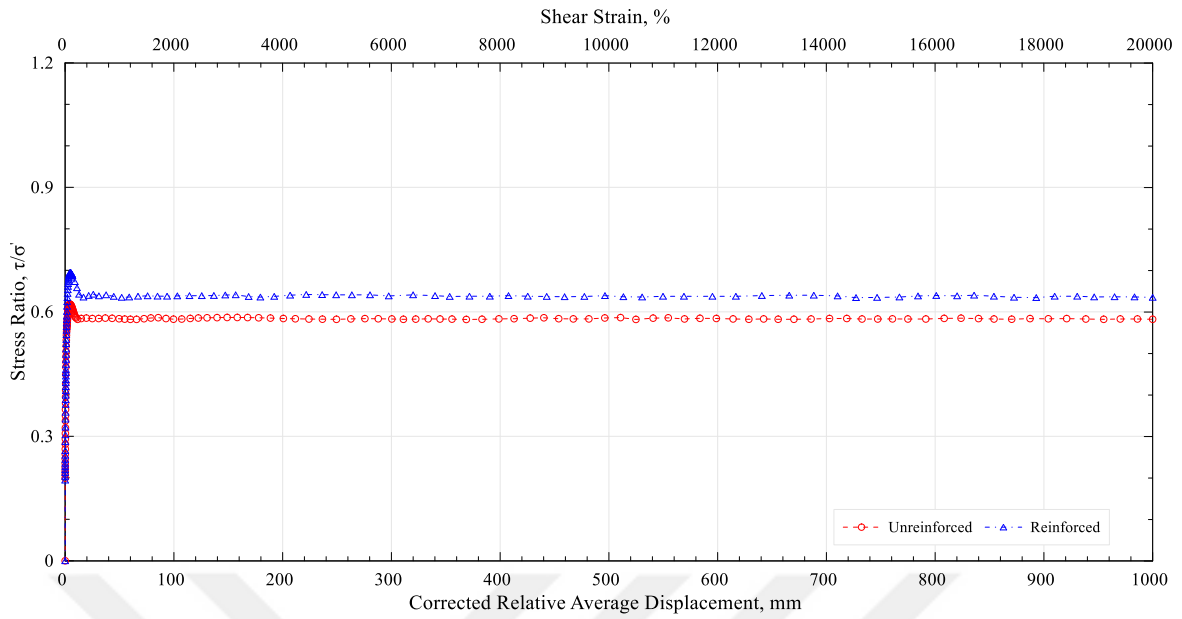
(c)

Figure 5.25. The stress ratio - Shear displacement relationship for ring shear ($e_0 = 0.60$):
 (a) 50 kPa, (b) 100 kPa, (c) 200 kPa

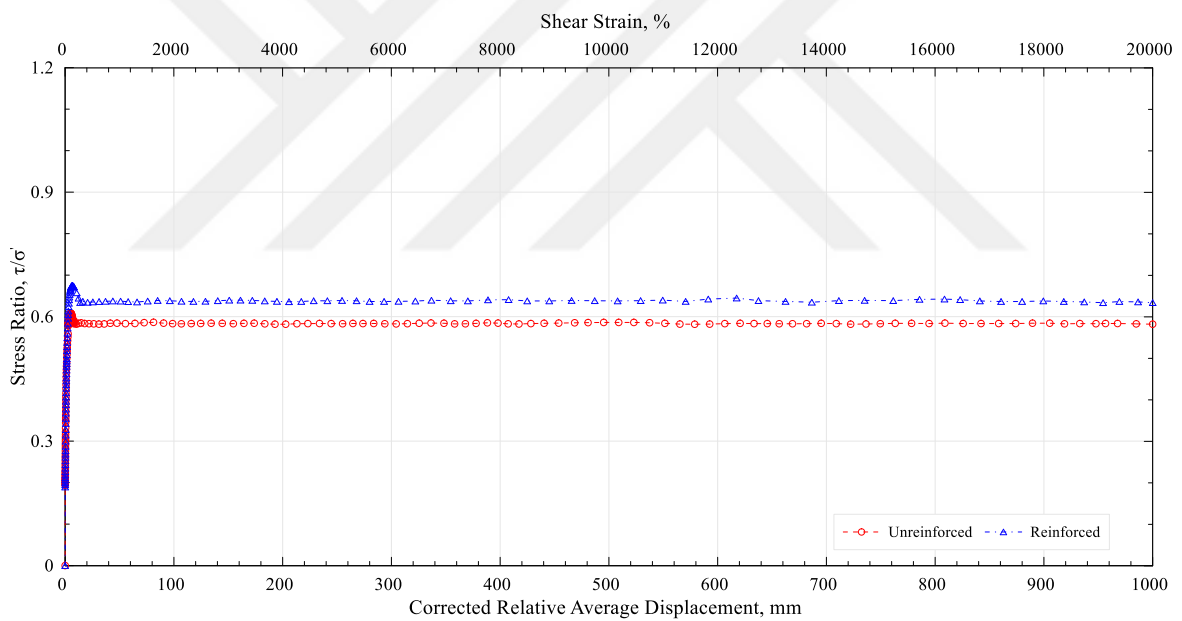
Figure 5.26 shows the effective stress ratio-shear displacement/strain curves obtained under the drained conditions of the very loose samples prepared in the high sample ratio such as $e_0 = 0.65$.



(a)



(b)



(c)

Figure 5.26. The stress ratio - Shear displacement relationship for ring shear ($e_0 = 0.65$):
 (a) 50 kPa, (b) 100 kPa, (c) 200 kPa

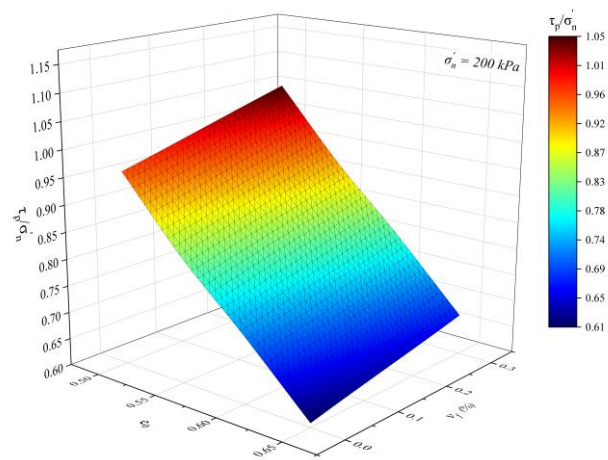
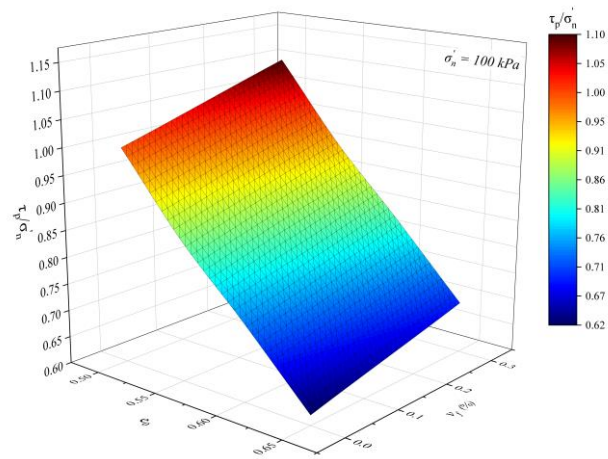
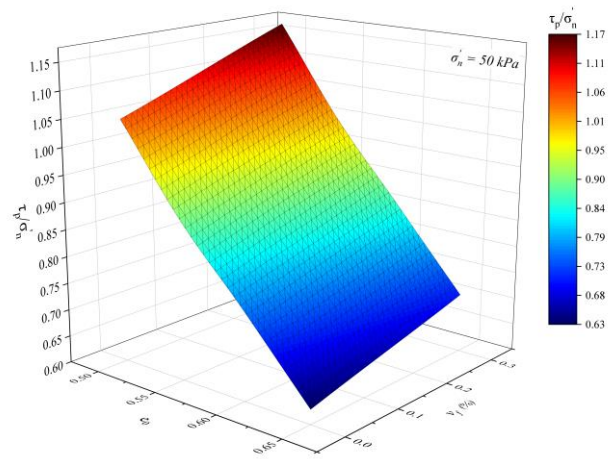
As seen from the figures, strength loss after the peak in very loose samples remained limited compared to the other void ratios. In this relationship in the definitions of the failure, related curves increased to a critical level in a parabolic way. Another critical condition drawing attention is that the change in the stress ratio is limited compared to the samples

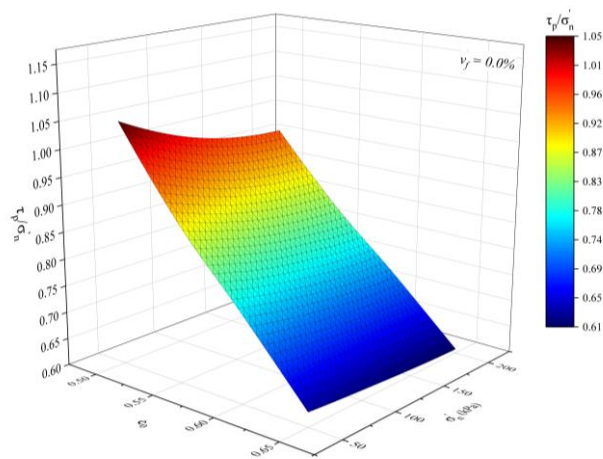
with less voids. Another significant comment to be made is that change in the reinforcement orientations limits the contribution of the reinforcement to the strength. The mechanism of this significant situation will be explained in detail in the next part.

The relationship between the peak (τ_p/σ'_n) and critical state effective stress ratio (τ_{cs}/σ'_n) as a function of effective normal stress (σ'_n), initial void ratio (e_0) and volumetric reinforcement concentration (v_f) are shown in Figure 5.27 and Figure 5.28, respectively. Graphics in Figure 5.27a, 5.27b, and 5.27c are scaled in the same range for the understanding of the effect of σ'_n on τ_p/σ'_n . Accordingly, increase in σ'_n causes to decrease the contribution of τ_p/σ'_n and v_f to the strength, increase in e_0 causes τ_p/σ'_n to decrease, however, the contribution of the v_f to the strength increased (Figure 5.27d, Figure 5.27e, Figure 5.27f). The reason for this is that grains limited in the ring reservoir such as ring shear are about the work they did against the effective normal stress for displacement. The presence of reinforcement increases the loss of energy.

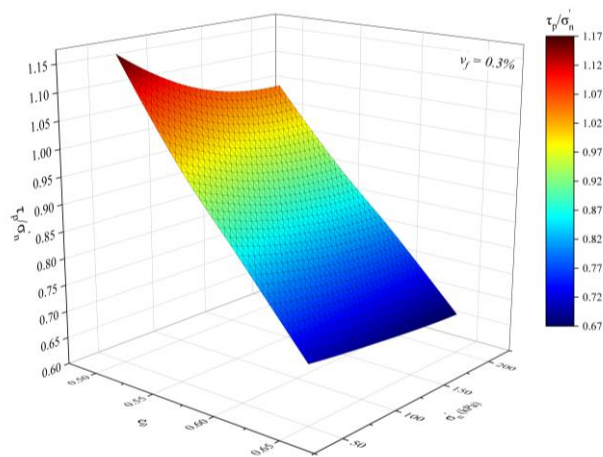
For obtaining the critical state effective stress ratios (τ_{cs}/σ'_n), samples are sheared until the $1m$ shear displacement. Even though these displacement values for the sands are too high, the main aim here is to find out the effect of the reinforcement on the greatest strain levels. As a result of the study, reinforcement orientation is seen in accordance with the cross-sectional area in the very big shear strains. This situation caused the contribution of the reinforcement τ_{cs}/σ'_n to remain at limited levels. Another significant thing is that its effect of σ'_n and e_0 on τ_{cs}/σ'_n and v_{fr} values remain less (Figure 5.28d, Figure 5.28e, Figure 5.28f). This result is due to the fact that grains (plates) such as clays for obtaining the critical stress ratios of the sands do not need vertical-parallel locations.

Ring shear test is a significant shearing test representing many geotechnical practices and having an increasing significance in the laboratories. This thesis study includes empirical comparison; therefore, it will not give any more detailed information about the ring shear test results. Researchers interested in the subject can benefit from Negussey (1989), Consoli, et al., (2005, 2007), Heineck et al., (2005), et al. for further research.

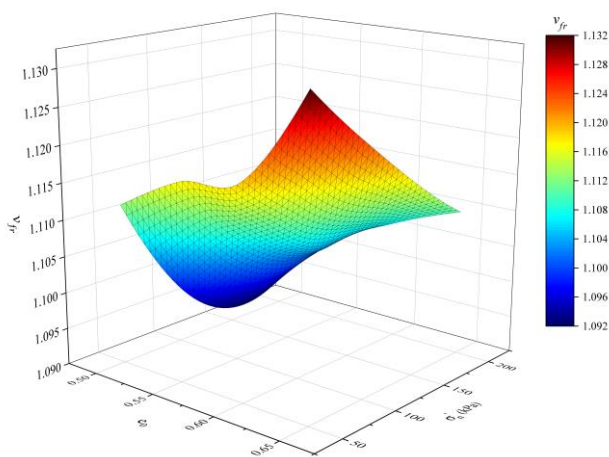




(d)

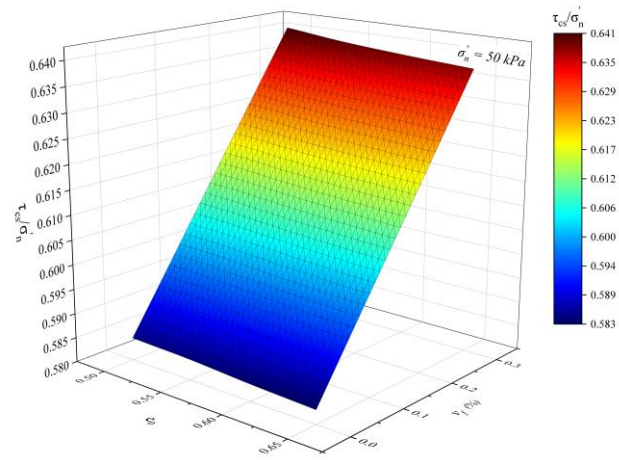


(e)

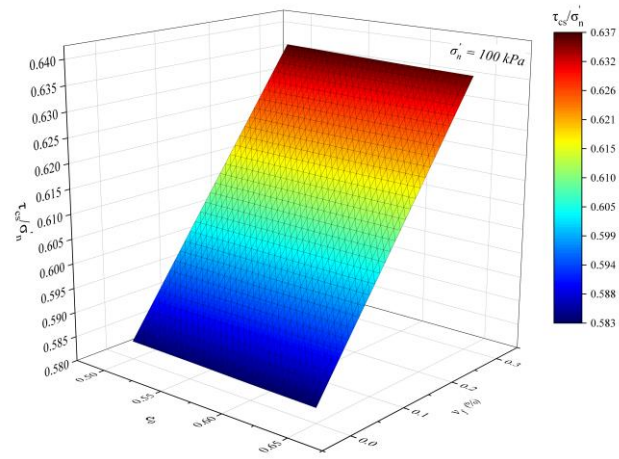


(f)

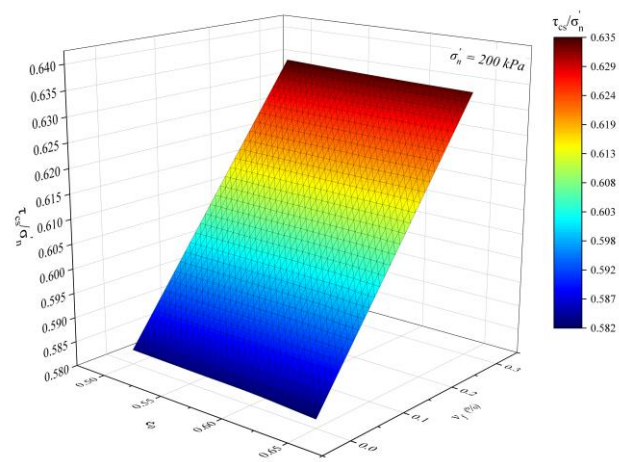
Figure 5.27. Effect of effective normal stress (σ'_n), initial void ratio (e_0) and volumetric reinforcement concentration (v_f) on the peak effective stress ratio for the ring shear tests (τ_p/σ'_n): (a) $\sigma'_n = 50 \text{ kPa}$, v_f - e_0 , (b) $\sigma'_n = 100 \text{ kPa}$, v_f - e_0 , (c) $\sigma'_n = 200 \text{ kPa}$, v_f - e_0 , (d) $v_f = 0.0\%$, σ'_n - e_0 , (e) $v_f = 0.3\%$, σ'_n - e_0 , (f) v_{fr} , σ'_n - e_0



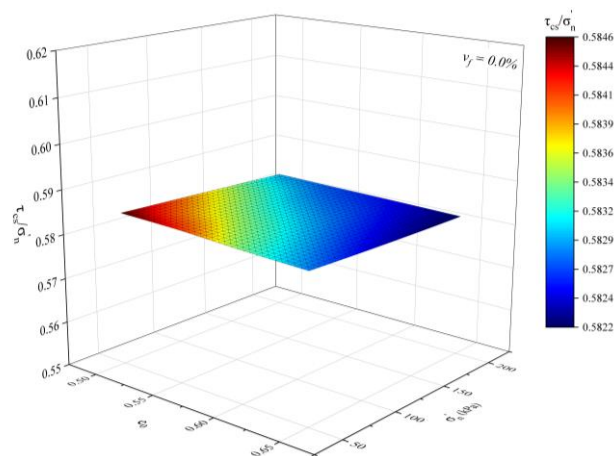
(a)



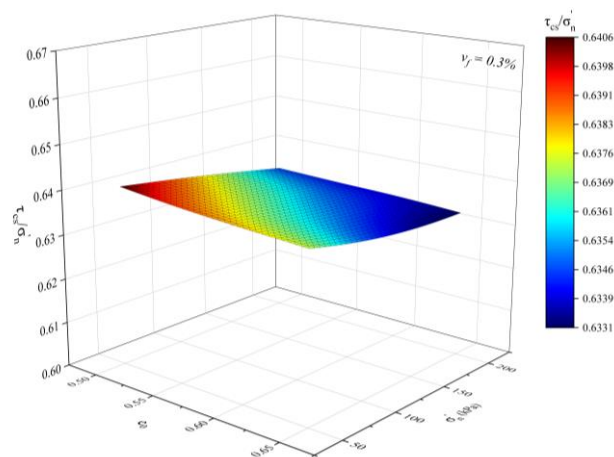
(b)



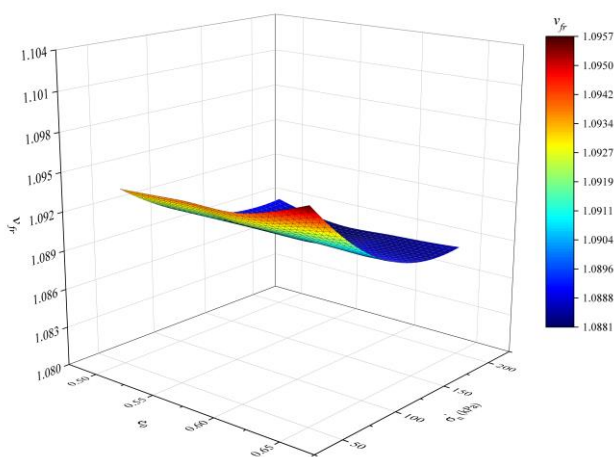
(c)



(d)



(e)



(f)

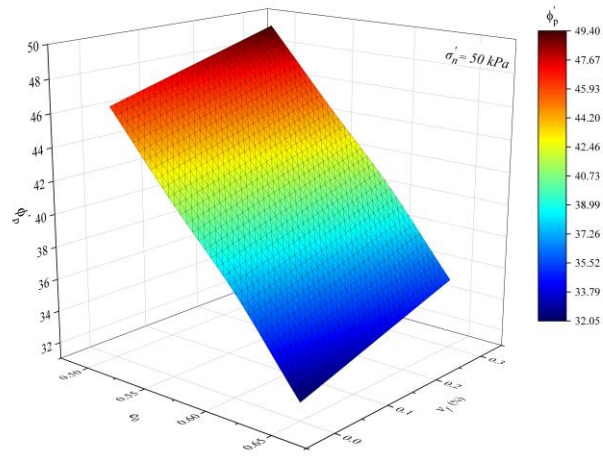
Figure 5.28. Effect of effective normal stress (σ'_n), initial void ratio (e_0) and volumetric reinforcement concentration (v_f) on the critical effective stress ratio for the ring shear tests (τ_{cs}/σ'_n): (a) $\sigma'_n = 50 \text{ kPa}$, v_f - e_0 , (b) $\sigma'_n = 100 \text{ kPa}$, v_f - e_0 , (c) $\sigma'_n = 200 \text{ kPa}$, v_f - e_0 , (d) $v_f = 0.0\%$, σ'_n - e_0 , (e) $v_f = 0.3\%$, σ'_n - e_0 , (f) v_{fr} , σ'_n - e_0

5.4.2. Shear strength parameters

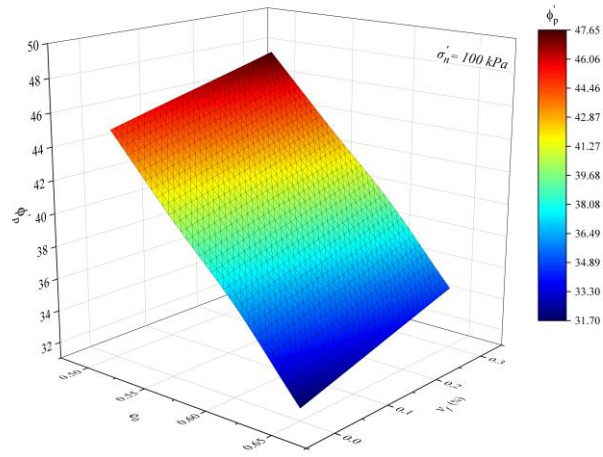
Ring shear test is another significant test used in determining the shear strength properties of soils. The devices used in this test are arranged in different orders depending on the definition of the plane of failure (e.g., Bishop et al., 1971; Bromhead, 1979; Sadrekarimi and Olson, 2009). Significant differences have been observed in the shear strength tests conducted with differently ordered devices on the same surface. Particularly for surfaces cohesionless such as sand which obtains its strength from friction and of which the peak effective friction angle varies widely, the subject becomes more critical.

Figure 5.29 shows the results of the peak effective friction angle (ϕ'_p) for unreinforced and reinforced states. It is seen that (ϕ'_p) is high where the initial void ratio is low, and that it exponentially decreases when the initial void ratio increases. The reason for this is that the ring shear method is extremely sensitive to geometrical interference. When the effect of effective normal stress (σ'_n) to ϕ'_p is examined, around $13^\circ - 14^\circ$ scattering was observed. The magnitude of the scattering may be considered as evidence to the situation explained above. In studies where the presence of reinforcement increases the strength in all values of e_0 , the greatest increase has been observed in the great values of e_0 . Another significant aspect is that the ring shear tests have reached high ϕ'_p values even in low reinforcement concentrations.

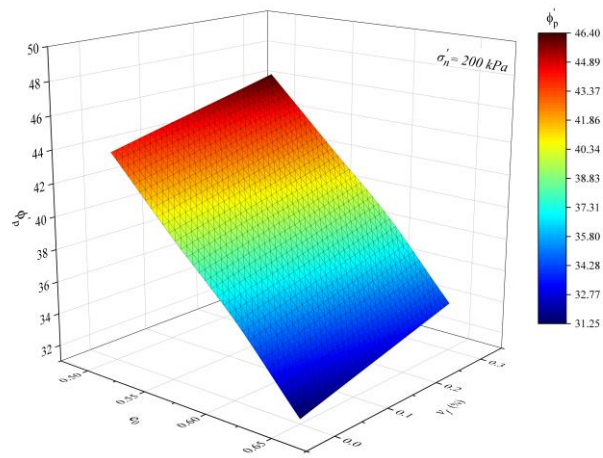
Figure 5.30 shows the friction angle (ϕ'_{CS}) of the effective critical state demonstrated with 3-D surfaces in different spaces and the increase rates of reinforcement to strength (v_{fr}). Due to the high displacement capacity of the ring shear device, it was observed that the effect of void ratio and effective normal stress on ϕ'_{CS} remained very limited. The reason for this is the fact that the particles were able to reach the strain levels they needed to reposition in critical state. When the presence of reinforcement is examined, it was observed that its contribution to strength remained limited (Figure 5.31). The reason for this is that particle-particle studies remain at low levels in large strains and that the reinforcement reaches undesired orientation positions.



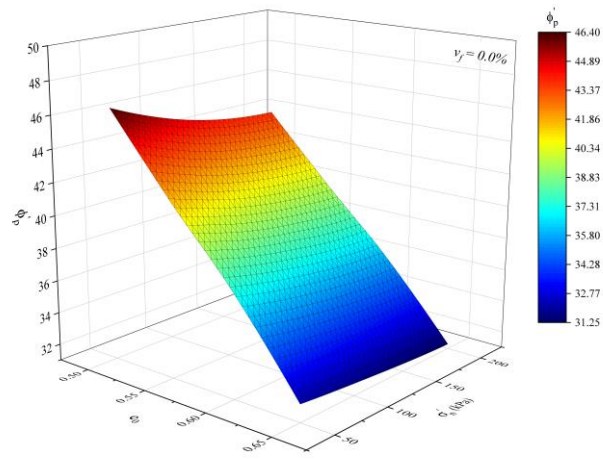
(a)



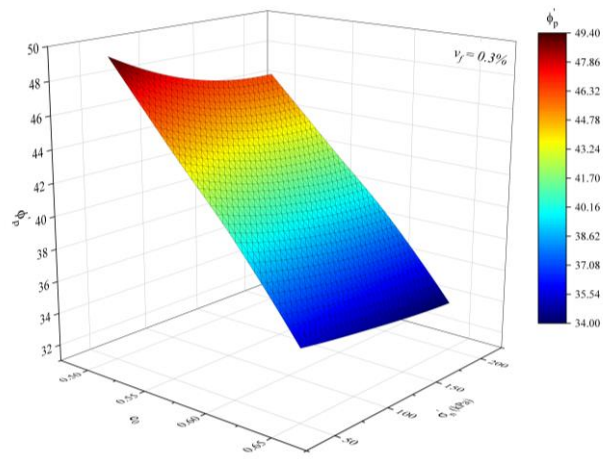
(b)



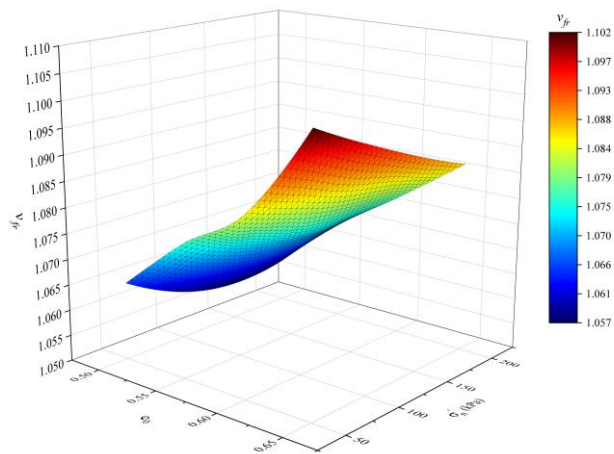
(c)



(d)

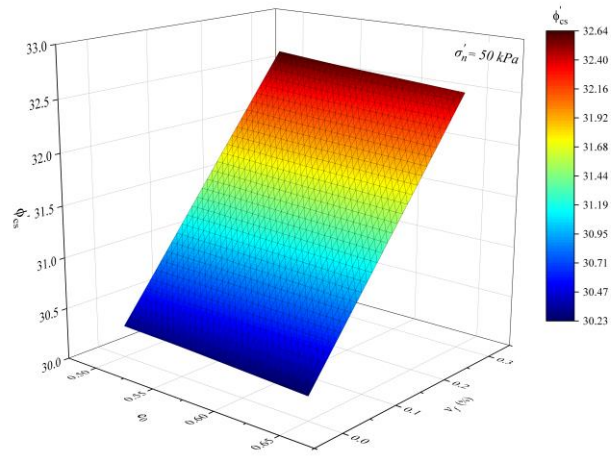


(e)

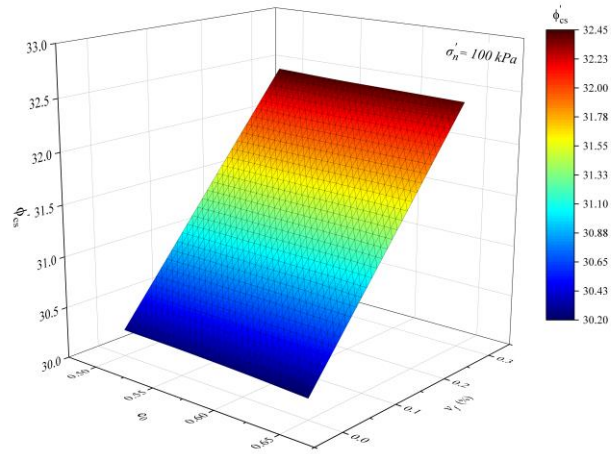


(f)

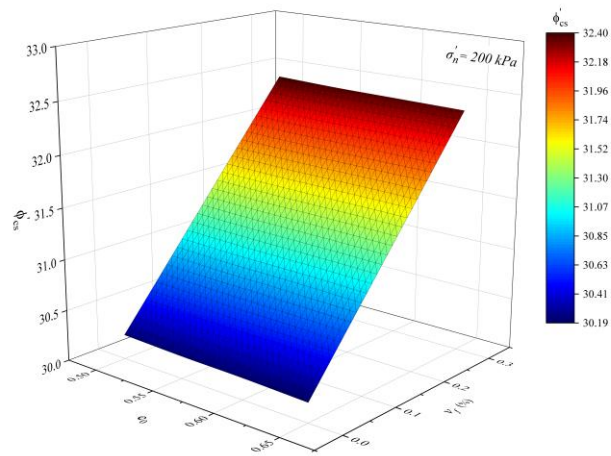
Figure 5.29. Effect of effective normal stress (σ'_n), initial void ratio (e_0) and volumetric reinforcement concentration (v_f) on the peak effective friction angle (ϕ'_p) for ring shear tests: (a) $\sigma'_n = 50 \text{ kPa}$, v_f - e_0 , (b) $\sigma'_n = 100 \text{ kPa}$, v_f - e_0 , (c) $\sigma'_n = 200 \text{ kPa}$, v_f - e_0 , (d) $v_f = 0.0\%$, σ'_n - e_0 , (e) $v_f = 0.3\%$, σ'_n - e_0 , (f) v_{fr} , σ'_n - e_0



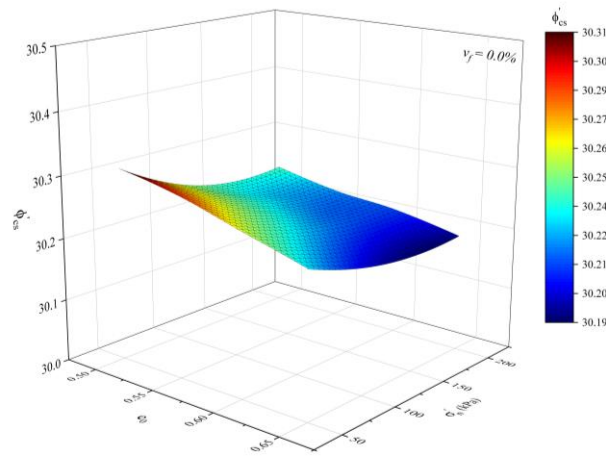
(a)



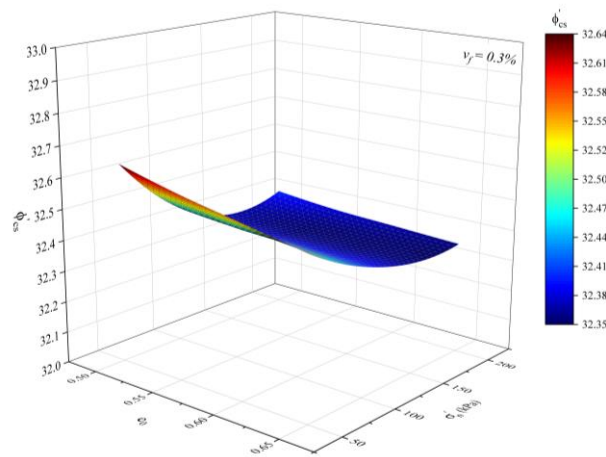
(b)



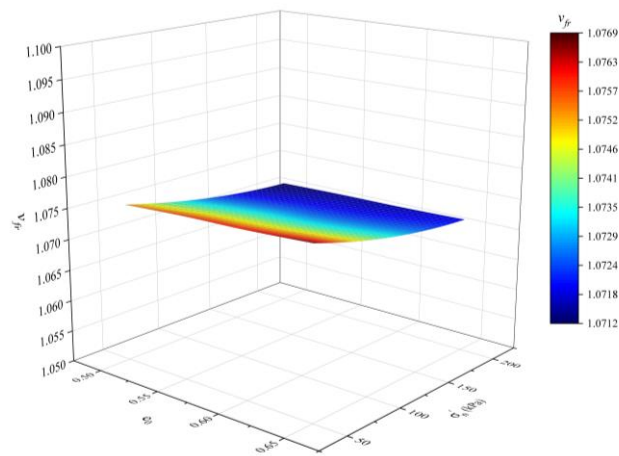
(c)



(d)



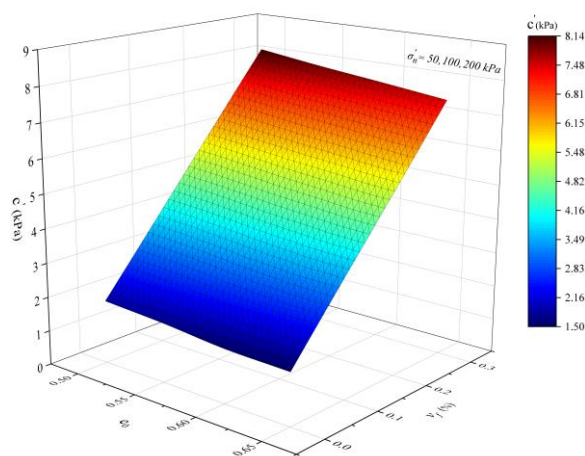
(e)



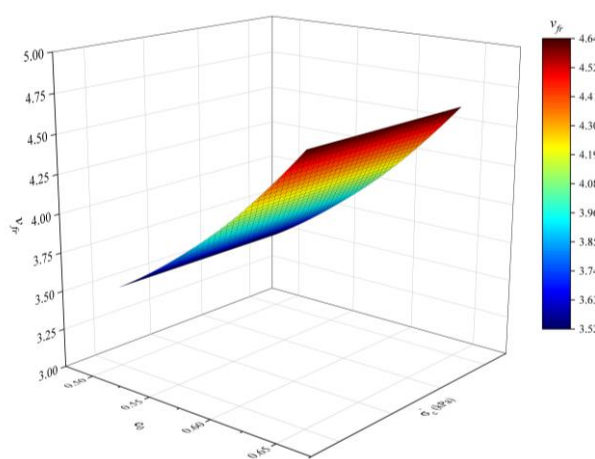
(f)

Figure 5.30. Effect of effective normal stress (σ'_n), initial void ratio (e_0) and volumetric reinforcement concentration (v_f) on the critical effective stress ratio (τ_{cs}/σ'_n) for ring shear tests: (a) $\sigma'_n = 50 \text{ kPa}$, v_f - e_0 , (b) $\sigma'_n = 100 \text{ kPa}$, v_f - e_0 , (c) $\sigma'_n = 200 \text{ kPa}$, v_f - e_0 , (d) $v_f = 0.0\%$, σ'_n - e_0 , (e) $v_f = 0.3\%$, σ'_n - e_0 , (f) v_{fr} , σ'_n - e_0

Figure 5.31 shows the ring shear test results for the effective cohesion term which is another shear strength parameter of soils. As so in the direct shear and triaxial tests, the effective cohesion strength which remained at low levels in unreinforced states showed a slight increase in the presence of reinforcement. The reason why the increase rate remains moderate is the limited occurrence of surface tension forces in dry and saturated samples. The main topic of discussion here is the unclarity whether the effect of the fiber reinforcement on the shear strength should be measured by cohesion or the friction angle. Discussions regarding the use of apparent cohesion in cohesionless soils for design purposes are presented in the next chapter.



(a)



(b)

Figure 5.31. Effect of initial void ratio (e_0) and volumetric reinforcement concentration (v_f), on cohesion parameter (c') in ring shear tests: (a) v_f - e_0 , (b) v_f - r

5.4.3. Volumetric strains

Volumetric strains of the soils are managed by a complex mechanism involving random displacements of the grains on the shear band. This mechanism is directly related to the physical and mechanical properties of the soil as well as the environmental factors to which it is exposed. For this reason, volumetric change curves should be considered as an analogy of stress-strain curves.

Volumetric changes can be achieved for any desired strain level with ring shear tests with large shear displacement capacities. It is important to take into account some of the limiting features of ring shear tests (e.g., soil extrusion) in order to accurately monitor these changes. Volumetric strain curves obtained from ring shear tests are shown in Figure 5.32. From the curves, the void ratio and normal stress have a significant effect on volumetric strain. On the other hand, it is seen that the presence of reinforcement reduces contraction and increases dilation. Finally, the important issue that attracts attention is the effect of the strain rate, which is increased a hundred times in ring shear tests after the peak, on the dilation.

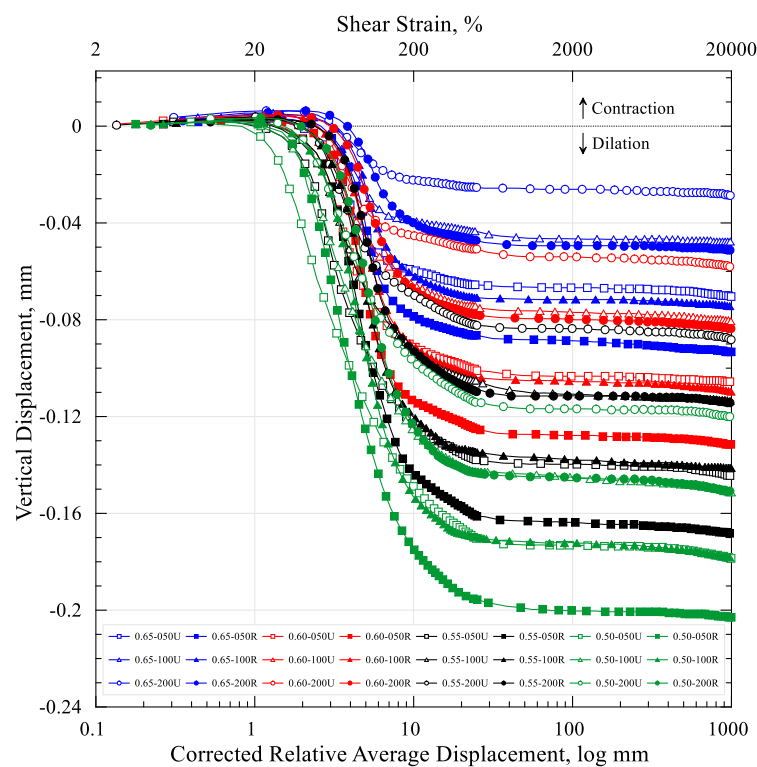


Figure 5.32. Volumetric strain curves obtained from ring shear tests

5.5. Comparative Analysis of Direct Shear, Triaxial and Ring Shear Test Methods

A soil must maintain the stability and deformation conditions under the effect of the loads it is subject to. Stability condition is related to the preservation of its stability as the result of load, and deformation condition is related to the pre failure condition of the soil and deformation not exceeding certain limits. For the examination of both situations, it is essential that the shear strength parameters of the related soil are very well known.

Analyzing the problems faced with regard to soil mechanics by only one experiment method is not possible. The main reason is the unique structure of the soil which is composed of different fractions, its relation with water, loading and deformation conditions it is subject to and the difference of the failure mechanism. Shear strength parameters of soils are measured by various methods working with different principles. Selection of the accurate deformation mode is possible by the true representation of the possible failure mechanism in the lab. In this study, methods of direct shear, triaxial and ring shear which are commonly applied in the measurement of engineering properties of the soils were used. In the chapter, comparative analysis results of the shear strength parameters of the soils, volumetric deformation parameters, and other issues were presented, respectively.

5.5.1. Shear strength parameters

In cohesionless soils, the shear strength is controlled by the friction that arise between the particles. The term friction defined has been explained on a macro level until this chapter. However, a micro level examination is also required in order to understand the frictional behavior of particles.

Hertz (1881) explained the surface potential occurred in the contact areas of deformable solids by examining the subject at micro level, hence he has been the pioneer of contact mechanics. Hertz suggested that the true contact areas of solids did not increase in a linear proportion with the increase in the load applied (N) and stated that the increase in the contact areas was a force function $(f^N)^{2/3}$ of the load. Thus, it was concluded that the friction coefficient partially decreased with the increase in the normal stress. The theory was developed for the definition of contract surfaces in different orders, the concept of adhesion

etc., for plastic (Bowden and Tabor, 1950, 1964) and elastic deformation states (Archard, 1953, 1957; Lodge and Howell, 1954) in order to make friction mechanism more understandable. Wider information related to the subject may be reached from sources related to tribology.

In his phenomenological criteria, Coulomb (1776) made an analogic assumption between the shear friction of solids and the internal friction of soils. This analogy, as explained in Chapter 3, is also valid for the term cohesion. In the first part of the chapter, experiment results regarding the internal friction angle tested for different deformation modes were provided, and following the chapter, experiment results related to cohesion term were given and a comparative analysis of these results was made.

Shear strength of a soil for a normal stress is represented with an envelope. This envelope of which the details have been mentioned in chapter 3 represents the functional relation between the shear stress and normal stress during failure. Although many hypotheses considering the common effect of this function were developed, Mohr-Coulomb failure theory is commonly used in many geotechnical applications due to its benefits. Cernica (1995) suggested that the failure on particularly cohesionless soils would be best explained by Mohr failure theory. Mohr-Coulomb equation is the idealized linear function of the curved Mohr failure envelope for a specific stress range encountered on the field. This idealized representation is very useful for the simplification of the analysis with the first-degree functions instead of high degree curves and obtaining accurate results in many geotechnical problems. In Mohr-Coulomb theory, neglect of intermediate principal stress ($\sigma_2 = 0$) has a role in the linear idealization of failure envelope. The assumption that the intermediate principal stress not having an effect on the failure of the soil is one of the reasons why the theory is widely accepted. For cohesionless soils, the curvature of the failure envelope is due to the repositioning of the particles during the deformation and the particle deformation that occurs under the effect of the normal stress forces. Since the shear strength angle (ϕ') decreases with normal stress, it is not constant. Therefore, taking the curvilinear envelope as an approximate straight line would lead to a (ϕ') value above the predicted safe stress interval. Another important example explaining the situation is the decrease in (ϕ') value with the increase in the depth of soil layer and confining pressure, hence the occurrence of deep failure surfaces which is more critical for geotechnical applications (e.g., deep

foundations, embankment dams). Stress values of pile tips and dam foundations reaching of 7 MPa is another evidence that shows the importance of the accurate definition of failure envelope.

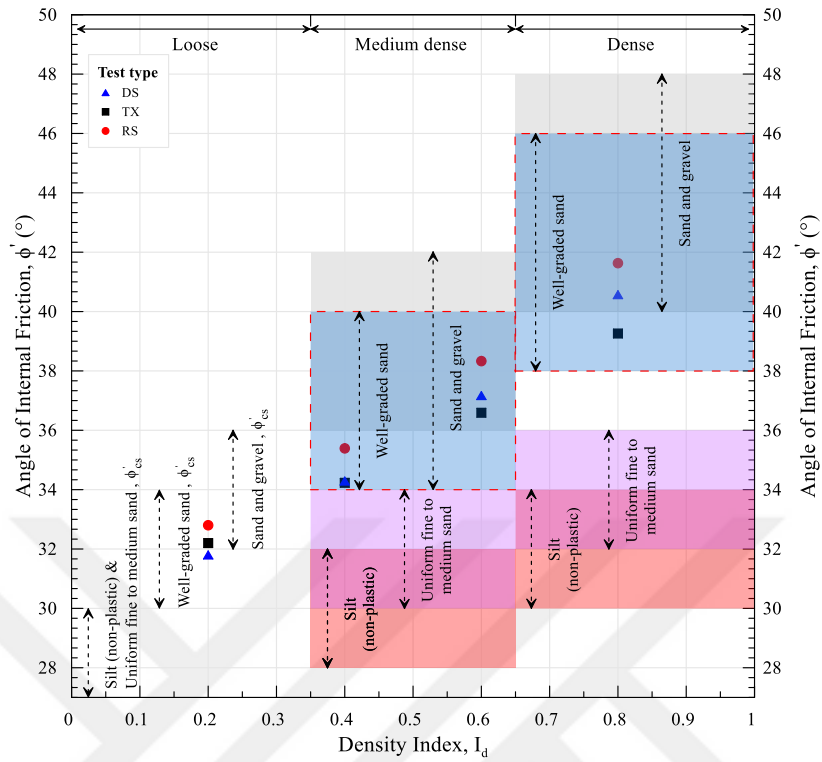
Although Bolton (1986) and Terzaghi et al. (1996) suggested that it would be appropriate to use the secant friction angle (ϕ'_s) for the idealized curved failure envelope in cohesionless soils ($c' = 0$), certain researchers (Berezantsev and Kovalov, 1968; Baligh, 1976; Duncan et al., 1980; Maksimović, 1989; Ueno, 2001; Baker, 2004) suggested that this approach would lead to over predictions and that using different parameters to define this expression would lead to more consistent results. In this study, secant and tangent friction angles were used as friction terms for both the peak and the critical state (due to being consistent with the selected surface type and stress range).

It is accepted that the curve of the failure envelope represents the effective friction angle (ϕ'), and τ axis represents the effective cohesion (c'). ϕ' is the angle between the failure envelope and the horizontal line. In geotechnical applications, this parameter is defined separately for peak and critical state depending on the soil strain. ϕ' , which is defined as the arctangent of the friction coefficient between the particles is controlled with shear strength on cohesionless soils. In these types of soils; shear strength is defined with the total strength including the strength deriving from the friction between the particle surfaces and the effect of geometrical interference preventing the relative movement of the particles. Accordingly, effective peak friction angle (ϕ'_p) was defined in Equation 5.1, and effective critical state friction angle (ϕ'_{cs}) was defined in Equation 5.2, as follows:

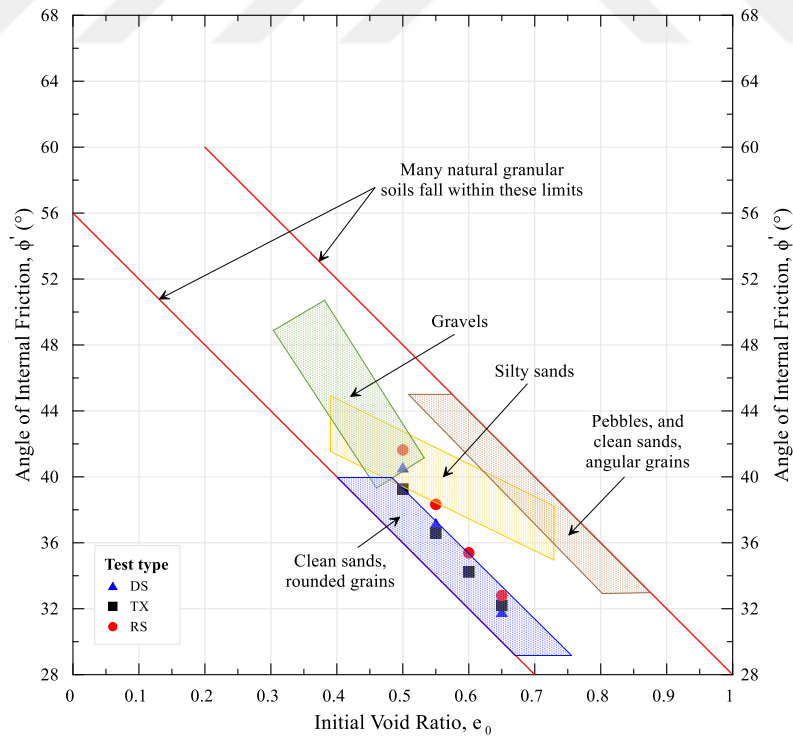
$$\phi'_p = \phi'_\mu + \phi'_d + \phi'_{cr} \quad (5.1)$$

$$\phi'_{cs} = \phi'_\mu + \phi'_{cr} \quad (5.2)$$

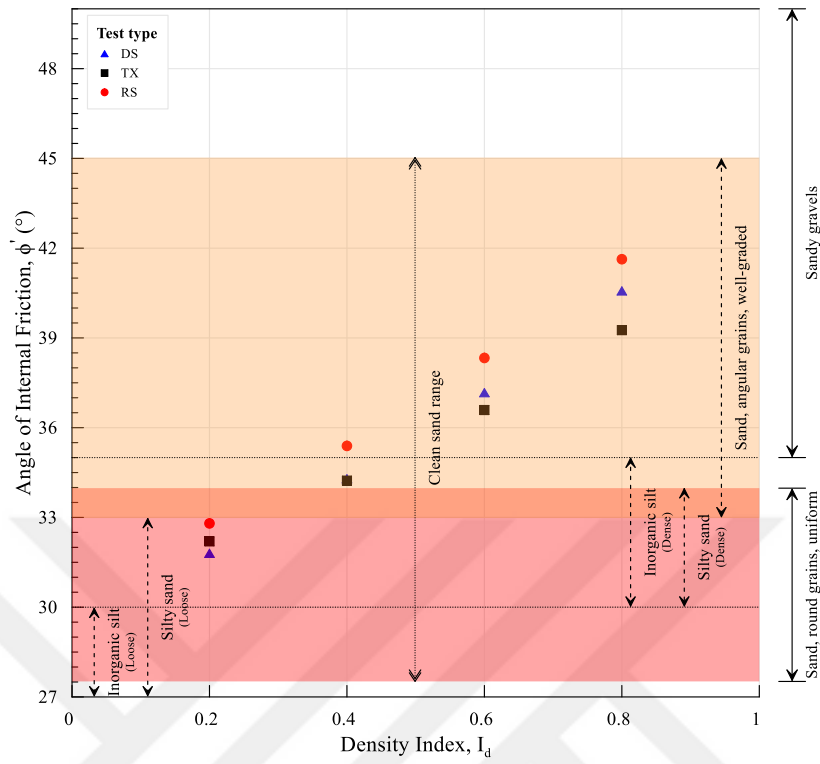
Here; interparticle sliding friction: ϕ'_μ , dilation or particle climbing: ϕ'_d , particle pushing and rearrangement: ϕ'_{cr} . The peak tangent obtained from each experiment method was compared with the typical effective peak friction angle ranges reproduced for granular materials (Figure 5.33).



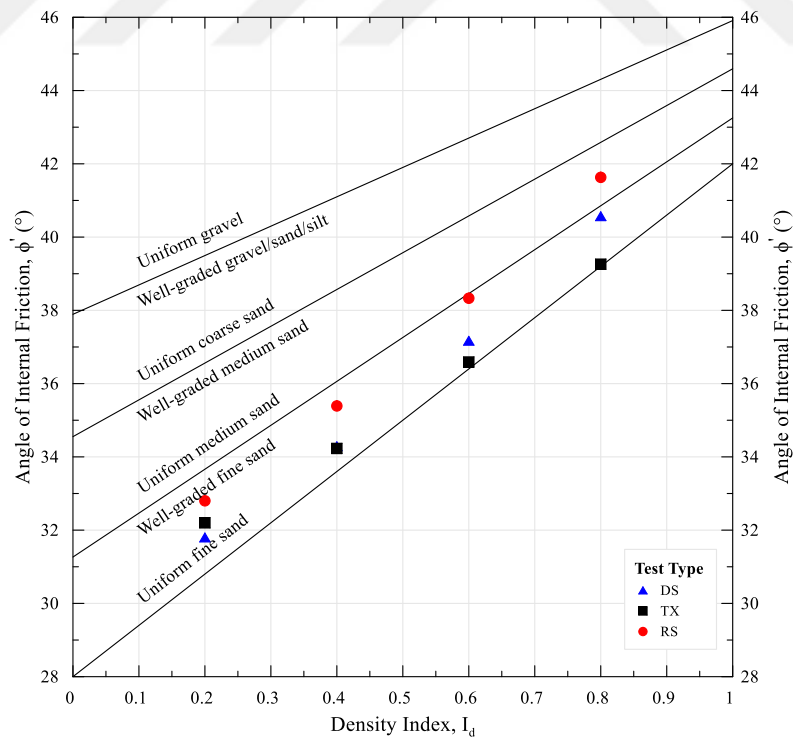
(a)



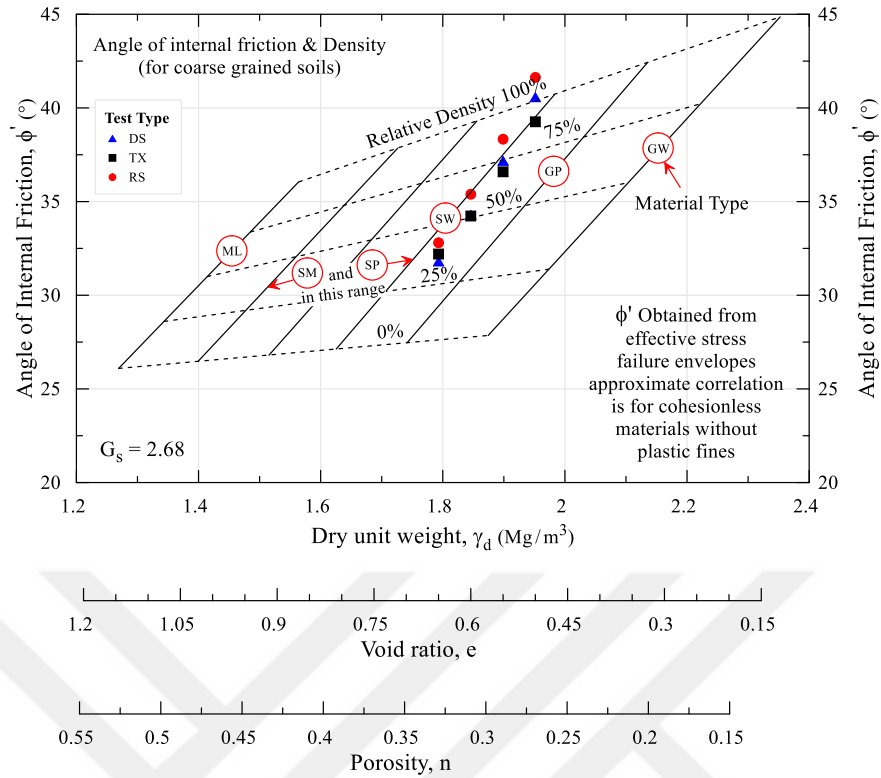
(b)



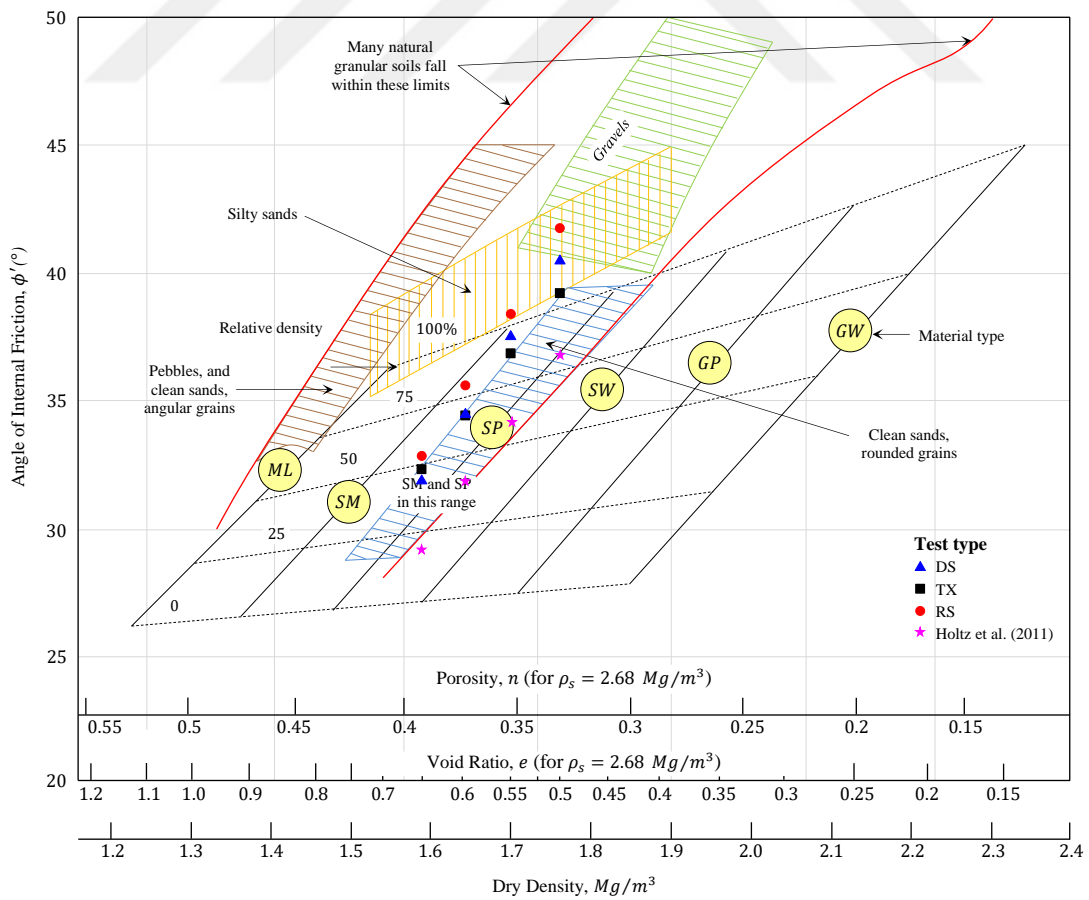
(c)



(d)



(e)

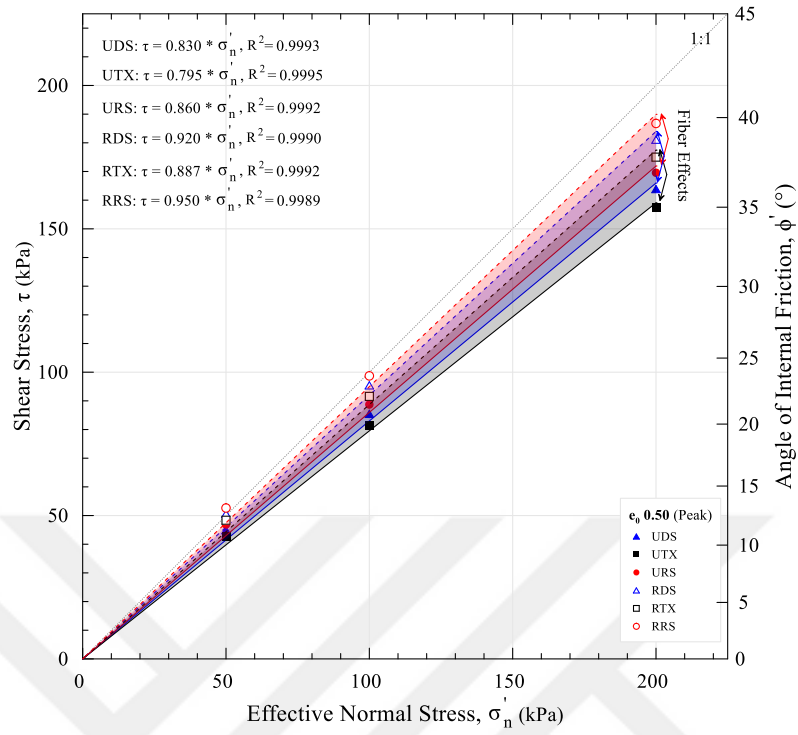


(f)

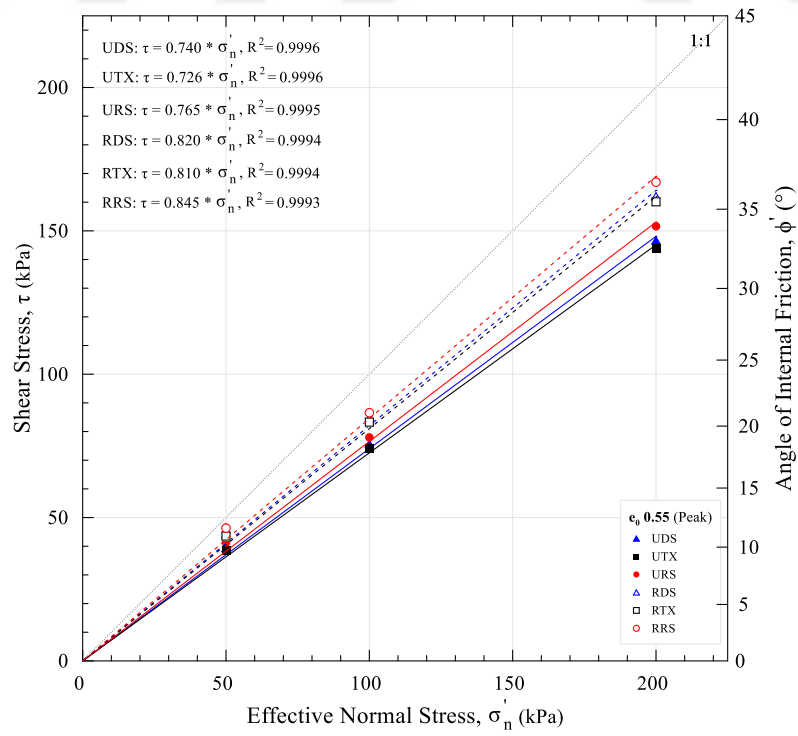
Figure 5.33. Comparison of effective friction angles with the general diagrams reproduced by triaxial method for typical intervals: (a) Hough (1957), (b) Means and Parcher (1963), (c) Terzaghi and Peck (1967), (d) Schmertmann (1978), (e) NAVFAC (1982), (f) Holtz et al., (2011)

When diagrams in Figure 5.33 are examined, it is seen that the peak effective friction angles obtained for direct shear, triaxial and ring shear tests are positioned within the related intervals. This result shows that the general ranges defined in literature are valid to a certain approach and is significant in terms of proving the consistency of the experiment results obtained. For each of the three methods, it was observed that the friction angles were close to each other in samples that were loosely packed and were positioned within the ranges defined for clean sand in the related diagrams. The geometrical interference contribution which increases with the decrease in the void ratio led to scatters in the friction angles obtained for direct shear, triaxial and ring shear tests. In these diagrams that were formed with the data of triaxial method, scatters of different methods are normal. Furthermore, when these diagrams are used for different experiment methods, clean sand material can occasionally be included in the pebble stone group. Therefore, these kinds of diagrams must only be used for appropriate experiment method, experiment condition (drainage, stress, etc.) and material properties and for control purposes. Another important point to mention is that, during the formation of these diagrams, the material factor (mechanical, index, etc.), definition of friction angles (secant or tangent) and the stress ranges have several uncertainties.

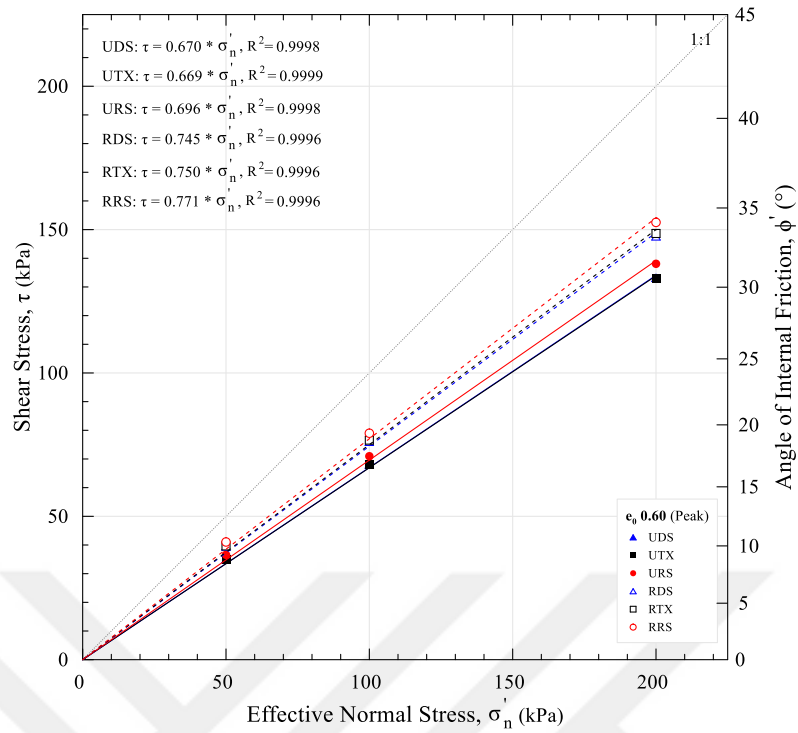
Shear strength parameters were examined separately for each test method in the previous section. Comparative analyses of the parameters of these analyses are performed in this section. Figure 5.34 shows the peak shear strength envelopes of reinforced and unreinforced samples for various test methods and void ratios. When the figures are analyzed, it is clear that the ring shear test produces greater effective shear strength angles for all void ratios. The difference between the test methods became more apparent as volumetric strain capacity increased with decreasing void ratio. Due to the limited deformation capabilities of the samples, the shear strength angles were relatively close to each other as the void ratio increased. However, composite samples must be evaluated on a separate basis.



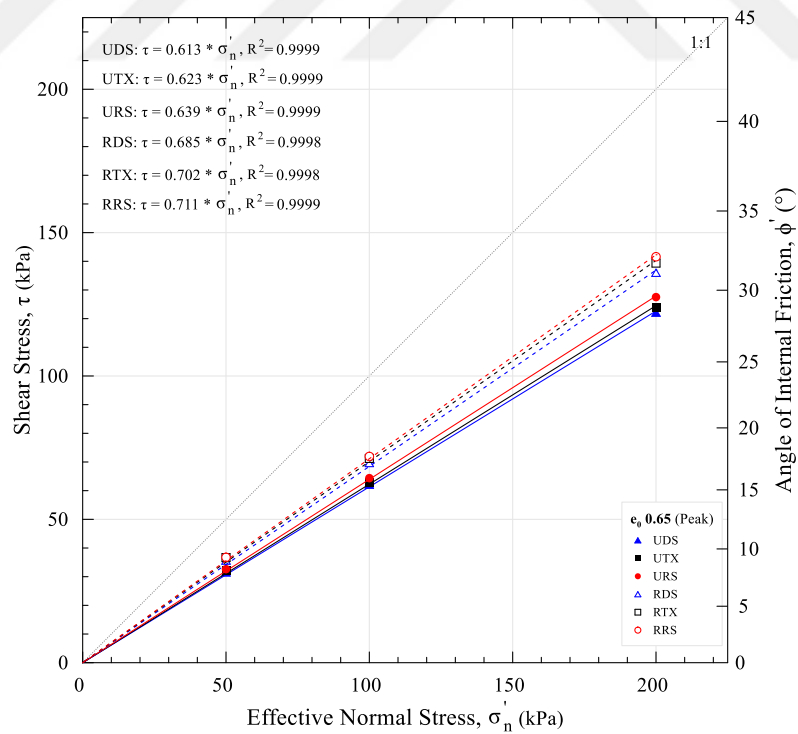
(a)



(b)



(c)



(d)

Figure 5.34. Peak shear strength failure envelopes for various initial void ratios: (a) $e_0 = 0.50$, (b) $e_0 = 0.55$, (c) $e_0 = 0.60$, and (d) $e_0 = 0.65$

The failure envelopes of the densely packed ($e_0 = 0.50$) samples are shown in Figure 5.34a. As can be observed, the ring shear test has the greatest effective friction angle and the least in the triaxial test ($\phi'_{rs} > \phi'_{ds} > \phi'_{tx}$). This correlation is valid in reinforced states. At this void ratio, where the grains are practically entirely interlocked at the start, the samples reach their peak under very minor strain. As a result, at this limited strain level, the energy spent on soil mass failure and the volumetric reaction of the soil mass to failure are the primary determinants of the effective friction angle. Within these principles, the effective peak friction angles of the direct shear and triaxial tests are found to be $\phi'_{ds} - \phi'_{tx} > 1.3^\circ$. Given the volumetric strain capacities of direct shear and triaxial testing, this difference is estimated to be greater than 2° in the densest order. The reason for this is that the triaxial method has poorer resistance to volumetric strains than other test methods. This result is consistent with the findings of Taylor (1939), Bishop (1954), and Rowe (1969), the primary studies on the subject. When the correlation between the direct shear test and the ring shear test is examined, it is found to be $\phi'_{rs} - \phi'_{ds} > 1^\circ$. Because both experiments are a form of plane strain test, this result is expected. Although the grains have considerable mobility in the shear band in the direct shear method, the fact that only two-dimensional motion is forced in the ring shear test is usually the cause of this outcome. When the results of ring shear and the triaxial tests are compared, the difference is greater than $\phi'_{rs} - \phi'_{tx} > 2.3^\circ$. This outcome is the result of the boundary conditions linked with the grains' ability to move against deformation.

When the effect of the presence of reinforcement on the results of the experimental methods was investigated, interesting results were achieved. Accordingly, it has been found that sand and fiber function more successfully in triaxial tests and contribute more to strength than other methods. As a result, the effective peak friction angle differences reported for the unreinforced condition have decreased. This is because the fiber orientation is better in the triaxial test, and the sand matrix and fiber reinforcement produce a more compact structure as a result of the experiment's structure. The effect of reinforcement on strength remained constant in direct shear and ring shear tests, both of which are types of plane strain tests.

The failure envelopes of the medium-densely packed ($e_0 = 0.55$) samples are shown in Figure 5.34b. While the inclinations of the envelopes belonging to the triaxial and direct shear methods are near to each other in the figure, the inclination is slightly larger in ring shear. The close proximity of the slopes compared to the denser position is due to the low level of dilation effect at this level. Accordingly, the tangent friction angles of the ring shear and the triaxial method stayed at the $\phi'_{rs} - \phi'_{tx} > 1.7^\circ$ level. This difference is greater than 2° under low stresses. This will be discussed in more detail in the following sections.

When the presence of reinforcement is investigated, it is observed that its contribution to the triaxial method is greater. As a result, a significant result was attained, as the difference between the triaxial and other shear tests in the unreinforced condition decreased by an average of 1.20 in the reinforced state. When the effect of the presence of reinforcement is compared, it is shown that the difference between direct shear and ring shear tests decreased by 1.06 in favor of direct shear. Another significant conclusion is that the role of reinforcement to strength is greater in comparison to $e_0 = 0.50$.

The failure envelopes of the loosely packed ($e_0 = 0.60$) samples are shown in Figure 5.34c. The effective friction angles obtained from direct shear and triaxial tests were found to be relatively similar to each other, in contrast to the earlier more densely packed void ratios. These two tests yielded about 1.10° higher effective friction angle results in the ring shear test ($\phi'_{rs} > \phi'_{ds} \approx \phi'_{tx}$). The reason for having nearly the same effective friction angle as the triaxial method for loosely packed sands in direct shear, a type of plane strain test, is due to the initial strain conditions.

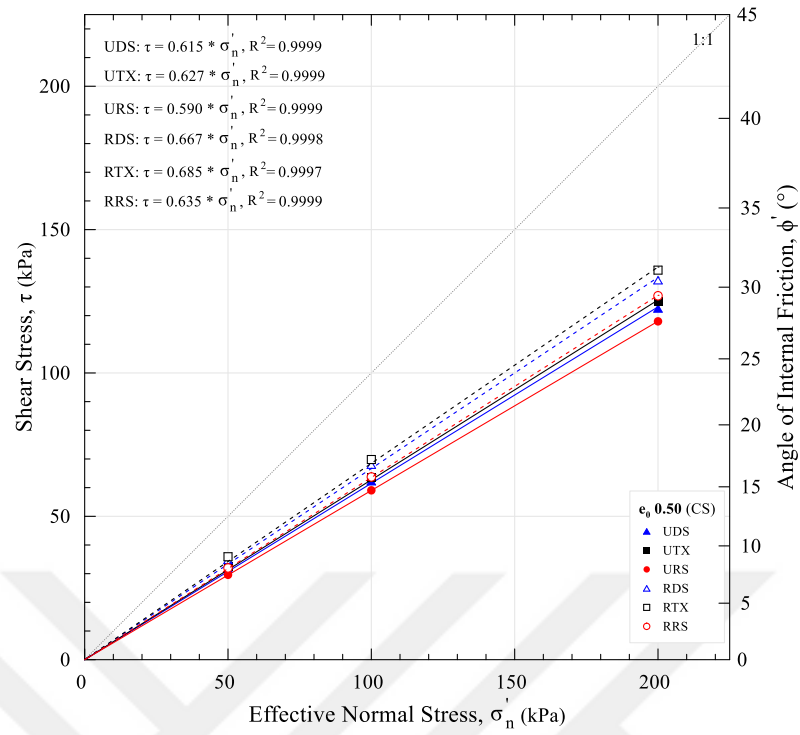
In the reinforced samples, on the other hand, a greater friction angle was obtained in the triaxial method than direct shear. When the triaxial test compared with the ring shear method, although it has a less effective friction angle, it has been observed that the difference between them decrease by 1.40 compared to the unreinforced condition in the presence of reinforcement. This result is significant in terms of demonstrating the various effects of the presence of reinforcement on the test methods.

Figure 5.34d shows the failure envelopes of very loosely packed ($e_0 = 0.65$) samples. According to the test results, ring shear produced the highest effective friction

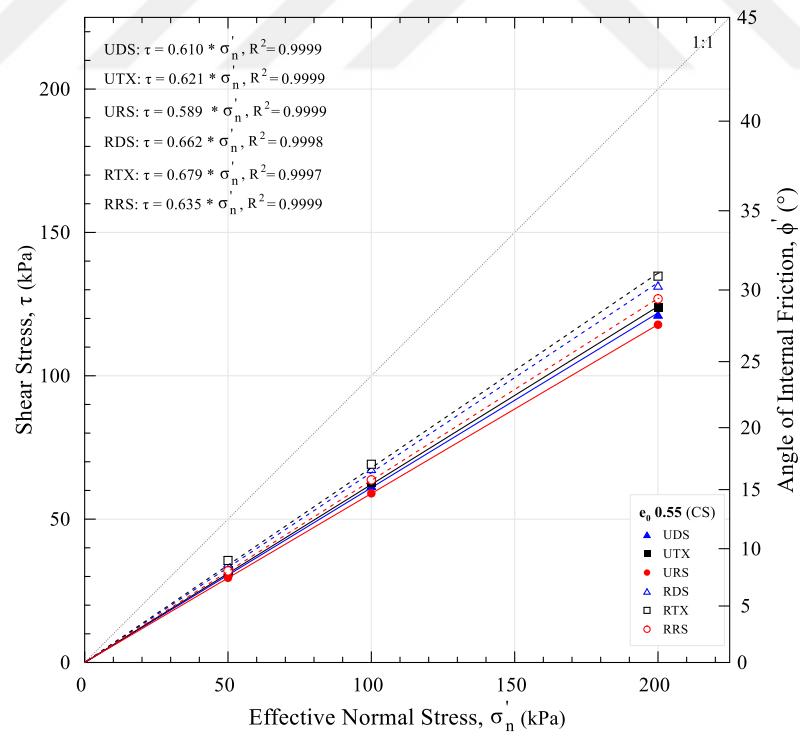
angle, whereas direct shear produced the lowest ($\phi'_{rs} > \phi'_{tx} > \phi'_{ds}$). This can be interpreted as the experimental boundary conditions of the direct shear method. Sand grains are far apart in very loose state. For methods with limited deformation capacity, such as direct shear, it is extremely difficult for these grains to come together with sufficient distortion to generate dilation, which contributes to strength. Furthermore, under shear strain, a suitable level and conditions for interlocking cannot be attained in a very loose condition since some of the sample tries to contract and the other part to pressure. Therefore, lower strength values are generally obtained in the direct shear method for very loose sands. This finding is compatible with the findings of Taylor (1939), Nash (1953), and Rowe (1969). The difference between direct shear and ring shear methods for this void ratio is about 1° .

The difference between the triaxial method and the ring shear method has decreased significantly in the presence of reinforcement. The explanation for this is that fiber reinforcing improves performance by forming a kind of link between sand grains that are far from each other. They do not, however, require reinforcement to form a connection between densely packed sand grains. At these levels, the effect of reinforcement on enhancing the ductility of the soils is more important than its contribution to strength.

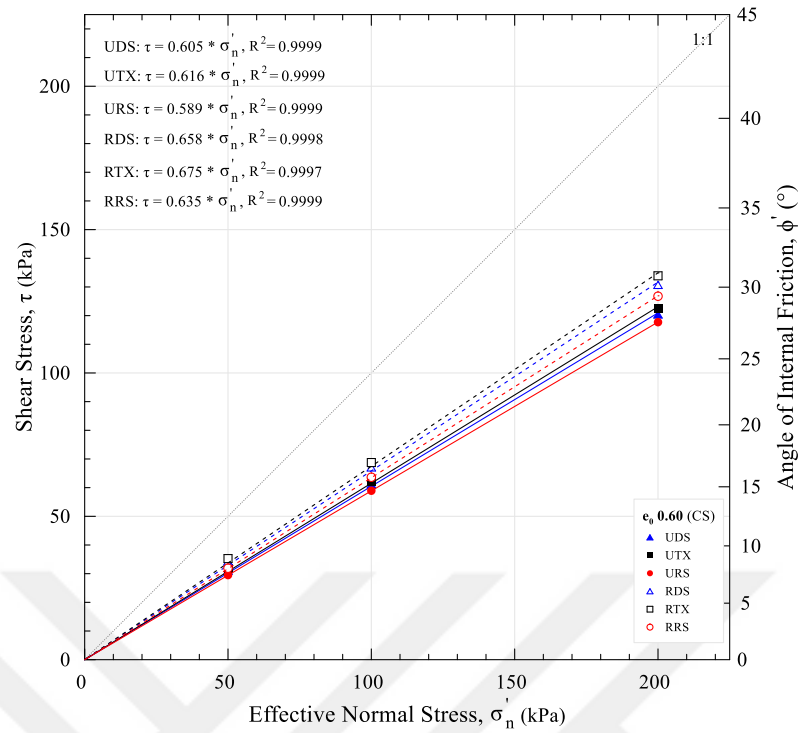
The critical state shear strength envelopes of reinforced and unreinforced specimens for various test methods and void ratios are shown in Figure 5.35. When the figures are reviewed, it is clear that the ring shear method produces the smallest critical state effective friction angles for all void ratios. Although it is known that the critical state friction angle is independent of the initial void ratio, it has been observed that this phenomenon affects triaxial and direct shear tests with very restricted strain capabilities. A similar situation was seen for the reinforced case, and the strain softening process was observed to increase after peaking. This scenario is directly related to the fact that reinforcing improves the ductility of composite samples.



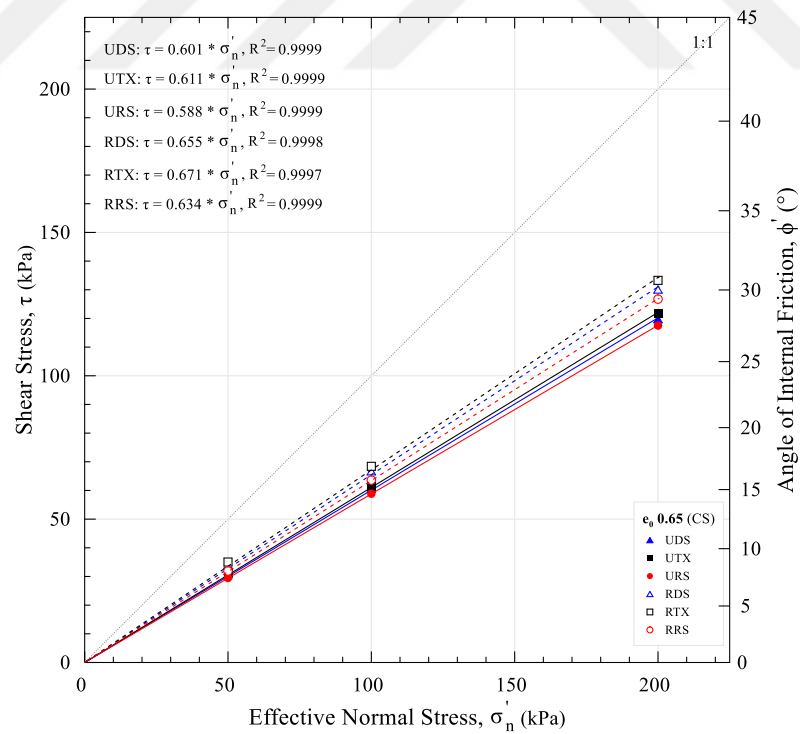
(a)



(b)



(c)



(d)

Figure 5.35. Critical shear strength failure envelopes for various initial void ratios: (a) $e_0 = 0.50$, (b) $e_0 = 0.55$, (c) $e_0 = 0.60$, and (d) $e_0 = 0.65$

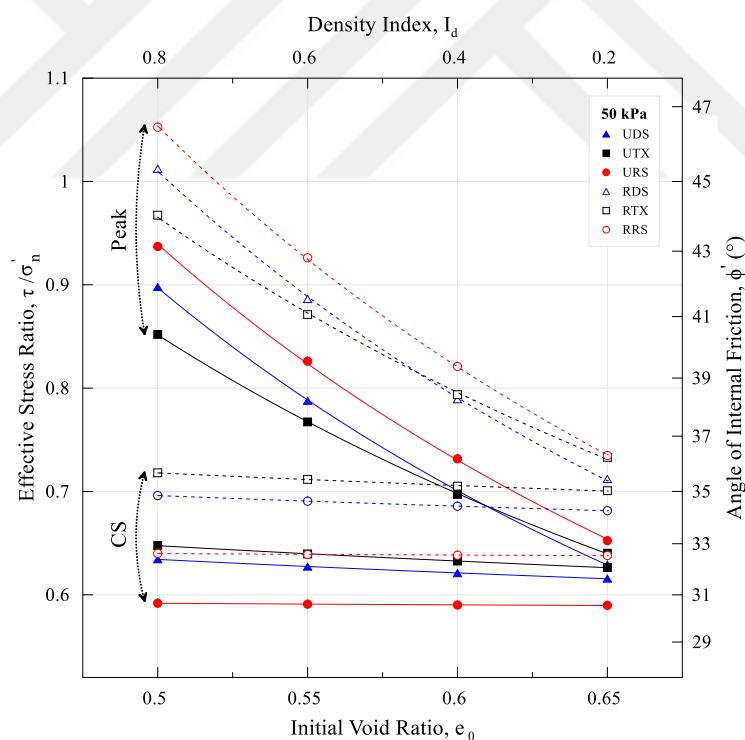
When the strain levels of sands of any density become large enough, their stress comes into contact with a permanent band. There is no volume change in the soil in this situation, and the stress value goes towards to a critical value. Although the orientation of the plates in fine-grained soils explains this condition, what is in granular soils is the stable settlement of the granular soils in the shear band. The concept of critical state is important for both sands and fine-grained soils. This concept is critical for applications such as fillings with a high sand percentage, earth-fill dams, slopes, and so on, as well as very large deformations and post-liquefaction stabilization analyses.

Figure 5.35 shows the critical state friction angles acquired using various test methods. As seen in the figures, the triaxial test produced the greatest effective critical state friction angle, while the ring shear test produced the lowest. This scenario can be interpreted as the fact that the strength of this phenomenon, the components of which are given in Equation 5.2, is primarily governed by the shape and mechanical properties of the grain and remains constant when evaluated under insufficient deformations. In direct shear and triaxial tests, this characteristic was approximately 1° for different void ratios. However, in the ring shear experiment, this change stayed at a low level. This is due to the fact that ring shear allows for nearly infinite deformation. The small differences in the ring shear test findings can be attributed to the final void ratio in the shear band and the non-uniform stress distribution in the band as a result of variability between the reinforced and unreinforced conditions. The triaxial test contributed the most to strength in the presence of reinforcement, as well as in the peak state. This is owing to the fact that the reinforcement in the triaxial test method can have varied orientations during sample preparation, and the softening is highly limited to the critical value after the peak because of the limited deformation capacity. However, at large deformations, the reinforcements in the shear bands are typically positioned horizontally in the ring shear test. Therefore, the contribution of these horizontally positioned shear-direction reinforcements to strength remains quite limited. In light of all of this data, the critical state friction angles determined by ring shear tests were applied to the relevant sand. For unreinforced specimens, this angle was estimated as $\phi'_{CS} = 30.50^\circ$ while for reinforced specimens, it was obtained as $\phi'_{CS} = 32.50^\circ$.

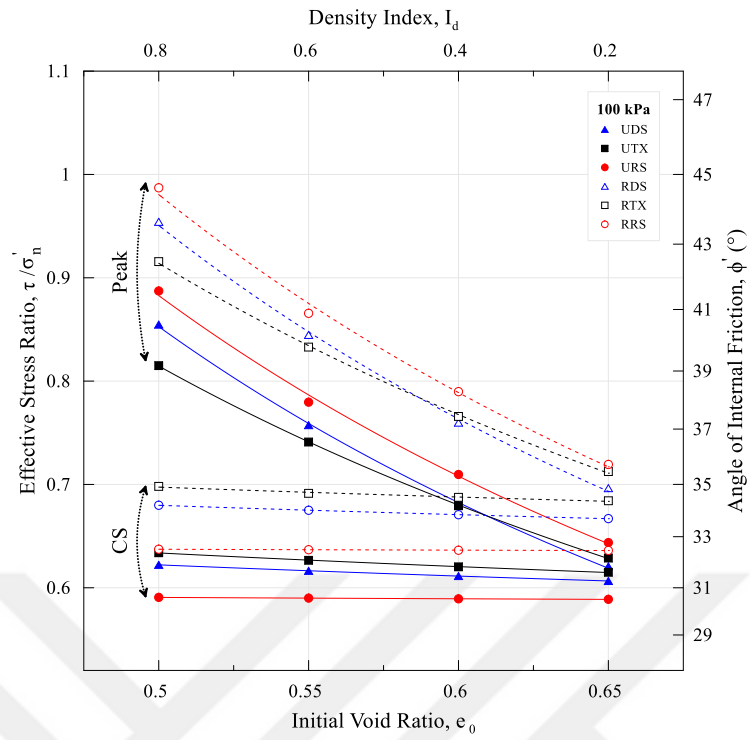
Figure 5.36 shows the effect of normal stress or confining pressure on the effective peak and critical state friction angles. When observed from the figures, the values of the

effective peak friction angles increase dramatically as normal or confining pressure decreases. This increase was much greater for samples that were densely packed, which contributed to more dilation. The suppression of dilation results in reduced friction angles as stresses increase. This phenomenon is a research issue in and of itself, and its relationship with the grain's friction coefficient at the micro level was detailed in the previous section.

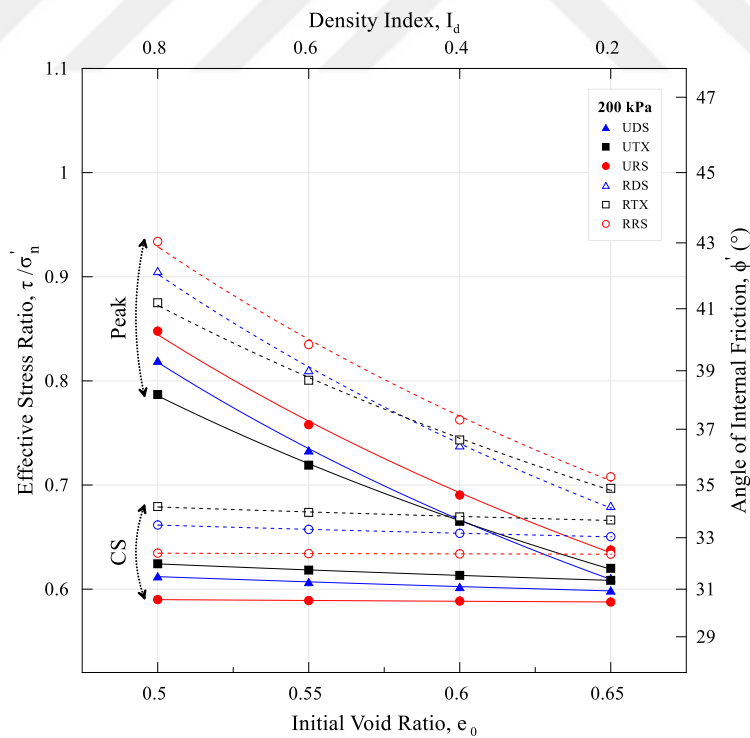
The concept of average stress is applied in geotechnical applications, as explained in Section 3.2. Although the "true contact area" is considered in this concept's analysis, this assumption is known as the positive bias for granular materials. This condition, which happens in grain contact zones and leads to grain breakage in the majority of cases, is critical for understanding the influence of stress differences. According to Holm (1941), Bowden and Tabor (1964), and Greenwood and Williamson (1966), friction is not a material constant and pioneering comparison analyses were done to elucidate the aforementioned phenomena.



(a)



(b)



(c)

Figure 5.36. The following are the relationships between effective peak and critical friction angles and density: (a) 50 kPa, (b) 100 kPa, and (c) 200 kPa

As seen in Figure 5.36, the contribution of dilation to strength increases dramatically as the void ratio decreases. The reason for this is that the grains are far apart in loosely packed sands, the shear band changes that occur as they get closer to each other and stress differences. In direct shear tests, for example, when displacements increase, the shear area of the sample decreases, and some sample remains in the passive position. This situation makes it questionable whether the loosely packed sand grains can come together and reach the desired void ratio in the peak with increasing strain. However, because the sample reaches the peak after only minor contraction in densely packed sands, the effect will be restricted. Another notable feature of the figures is that, as compared to other test methods, the change of the effective friction angles obtained from triaxial tests with increasing density is fairly limited. The reason for this can be interpreted as the sample's less resistance to volumetric strains increasing with the decrease of the void ratio and geometrical interference capacity of the sample.

When the influence of reinforcement on the sand matrix was investigated, it was observed that reinforcement contributed to the strength of all test methods. This effect was greater in the triaxial method, the reasons for which were discussed in the previous section. As a result, when the figures are closely studied, the effective peak friction angles of the direct shear and triaxial methods, which meet at a density index of 0.3 in the unreinforced condition, only meet at a density index of 0.5 in the presence of reinforcement. Despite the fact that the study utilized a very low reinforcement concentration, this result is quite relevant. On the other hand, the presence of reinforcement has been found to have little effect on the range of peak friction angles. This result can help determine whether the reinforcement should be evaluated based on solid, void, or relative density.

One of the most controversial part of the subject is the variation of the critical state effective friction angle with normal or confining pressure. Although some researchers claim that stress has no effect on this angle (Negussey et al., 1988; Verdugo, 1992), others (Ponce and Bell, 1971; Fukushima and Tatsuoka, 1984) have demonstrated that stress has an influence on this angle. According to recent studies (Quinteros, 2014; Rousé, 2018), this angle is particularly critical for normal or confining pressures below 50 *kPa*. The critical state friction angle, as is well known, is independent of the initial void ratio. The ring shear test achieved the lowest effective critical friction angle, as described in the previous section.

In the direct shear and triaxial tests, this angle was shown to be greater than 1° degree. Because the deformation capacities of the triaxial and direct shear methods are limited, it has been observed that this angle is affected by the void ratio and normal stress. This angle was shown to be independent of the initial void ratio and only partially independent of the normal stress in ring shear tests. A comparison of the effective critical friction angles obtained from direct shear, triaxial, and ring shear test methods with a large number of direct shear and triaxial literature data are shown in Figure 5.37. The experimental results, as can be seen, are consistent with the literature.

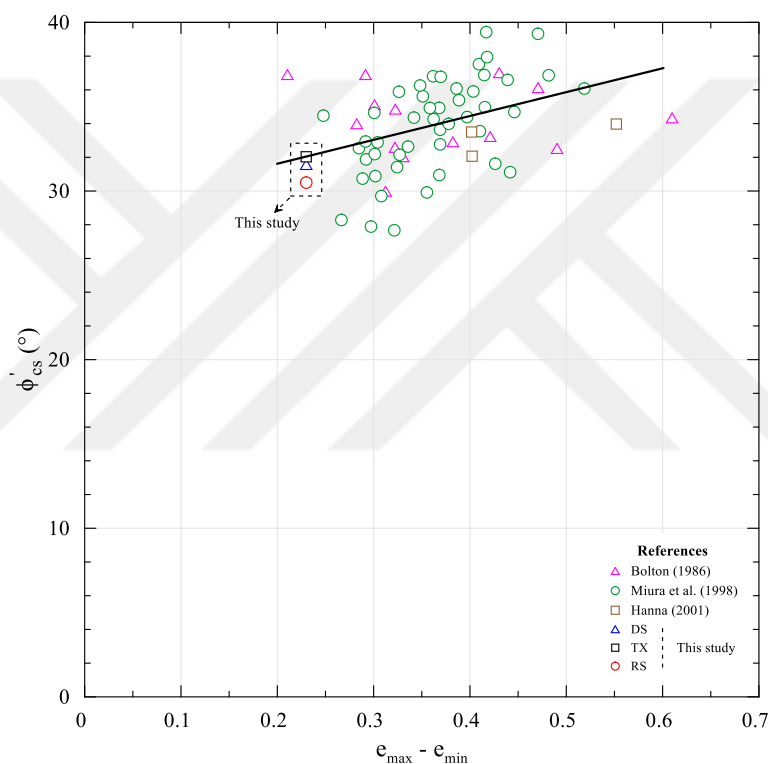


Figure 5.37. Correlation of ϕ'_{cs} with index properties for sands (Knappett and Craig, 2019)

When the influence of reinforcement on the effective critical friction angle is investigated, we notice that it varies in a narrower range for all three stress levels than without reinforcement. The reason for this is the effective action of the reinforcement with the sand matrix under the effect of kinetic friction and grain rearrangement (or rolling) in the critical state where there is no dilation. Another significant finding is that in the presence of reinforcement, higher strain levels are required to achieve the critical state. When the findings of the direct shear and triaxial methods are compared to the ring shear test, this result is confirmed.

One of the main aims of this thesis is to develop practical correlations between direct shear, triaxial, and ring shear test methods. A wide range of standardized experimental data were used for this purpose. Because plane strain conditions more reliably model field stress conditions in many important geotechnical applications, correlations obtained from direct shear, triaxial, and ring shear tests are associated with plane strain data in the following step, and new correlations are obtained for each test method. When these correlations were compared to the literature data, it was observed that the results were quite compatible.

Figure 5.38 shows the test results obtained using the direct shear and triaxial methods. The analyses used a total of 84 standardized test data sets with varying initial void ratios and stresses. Because the experimental practice of both methods is based on different principles, the relationship between them cannot be expressed with a single coefficient. As a result, depending on the test boundary conditions, triaxial friction angles were obtained in very loose samples and greater effective friction angles were obtained in dense samples using the direct shear method. The figure shows the reference line ($\phi'_{ds} = \phi'_{tx}$) that reflects this relationship.

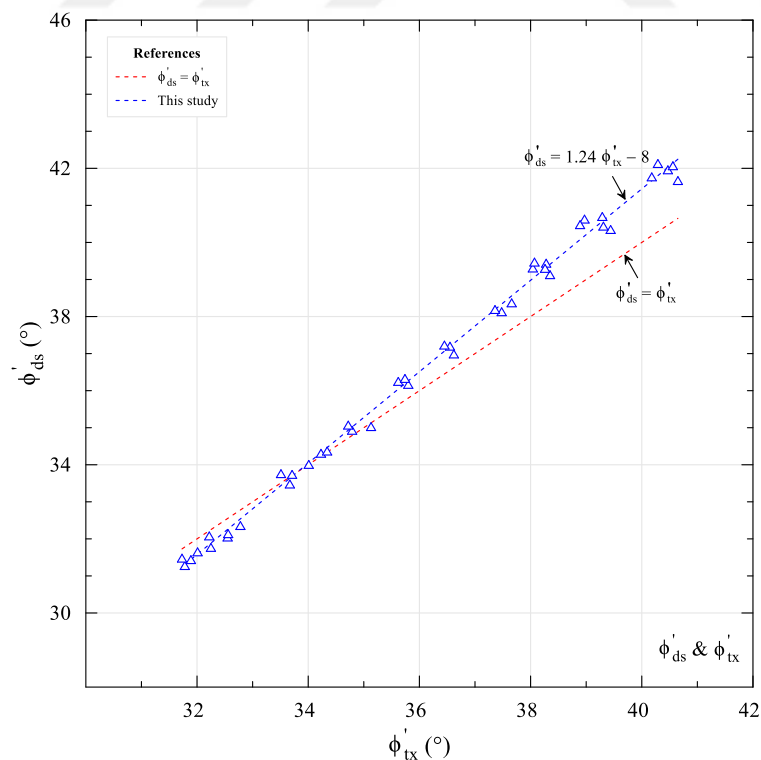


Figure 5.38. Maximum strength under direct shear and triaxial test (ϕ'_{ds} & ϕ'_{tx})

Correlation analyses are used to determine whether there is a relationship between two or more variables, as well as the direction, strength, and degree of variation of that relationship. The correlation coefficient (R) is used to measure the direction and strength of the variables in these analyses, and the coefficient of determination (R^2) is used to measure how the variables change with each other. In brief, this expression is an estimate of co-change based on variable relationships.

When Figure 5.38 is examined, it is clear that both variables are changing in the same direction. This indicates a positive correlation relationship. When the variable distributions are examined, it is observed that the correlation type is in the form of a linear function. In correlation analysis, variables are represented by a variety of functions (e.g., linear, logarithmic, exponential, power, polynomial).

When the standardized test results of the direct shear and triaxial methods were analyzed following relationships were obtained:

$$\phi'_{ds} = 1.24 \phi'_{tx} - 8 \quad (5.3)$$

&

$$\phi'_{tx} = 0.81 \phi'_{ds} + 6.4 \quad (5.4)$$

Kulhawy and Mayne (1990) derived a new plane strain-based relationship by combining Rowe's (1962, 1969) theoretical expression with certain assumptions based on stress-dilation relationships and Bolton's (1986) equations ($\tan \phi'_{ds} = \tan 1.12\phi'_{tx} \cos \phi'_{cs}$). The association of this semi-theoretical relationship with the derived equations is shown in Figure 5.39. The trigonometric relationship proposed by Kulhawy, and Mayne (1990) is in accordance with the linear equation derived from direct shear and triaxial test results, as shown in the figure. The difference between both equations is less than 1° at high density ($e_0 = 0.5$). While making this comparison, keep in mind that one of the most important studies on the subject, Kulhawy and Mayne (1990), has a semi-theoretical relationship based on certain assumptions. The above practical equations, which were derived in linear form using a large number of standardized experimental data, are also in strong agreement with the theoretical relations.

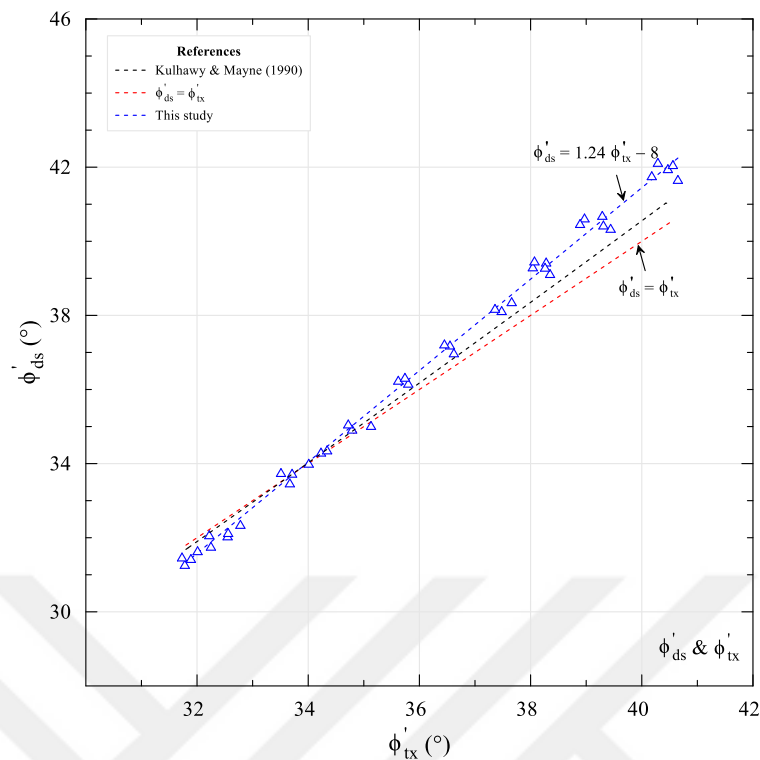


Figure 5.39. Comparison of the derived equation with the theoretical relations (ϕ'_{ds} & ϕ'_{tx})

Figure 5.40 shows the test results from the ring shear and triaxial methods. The analyses used a total of 84 standardized test data sets with varying initial void ratios and stresses. Because of the boundary conditions, the ring shear test has achieved higher values than the triaxial test under all conditions. When the relationship between the variables was investigated, it was observed that the correlation was positive and linear. Furthermore, the coefficients indicating the strength of the correlation and the change between the variables were obtained as 0.997 and 0.994, respectively. The figure shows the reference line ($\phi'_{ds} = \phi'_{tx}$), which clarifies the relationship between the two variables.

The following linear relationships were obtained after analyzing the standardized test results of the ring shear and triaxial methods:

$$\phi'_{rs} = 1.25 \phi'_{tx} - 7.4 \quad (5.5)$$

&

$$\phi'_{tx} = 0.80 \phi'_{rs} + 5.9 \quad (5.6)$$

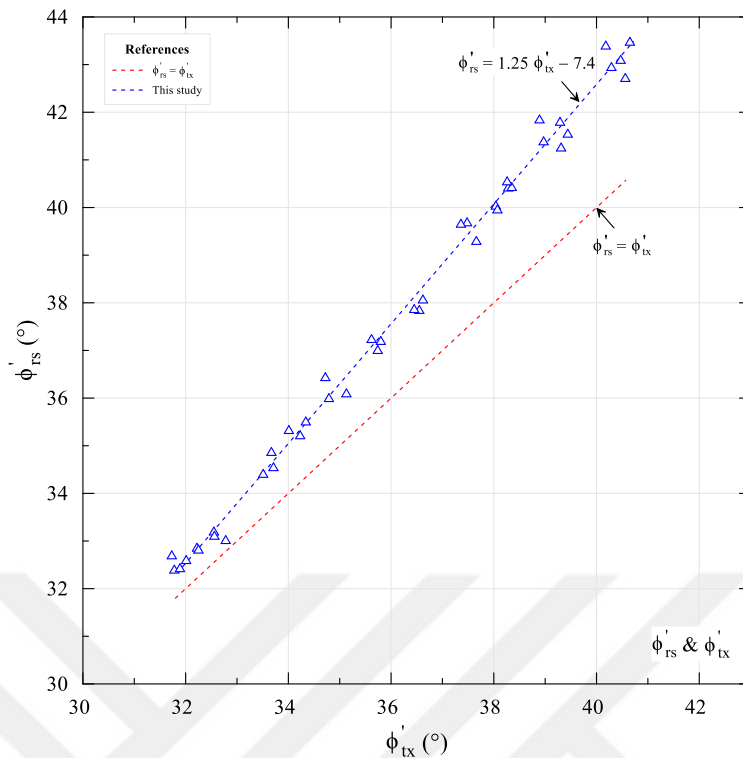


Figure 5.40. Maximum strength under ring shear and triaxial test (ϕ'_{rs} & ϕ'_{tx})

Figure 5.41 shows the test results obtained using the ring shear and direct shear methods. The analyses used a total of 84 standardized test data sets with varying initial void ratios and stresses. Because both methods are based on shearing a predetermined plane, the experimental procedures are similar. As a result, the relationship between them could be expressed using a single coefficient. In ring shear test, greater effective friction angles were obtained for each density level than in direct shear tests. The figure shows the reference line ($\phi'_{ds} = \phi'_{tx}$) that provides a better understanding of this relationship. The parameters of correlation between the variables were $R = 0.999$ and $R^2 = 0.998$.

The following linear relationships were obtained after analyzing the standardized test results of the ring shear and direct shear methods:

$$\phi'_{rs} = 1.03 \phi'_{ds} \tag{5.7}$$

&

$$\phi'_{ds} = 0.97 \phi'_{rs} \tag{5.8}$$

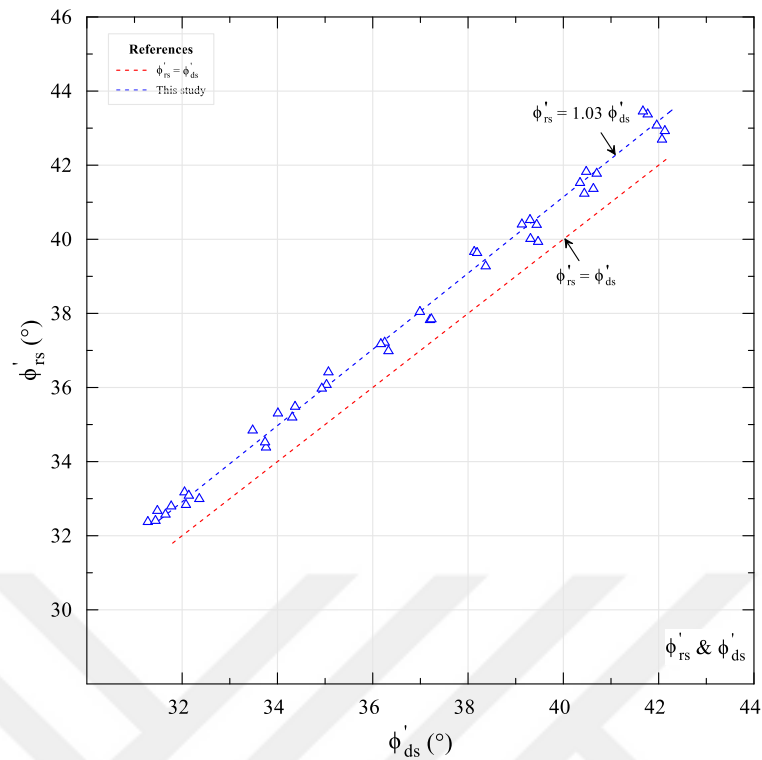


Figure 5.41. Maximum strength under ring shear and direct shear test (ϕ'_{rs} & ϕ'_{ds})

In the literature, no relationship has been established between the ring shear test and other laboratory tests for cohesionless soils such as sand. One of the main aims of this thesis is to help eliminate the deficiency in this subject.

Plane strain tests take an important place among test methods because they more accurately model field stress conditions in a wide range of important geotechnical applications. In these tests, which allow only vertical and horizontal strains, lateral strain is not permitted (theoretically, $\varepsilon_2 = 0$). The intermediate principal stress can be measured with a dimensionless coefficient ($b = (\sigma'_2 - \sigma'_3)/(\sigma'_1 - \sigma'_3)$) or directly in this test method, which has procedures similar to the triaxial method. This test method was extensively discussed in the section on literature review. Researchers interested in this test method can find detailed information from Wade (1963), Leussink and Wittke (1964), Henkel and Wade (1966), Al-Hussaini (1967), Finn et al. (1967), Wightman (1967), Barden et al. 1969, Peters et al. (1988), Alshibli et al. (2004), Wanatowski (2005), in addition to the studies presented in the sand literature research section.

The analysis and design parameters required in geotechnical applications are generally obtained in laboratories by testing field samples. As a result, in the laboratory, an accurate representation of the current stress and deformation conditions of the soil in the field is critical. Although many geotechnical applications represent plane strain conditions, the devices to perform these tests are few and expensive and are usually found in university laboratories. As a result, for many cases, various relationships are used to transition from strength parameters to plane strain of the triaxial and direct shear test methods.

Because of its advantages, triaxial test is commonly used in geotechnical applications. Therefore, many relationships have been derived between the plane strain test and similar principles. The intent of Figure 5.42 is to derive a linear relationship between the most commonly used of these relationships. It is aimed that by using the effective friction angles obtained from the triaxial test method, a linear relationship represented by a constant factor can be established between a total of 462 variables.

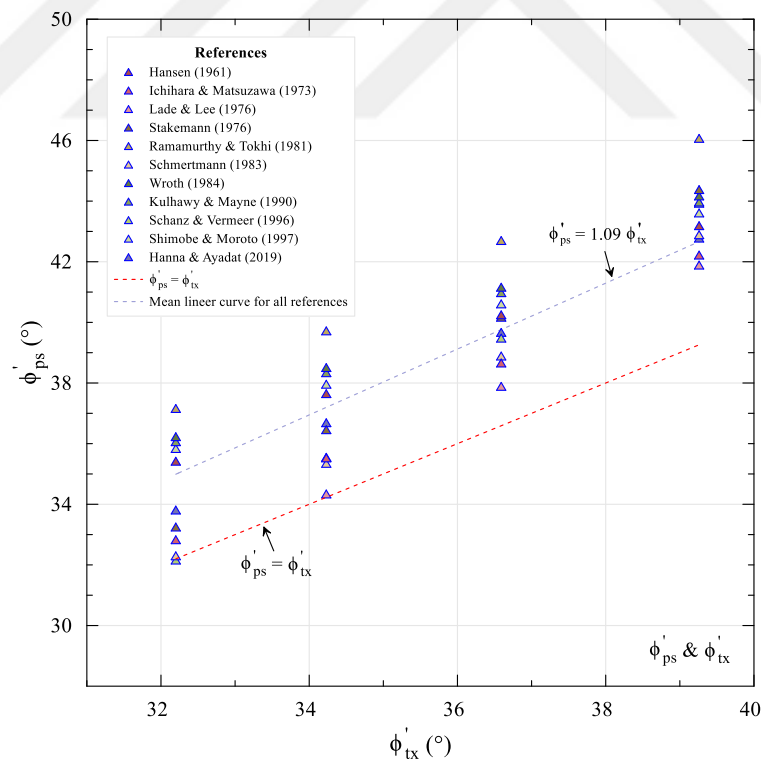


Figure 5.42. Maximum strength under plane strain and triaxial test (ϕ'_{ps} & ϕ'_{tx})

As a result, between the plane strain and the triaxial method, a linear equation with a constant coefficient of $\phi'_{ps} = 1.087 \phi'_{tx}$ was obtained. In practice, the constant coefficient can be set at $1.087 \approx 1.090$:

$$\phi'_{ps} = 1.09 \phi'_{tx} \quad (5.9)$$

&

$$\phi'_{tx} = 0.92 \phi'_{ps} \quad (5.10)$$

Figure 5.43 shows that the above equations agree strongly with the experimental results of Wanatowski and Chu (2007) when compared on the same basis ($\phi'_{ps} = a \phi'_{tx}$).

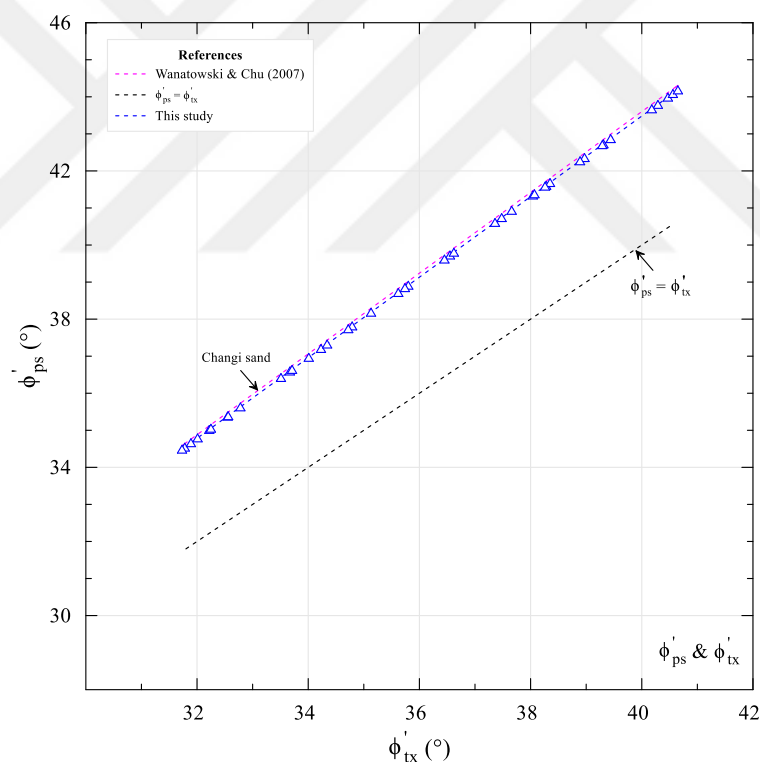


Figure 5.43. Maximum strength under plane strain and triaxial test (ϕ'_{ps} & ϕ'_{tx})

Without doubt, direct shear is one of the most preferred test due to its practicality, easy application, availability, and other significant advantages. Therefore, researchers have placed a high value on its relationship with the plane strain experiment, and theoretical relationships have been derived between them using various assumptions (Davis, 1968;

Rowe, 1969 et al.). According to Hanna et al. (1987), these derived theoretical relationships overestimate real-world experiments. This is, without doubt, to be expected for samples sheared different types of bases. The derived theoretical relationships are explained in details in the literature research section.

While associating plane strain and direct shear, the relationship of both tests with the triaxial test was utilized. Therefore, combining Equations 5.4 and 5.10, the following equations are obtained:

$$\phi'_{ps} = 0.88 \phi'_{ds} + 7 \quad (5.11)$$

&

$$\phi'_{ds} = 1.14 \phi'_{ps} - 8 \quad (5.12)$$

The ring shear test with rotational shear kinematics overcomes the displacement constraints of the laboratory tests. This test, which was previously used only to determine the ultimate (residual) strength of fine-grained soils, is now being used with increasing interest in testing various sand properties. One of the most important findings from our thesis study is that standard laboratory tests are insufficient for determining the critical strengths of sands. Ring shear tests can be used to solve this problem. Ring shear tests, on the other hand, have been used in a limited number of cases to determine the effective peak friction angles of sands. This is due to the same reason as described above for the plane strain test. The relationships of both tests with the triaxial test were used to establish a relationship between plane strain and ring shear tests, as in direct shear. Therefore, combining Equations 5.6 and 5.10, the following equations are obtained:

$$\phi'_{ps} = 0.87 \phi'_{rs} + 6.4 \quad (5.13)$$

&

$$\phi'_{rs} = 1.15 \phi'_{ps} - 7.4 \quad (5.14)$$

Table 5.1 shows the results of the direct shear, triaxial, ring shear, and plane strain test methods.

Table 5.1. Internal friction angle relationships for direct shear, triaxial, ring shear, and plane strain tests

Test Type	Friction Angle (degrees)			
	Direct shear	Triaxial	Ring shear	Plane strain
Direct shear	$1.00 \phi'_{ds}$	$1.24 \phi'_{tx} - 8$	$0.97 \phi'_{rs}$	$1.14 \phi'_{ps} - 8$
Triaxial	$0.81 \phi'_{ds} + 6.4$	$1.00 \phi'_{tx}$	$0.80 \phi'_{rs} + 5.9$	$0.92 \phi'_{ps}$
Ring shear	$1.03 \phi'_{ds}$	$1.25 \phi'_{tx} - 7.4$	$1.00 \phi'_{rs}$	$1.15 \phi'_{ps} - 7.4$
Plane strain	$0.88 \phi'_{ds} + 7$	$1.09 \phi'_{tx}$	$0.87 \phi'_{rs} + 6.4$	$1.00 \phi'_{ps}$

Cohesion is another important parameter in determining soil shear strength. The fact that the cohesion and internal friction angles of the same soil have different values under different loading conditions indicates that these parameters are mathematical expressions that represent the strength under different conditions rather than being an intrinsic property of the soil. As a result, it is important to understand that these parameters have no physical meaning. Cohesion cannot be mentioned in the case of sands that do not contain fine material. Salgado (2006), on the other hand, interpreted the cohesion obtained from laboratory tests for sands as a graphical fit parameter.

Some researchers have shown that the presence of reinforcement increases sand cohesion (Nataraj and McManis, 1997; Romero, 2003; Diambra, 2010), while others have found that it has no effect (Gray and Ohashi, 1983; Maher and Gray, 1990; Ranjan et al., 1996). According to some researchers, the increased strength of sand with reinforcement is due to cohesion rather than internal friction (di Prisco and Nova, 1993; Oancea, 1996; Consoli et al., 2003). As can be seen, it is unclear whether the effect of reinforcement on soil shear strength will be measured by cohesion or friction angle. All these uncertainties become clearer in studies of structural modeling of the reinforcement-soil relationship (Ding and Hargrove, 2006; Ibraim et al., 2012; Diambra et al., 2013). Therefore, additional research on the subject is required.

Figure 5.44 shows the effect of reinforcement on effective cohesion (c') for direct shear, triaxial, and ring shear tests. While the strengths in the shear tests were close to each other, the triaxial method produced slightly more apparent cohesion. The reason for this is that the interaction of reinforcement and sand grains with each other is increased due to the triaxial test conditions. Another important finding from the experiments is that the effective cohesion value increases slightly as the void ratio decreases. This is due to the increasing interactions between the grains and the reinforcement, which are close to each other, resulting in a very compact composite. In contrast, in the triaxial test, which differs from other shear tests, specific procedures are followed to saturate the sample. The pore water pressure coefficients control the degree of saturation of the sample in this test, so full saturation is achieved with certain approaches. This describes the effects of pressure forces applied to soil particles as a result of surface tensions at the point where water meniscus occurs between grain-grain or grain-reinforcement. These capillary effects are reflected in the strength tests as a little more cohesion.

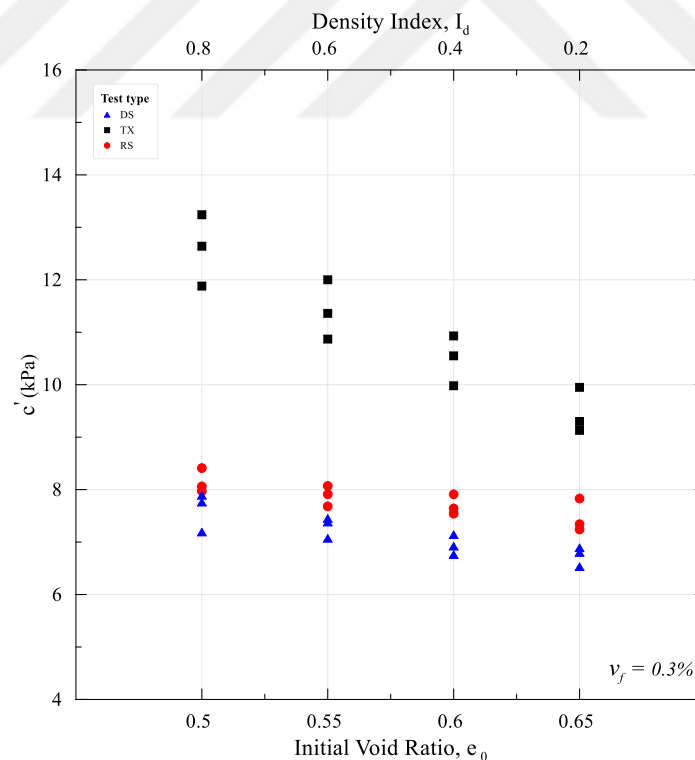


Figure 5.44. Cohesion strengths of reinforced specimens (ϕ'_{ds} & ϕ'_{tx} & ϕ'_{rs})

The low concentration of reinforcement used in the study ($v_f = 0.3\%$) explains why the test method results are so close to each other. For the reasons stated above, it is predicted that as reinforcement concentrations increase, the apparent cohesion increase will be more pronounced in the triaxial method.

Although it has been demonstrated experimentally that the reinforcement contributes to apparent cohesion in sands, the water meniscus between the grain-grain or grain-reinforcement will completely vanish in saturated soil when the moist soil dries out or the water completely fills the soil voids. On the other hand, as detailed in the previous section, some of the components that constitute cemented sand easily lose their strength due to the reaction with water. As a result, it would be more appropriate not to use the extra strengths created by cementation and the electrostatic attraction forces between grain-grain or grain-reinforcement formed under the influence of slightly moist in the analysis for design purposes. Undoubtedly, this interpretation is valid for the style and type of geosynthetic reinforcement used in this study. As is well known, there are numerous styles and types of geosynthetic reinforcements that interact with the soil via various mechanisms. The tensile forces formed by absorbing the shear forces that cause the composite soil to fail increase the strength capacity of the soil. Undoubtedly, the interaction will vary depending on the soil medium's loading conditions and the properties of the geosynthetic reinforcement. On this basis, it would be more appropriate to evaluate the relationship between soil-reinforcement and internal friction angle-cohesion.

Finally, it is important to note that the data presented in this section applies to coarse-grained soils such as sand. The relationship between fine-grained soils and geosynthetic reinforcement is assessed on a variety of criteria.

5.5.2. Volumetric strain parameters

The volumetric strain capacities of soils against failure under load are directly related to their shear strength parameters. As a result, the subject should be evaluated along with the shear strength parameters. Studies on the volumetric strains of soils are given in Chapter 2 and detailed information on their theoretical relationships are given in Chapter 3. In this section, the results of the direct shear, triaxial and ring shear test methods are discussed and comparative analysis are presented.

Volumetric strain curves of direct shear, triaxial and ring shear test methods are presented in the previous section. These curves are very important in terms of representing the volumetric change of the soil mass against defeat during shearing. As can be seen from the curves, the soils exposed to strain are first contracted somewhat and then they dilate and fall to a critical level where there is no volumetric change. Undoubtedly, the level of volumetric strain at failure constitutes the most important part of this whole process. Volumetric strain of soil (ε_v) is defined as the ratio of the change of soil volume (ΔV) to the initial volume (V_0) of the soil:

$$\varepsilon_v = \frac{\Delta V}{V_0} \quad (5.15)$$

Volumetric strains of direct shear, triaxial and ring shear test methods are shown in Figure 5.45. As can be clearly seen from the figures, the greatest volumetric strains were obtained in the triaxial test method. In the direct shear and ring shear tests, shearing according to the same principle, strains close to each other but lower than in the triaxial tests were obtained. The reason for this significant difference is that the volumetric strain in the shear band during shear is suppressed depending on the experimental method. This suppression is very important since it is the source of dilation that makes the main contribution to the strength of the soils, as has been mentioned a lot before.

When the effect of normal and confining pressure on volumetric strains while shearing soil samples was examined, it was seen that the difference between the test methods increased even more with the decrease in the applied stresses. The reason for this increase is

the freedom of the relative movements of the grains on the shear band to each other with the decrease of the applied stress.

When the effect of the initial void ratio on volumetric strains was examined, it was observed that volumetric strains increased significantly with the decreasing void ratio. This increase, in particular, has been more prominent in low stress conditions. The reason for this is that as the initial void ratio decreases, the movement of the grains relative to each other becomes more difficult under shear stress and the energy losses increase as a result of the volumetric dilation of the soil under pressure.

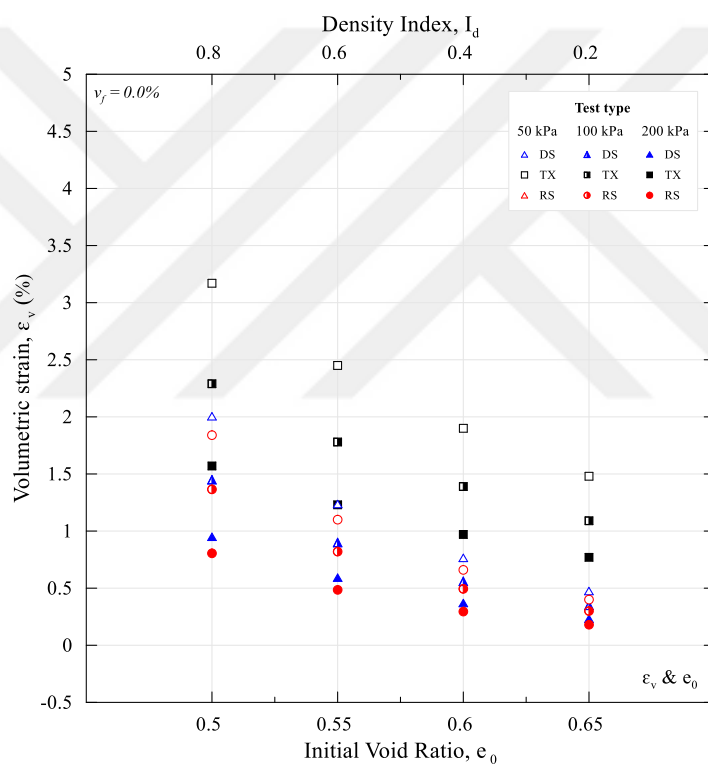


Figure 5.45. Volumetric strain at failure in direct shear, triaxial and ring shear tests versus initial void ratio ($v_f = 0.0\%$)

The effect of the presence of reinforcement on the volumetric strains for different test methods is shown in Figure 5.46. As can be seen from the figure, greater volumetric strains were obtained in triaxial tests for each initial void ratio and stress level. Direct shear and ring shear tests were observed to have volumetric strains close to each other but lower than the triaxial method. When the effect of normal or confining pressure on volumetric strains was examined, it was observed that the difference was more than 2 times for the

lowest and highest stress conditions. On the other hand, a similar ratio was obtained for low and high initial void ratios.

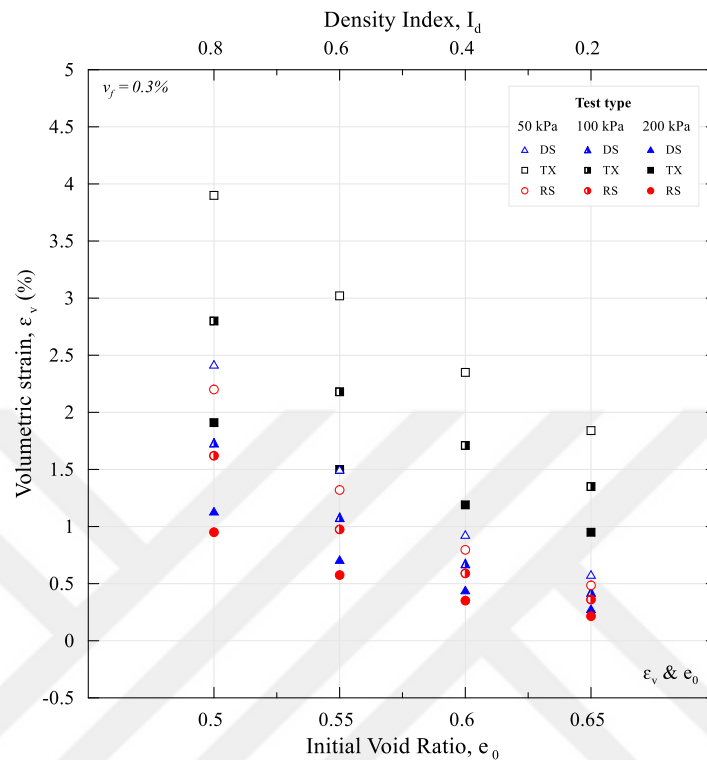


Figure 5.46. Volumetric strain at failure in direct shear, triaxial and ring shear tests versus initial void ratio ($v_f = 0.3\%$)

When the cases with and without reinforcement were compared, it was seen that the presence of reinforcement significantly increased the volumetric strains in all three test methods. This increase was between 20% - 25% on average for different void ratios and stress levels. This increase is normal since the presence of reinforcement makes the samples more compact. When the increase rates were compared among themselves, it was seen that the reinforcement affected volumetric strains more at high void ratios and low confining pressures. This result is quite significant. Soils need more reinforcement presence when there is an increase in the initial void ratio and low confining pressures. When the experimental methods were compared, the greatest increase in volumetric strain was observed in triaxial tests. This is due to the relationship between triaxial tests and reinforcement.

Although the reinforcement concentration used in the study is very low, it is important that it affects volumetric strain so much. Another important issue to be mentioned

is the confusion of the concept of volumetric strain with stiffness and ductility. While ε_v is a strain characteristic of the soil, stiffness and ductility are defined as the strength characteristic of the soil. As mentioned in the previous section, it has been observed that the presence of reinforcement decreases the stiffness of the soil while increasing its ductility. This situation is important in terms of showing the importance of the use of geosynthetics for the soils as it increases the energy capacity required for the soil to be failure.

In addition to volumetric strain where dilation is at its maximum value, the parameter representing the level of volumetric strain at the beginning of dilation is also important. Soils in the shearing phase are first contracted a little. The level of this volumetric contraction is important because it is used to define the parameters constituting the shear strength with the internal energy principle. As it is known, these definitions form the basis of flow rules derived from dilation.

Figure 5.47 shows the volumetric contractions (ε_c) of direct shear, triaxial and ring shear test methods for unreinforced samples.

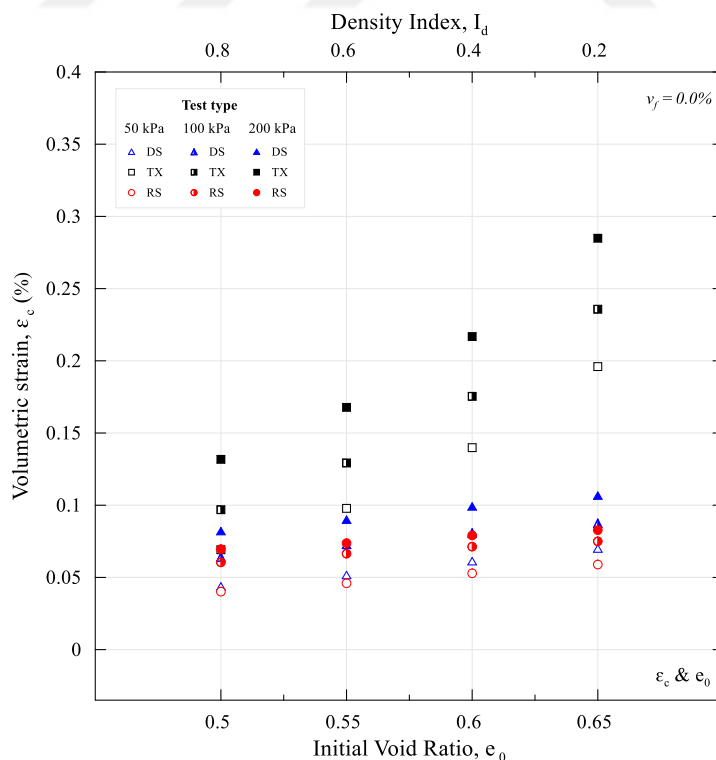


Figure 5.47. Volumetric strain at onset dilation failure in direct shear, triaxial and ring shear tests versus initial void ratio ($v_f = 0.0\%$)

As seen in Figure 5.47, volumetric strains decreased with the decrease of the void ratio. The reason for this is that since the grains are sufficiently close to each other, they can pass into the dilation phase without the need for further contraction. When the effect of the applied load is examined, it is seen that the contraction is higher with the increase of normal or confining pressure. This is due to the fact that grains are forced to contract rather than dilate with increasing normal or confining pressure.

When the results of all three experimental methods were compared, it was observed that volumetric contraction strains were higher in the triaxial method and least in the ring shear method. This shows that in ring shear tests, grains work more on volumetric dilation than on volumetric contraction. As a natural consequence of this, dilation contribute more to strength in ring shear tests.

Figure 5.48 shows the volumetric contractions (ϵ_c) of direct shear, triaxial and ring shear test methods for reinforced samples.

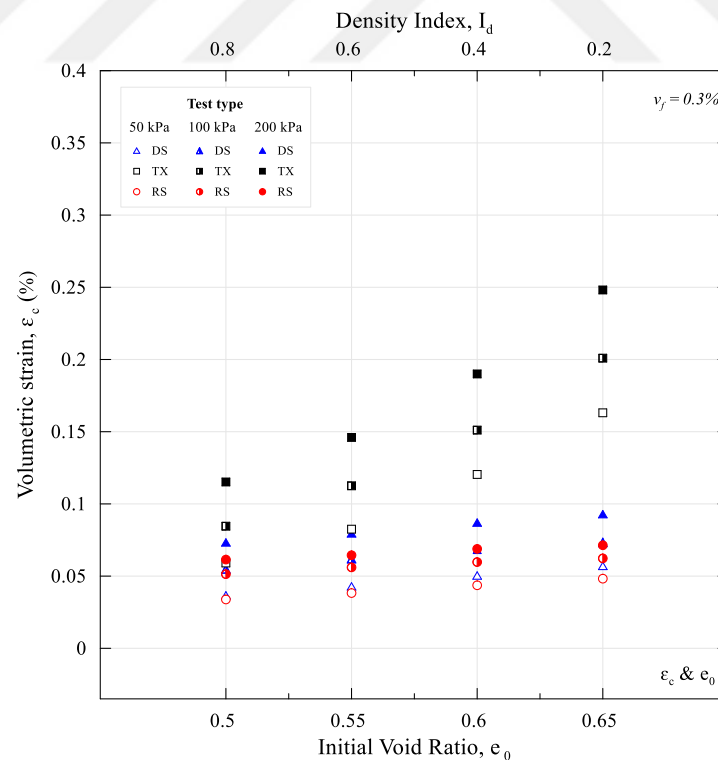


Figure 5.48. Volumetric strain at onset dilation failure in direct shear, triaxial and ring shear tests versus initial void ratio ($v_f = 0.3\%$)

As can be seen in Figure 5.48, the effect of the initial void ratio and the applied load on volumetric contraction has a similar trend to that of unreinforced samples. However, since the soil has a more compact structure in its reinforced presence, the amount of volumetric contraction has decreased by 15% – 20%. This effect was greater with the increase in the void ratio and the decrease in normal or confining pressure. Undoubtedly, this has been more distinct for the triaxial method. Finally, the most important point to be mentioned is the fact that the presence of reinforcement reduces the required void ratio for the transition to dilation while increasing the accessibility to this void ratio.

As known, the presence of dilation is definitely mentioned for cohesionless soils except for the loose sands. Dilation is one of the important geotechnical issues whose importance is increasingly understood as it plays a key role in the soil-structure response to any loading condition. Traditionally, the shear strength of cohesionless soils is defined by peak and critical friction angles. The relationship between these two main parameters is also explained by the phenomenon called dilation. Recognizing this important relationship, Taylor (1948) stated that the strength of the sands was a measure of the dilation during shearing and explained this for the first time by modifying Coulomb's (1773) concept of shear strength using the external energy principle and direct shear method. Later, different experimental methods were used to develop this relationship, and a large number of theoretical and experimental relationships were derived on various principles (Skempton and Bishop, 1950; Bishop, 1954; Rowe 1962, 1969; Schofield and Wroth, 1968; de Jong, 1976; Bolton, 1986; Collins et al., 1992). Detailed information about these relationships and the details of the most important studies on the subject are explained in the previous sections.

Various relationships derived from different principles (e.g., Mohr Circle of Strains; Vermeer and de Borst, 1984; Vaid and Sasitharan, 1991) are used in defining the dilation angle. Although these relationships also valid for one or more test methods, they are based on certain practical assumptions. Therefore, it is usual that the difference between the dilation angles calculated depending on the methods selected for the same sand is greater than 10° . This situation becomes more critical, especially with increasing density. Since very detailed information and visuals are shared in the previous sections on the subject, only the presentation of the test results and comparative analyses between the test methods will be given in this section.

The following definitions below were used to calculate the maximum dilation angles for direct shear, triaxial and ring tests.

In direct shear and ring shear tests:

$$\psi = \arctan \left\{ -\frac{d\varepsilon_v}{d\varepsilon_\gamma} \right\} \quad (5.16)$$

In triaxial test:

$$\psi = \arcsin \left\{ \frac{-(d\varepsilon_v/d\varepsilon_a)}{2 - (d\varepsilon_v/d\varepsilon_a)} \right\} \quad (5.17)$$

where $d\varepsilon_v$, $d\varepsilon_a$ and $d\varepsilon_\gamma$ are incremental changes in volumetric strain, axial strain, and shear strain, respectively. The definitions of the dilatancy angles are the most commonly referred to in the literature (e.g., Bolton 1986).

The maximum dilation angles of the unreinforced and reinforced samples measured for direct shear, triaxial, and ring shear test methods are shown in Figure 5.49 and Figure 5.50, respectively. The maximum dilation angle is known to be dependent on soil density, normal and confining pressure, and stress path. When the effect of the initial void ratio was examined, it was seen that the dilation angle increased with the decrease of the void ratio (Figure 5.51). It has been observed that the dilation angle increases with the decrease in normal or confining pressure. This can be interpreted as suppression of dilation under high stress conditions. When the common effect of density and stress was examined, the maximum dilation angles are obtained under low initial void ratio and low stress.

When the results of the maximum dilation angles of the reinforced samples were evaluated, it was seen that the general trend was similar to that of the samples without reinforcement (Figure 5.52). Since the samples reach a more compact structure in the presence of reinforcement, peak and critical friction angles will increase. Accordingly, dilation angles are expected to increase slightly. It was observed that the rate of this increase was at different levels depending on the test method, the void ratio and the stresses applied.

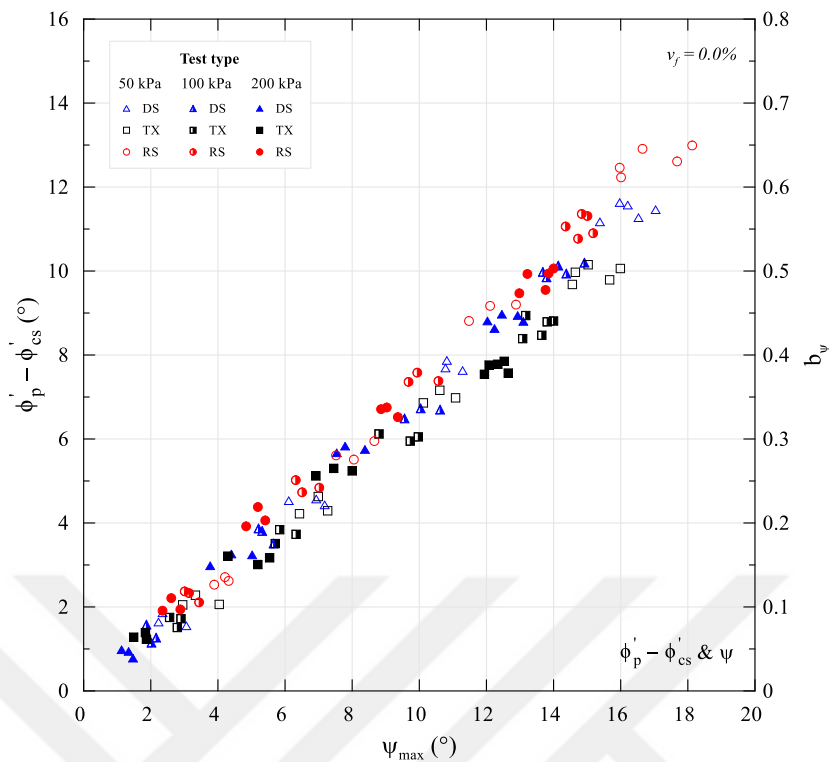


Figure 5.49. Variations of the excess friction angle ($\phi'_p - \phi'_{cs}$) with the angle of dilation (ψ) for unreinforced specimens

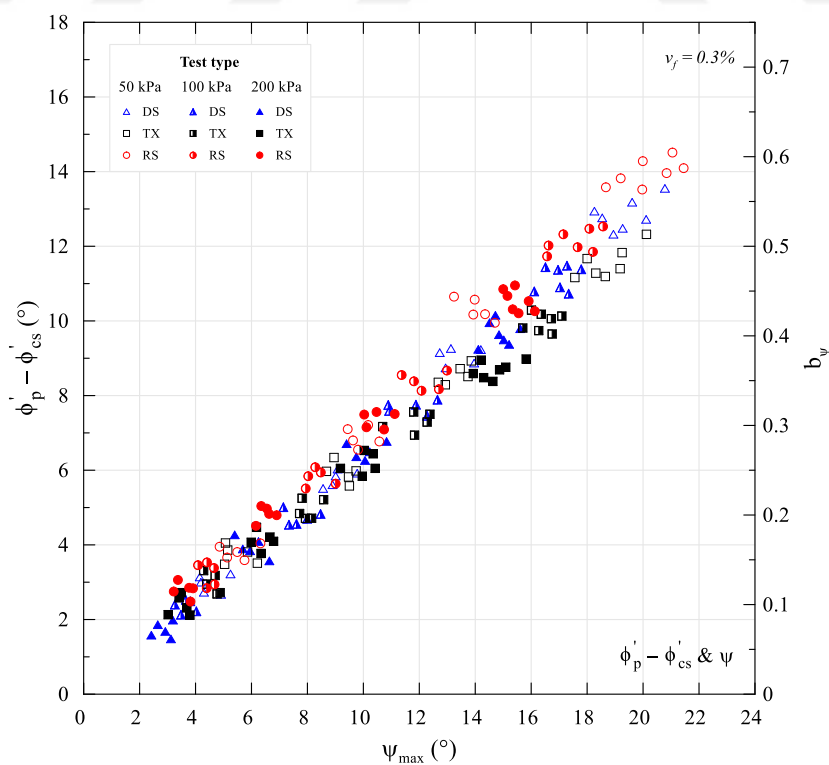


Figure 5.50. Variations of the excess friction angle ($\phi'_p - \phi'_{cs}$) with the angle of dilation (ψ) for reinforced specimens

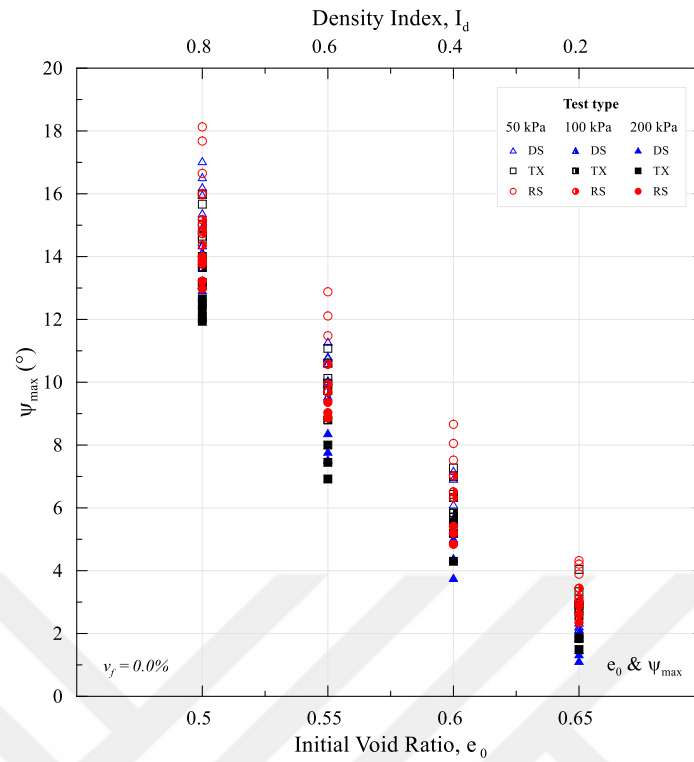


Figure 5.51. Influence of initial void ratio on maximum dilation angle for unreinforced specimens

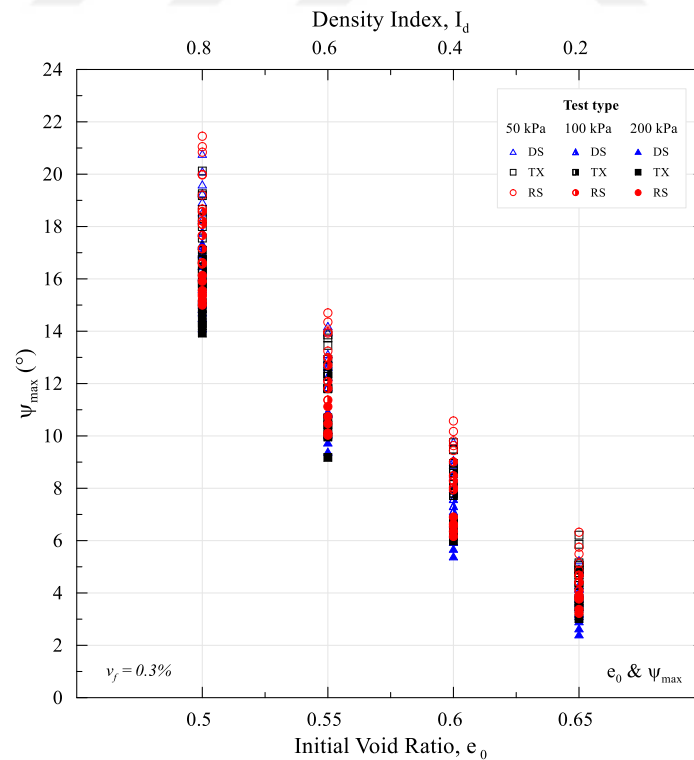


Figure 5.52. Influence of initial void ratio on maximum dilation angle for reinforced specimens

When the maximum dilation angles (ψ_{max}) obtained from direct shear, triaxial and ring shear test methods were compared, it was seen that the greatest values of this angle were reached in ring shear tests. It was observed that the maximum dilation angles obtained from the experimental methods were very close to each other in loosely packed sands, and the difference between these angles increased with the decreasing initial void ratio when the effect of the initial void ratio on the dilation angle was examined. When the effect of normal and confining pressure on ψ_{max} was examined, it was seen that the difference between the dilation angles obtained from different experimental methods decreased with the increase of the applied loads, and the difference between the dilation angles increased with the decrease of the applied loads. The reason for these differences between the dilation angles is that in the shear tests, while the particles in the shear band are forced to move only in two dimensions, in the triaxial test representing axisymmetric conditions, there are three different directions in which the grain can move. This state of freedom, which prevents particle movement, is reflected to us as dilation, or in other words, as additional strength.

Dilation angle is strongly correlated with effective peak friction (ϕ'_p) and critical state friction (ϕ'_{cs}) angle. Thus, dilation was initially defined as the difference between peak and critical friction terms, later it was expressed as a strength component in the form of an approximate expression representing certain conditions of these friction parameters. A total of 126 experimental data obtained from direct shear, triaxial, and ring shear tests were used in order to investigate this important relationship between ϕ'_p and ψ_{max} (Figure 5.53). In the figure, it is clearly seen that ϕ'_p is a result of dilation. This finding is important in terms of showing the effect of dilation on ϕ'_p which is frequently mentioned in the thesis study. For each test method, the following relationships are derived in unreinforced samples:

In direct shear:

$$\phi'_p - \phi'_{cs} = 0.70\psi \quad (5.18)$$

In triaxial:

$$\phi'_p - \phi'_{cs} = 0.64\psi \quad (5.19)$$

In ring shear:

$$\phi'_p - \phi'_{cs} = 0.74\psi \quad (5.20)$$

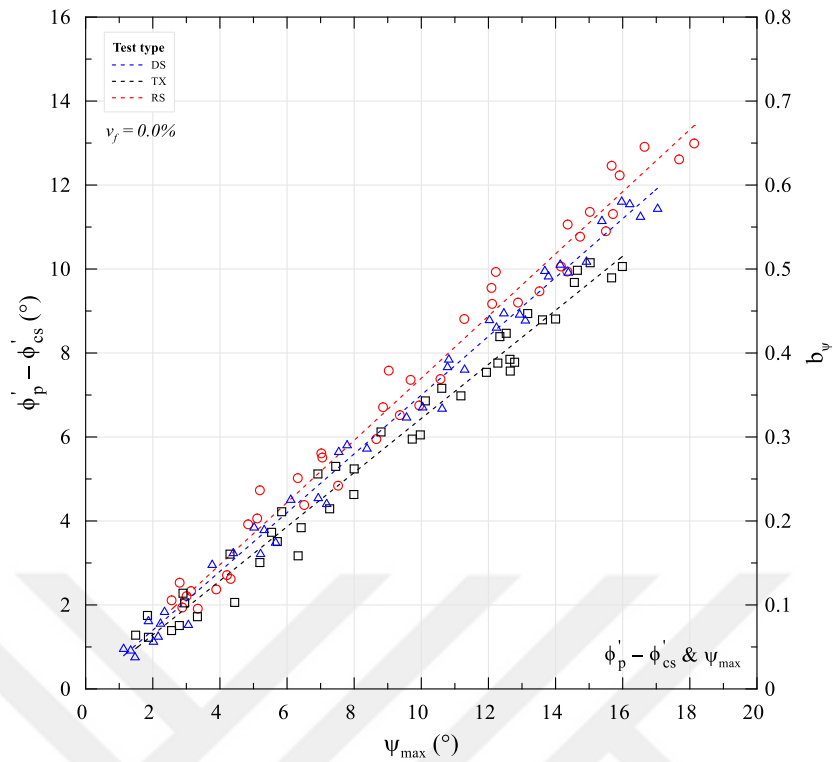


Figure 5.53. Relationship between effective peak friction angle and maximum dilation angle for unreinforced specimens

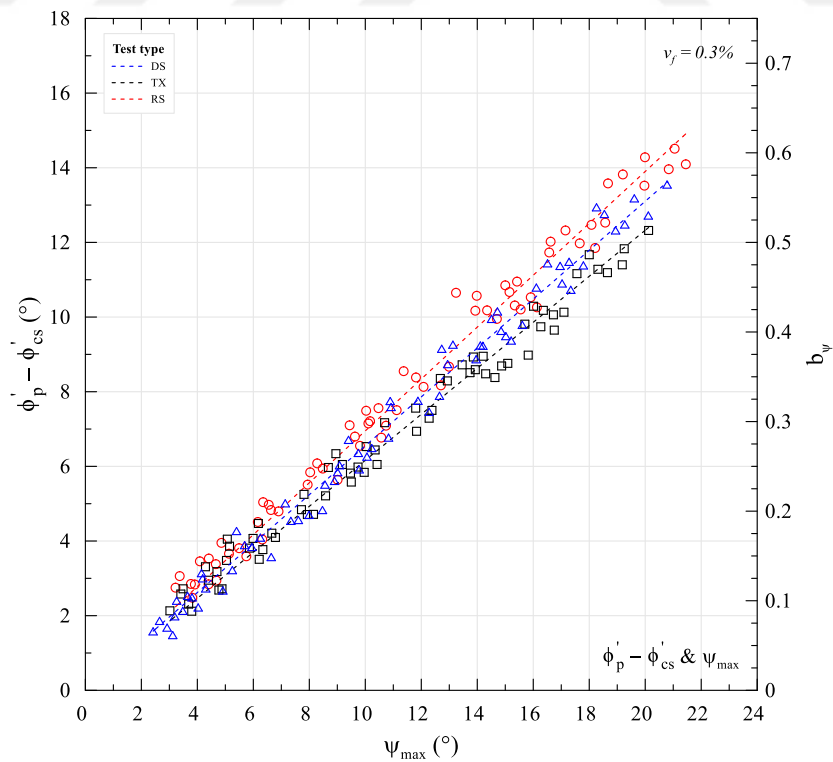


Figure 5.54. Relationship between effective peak friction angle and maximum dilation angle for reinforced specimens

As can be seen from the equations in the derived basis for each experimental method, the contribution of each experimental method to the dilation component is different. This is expected due to the boundary conditions of the experimental methods. The relationship between effective peak and critical friction angles and the dilation angle can be easily monitored with the b_ψ dilation coefficient defined in the right column.

For each experimental method, comprehensive research has been conducted by using a total of 198 experimental data to investigate the effect of the presence of reinforcement on dilation (Figure 5.54). The results of the experiment showed that the presence of reinforcement increased the dilation of each case. This increase is the main source of the presence of reinforcement to increase the shear strength of soils. Another noticeable factor is that the contribution of reinforcement to dilation is higher with the decrease in density and applied loads. Another important point that should not be overlooked is that the critical friction angle value increases in the presence of reinforcement. This situation is important in terms of showing that effective peak and effective critical state friction angles should be taken into account when evaluating their relationship with dilation angle. Thus, effective critical state friction angle has always been one of the most important parameters for many flow rules derived (e.g., Taylor, 1948; Rowe, 1962; Atkinson and Bransby, 1978; Bolton, 1986). For the direct shear, triaxial, and ring shear test methods, the following relationships are derived for the reinforced samples:

In direct shear:

$$\phi'_p - \phi'_{cs} = 0.66\psi \quad (5.18)$$

In triaxial:

$$\phi'_p - \phi'_{cs} = 0.61\psi \quad (5.19)$$

In ring shear:

$$\phi'_p - \phi'_{cs} = 0.70\psi \quad (5.20)$$

These relationships are important in terms of showing the effect of the change in the critical friction angle (ϕ'_{cs}) on the dilation parameter. Today, there is no consensus on opinion about which principle will be used in the selection of the ϕ'_{cs} used in the definition

of stress-dilation relations. This important uncertainty has been the subject of many studies conducted today.

In the last part of the thesis study, the dilation parameters obtained from direct shear, triaxial and ring shear tests were compared with the leading studies related to the subject (Figure 5.55). In the comparison, the generally accepted parameters of Bolton's (1986) study were accepted as the limit. In Figure 5.55, it is seen that the relationships obtained for direct shear and triaxial methods are in accordance with the literature. No published studies have reported on the comparison of ring shear tests. One of the most important objectives of this thesis study is to fill this gap in the literature by explaining the strength and dilation behaviors of ring shear tests for cohesionless soils.

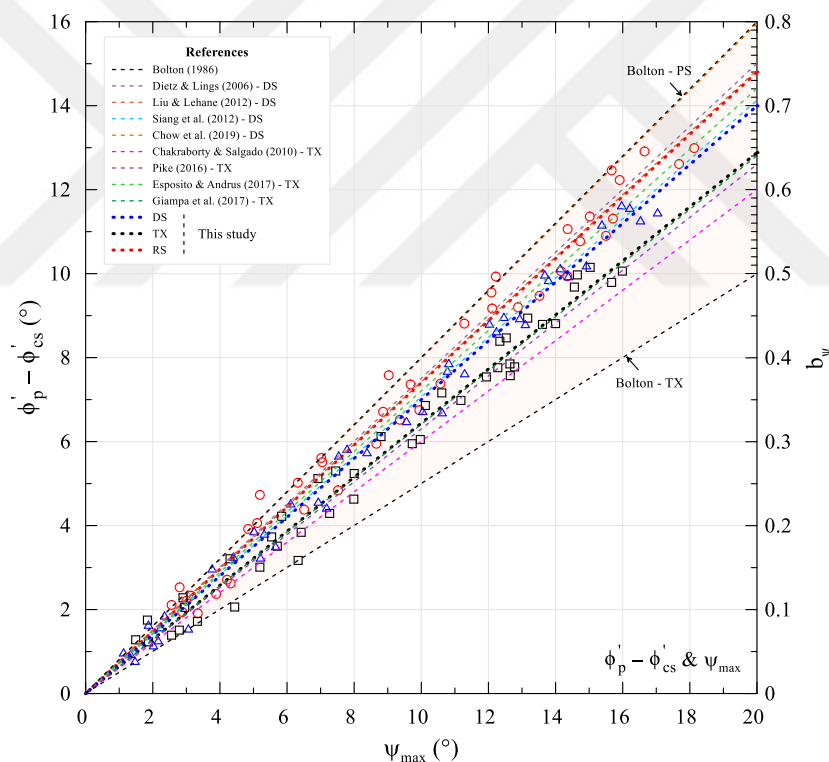


Figure 5.55. Relationship between excess friction angle and maximum dilation angle

The presence of gravel is very important in geotechnical applications for cohesive soils. Therefore, many important studies have been conducted to understand the stress-dilation behavior of cohesionless soils containing gravel. The presence of gravel is not within the scope of this thesis study. Researchers who are interested in this subject may use Fannin et al. (2005), Simoni and Houlsby (2006), Nicks et al. (2015), Strahler et al. (2016a) sources.

6. CONCLUSIONS AND RECOMMENDATIONS

In this study, the results of direct shear, triaxial, and ring shear test methods of sand soil were evaluated based on stress-strain and stress-dilation, and comparative analyzes were performed. The results of the analysis were associated with the plane strain method, which reliably models the field stress conditions in many geotechnical applications and significant correlations were found between the test methods. In the study, the geosynthetic material, which has increasing importance and use, was examined in terms of its effect on different test methods, and significant findings were obtained. A total of 1203 tests were performed and comprehensive research was conducted to establish strong relationships between the parameters obtained from different test methods. Detailed analysis of the results obtained from the test methods based on cause and effect was presented in Part 5. In this part, the findings concerning the results of the study were summarized.

When the normalized effective peak stress ratios were compared, the highest values were obtained in the ring shear test and the lowest values were obtained in the triaxial test at low void ratios, and in the direct shear test at high void ratios.

When the normalized effective critical stress ratios were compared, the highest values were obtained in the triaxial method and the lowest values were obtained in the ring shear method.

Since the effective peak and critical internal friction angles are the arctangents of the effective stress ratio, evaluations should be made based on this information. It has been observed that the effective cohesion strengths were at negligible levels for the test methods.

Looking at the effect of the initial void ratio and the applied stresses on the normalized effective stress ratios, it was observed that the difference between the test methods decreased significantly in the increasing void ratio and stresses, and the difference increased in the decreasing void ratio and stresses.

When the effective peak friction angles obtained from the test methods were compared with a large number of diagrams where cohesionless soils were standardized, it was observed that they were quite in accordance with the literature data. The effective critical friction angles obtained for each test method were also in accordance with literature.

A huge number of effective peak friction angles obtained from different test methods were compared each other and strong relationships were observed between them. These derived relationships were compared with the literature data and their consistency was demonstrated.

The results obtained from direct shear, triaxial, and ring shear tests were associated with the plane strain method and useful relationships were derived between the test methods. The consistency of these relationships was demonstrated using data from different studies.

When the volumetric strain ratios at the time of failure were compared, the highest values were obtained in the triaxial tests, and the lowest values were obtained in ring shear tests.

Looking at the effect of the initial void ratio and the applied stresses to the strains at the time of failure, it was observed that the difference between the decreasing void ratio and the test methods in stresses increased considerably, while the difference between the increasing void ratio and stresses decreased.

When the volumetric compression strain ratios at the beginning of dilation were compared, the highest values were obtained in triaxial tests, and the smallest values were obtained in ring shear tests.

Looking at the effect of the initial void ratio and the applied stresses to the volumetric strains at the beginning of the dilation, it was observed that the difference between the test methods increased significantly in the increasing void ratio and stresses, and the difference decreased in the decreasing void ratio and stresses.

When the dilation angles at the time of failure were compared, the largest values were obtained in ring shear tests and the smallest values were obtained in the triaxial shear method in low void ratios, and the direct shear method in high void ratios.

Looking at the effect of the initial void ratio and applied stresses on the dilation angles at the time of failure, it was observed that the difference between the test methods decreased in increasing void ratio and stresses, and the difference increased in decreasing void ratio and stresses.

The dilation angles at failure were compared with the effective peak and effective critical friction angles and significant relationships were derived for each test method. The consistency of this relationships is demonstrated by comparing a large number of literature data and flow rules.

When the effect of the presence of reinforcement on the normalized effective peak and critical stress ratios was analyzed, it was observed that it contributed to the strength for each test method. The rate of this contribution was greater for effective peak stress ratios.

When the effect of the presence of reinforcement on the initial void ratio and applied stresses on the normalized effective stress ratios is examined, it was observed that the contribution to the strength is more at decreasing void ratio and stresses.

It was found that the presence of reinforcement slightly increased the effective cohesion strengths. Accordingly, the highest cohesion strength values were obtained from triaxial tests, and the lowest values were obtained from ring shear tests.

Looking at the effect of the presence of reinforcement on the volumetric strains at the time of failure, it was observed that it increased the strains for each test method. The rate of this increase was found to be greater in triaxial tests.

When the effect of the presence of reinforcement on the strains at the initial moment when the dilation is zero, it was observed that it reduced the strains for each test method. The rate of this decrease was greater in triaxial tests.

The presence of reinforcement was observed to increase the dilation angles at the time of failure. The largest values of this increase were reached in the ring shear tests, the smallest values were obtained in the direct shear tests at low void ratios and in the triaxial tests at high void ratios.

Looking at the effect of the presence of reinforcement on the initial void ratio and the applied stresses on the dilation angles at the time of failure, it was observed that the difference between the test methods decreased in increasing void ratio and stresses, and the difference increased in decreasing void ratio and stresses.

Relationships were derived for each test method by comparing the increasing dilation angle of the presence of reinforcement and its effect on effective peak and effective critical friction angles. When these relationships compared with the relationships derived for the unreinforced case, the effect of the effective critical friction angle on the flow rules was clearly seen.

Finally, the presence of reinforcement was found to decrease the stiffness properties of composite samples and increased their ductility properties.

This study can be developed for the different physical or mechanical properties of sand or reinforcement, very low stress conditions or very high stress conditions that contain the effect of particle crushing, presence of fines, loading mode, stress path and for the drained conditions. Moreover, the effects of special processes that change the strength characteristics of sands such as anisotropic deposit, pozzolanic admixture or cementation can be examined with different test methods and competitive analysis can be conducted.

Experimental studies are long-term tasks that require hard effort. Therefore, it should be done with passion. Just like everything else in life...

LIST OF REFERENCES

- Adams, F.D., Nicholson, J.T., 1900, An experimental investigation into the flow of marble, *Philosophical Transactions of the Royal Society of London*, A:195, 363-401.
- Al-Hussaini, M.M., 1967, *The Behavior of Sand Under Plane Strain Conditions*, PhD. Thesis, Georgia Institute of Technology, p.166.
- Al-Refeai, T.O., 1991, Behavior of granular soils reinforced with discrete randomly oriented inclusions, *Geotextiles and Geomembranes*, 10(4), 319-333.
- Alshibli, K.A., Batiste, S.N., Sture, S., 2003, Strain localization in sand: Plane strain versus triaxial compression, *Journal Of Geotechnical And Geoenvironmental Engineering (ASCE)*, 129(6), 483-494.
- Alshibli, K.A., Godbold, D.L., Hoffman, K., 2004, The Louisiana plane strain apparatus for soil testing, *Geotechnical Testing Journal*, 27(4), 337-346.
- Amontons, M., 1699, De la resistance cause'e dans les machines "*Tant par les frottemens des parties qui les compofent, que par la roideur des cordes qu'on y employe, & la maniere de calculer l'un & l'autre*", *Mémoires de l'Académie Royale des Sciences*, Amsterdam, 206-227.
- Archard, J.F., 1953, Elastic deformation and the contact of surfaces, *Nature*, 172, 918-919.
- Archard, J.F., 1957, Elastic deformation and the laws of friction, *Proceedings of the Royal Society (Series A-Mathematical Physical and Engineering Sciences)*, 243(1233), 190-205.
- Arteaga, C.B., 1989, *The Shear Strength of Ottawa Sand Mixed with Discrete Short Length Plastic Fibers*, Master's Thesis, Mississippi State University, p.153.
- Arthur, J.R.F., Menzies, B.K., 1972, Inherent anisotropy in a sand, *Géotechnique*, 22(1), 115-128.
- Arthur, J.R.F., Phillips, A.B., 1975, Homogeneous and layered sand in triaxial compression, *Géotechnique*, 25(4), 799-815.
- ASTM., 2011, *Standard Test Method for Direct Shear Test of Soils Under Consolidated Drained Conditions (D3080/D3080M-11)*, ASTM International, p.9.
- ASTM., 2013, *Standard Test Method for Torsional Ring Shear Test to Determine Drained Residual Shear Strength of Cohesive Soils (D6467-13^{e1})*, ASTM International, p.7.
- ASTM., 2014, *Standard Test Methods for Specific Gravity of Soil Solids by Water Pycnometer (D854-14)*, ASTM International, p.8.

LIST OF REFERENCES (Continued)

- ASTM., 2016, Standard Test Methods for Maximum Index Density and Unit Weight of Soils Using a Vibratory Table (D4253-16^{e1}), ASTM International, p.14.
- ASTM., 2016, Standard Test Methods for Minimum Index Density and Unit Weight of Soils and Calculation of Relative Density (D4254-16), ASTM International, p.9.
- ASTM., 2017, Standard Test Methods for Particle-Size Distribution (Gradation) of Soils Using Sieve Analysis (D6913/D6913M-17), ASTM International, p.34.
- ASTM., 2018, Standard Test Method for Torsional Ring Shear Test to Measure Drained Fully Softened Shear Strength and Stress Dependent Strength Envelope of Fine-Grained Soils (D7608-18), ASTM International, p.6.
- ASTM., 2019, Standard Test Methods for Laboratory Determination of Water (Moisture) Content of Soil and Rock by Mass (D2216-19), ASTM International, p.7.
- ASTM., 2020, Standard Test Method for Consolidated Drained Triaxial Compression Test for Soils (D7181-20), ASTM International, p.12.
- ASTM., 2020, Standard Test Methods for Determination of Maximum Dry Unit Weight of Granular Soils Using a Vibrating Hammer (D7382-20), ASTM International, p.15.
- Atkinson, J.H., Bransby, P.L., 1978, *The Mechanics of Soils*, McGraw-Hill University Series in Civil Engineering, McGraw-Hill, p.375.
- Baker, R., 2004, Nonlinear Mohr envelopes based on triaxial data, *Journal of Geotechnical and Geoenvironmental Engineering (ASCE)*, 130(5), 498-506.
- Baligh, M.M., 1976, Cavity expansion in sands with curved envelopes, *Journal of the Geotechnical Engineering Division (ASCE)*, 102(11), 1131-1146.
- Barden, L., Ismail, H., Tong, P., 1969, Plane strain deformation of granular material at low and high pressures, *Géotechnique*, 19(4), 441-452.
- Bareither, C.A., Benson, C.H., Edil, T.B., 2008, Comparison of shear strength of sand backfills measured in small-scale and large-scale direct shear tests, *Canadian Geotechnical Journal*, 45(9), 1224-1236.
- Bell, A.L., 1915, The lateral pressure and resistance of clay and the supporting power of clay foundations, *Minutes of the Proceedings of the Institution of Civil Engineers, Part 1*: 199, 233-272.
- Beltrami, E., 1885, Sulle condizione di resistenza dei corpi elastici, II. *Nuovo Cimento, Società Italiana di Fisica*, 18, 145-155.

LIST OF REFERENCES (Continued)

- Berezantsev, V.G. Kovalev, I.V., 1968, Consideration of the curvilinear of the shear graph when conducting tests on model foundations, *Soil Mechanics and Foundation Engineering*, 5(1), 3-8.
- Bishop, A.W., 1950, Measurement of the shear strength of soils (Discussion), *Géotechnique*, 2(1), 113-116.
- Bishop, A.W., 1954, Shear characteristics of a saturated silt, measured in triaxial compression (Correspondence), *Géotechnique*, 4(1), 43-45.
- Bishop, A.W., Henkel, D.J., 1957, *The Measurement of Soil Properties in the Triaxial Test*, Edward Arnold Ltd., p.190.
- Bishop, A.W., 1966, The strength of soils as engineering materials, *Géotechnique*, 16(2), 91-130.
- Bishop, A.W., 1971, Shear strength parameters for undisturbed and remoulded soils specimens, In *Proceedings of the Roscoe Memorial Symposium on Stress-Strain Behaviour of Soils*, Henley-on-Thames: G.T. Foulis, 3-59.
- Bishop, A.W., Green, G.E., Garga, V.K., Andresen, A., Brown, J.D., 1971, A new ring shear apparatus and its application to the measurement of residual strength, *Géotechnique*, 21(4), 273-328.
- Bolton, M.D., 1979, *A Guide to Soil Mechanics*, Macmillan Education Ltd., London, p.439.
- Bolton, M.D., 1986, The strength and dilatancy of sands, *Géotechnique*, 36(1), 65-78.
- Bolton, M.D., 1987, Discussion: The strength and dilatancy of sands, *Géotechnique*, 37(2), 219-226.
- Bolton, M.D., 2018, The strength and dilatancy of geomaterials, The Hong Kong University of Science and Technology, IAS Distinguished Lecture, p.55.
- Bowden, F.P., Tabor, D., 1950, *Friction and Lubrication of Solids - Part I*, Clarendon Press, p.372.
- Bowden, F.P., Tabor, D., 1964, *Friction and Lubrication of Solids - Part II*, Clarendon Press, p.544.
- Boyle, S.R., 1995, *Deformation Prediction of Geosynthetic Reinforced Soil Retaining Walls*, PhD. Thesis, University of Washington, p.391.
- Bromhead, E.N., 1979, A simple ring shear apparatus, *Ground Engineering*, 12(5), 40-44.

LIST OF REFERENCES (Continued)

- BS., 1990, Methods of test for soils for civil engineering purposes - Part 7: Shear strength tests (total stress) (BS 1377-7), British Standards Institution, p.56.
- Budhu, M., 1979, Simple Shear Deformation of Sands, PhD. Thesis, University of Cambridge, p.301.
- Buisman, A.S.K., 1934, Proefondervindelicke bepaling van de greas van inwendig evenwicht van een grondmassa, De Ingenieur, B:49(26), 83-88.
- Casagrande, A., 1936, Characteristics of cohesionless soils affecting the stability of slopes and earth fills, Journal of the Boston Society of Civil Engineers, 23(1), 13-32.
- Casagrande, A., W.L., Shannon, 1948, Stress-deformation and strength characteristics of soils under dynamic loads, Proceedings of the Second International Conference on Soil Mechanics and Foundation Engineering, Rotterdam, 5, 29-34.
- Castro, G., 1969, Liquefaction of Sands, PhD. Thesis, Harvard University, p.125.
- Cauchy, A.L., 1823, Recherches sur l'équilibre et le mouvement intérieur des corps solides ou fluides, élastiques ou non élastiques, Bulletin des Sciences par la Société Philomatique, Paris, 9-13.
- Cauchy, A.L., 1827, De la pression ou tension dans un corps solide, Exercices de Mathématiques 2, Paris, 42-56.
- CEN., 1987, Methods of Testing Cement - Part 1: Determination of Strength (EN 196-1), Comité Européen de Normalisation, p.32.
- CEN., 1994, Methods of Testing Cement - Part 1: Determination of Strength (EN 196-1), Comité Européen de Normalisation, p.36.
- CEN., 2005, Methods of Testing Cement - Part 1: Determination of Strength (EN 196-1), Comité Européen de Normalisation, p.36.
- CEN., 2016, Methods of Testing Cement - Part 1: Determination of Strength (EN 196-1), Comité Européen de Normalisation, p.38.
- Cernica, J.N., 1995, Geotechnical Engineering: Soil Mechanics, John Wiley & Sons, Inc., New York, p.453.
- Chakraborty, T., Salgado, R., 2010, Dilatancy and shear strength of sand at low confining pressures, Journal of Geotechnical and Geoenvironmental Engineering (ASCE), 136(3), 527-532.

LIST OF REFERENCES (Continued)

- Chow, S.H., Roy, A., Herduin, M., Heins, E., King, L., Bienen, B., O'Loughlin, C., Gaudin, C., Cassidy, M., 2019, Characterisation of UWA Superfine Silica Sand (GEO 18844), Oceans Graduate School, p.33.
- Collin, A., 1846, Recherches Expérimentales sur les Glissements Spontanés des Terrains Argileux Accompagnées de Considérations sur Quelques Principes de la Mécanique Terrestre, Carilian-Goeury et V^{or} Dalmont, Paris, p.168.
- Collins, I.E., Pender, M.J., Wang, Y., 1992, Cavity expansion in sands under drained loading conditions, *International Journal for Numerical and Analytical Methods in Geomechanics*, 16(1), 3-23.
- Consoli, N.C., Casagrande, M.D.T., Coop, M.R., 2005, Behavior of a fiber-reinforced sand under large shear strains, *Proceedings of the Sixteen International Conference on Soil Mechanics and Geotechnical Engineering*, 3, 1331-1334.
- Consoli, N.C., Casagrande, M.D.T., Coop, M.R., 2007, Performance of a fibre-reinforced sand at large shear strains, *Géotechnique*, 57(9), 751-756.
- Consoli, N.C., Casagrande, M.D.T., Prietto, P.D.M., Thomé, A., 2003, Plate Load Test on Fiber-Reinforced Soil, *Journal of Geotechnical and Geoenvironmental Engineering*, 129(10), 951-955.
- Consoli, N.C., Heineck, K.S., Casagrande, M.D.T., Coop, M.R., 2007, Shear strength behavior of fiber-reinforced sand considering triaxial tests under distinct stress paths, *Journal of Geotechnical and Geoenvironmental Engineering (ASCE)*, 133 (11), 125-136.
- Cornforth, D.H., 1961, Plane Strain Failure Characteristics of a Saturated Sand, PhD. Thesis, University of London, p.341.
- Cornforth, D.H., 1964, Some experiments on the influence of strain conditions on the strength of sand, *Géotechnique*, 14(2), 143-167.
- Coulomb, C.A., 1773/1776, Essai sur une application des règles de Maximis & Minimis à quelques Problèmes de Statique, relatifs à l'Architecture, *Mémoires de Mathématique et de Physique, Présentés à l'Académie Royale des Sciences, par divers Savans, & lûs dans fes Affemblées*, 7, 343-382.
- Culmann, K., 1866, *Die Graphische Statik*, Verlag Von Meyer & Zeller, Zürich, p.740.
- Da Vinci, L., 1493, Leonardo's notebooks: Law of friction, Victoria and Albert Museum, London, Forster Codex (3), 72r.

LIST OF REFERENCES (Continued)

- Davis, E.H., 1968, Theories of plasticity and failures of soil masses, *Soil Mechanics: Selected Topics* (Editor: Lee, I.K.), Butterworths & Co., 341-380.
- De Beer, E., 1967, Shear strength characteristics of the “Boom Clay”, *Geotechnical Conference Oslo 1967 on Shear Strength Properties of Natural Soils and Rocks*, Oslo, 1, 83-88.
- De Josselin de Jong, G., 1976, Rowe’s stress-dilatancy relation based on friction, *Géotechnique*, 26(3), 527-534.
- Dev, K.L., Pillai, R.J., Robinson, G., 2016, Drained angle of internal friction from direct shear and triaxial compression tests, *International Journal of Geotechnical Engineering*, 10(3), 283-287.
- di Prisco, C., Nova, R., 1993, A constitutive model for soil reinforced by continuous threads, *Geotextiles and Geomembranes*, 12(2), 161-178.
- Diambra, A., 2010, *Fibre Reinforced Sands: Experiments and Constitutive Modelling*, PhD Thesis, University of Bristol, p.266.
- Diambra, A., Ibraim, E., 2015, Fibre-reinforced sand: interaction at the fibre and grain scale, *Géotechnique*, 65(4), 296-308.
- Diambra, A., Ibraim, E., Russell, A.R., Wood, D.M., 2013, Fibre reinforced sands: From experiments to modelling and beyond, *International Journal for Numerical and Analytical Methods in Geomechanics*, 37(15), 2427-2455.
- Diambra, A., Ibraim, E., Wood, D.M., Russell, A.R., 2010, Fibre reinforced sands: Experiments and modelling, *Geotextiles and Geomembranes*, 28(3), 238-250.
- Diambra, A., Russell, A.R., Ibraim, E., Wood, D.M., 2007, Determination of fibre orientation distribution in reinforced sands, *Géotechnique*, 57(7), 623-628.
- Dietz, M.S., Lings, M.L., 2006, Postpeak strength of interfaces in a stress-dilatancy framework, *Journal of Geotechnical and Geoenvironmental Engineering (ASCE)*, 132(11), 1474-1484.
- Ding, D., Hargrove, S.K., 2006, Nonlinear stress-strain relationship of soil reinforced with flexible geofibers, *Journal of Geotechnical and Geoenvironmental Engineering (ASCE)*, 132(6), 791-791.
- Dos santos, A.P.S., Consoli, N.C., Baudet, B.A., 2010, The mechanics of fibre-reinforced sand, *Géotechnique*, 60(10), 791-799.

LIST OF REFERENCES (Continued)

- Drucker, D.C., 1953, Limit analysis of two and three dimensional soil mechanics problems, *Journal of the Mechanics and Physics of Solids*, 1(4), 217-226.
- Drucker, D.C., Prager, W., 1952, Soil mechanics and plastic analysis or limit design, *Quarterly of Applied Mathematics*, 10(2), 157-165.
- Duncan, J.M., Byrne, P., Wong, K.S., Mabry, P., 1980, Strength, Stress-Strain and Bulk Modulus Parameters for Finite Element Analyses of Stresses and Movements in Soil Masses (Report No.: UCB/GT/80-01), College of Engineering Office of Research Services University of California, Berkeley (CA), p.80.
- ELE., 1993, Operating Instructions - Digital Tritest 50 (25-3516), ELE International, 3, p.11.
- ELE., 2015, Operating Instructions - Digital Direct/Residual Shear Apparatus (26-2114), ELE International, 4, p.28.
- ELE., 2019, Product catalogue - Civil & environmental engineering test equipment catalogue - Part 2: Soil testing equipment, ELE International, 13, 13-113.
- EN., 2007, Eurocode 7: Geotechnical Design - Part 2: Ground Investigation and Testing (EN 1997-2), European Committee for Standardization, p.202.
- Esposito III, M.P., Andrus, R.D., 2017, Peak shear strength and dilatancy of a Pleistocene age sand, *Journal of Geotechnical and Geoenvironmental Engineering (ASCE)*, 143(1), 04016079(p.11).
- Euler, L., 1757, Continuation des recherches sur la théorie du mouvement des fluides, *Mémoires de l'Académie Royale des sciences (Berlin)*, 11, 316-361.
- Euler, L., 1771, Sectio tertia de motu fluidorum lineari potissimum aquae, *Novi Commentarii Academiae Scientiarum Petropolitanae*, 15, 219-360.
- Falorca, I.M.C.F.G., Pinto, M.I.M., 2011, Effect of short, randomly distributed polypropylene microfibres on shear strength behaviour of soils, *Geosynthetics International*, 18(1), 2-11.
- Fannin, R.J., Eliadorani, A., Wilkinson, J.M.T., 2005, Shear strength of cohesionless soils at low stress, *Géotechnique*, 55(6), 467-478.
- Fernandes, M.M., 2020, Analysis and Design of Geotechnical Structures, CRC Press (Taylor & Francis Group), p.754.
- Finn., W.D.L., Wade, N.H., Kenneth, L.L., 1967, Volume changes in triaxial and plane strain tests, *Journal of the Soil Mechanics and Foundations Division (ASCE)*, 93(6), 297-308.

LIST OF REFERENCES (Continued)

- FHWA., 2007, Geotechnical Technical Guidance Manual, United States Department of Transportation (Federal Highway Administration), p.291.
- Fukushima, S., Tatsuoka, F., 1984, Strength and deformation characteristics of saturated sand at extremely low pressures, *Soils and Foundations*, 24(4), 30-48.
- GCP., 2020, STRUX® 90/40 Synthetic Macro Fibers, Product Data Sheets, GCP Applied Technologies Inc., p.5.
- Georgiadis, K., Potts, D.M., Zdravkovic, L., 2004, Modelling the shear strength of soils in the general stress space, *Computers and Geotechnics*, 31(5), 357-364.
- Giampa, J.R., Bradshaw, A.S., Schneider, J.A., 2017, Influence of dilation angle on drained shallow circular anchor uplift capacity, *International Journal of Geomechanics (ASCE)*, 17(2), 04016056(p.11).
- Giampa, J., Bradshaw, A., 2018, A simple method for assessing the peak friction angle of sand at very low confining pressures, *Geotechnical Testing Journal (ASTM)*, 41(4), 639-647.
- Gilboy, G., 1936, Improved soil testing methods, *Engineering News-Record*, 110(21), 732-734.
- Goodrich, E.P., 1904, Lateral earth pressure and related phenomena (No: 983), *Transactions of the American Society of Civil Engineers (ASCE)*, 53, 272-321.
- Gray, D.H., Ohashi, H., 1983, Mechanics of Fiber Reinforcement in Sand, *Journal of Geotechnical Engineering (ASCE)*, 109(3), 335-353.
- Gray, D.H., Al-Refeai, T.O., 1986, Behavior of fabric-versus fiber-reinforced sand, *Journal of Geotechnical Engineering (ASCE)*, 112(8), 804-820.
- Gray, D.H., Maher, M.H., 1989, Admixture stabilization of sands with random fibers, *Proceedings of the Twelfth International Conference on Soil Mechanics and Foundation Engineering, Rio De Janeiro*, 2, 1363-1366.
- Green, G.E., 1972, Strength and deformation of sand measured in an independent stress control cell, *Proceedings of the Roscoe Memorial Symposium: Stress-strain Behaviour of Soils*, G. T. Foulis & Co. Limited, Cambridge, 285-323.
- Green, G.E., Reades, D.W., 1975, Boundary conditions, anisotropy and sample shape effects on the stress-strain behaviour of sand in triaxial compression and plane strain, *Géotechnique*, 25(2), 333-356.

LIST OF REFERENCES (Continued)

- Greenwood, J.A., Williamson, J.B.P., 1966, Contact of nominally flat surfaces, *Proceedings of the Royal Society (Series A-Mathematical Physical and Engineering Sciences)*, 295(1442), 300-319.
- Gruner, H.E., Haefeli, R., 1934, Beitrag zur untersuchung des physikalischen und statischen verhaltens kohärenter bodenarten, *Schweizerische Bauzeitung*, 103(15), 171-174.
- Guida, G., Sebastiani, D., Casini, F., Miliziano S., 2019, Grain morphology and strength dilatancy of sands, *Géotechnique Letters*, 9(4), 245-253.
- Guo, P., 2008, Modified direct shear test for anisotropic strength of sand, *Journal of Geotechnical and Geoenvironmental Engineering (ASCE)*, 134(9), 1311-1318.
- Habib, P., 1953, Influence de la variation de la contrainte principale moyenne sur la résistance au cisaillement des sols, *Proceedings of the Third International Conference on Soil Mechanics and Foundation Engineering, Zurich*, 1, 131-136.
- Haefeli, R., 1938, Mechanische eigenschaften von lockergesteinen, *Schweizerische Bauzeitung*, 111(24), 299-303; 111(26), 321-325.
- Hanna, A.M., 2001, Determination of plane-strain shear strength of sand from the results of triaxial tests, *Canadian Geotechnical Journal*, 38(6), 1231-1240.
- Hanna, A.M., Ayadat, T., 2019, Comparative study of shear strength characteristics of dry cohesionless sands from triaxial, plane-strain and direct shear tests, *Geomechanics and Geoengineering*, 1-13.
- Hanna, A.M., Massoud, N., 1981, Interlocking of granular materials in two and three-dimensional shear failure, *Proceeding of the Eight Canadian Congress of Applied Mechanics [CANCAM81], Moncton N.B.*, 336-343.
- Hanna, A.M., Massoud, N., Youssef, H., 1987, Prediction of plane strain angle of shearing resistance from direct shear test results, *Proceedings of the International Symposium on Prediction and Performance in Geotechnical Engineering, University of Calgary*, 369-376.
- Hansen, J.B., 1961, A general formula for bearing capacity, *The Danish Geotechnical Institute*, 11, 38-46.
- Hardin, B.O., 1985, Crushing of soil particles, *Journal of Geotechnical and Geoenvironmental Engineering, ASCE*, 111(10), 1177-1192.
- Head, K.H., 1998, *Manual of Soil Laboratory Testing: Volume 3: Effective Stress Tests (Second Edition)*, John Wiley & Sons, Inc., Chichester, p.428.

LIST OF REFERENCES (Continued)

- Head, K.H., Epps, R.J., 2014, Manual of Soil Laboratory Testing: Volume 3: Effective Stress Tests (Third Edition), Whittles Publishing (CRC Press), Caithness, p.414.
- Heineck, K.S., Coop, M.R., Consoli, N.C., 2005, Effect of microreinforcement of soils from very small to large shear strains, *Journal of Geotechnical and Geoenvironmental Engineering (ASCE)*, 131 (8), 1024-1033.
- Henkel, D.J., Wade, N.H., 1966, Plane strain tests on a saturated remolded clay, *Journal of Soil Mechanics and Foundations Division (ASCE)*, 92(6), 67-80.
- Hennes, R.G., 1953, The strength of gravel in direct shear, *Symposium on Direct Shear Testing of Soils, ASTM Special Technical Publication (STP131)*, Baltimore (MD), 51-62.
- Hertz, H., 1881, Ueber die Berührung fester elastischer Körper (On the contact of elastic solids), *Journal für die Reine und Angewandte Mathematik*, 92, 156-171.
- Holm, R., 1941, *Die Technische Physik der Elektrischen Kontakte*, Springer-Verlag Berlin Heidelberg GmbH, Berlin (Siemensstadt), p.337.
- Holtz, R.D., Kovacs, W.D., Sheahan, T.C., 2011, *An Introduction to Geotechnical Engineering (2nd Edition)*, Pearson Education, Inc., Upper Saddle River (NJ), p.864.
- Horn, H.M., Deere, D.U., 1962, Frictional characteristics of minerals, *Géotechnique*, 12(4), 319-335.
- Hough, B.K., 1957, *Basic Soils Engineering*, The Ronald Press, New York, p.513.
- Houlsby, G.T., 1991, How the dilatancy of soils affects their behaviour, In *Proceedings of the Tenth European Conference on Soil Mechanics and Foundation Engineering*, Florence, 4, 1189-1202.
- Housel, W.S., 1936, Internal stability of granular materials, *Proceedings of the American Society for Testing Materials*, 36(2), 426-468.
- Hunger, O., Morgenstern, N.R., 1984, High velocity ring shear tests on sand, *Géotechnique*, 34(3), 415-421.
- Hvorslev, M.J., 1936a, Conditions of failure for remoulded cohesive soils, *Proceedings of the First International Conference on Soil Mechanics and Foundation Engineering*, Cambridge (MA), 3, 51-53.
- Hvorslev, M.J., 1936b, A ring shearing apparatus for the determination of the shearing resistance and plastic flow of soils, *Proceedings of the First International Conference on Soil Mechanics and Foundation Engineering*, Cambridge (MA), 2, 125-129.

LIST OF REFERENCES (Continued)

Hvorslev, M.J., 1937, Über die Festigkeitseigenschaften Gestörter Bindiger Böden, Danmarks Naturvidenskabelige Samfund, Ingeniørvidenskabelige Skrifter, København, A:45, p.159.

Hvorslev, M.J., 1939, Torsion shear tests and their place in the determination of the shearing resistance of soils, Symposium on Shear Testing of Soils, Proceedings of the American Society for Testing Materials, 39, 999-1022.

Ibraim, E., Fourmont, S., 2006, Behaviour of sand reinforced with fibres, Proceedings of the Geotechnical Symposium: Geomechanics: Laboratory Testing, Modelling and Applications (Ling, H.I., Callisto, L., Leshchinsky, D., Koseki, J., (eds), 2007, Soil Stress-Strain Behavior: Measurement, Modeling and Analysis, Solid Mechanics and Its Applications, 146), 807-818.

Ibraim, E., Diambra, A., Wood, D.M., Russel, A.R., 2010, Static liquefaction of fibre reinforced sand under monotonic loading, Geotextiles and Geomembranes, 28(4), 374-385.

Ibraim, E., Diambra, A., Russel, A.R., Wood, D.M., 2012, Assessment of laboratory sample preparation for fibre reinforced sands, Geotextiles and Geomembranes, 34, 69-79.

Ichihara, M., Matsuzawa, H., 1973, Application of plane strain test to earth pressure, Proceedings of The Eighth International Conference on Soil Mechanics and Foundation Engineering, Moscow, 1, 185-190.

ISO., 1968, Cement and Lime (ISO/R 679), International Organization for Standardization, p.12.

ISO., 2018, Geotechnical investigation and testing - Laboratory testing of soil - Part 10: Direct Shear Tests (ISO 17892-10), International Organization for Standardization, p.23.

JGS, 1979, Mechanical tests on soil (II), Standards on soil tests, Japanese Geotechnical Society, 423-593.

Jefferies, M., Been, K., 2016, Soil Liquefaction: A Critical State Approach (Second Edition), Applied Geotechnics Series, CRC Press, p.734.

Jewell, R.A., 1980, Some Effects of Reinforcement on the Mechanical Behaviour of Soils, PhD. Thesis, University of Cambridge, p.320.

Jewell, R.A., 1989, Direct shear tests on sand, Géotechnique, 39(2), 309-322.

Jewell, R.A., Wroth, C.P., 1987, Direct shear tests on reinforced sand, Géotechnique, 37(1), 53-68.

LIST OF REFERENCES (Continued)

- Jürgenson, L., 1934, The shearing resistance of soils, *Journal of the Boston Society of Civil Engineers*, 21(3), 242-275.
- Kaibori, M., 1980, Direct Shear Test on Saturated Toyoura Standard Sand, Master's Thesis, Kyoto University, p.93.
- Kármán, T.V., 1910, Mitől függ az anyag igénybevétele?, *A Magyar Mérnök és Építész Egylet Közlönye*, 44(10), 212-226.
- Kármán, T.V., 1911, Festigkeitsversuche unter allseitigem druck, *Zeitschrift des Vereins Deutscher Ingenieure*, 42:55(2), 1749-1757.
- Kenney, T.C., 1967, The influence of mineral composition on the residual strength of natural soils, *Geotechnical Conference Oslo 1967 on Shear Strength Properties of Natural Soils and Rocks*, Oslo, 1, 123-129.
- Kjellman, W., 1936, Report on an apparatus for consummate investigation of the mechanical properties of soils, *Proceedings of the First International Conference on Soil Mechanics and Foundation Engineering*, Cambridge (MA), 2, 16-20.
- Knappett, J, Craig, R.F., 2019, *Craig's Soil Mechanics (9th Edition)*, CRC Press, p.654.
- Ko, H.Y., Scott, R.F., 1968, Deformation of sand at failure, *Journal of the Soil Mechanics and Foundations Division (ASCE)*, 94(4), 883-898.
- Koerner, R.M., 1970, Effect of particle characteristics on soil strength, *Journal of the Soil Mechanics and Foundations Division (ASCE)*, 96(4), 1221-1234.
- Koerner, R.M., 2012, *Designing with Geosynthetics: Volume 1 (Sixth Edition)*, Xlibris Corporation, Inc., USA, p.528.
- Krey, H., 1926, *Erddruck, Erdwiderstand und Tragfähigkeit des Baugrundes: Gesichtspunkte für die Berechnung, Praktische Beispiele und Erddrucktabellen (Dritte Umgearbeitete und Erweiterte Auflage)*, Verlag von Wilhelm Ernst & Sohn, Berlin, p.296.
- Kulhawy, F.H., Mayne, P.W., 1990, Manual on estimating soil properties for foundation design, Electric Power Research Institute (Cornell University Geotechnical Engineering Group), EPRI report: EL-6800, Research project: 1493-6, p.308.
- La Gatta, D.P., 1970, Residual Strength of Clay and Clay-Shales by Rotation Shear Tests, Harvard Soil Mechanics Series No: 86, Cambridge (MA); U.S Army Engineer Waterways Experiment Station Contract Report: S-70-5, Vicksburg (MS), p.220.

LIST OF REFERENCES (Continued)

- La Rochelle, P., Leroueil, S., Trak, B., Blais-Leroux, L., Tavenas, F., 1988, Observational approach to membrane and area corrections in triaxial tests, *Advanced Triaxial Testing of Soil and Rock*, ASTM Special Technical Publication (STP977), Baltimore (MD), 715-731.
- Ladd, C.C., Foott, R., Ishihara, K., Schlosser, F., Poulos, H.G., 1977, Stress-deformation and strength characteristics, *The Ninth International Conference on Soil Mechanics and Foundation Engineering*, Tokyo, 2, 421-494.
- Ladd, R.S., 1978, Preparing test specimens using undercompaction, *Geotechnical Testing Journal (ASTM)*, 1(1), 16-23.
- Lade, P.V., 1972, *The Stress-Strain and Strength Characteristics of Cohesionless Soils*, PhD. Thesis, University of California, p.765.
- Lade, P.V., Duncan, J.M., 1973, Cubical triaxial tests on cohesionless soil, *Journal of the Soil Mechanics and Foundations Division (ASCE)*, 99(10), 793-812.
- Lade, P.V., Duncan, J.M., 1975, Elastoplastic stress-strain theory for cohesionless soil, *Journal of the Geotechnical Engineering Division (ASCE)*, 101(10), 1037-1053.
- Lade, P.V., Lee, K.L., 1976, *Engineering Properties of Soils*, Engineering Report UCLA-ENG-7652, School of Engineering and Applied Sciences, University of California, p.145.
- Lade, P.V., Yamamuro, J.A., Bopp, P.A., 1996, Significance of particle crushing in granular materials, *Journal of Geotechnical and Geoenvironmental Engineering (ASCE)*, 122(4), 309-316.
- Lam, W.K., Tatsuoka, F., 1988, Effects of initial anisotropic fabric and σ_2 on strength and deformation characteristics of sand, *Soils and Foundations*, 28(1), 89-106.
- Lancelot, L., Shahrour, I., Al Mahmoud, M., 2006, Failure and dilatancy properties of sand at relatively low stresses, *Journal of Engineering Mechanics (ASCE)*, 132(12), 1396-1399.
- Lau, C.K., Bolton, M.D., 2011, The bearing capacity of footings on granular soils. I: Numerical analysis, *Géotechnique*, 61(8), 627-638.
- Lee, K.L., 1970, Comparison of plane strain and triaxial tests on sand, *Journal of the Soil Mechanics and Foundations Division (ASCE)*, 96(3), 901-923.
- Lee, K.L., Farhoomand, I., 1967, Compressibility and crushing of granular soil in anisotropic triaxial compression, *Canadian Geotechnical Journal*, 4(1): 68-86.
- Lee, K.L., Seed, H.B., 1967, Drained strength characteristics of sands, *Journal of Soil Mechanics and Foundations Division (ASCE)*, 93, 117-141.

LIST OF REFERENCES (Continued)

- Lee, K.L., Seed, H.B., Dunlop, P., 1966, The Effect of Transient Loading on the Strength of Sand, Highway Research Board, Washington (DC), p.40.
- Lee, W.F., 2000, Internal Stability Analyses of Geosynthetic Reinforced Retaining Walls, PhD. Thesis, University of Washington, p.416.
- Lehane, B.M., Liu, Q.B., 2013, Measurement of shearing characteristics of granular materials at low stress levels in a shear box, *Geotechnical and Geological Engineering*, 31, 329-336.
- Leibniz, G.W., 1684, Nova methodus pro maximis et minimis: itemque tangentibus, quae nec fractas, nec irrationales quantitates moratur, & singulare pro illis calculi genus, *Acta Eruditorum*, Anno M DC LXXXIV publicata, ac Serenissimo Fratrum Pari, 467-473.
- Leygues, M.L., 1885, Nouvelle recherche sur la poussée des terres et le profil de revêtement le plus économique (No:98), *Annales des Ponts et Chaussées*, Sixth Série: 2(10), 788-1003.
- Leussink, H., Wittke, W., 1964, Difference in triaxial and plain strain shear strength, *Laboratory Shear Testing of Soil*, ASTM Special Technical Publication (STP361), Baltimore (MD), 77-89.
- Leussink, H., Wittke., W., Weseloh, K., 1966, Unterschiede im Scherverhalten rolliger Erdstoffe und Kugelschüttungen im Dreiaxial und Biaxialversuch, *Veröffentlichungen des Institutes für Bodenmechanik und Felsmechanik*, Universität Karlsruhe, 21, p.70.
- Lings, M.L., Dietz, M.S., 2004, An improved direct shear apparatus for sand, *Géotechnique*, 54(4), 245-256.
- Liu, Q.B., Lehane, B.M., 2012, The influence of particle shape on the (centrifuge) cone penetration test (CPT) end resistance in uniformly graded granular soils, *Géotechnique*, 62(11), 973-984.
- Lodge, A.S., Howell, H.G., 1954, Friction of an elastic solid, *Proceedings of the Physical Society (Section B)*, 67(2), 89-97.
- Newton, I., 1686, *Philosophiæ Naturalis Principia Mathematica* (“The Mathematical Principles of Natural Science”), Imprimatur Samuel Pepys Regalis Societas Præses, Londini (“London”), p.510.
- Maher, M.H., Gray, D.H., 1990, Static response of sand reinforced with randomly distributed fibers, *Journal of Geotechnical Engineering (ASCE)*, 116(11), 1661-1677.

LIST OF REFERENCES (Continued)

- Maksimović, M., 1989, Nonlinear failure envelope for coarse-grained soils, *Journal of Geotechnical Engineering (ASCE)*, 115(4), 581-586.
- Marachi, N.D., Duncan, J.D., Chan, C.K., Seed, H.B., 1981, Plane-strain testing of sand, *Laboratory Shear Strength of Soil*, ASTM Special Technical Publication (STP740), Baltimore (MD), 294-302.
- Marsal, R.J., 1967, Large Scale Testing of Rockfill Materials, *Journal of the Soil Mechanics and Foundations Division (ASCE)*, 93(2), 27-43.
- Matsuoka, H., 1974, Stress-strain relationships of sands based on the mobilized plane, *Soils and Foundations*, 14(2), 47-61.
- Matsuoka, H., Nakai, T., 1974, Stress-deformation and strength characteristics of soil under three different principal stresses, *Proceedings of Japan Society of Civil Engineers*, 232, 59-70.
- Maxwell, J.C., 1856, Origins of James Clerk Maxwell's electric ideas, as described in familiar letters to William Thomson, In Joseph Larmor (Ed.), Cambridge University Press (1937), 31-33.
- Means, R.E., Parcher, J.V., 1963, *Physical Properties of Soils*, Charles Edward Merrill Books Publishing Company Inc., Columbus, p.464.
- Medzvieckas, J., Dirgėlienė, N., Skuodis, Š., 2017, Stress-strain states differences in specimens during triaxial compression and direct shear tests, *Procedia Engineering (Modern Building Materials Structures and Techniques, 2016)*, 172, 739-745.
- Meehan, C.L., Brandon, T.L., Duncan, J.M., 2007, Measuring drained residual strengths in the Bromhead ring shear, *Geotechnical Testing Journal (ASTM)*, 30(6), 466-473.
- Menzies, B.K., 1970, *Stress-strain Anisotropy in Sands*, PhD. Thesis, University of London, p.129.
- Merry, S.M., Lawton, E.C., 2012, A review of shear stress sign convention in interpreting Mohr's Circle using the pole of planes method, *ASCE, GeoCongress 2012*, 1263-1272.
- Meyerhof, G.G., 1956, Penetration tests and bearing capacity of cohesionless soils, *Journal of the Soil Mechanics and Foundations Division (ASCE)*, 82(1), 1-19.
- Michalowski, R.L., 2008, Limit analysis with anisotropic fibre-reinforced soil, *Géotechnique*, 58(6), 489-501.

LIST OF REFERENCES (Continued)

- Michalowski, R.L., Čermák, J., 2002, Strength anisotropy of fiber-reinforced sand, *Computers and Geotechnics*, 29(4), 279-299.
- Michalowski, R.L., Čermák, J., 2003, Triaxial compression of sand reinforced with fibers, *Journal of Geotechnical and Geoenvironmental Engineering (ASCE)*, 129(2), 125-136.
- Michalowski, R.L., Zhao, A., 1996, Failure of fiber-reinforced granular soils, *Journal of Geotechnical Engineering*, 122(3), 226-234.
- Mirata, T., Erzin, Y., 2007, Strength of sands in wedge shear, triaxial shear, and shear box tests, *Geotechnical Testing Journal (ASTM)*, 30(2), 152-163.
- Mitchell, J.K., Soga, K., 2005, *Fundamentals of Soil Behavior (3rd Edition)*, John Wiley & Sons, Inc., New Jersey, p.592.
- Miura, N., Yamanouchi, T., 1973, Compressibility and drained shear characteristics of a sand under high confining pressures, *Technology Reports of the Yamaguchi University*, 1(2), 271-290.
- Mohr, O., 1882, Ueber die darstellung des spannungszustandes und des deformationszustandes eines körperelementes und über die anwendung derselben in der festigkeitslehre, *Der Civilingenieur*, 30, 113-156.
- Mohr, O., 1900, Welche umstände bedingen die elastizitätsgrenze und den bruch eines materiales? *Zeitschrift des Vereines Deutscher Ingenieure*, 44(2), 1524-1530; 1572-1577.
- Musschenbroek, P.V., 1729, *Physicæ Experimentales et Geometricæ, De Magnete, Tuborum Capillarium Vitreorumque Speculorum Attractione, Magnitudine Terræ, Cohærentia Corporum Firmorum, Dissertationes ut et Ephemerides Meteorologicæ Ultrajectinæ, Lugduni Batavorum*, p.685.
- Nagaraj, T.S., Somashekar, B.V., 1979, Stress deformation and strength of soils in plane strain, *Proceedings of the sixth Asian Regional Conference on Soil Mechanics and Foundation Engineering*, Singapore, 1, 43-46.
- Nash, K.L., 1953, The shearing resistance of a fine closely graded sand, *Proceedings of the Third International Conference on Soil Mechanics and Foundation Engineering*, Zurich, 1, 160-164.
- Nataraj, M.S., McManis, K.L., 1997, Strength and deformation properties of soils reinforced with fibrillated fibers, *Geosynthetics International*, 4(1), 65-79.

LIST OF REFERENCES (Continued)

- NAVFAC., 1982, Soil Mechanics: Design Manual 7.1, Naval Facilities Engineering Command, Department of the Navy, Alexandria, p.382.
- NAVFAC., 1986, Soil Mechanics: Design Manual 7.01, Naval Facilities Engineering Command, Department of the Navy, Washington (DC), p.390.
- Navier, P.M., 1822, Mémoire sur les lois du mouvement des fluides, Lu à l'Académie royale des Sciences, 389-441.
- Negussey, D., Wijewickreme, W.K.D., Vaid, Y.P., 1988, Geomembrane interface friction, Canadian Geotechnical Journal, 26(1), 165-169.
- Newland, P.L., Allely, B.H., 1957, Volume changes in drained triaxial tests on granular materials, Géotechnique, 7(1), 17-34.
- Nicks, J.E., Gebrenegus, T., Adams, M.T., 2015, Strength Characterization of Open-Graded Aggregates for Structural Backfills (FHWA-HRT-15-034), Office of Infrastructure Research and Development, U.S. Department of Transportation, The Federal Highway Administration, p.154.
- Noorzad, R., Zarinkolaei, S.T.G., 2015, Comparison of mechanical properties of fiber-reinforced sand under triaxial compression and direct shear, Open Geosciences, 1, 547-558.
- Novosad, J., 1964, Studies on granular materials (Part 2: Apparatus for measuring the dynamic angle of internal and external friction of granular materials "Angles of friction of granular materials at high shearing speeds and small normal stresses were measured on a modified Hvorslev shearing apparatus"), Collection of Czechoslovak Chemical Communications, 29, 2697-2701.
- O'Kelly, B.C., 2015, Effective stress strength testing of peat, Environmental Geotechnics, 2(1), 34-44.
- Oancea, A., 1996, Triaxial compression of soils reinforced with discrete synthetic fibres, Master's Thesis, Carleton University, p.178.
- Oda, M., 1971, Studies on anisotropy in granular sand, Report of Department of Foundation Engineering, Faculty of Science and Engineering, Saitama University, 1, 1-34.
- Oda, M., Koishikawa, I., Higuchi, T., 1978, Experimental study of anisotropic shear strength of sand by plane strain test, Soils and Foundations, 18(1), 25-38.

LIST OF REFERENCES (Continued)

- Okada, Y., Sassa, K., Fukuoka, H., 1988, Comparison of shear behaviour of sandy soils by ring-shear test with conventional shear tests, Proceedings of the IUFRO Division 8 Conference Environmental Forest Science, Environmental Forest Science, 623-632.
- Palmeira, E.M., 1987, The Study of Soil-reinforcement Interaction by Means of Large Scale Laboratory Tests, PhD. Thesis, University of Oxford, p.237.
- Peck, R.B., Hanson, W.E., Thornburn, T.H., 1974, Foundation Engineering (2nd Edition), John Wiley & Sons, Inc., New York, p.544.
- Pells, P.J.N., Maurenbrecher, P.M., Elges, H.F.W.K., 1973, Validity of results from the direct shear test, Proceedings of the eighth international conference on soil mechanics and foundation engineering, Moscow, 1, 333-338.
- Peters, J.F., Lade, P.V., Bro, A., 1988, Shear band formation in triaxial and plane strain tests, Advanced Triaxial Testing of Soil and Rock, ASTM Special Technical Publication (STP977), Baltimore (MD), 604-627.
- Pike, K., 2016, Physical and Numerical Modelling of Pipe/Soil Interaction Events for Large Deformation Geohazards, PhD. Thesis, 52(8), Memorial University of Newfoundland, p.402.
- Poisson, S.D., 1831, Mémoire sur les équations générales de l'équilibre et du mouvement des corps solides élastiques et des fluides, Journal de l'Ecole Polytechnique, 13, 1-174.
- Ponce, V.M., Bell, J.M., 1971, Shear strength of sand at extremely low pressures, Journal of the Soil Mechanics and Foundations Division, 97(4), 625-638.
- Proctor, D.C., Barden, L., 1969, A note on the drained strength of sand under generalized strain conditions, Géotechnique, 19(3), 424-426.
- Procter, D.C., Barton, R.R., 1974, Measurements of the angle of interparticle friction, Géotechnique, 24(4), 581-604.
- Punetha, P., Mohanty, P., Samanta, M., 2017, Microstructural investigation on mechanical behavior of soil-geosynthetic interface in direct shear test, Geotextiles and Geomembranes, 45(3), 197-210.
- Quinteros, V.S., 2014, Observations on the Mobilization of Strength in Reinforced Soil Structures, Master's Thesis, The University of British Columbia, p.88.
- Rahman, M.S., Ülker, M.B.C., 2018, Modeling and Computing for Geotechnical Engineering - An Introduction, CRC Press (Taylor & Francis Group), p.506.

LIST OF REFERENCES (Continued)

- Ramamurthy, T., Tokhi, V.K., 1981, Relation of triaxial and plane strain strengths, Proceedings of the Tenth International Conference on Soil Mechanics and Foundation Engineering, Stockholm, 1, 755-758.
- Ramamurthy, T., Tokhi, V.K., 1989, Plane strain strength from triaxial test, Proceedings of the Twelfth International Conference on Soil Mechanics and Foundation Engineering, Rio De Janeiro, 1, 749-752.
- Ranjan, G., Vasan, R.M., Charan, H.D., 1994, Behaviour of plastic-fibre-reinforced sand, Geotextiles and Geomembranes, 13(8), 555-565.
- Ranjan, G., Vasan, R.M., Charan, H.D., 1996, Probabilistic analysis of randomly distributed fiber-reinforced soil, Journal of Geotechnical Engineering (ASCE), 122(6), 419-426.
- Rankine, W.J.M., 1843, On the causes of the unexpected breakage of the journals of railway axles; and on the means of preventing such accidents by observing the law of continuity in their construction, Minutes of Proceedings, Institution of Civil Engineers, 2, 105-107.
- Rankine, W.J.M., 1857, On the stability of loose earth, Philosophical Transactions of the Royal Society of London, 147, 9-27.
- Rawat, P.C., 1976, Shear Behaviour of Cohesionless Materials Under Generalized Conditions of Stress and Strain, PhD. Thesis, Indian Institute of Technology Delhi, p.415.
- Reades, D.W., 1972, Stress-strain Characteristics of a Sand Under Three-Dimensional Loading, PhD. Thesis, University of London, p.878.
- Reades, D.W., Green, G.E., 1974, Discussion on "cubical triaxial tests on cohesionless soil", Journal of Geotechnical Engineering Division (ASCE), 100(9), 1065-1067.
- Rendulic, L., 1933/1935, Der hydrodynamische Spannungsausgleich in zentral entwässerten Tonzylindern, Wasserwirtschaft und Technik, 2, 250-253; 269-273.
- Reynolds, O., 1883, An experimental investigation of the circumstances which determine whether the motion of water shall be direct or sinuous, and of the law of resistance in parallel channels, Philosophical Transactions of the Royal Society of London, 174, 935-985.
- Reynolds, O., 1885, On the dilatancy of media composed of rigid particles in contact. With experimental illustrations, The London, Edinburgh and Dublin Philosophical Magazine and Journal of Science, 5:20(127), 469-481.
- Riemer, M.F., 1999, Plane Strain Testing of Sand Specimens for RMC Test Wall Modeling, Test Report, Berkeley (CA), 4.p.

LIST OF REFERENCES (Continued)

- Roberts, J.E., De Souza, J.M., 1958, The compressibility of sands, *Proceedings of the American Society for Testing Materials*, 58, 1269-1277.
- Romero, R.J., 2003, *Development of A Constitutive Model for Fiber-Reinforced Soils*, PhD. Thesis, University of Missouri, p.183.
- Roscoe, K.H., 1970, The influence of strains in soil mechanics, *Géotechnique*, 20(2), 129-170.
- Roscoe, K.H., Burland, J.B., 1968, *On the generalized stress-strain behaviour of 'wet' clay*, *Engineering Plasticity*, Cambridge University Press, 535-608.
- Rousé, C., 2018, Relation between the critical state friction angle of sands and low vertical stresses in the direct shear test, *Soils and Foundations*, 58(5), 1282-1287.
- Rowe, P.W., 1962, The stress-dilatancy relation for static equilibrium of an assembly of particles in contact, *Proceedings of the Royal Society (Series A-Mathematical and Physical Sciences)*, 269(1339), 500-527.
- Rowe, P.W., 1963, Stress-dilatancy, earth pressures and slopes, *Journal of the Soil Mechanics and Foundations Division (ASCE)*, 89(3), 37-61.
- Rowe, P.W., 1964a, Closure to discussion on Stress-dilatancy, earth pressures and slopes, *Journal of the Soil Mechanics and Foundations Division (ASCE)*, 90(4), 145-180.
- Rowe, P.W., 1964b, Discussion on Some experiments on the influence of strain conditions on the strength of sand, *Géotechnique*, 14(4), 361-364.
- Rowe, P.W., 1969, The relation between the shear strength of sands in triaxial compression, plane strain and direct, *Géotechnique*, 19(1), 75-86.
- Rowe, P.W., Barden, L., Lee, I.K., 1964, Energy components during the triaxial cell and direct shear tests, *Géotechnique*, 14(3), 247-261.
- Saada, A.S., Townsend, F.C., 1981, *Laboratory strength testing of soils*, *Laboratory Shear Strength of Soil*, ASTM Special Technical Publication (STP740), Baltimore (MD), 7-77.
- Sack, W.A., 1960, *Factors Affecting the Shear Strength of Cohesionless Soil*, Master's Thesis, Michigan State University, p.64.
- Sadek, S., Najjar, S.S., Freiha, F., 2010, Shear strength of fiber-reinforced sands, *Journal of Geotechnical and Geoenvironmental Engineering (ASCE)*, 136(3), 490-499.

LIST OF REFERENCES (Continued)

- Sadrekarimi, A., 2009, Development of a New Ring Shear Apparatus for Investigating the Critical State of Sands, PhD. Thesis, University of Illinois at Urbana-Champaign, p.452.
- Sadrekarimi, A., Olson, S.M., 2009, A new ring shear device to measure the large displacement shearing behavior of sands, *Geotechnical Testing Journal (ASTM)*, 32(3), 197-208.
- Sadrekarimi, A., Olson, S.M., 2010, Particle damage observed in ring shear tests on sands, *Canadian Geotechnical Journal*, 47(5), 497-515.
- Sadrekarimi, A., Olson, S.M., 2011, Yield strength ratios, critical strength ratios, and brittleness of sandy soils from laboratory tests, *Canadian Geotechnical Journal*, 48(3), 493-510.
- Sadrekarimi, A., Olson, S.M., 2014, Residual state of sands, *Journal of Geotechnical and Geoenvironmental Engineering (ASCE)*, 140(4), 04013045(p.10).
- Salgado, R., 2006, *The Engineering of Foundations*, McGraw-Hill Education, p.896.
- Salgado, R., Bandini, P., Karim, A., 2000, Shear strength and stiffness of silty sand, *Journal of Geotechnical and Geoenvironmental Engineering (ASCE)*, 126(5), 451-462.
- Sassa, K., 2000, Mechanism of flows in granular soils, *An International Conference on Geotechnical & Geological Engineering (GeoEng2000)*, 1, 1671-1702.
- Sauter, D.W., Taoufik, M., Boisson, C., 2017, Polyolefins, a success story, *Polymers (MDPI)*, 9(6), p.13.
- Scarlett, B., Todd, A.C., 1969, The critical porosity of free flowing solids, *Journal of Engineering for Industry (ASME)*, 91(2), 478-487.
- Schanz, T., Vermeer, P.A., 1996, Angles of friction and dilatancy of sand, *Géotechnique*, 46(1), 145-151.
- Schlosser, F., Long, N.T., 1974, Recent results of French research on reinforced earth, *Journal of the Construction Division (ASCE)*, 100(3), 233-237.
- Schmertmann, J.H., 1978, Guidelines for CPT Performance and Design (Report FHWA-TS-78-209), United States Department of Transportation, p.158.
- Schmertmann, J.H., 1983, Revised procedure for calculating K_0 and OCR from DMT 's with $I_D > 1.2$ and which incorporate the penetration force measurement to permit calculating the plane strain friction angle, *DMT Workshop 1*, Gainesville (FL), p.5.

LIST OF REFERENCES (Continued)

- Schofield, A.N., 1998, The Mohr Coulomb error, *Mécanique & Géotechnique*, Laboratoire de Mécanique des Solides École Polytechnique, 19-27.
- Schofield, A.N., Wroth, P., 1968, *Critical State Soil Mechanics*, McGraw Hill, Maidenhead, p.310.
- Senetakis, K., Coop, M.R., Todisco, M.C., 2013, The inter-particle coefficient of friction at the contacts of Leighton Buzzard sand quartz minerals, *Soils and Foundations*, 53(5), 746-755.
- Shimobe, S., Moroto, N., 1997, Classical study on strength parameters of granular soils, *Deformation and Progressive Failure in Geomechanics (The International Symposium on Deformation and Progressive Failure in Geomechanics: IS-Nagoya'97)*, 271-276.
- Siang, A.J.L.M., Wijeyesekera, D.C., bin Zainorabidin, A., bin Hj Bakar, I., 2012, Effect of particle grading size and shape on density, dilatancy and shear strength of sands, *Malaysian Journal of Science*, 31(2), 161-174.
- Simoni, A., Houlsby, G.T., 2006, The direct shear strength and dilatancy of sand-gravel mixtures, *Geotechnical and Geological Engineering*, 24, 523-549.
- Skempton, A.W., Bishop, M.A., 1950, The measurement of the shear strength of soil, *Géotechnique*, 2(2), 90-108.
- Skempton, A.W., 1964, Long-term stability of clay slopes, *Géotechnique*, 14(2), 77-102.
- Soriano, I., Ibraim, E., Andò, E., Diambra, A., Laurencin, T., Moro, P., Viggiani, G., 2017, *Granular Matter*, 19(75), p.14.
- Sowers, G.F., 1964, Strength testing of soils, *Laboratory Shear Testing of Soil*, ASTM Special Technical Publication (STP361), Baltimore (MD), 3-21.
- Stakemann, O., 1976, Failure Conditions for G12-Sand and Plane Strain Model Tests, The Danish Geotechnical Institute, I.M'76-1, p.96.
- Stanton, T.E., Hveem, F.N., 1934, Role of the laboratory in the preliminary investigation and control of materials for low cost bituminous pavements, *Proceedings of the Fourteenth Annual Meeting of the Highway Research Board*, 14 (2), 14-54.
- Stark, T.D., Eid, H.T., 1993, Modified Bromhead ring shear apparatus, *Geotechnical Testing Journal (ASTM)*, 16(1), 100-107.

LIST OF REFERENCES (Continued)

- Stokes, G.G., 1845, On the theories of the internal friction of fluids in motion, and of the equilibrium and motion of elastic solids, Transactions of the Cambridge Philosophical Society, 8, 75-129.
- Strahler, A., Stuedlein, A.W., Arduino, P.W., 2015, Stress-strain response and dilatancy of sandy gravel in triaxial compression and plane strain, Journal of Geotechnical and Geoenvironmental Engineering (ASCE), 142(4), 04015098(p.11).
- Strahler, A., Stuedlein, A.W., Arduino, P.W., 2016, Erratum for “Stress-strain response and dilatancy of sandy gravel in triaxial compression and plane strain”, Journal of Geotechnical and Geoenvironmental Engineering (ASCE), 142(10), 08216003(p.2).
- Strahler, A., Stuedlein, A.W., Arduino, P.W., 2018, Three-dimensional stress-strain response and stress-dilatancy of well-graded gravel, International Journal of Geomechanics (ASCE), 18(4), 04018014(p.10).
- Stroud, M.A., 1971, The Behaviour of Sand at Low Stress Levels in the Simple Shear Apparatus, PhD. Thesis, University of Cambridge, p.354.
- Sture, S., Costes, N.C., Batiste, S.N., Lankton, M.R., AlShibli, K.A., Jeremic, B., Swanson, R. A., Frank, M., 1998, Mechanics of granular materials at low effective stresses, Journal of Aerospace Engineering (ASCE), 11(3), 67-72.
- Superfeskys, M.J., Williams, G.P., 1978, Shear Strength of Surface-mine Spoils Measured by Triaxial and Direct Shear Methods, Forest Service General Technical Report (NE-39), United States Department of Agriculture, Broomall (PA), p.15.
- Sutherland, H.B., Mesdary, M.S., 1969, The influence of the intermediate principal stress on the strength of sand, Proceedings of the Seventh International Conference on Soil Mechanics and Foundation Engineering, Mexico City, 1, 391-399.
- Tatsuoka, F., 1985, On the angle of interface friction for cohesionless soils, Soils and Foundations, 25(4), 135-141.
- Tatsuoka, F., Sakamoto, M., Kawamura, T., Fukushima, S., 1986, Strength and deformation characteristics of sand in plane strain compression at extremely low pressures, Soils and Foundations, 26(1), 65-84.
- Taylor, D.W., 1939, A comparison of results of direct shear and cylindrical compression tests, Symposium on Shear Testing of Soils, Proceedings of the American Society for Testing Materials, 39, 1058-1070.

LIST OF REFERENCES (Continued)

- Taylor, D.W., 1948, Fundamentals of Soil Mechanics, John Wiley & Sons, Inc., New York, p.712.
- Terzaghi, K., 1920, Old earth pressure theories and new test results, Engineering News-Record, 85, 632-637.
- Terzaghi, K., 1924, Die Theorie der hydrodynamischen Spannungserscheinungen und ihr erdbautechnisches Anwendungsgebiet, Proceedings of the first International Congress for Applied Mechanics, Delft, 288-294.
- Terzaghi, K., 1925, Principles of Soil Mechanics, Engineering News Record, 95, p.1068.
- Terzaghi, K., 1943, Theoretical Soil Mechanics, John Wiley & Sons, Inc., New York, p.528.
- Terzaghi, K., Casagrande, A., 1932, The design of the shearing apparatus (Recent developments in soil testing apparatus as a report in: Rutledge, P.C., 1935, Journal of the Boston Society of Civil Engineers, 22(4), 223-250), Massachusetts Institute of Technology, Cambridge (MA).
- Terzaghi, K., Peck, R.B., 1948, Soil Mechanics in Engineering Practice, John Wiley & Sons, Inc., p.566.
- Terzaghi, K., Peck, R.B., 1967, Soil Mechanics in Engineering Practice (2nd Edition), John Wiley & Sons, Inc., New York, p.729.
- Terzaghi, K., Peck, R.B., Mesri, G., 1996, Soil Mechanics in Engineering Practice (3rd ed.), John Wiley & Sons, Inc., p.512.
- Tiedemann, B., 1937, Über die schubfestigkeit bindiger böden, Die Bautechnik, 15(30), 400-403; 15(33), 433-435.
- Tika, T.E., Vaughan, P.R., Lemos, L.J.L.J., 1996, Fast shearing of pre-existing shear zones in soil, Géotechnique, 46(2), 197-233.
- Tresca, H.E., 1864, Mémoires sur l'écoulement des corps solides, soumis à de fortes pressions, Comptes Rendus Hebdomadaires des Séances de l'Académie des Sciences, 59, 754-758.
- TSE., 2016, Çimento Deney Metotları - Bölüm 1: Dayanım Tayini (TS EN 196-1), Türk Standardları Enstitüsü, s.35.
- Ueno, K., Miura, K., Kusakabe, O., Nishimura, M., 2001, Reappraisal of size effect of bearing capacity from plastic solution, Journal of Geotechnical and Geoenvironmental Engineering (ASCE), 127(3), 275-281.

LIST OF REFERENCES (Continued)

- Vaid, Y.P., Sasitharan, S., 1992, The strength and dilatancy of sand, *Canadian Geotechnical Journal*, 29(3), 522-526.
- Venant, S.B., 1837, *Leçons de mécanique appliquée faites par intérim, par M. de St-Venant, Ingénieur des Ponts et Chaussées, Paris, (Lithographed Course; referred to by Todhunter and Pearson, 1886, History of Elasticity, Cambridge, 1, p.831).*
- Venant, S.B., 1843, Note à joindre au mémoire sur la dynamique des fluides (1834), *Comptes Rendus des Séances de l'Académie des Sciences*, 17, 1240-1243.
- Venkatramaiah, C., 2018, *Geotechnical Engineering (Sixth Edition)*, New Age International Publishers, p.976.
- Verdugo, R., 1992, The critical state of sands: Discussion, *Géotechnique*, 42 (4), 655-663.
- Vermeer, P.A., de Borst, R., 1984, Non-associated Plasticity for Soils, *Concrete and Rock, Heron*, 29(3), p.64.
- Vesic, A.S., Clough, G.W., 1968, Behavior of granular materials under high stresses, *Journal of the Soil Mechanics and Foundations Division (ASCE)*, 94(3), 661-688.
- Vidal, H., 1969, The principle of reinforced earth (Soil theories: Reinforced earth, displacements, bearing and seepage), *National Research Council (Series: Highway Research Record)*, 282, 1-16.
- Villet, W.C.B., Mitchell, J.K., 1981, Cone resistance, relative density and friction angle, In *Proc. Session on Cone Penetration Testing and Experience (ASCE National Convention)*, New York, 178-208.
- VJTech., 2018, Product catalogue - Ring Shear Pro Testing System (VJT5600A/01), *Building Better Technology for the Civil Engineering Industry*, VJ Tech Limited, 9, 37-38.
- Wade, N.H., 1963, *Plane Strain Failure Characteristics of a Saturated Clay*, PhD. Thesis, University of London, p.308.
- Wan, R.G., Guo, P.J, 1998, A Simple constitutive model for granular soils: Modified stress-dilatancy approach, *Computers and Geotechnics*, 22(2), 109-133.
- Wanatowski, D., 2005, *Strain Softening and Instability of Sand Under Plane-Strain Conditions*, PhD. Thesis, Nanyang Technological University, p.345.
- Wanatowski, D., Chu, J., 2006, Stress-strain behavior of a granular fill measured by a new plane-strain apparatus, *Geotechnical Testing Journal (ASTM)*, 29(2), 149-157.

LIST OF REFERENCES (Continued)

- Wanatowski, D., Chu, J., 2007a, Drained behaviour of Changi sand in triaxial and plane-strain compression, *Geomechanics and Geoengineering: An International Journal*, 2(1), 29-39.
- Wanatowski, D., Chu, J., 2007b, A New Plane-Strain Apparatus and Plane-Strain Tests on Sand, *Proceedings of the 16th Southeast Asian Geotechnical Conference*, 1, 393-398.
- Westerberg, N., 1921, Jordtryck i kohesionära jordarter, *Teknisk Tidskrift, Väg & Vattenbyggnadskonst*, 51(3), 25-29; 51(4), 61-65; 51(5), 61-65.
- Wightman, A., 1967, The Stress-Dilatancy of Sands During Plane Strain Compression, Master's Thesis, The University of Manchester, p.114.
- Wood, D.M., 1990, *Soil Behaviour and Critical State Soil Mechanics*, Cambridge University Press, p.488.
- Wood, D.M., 2009, *Soil Mechanics: A One-Dimensional Introduction*, Cambridge University Press, p.254.
- Wood, D.M., 2013, Soils in space, *Constitutive Modeling of Geomaterials: Advances and New Applications*, Springer Series in Geomechanics and Geoengineering, 239-246.
- Wroth, C.P., 1984, The interpretation of in situ soil tests, *Géotechnique*, 34(4), 449-489.
- Yetimoglu, T., Salbas, O., 2003, A study on shear strength of sands reinforced with randomly distributed discrete fibers, *Geotextiles and Geomembranes*, 21(2), 103-110.
- Zhang, H., Garga, V.K., 1997, Quasi-steady state: A real behaviour?, *Canadian Geotechnical Journal*, 34(5), 749-761.
- Zhao, H.F., Zhang, L.M., Chang, D.S., 2013, Behavior of coarse widely graded soils under low confining pressures, *Journal of Geotechnical and Geoenvironmental Engineering (ASCE)*, 139(1), 35-48.
- Zornberg, J.G., 2002, Discrete framework for limit equilibrium analysis of fibre-reinforced soil, *Géotechnique*, 52(8), 593-604.